

ADAPTIVE TRAITS FOR TEMPORAL CODING IN THE AUDITORY BRAINSTEM

MIHAI STANCU



Graduate School of
Systemic Neurosciences

LMU Munich



DISSERTATION AT THE
GRADUATE SCHOOL OF SYSTEMIC NEUROSCIENCES
LUDWIG-MAXIMILIANS-UNIVERSITÄT MÜNCHEN

APRIL 2023

Supervisor

PD Dr. Conny Kopp-Scheinflug

Chair: Prof. Benedikt Grothe

LMU Martinsried

First Reviewer: PD Dr. Conny Kopp-Scheinflug

Second Reviewer: Prof. Dr. Benedikt Grothe

Date of Submission: 11.04.2023

Date of Defense: 27.11.2023

Table of Contents

Acknowledgements.....	ii
1. Introduction	1
1.1 The brain	1
The dendrites	3
The axon initial segment.....	5
The axon and the myelin around it.....	6
The synaptical terminal.....	9
1.2 The auditory pathway	11
1.3 Potassium channels.....	15
1.4 Semantics, adaptation & (en)coding.....	17
Coding & encoding.....	17
Adaptation	18
Time and the brain.....	19
1.5 Motivation & objectives of the thesis.....	20
2. Chapter 2 – Myelin.....	21
3. Chapter 3 – Potassium channels.....	31
4. Discussion & further directions.....	66
4.1 Efficient coding.....	68
4.2 Active efficient coding.....	69
4.3 Predictive coding.....	72
4.4 Cochlear implants	75
4.5 Dyslexia	77
4.6 Hearing loss and tinnitus.....	79
5. Conclusion.....	80
6. Bibliography	83
Author Contributions	104

Acknowledgements

Being grateful is, in my opinion, one of the most graceful and elegant states the human mind can be in. It harbors fulfillment, energy and humbleness, all of which are required to steer ourselves in blissful awe, witnessing the never-ending and terrifying beauty of the universe.

I truly believe it is the people we have around us are the ones giving us shape, constantly bringing us meaning and joy, so for me it is necessary to start this work by acknowledging their glittering presence.

sic itur ad astra

Thank you to my family, you are everything for me. Your unconditional and never-ending support made me who I am.

Vā multumesc dim suflet!

Thank you to my loved ones and my friends, you painted my life in the boldest colours, making it all worth it to the very last bit. You took care of my soul, in ways you wouldn't even know. I would not change a single moment with you.

To our department and the GSN, you are beautiful people, with whom I've shared so many good moments and stories! You will always have my gratitude.



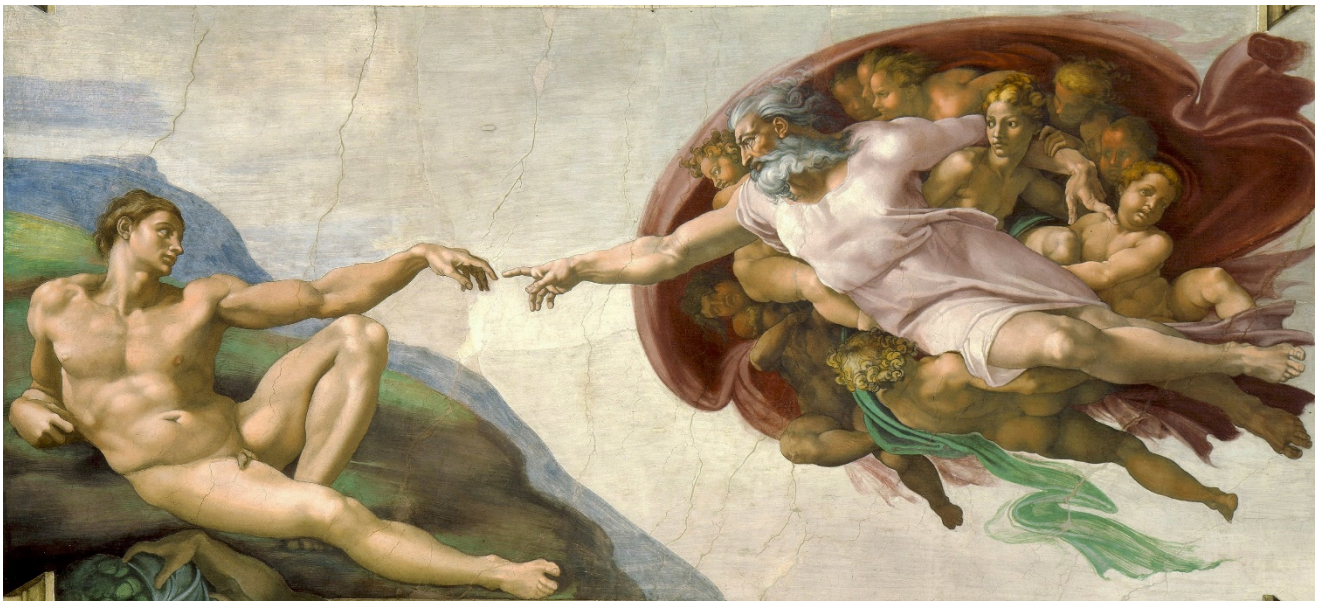
Salvador Dalí, The Endless Enigma, 1938

Conny, it's been almost a decade since we've met. You decided to trust me with a summer opportunity, which ultimately led to me joining you a few years later and pursuing this PhD. I am sure that you know that words could never reach the horizon of gratitude, respect, value and love that I have for you, but I will try. You are an elegant and noble soul, from whom I've learned a tremendous amount of science, as well as other notions and ideas, that are at least as valuable. You provided me with more than guidance or simple work duties these years, you were my second family, for quite a while now! I want you to know that these years spent in your lab represent the most prolific period of my life, in which I grew beautifully. Thank you for being the way you are, never change! Having you along my life's path is a blessing.

Benedikt, I would like to juggle your memory for a second. In the first retreat we had at the GSN, not even two weeks after coming to Munich, you came to us, the new PhD students and started by strongly asking us not to address you by any academic title or by your family name, just simply "Benedikt". It was the first glimpse of the man you proved to be. You showed us humbleness, which is one of the traits of genuine human greatness. Lots of other gracious acts and decisions followed, from which I benefitted, either directly or indirectly. I would like to say thank you for what you've done for all of us, past, present and future people. Your efforts, sheer will, uncompromised dedication and sacrifices made it possible that science and its people thrive and explore and create. I will do my best to keep adding to this effort, so that true beauty is further nourished.

Jan, you are an amazing man. I had no idea we will be crossing paths, but I am delighted that we did. I enjoyed working with you in the lab, your expertise is invaluable and your spirit is unmatched. I loved being able to share experiments, stories, travels and even some car tinkering with you! Thank you for your contribution to my upbringing, it means a lot!

1. Introduction



Michelangelo, Creation of Adam, 1508-1512.

Frank Lynn Meshberger, M.D proposed that the painting may be hiding an **anatomical depiction of the human brain** and that the depicted God is superimposed on the emotional side of the brain, the limbic system. ⁴⁵⁰

1.1 The brain

Throughout much of human history, the true purpose and function of the brain remained shrouded in mystery. One of the earliest theories regarding the brain's role came from Aristotle, who viewed the brain as a secondary organ that primarily functioned to cool the heart and allowed for the circulation of spirits. Interestingly, he also introduced the concept of the *sensus communis*, which eventually became known as "common sense". Essentially, Aristotle believed that all of our intellectual knowledge originated from our sensory experiences, stating that "There is nothing in the intellect that is not in the senses". Despite the advancements made in modern neuroscience, Aristotle's early theories on the brain and cognition remain a testament to the complex and enduring history of human understanding. Starting with the Roman doctor Galen, who observed that the brain was linked decisively to behaviour (and thus assigning the "seat of the soul" to the brain), many others followed and, step-by-step, described the brain more accurately, to what we have today.

We are now privileged to reliably consider the nervous system to be the only organised biological structure that deals exclusively with information, be it collecting, processing or exchanging it with the outer environment or the inner parts of the organism. While information exchange and processing exists in almost all kinds of tissue or cells, we could also find other functions of that tissue: the heart has its own signal generating mechanisms, but it also pumps blood into the circulatory system, the glands cells have intricate tuning mechanisms, but they also secrete different substances needed to carry out tasks. The nervous system can be safely regarded as the only "information for the sake of information" type. This specialized separation of tasks and responsibilities within an organism allows for better performance and a better outcome in terms of survival and fitness.

For living organisms, information needs a physical support in order to be handled. That support is, in simple terms, the notion of *change*. To illustrate this, I will use two equally feasible mechanisms, both of which would use particle movement.

For the first proposition, I will take refer to molecular diffusion, one of the many phenomena derived from the physical laws of the universe that we live in. It is the thermal motion of all liquid or gas particles at temperatures above absolute zero and in time it leads to equal distribution of particles within a given space. If one creates a content gradient between two spaces and then allows passage between the two, an equilibrium state will be reached, and we can observe a *change* between the initial and final state. The second proposition would be similar, but in the opposite direction: we can initiate the change, starting from a single space with no gradient in which we create a gradient and then isolate the extremities accordingly. The end result, again, produces *change*.

If we take into account the biological substrate in which *change* needs to be created, we can see that there would be a *time* difference between the two propositions: the latter simply takes more time to happen through molecular machinery. Since time is a scarce resource for living organisms and quick action is almost always required, we evolved to use the first example as our underlying means of representing information. Neurons, like any other cell type, are circumscribed by a membrane, which is specialized in working with *change*. The membrane is a lipid bilayer that is impermeable for most ions and molecules and thus creates and maintains an imbalance in ionic concentrations between the inner and outer sides of it. This imbalance is disrupted for brief periods of time, which is then interpreted as information. These brief disruptions are called action potentials (APs). This is a simplified description of a much more complex process, but it highlights the core principle of how information is handled in our nervous system. If the membrane would try to produce imbalance starting from equilibrium and use that *change* as support for information, it would simply take a lot more time, during which plenty of actions could happen in the outer or inner environments; most of them would be detrimental to the organism.

Across different modalities like vision, audition, touch, taste or smell, there is a common blueprint across all types of neurons. They must generate a sequence of four physiological signals at four different anatomical sites – the input signal at the dendrites, the trigger signal at the AIS, the conducting signal at the axon and the output signal at the synaptic terminal. By taking these into account, we can put forward a model neuron, whose components cater to each type of signal: receptive, integrative, long-range transmission and the final secretory component. Overall, it is the expression of the dynamic polarization principle, enunciated by Ramón y Cajal^{1,2}. The pursue of this thesis is to describe the known modulation sites in the model neuron and add a further contribution to understanding it, operating within the context of auditory pathway research.

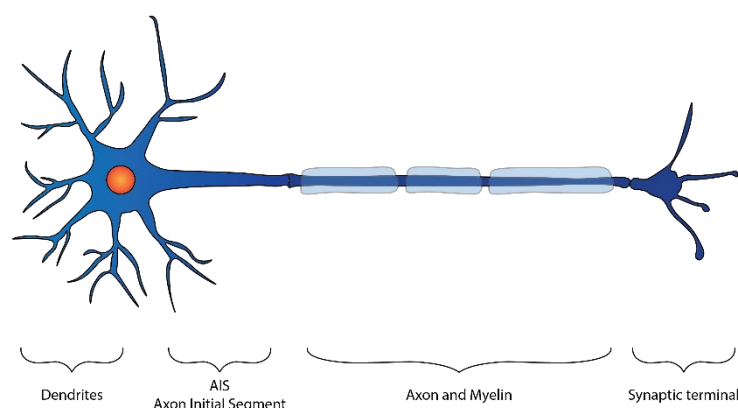


Figure 1. Model neuron

The dendrites

The dendrites are structures that serve as receptors and initial processing sites for received information. They extend from the cell bodies, forming structures called processes. The nature of the input also dictates the ramification degree that these processes have. Dendrites receive synaptic inputs on their bodies, dendritic spines or specialized structures that have synapses on them³. All these peculiar features come in different flavors, varying widely in terms of local connectivity and the molecular signaling necessities. Special imaging techniques showed that the dendritic synaptic specialisations come with significant differences in size, localization and internal composition. Furthermore, genetic, acquired, environmental and memory-related factors, along with personal pathological history across an individual's life can influence and determine the shape and the composition of dendrites and their synaptic connections³.

Some modern approaches that study the dendrites, the axons and the glial cells started showing proof that the conventional model in which the information transmission only happens in the cell body-axon-dendrite direction might actually be wrong³⁻⁵. The classical understanding was that dendrites are a receptor field or structure of the neurons, with axons passing on signals coming from the cell body to other neurons, but this has been challenged by modern imaging studies, which show atypical functionality, with dendrites acting as an output relay as well. In certain regions of the nervous system, the dendrites make reciprocal synapses with other dendrites, having both pre- and post-synaptic components. All this while axons can act as receptors, forming axo-axonal connections throughout the brain. Furthermore, another type of connections, called gap junctions, are found between dendrites, axons and glial structures. These serve as bidirectional communication sites between adjacent membranes. Despite being less common, the gap junctions, along with the connections among pairs of dendrites or axons still play significant roles in making direct communication between neural cells and for its modulation³. The dendritic arborizations with a high level of complexity can harbour thousands of synapses. The spherical shape of neuronal bodies limits their surface available for input connections. The dendrites complement this by massively increasing the area without a substantial increase in cell volume. Furthermore, packing this surface as dendritic trees enable a compact placement of numerous neurons together and expands the accessibility to multiple axons. Despite all this, a fully expanded dendritic tree does not translate to an increased synapse density. For example, only about a fifth of the axons that are in direct contact with a dendrite of a pyramidal cell in the hippocampus actually make a synapse with that dendrite. The combined surface of those synapses only takes about a tenth of the total surface of the dendrites⁴⁻⁶. The imaging studies imply that increasing the synaptic connectivity might not be the main purpose of the dendrites or any other synaptic specializations (i.e., spines, growths)⁷⁻⁹.

Neurons situated in the brain stem function as coincidence detectors for auditory information. They possess the ability to fire rapidly, generating up to 1000 spikes per second, and operate on a timescale ranging from tens to hundreds of microseconds. This remarkable speed is attributed to their distinct morphology, synaptic characteristics, and the existence of voltage-sensitive conductance, leading to low input resistances and brief time constants. These neurons boast extraordinary temporal resolution, making them highly receptive to the morphological and biophysical attributes of dendrites and the spatial distribution of synaptic inputs. Octopus cells utilize dendritic filtering to counterbalance delays caused by cochlear traveling waves when identifying broadband transient sounds. Conversely, the primary cells of the medial superior olivary nucleus rely on dendrites to improve the detection of simultaneous inputs from both ears. Octopus cell dendrites extend across the tonotopically organized bundle of auditory nerve fibers as they cross the dorsal cochlear nucleus.

In mice, these primary branches have a diameter of roughly 4 μm and lengths that range from 100 to 200 μm . Each mouse octopus cell obtains input from at least 60 auditory nerve fibers, and approximately 200 octopus cells receive input from a total of 12,000 fibers. This convergence of inputs grants octopus cells an extensive tuning spectrum.

In contrast, MSO neurons have a bipolar structure, with excitatory inputs from both ipsilateral and contralateral sources allocated to the distal ends of their lateral or medial dendritic arbors, respectively. Each MSO cell acquires at least two to four similarly and acutely tuned excitatory axons on either side. MSO neurons create a sheet on each side, arranging frequency in the dorsoventral dimension. It remains uncertain whether there is a systematic mapping of optimal ITDs within the nucleus in all mammals. MSO neuron dendrites are comparatively thick, spanning roughly 100 to 200 μm in length, but exhibit few branches. Glycinergic inhibition, originating from the medial and lateral nuclei of the trapezoid body, specifically targets the soma and proximal dendrites. The ability to detect minor timing discrepancies is enhanced through a combination of excitatory inputs and inhibition¹⁰⁻¹².

Both octopus and MSO cells leverage dendritic morphology to amplify coincidence detection in ways that are biologically significant. In octopus cells, dendritic electrotonic filtering counteracts traveling wave delays, resulting in the generation of substantial, rapidly ascending summed EPSPs at the soma¹³. Conversely, MSO neurons display more efficient and linear summation of subthreshold inputs when distributed across multiple tufts instead of a single tuft¹⁴. Additionally, the substantial diameter of both octopus and MSO dendrites lowers axial resistance, enabling current flow from synapses to the soma and axon, thereby reducing EPSP duration.

EPSCs in octopus cells, originating from stimulated fibers, rise over approximately 0.5 ms and decay with time constants of around 0.7 ms¹⁵. Both octopus and MSO cells preserve the timing of fast synaptic currents as quickly ascending and descending EPSPs, but noticeable synaptic depression occurs during repetitive stimulation¹⁵⁻¹⁷. In vivo, responses to a series of clicks at 500 Hz display a 200 μs latency shift across the initial 10 clicks, likely attributable to synaptic depression¹⁸. NMDA receptors are present in mature organisms; however, their functional influence diminishes with age due to gKL activation by the AMPA component of EPSPs, which speeds up membrane repolarization and conceals NMDA receptor-mediated depolarization^{15,19}. In octopus cells of mice, glycinergic and GABAergic inhibition are physiologically inconsequential, while accurately timed glycinergic currents from two to four robust inputs in MSO cells impact both the position and amplitude of ITD curves^{10,20,21}.

Neuronal computations rely on their time course. Neurons function as "integrators" when their integration time is extended compared to the firing rate, and as "coincidence detectors" when it is brief relative to the input firing rate²². Octopus and MSO cells are regarded as some of the most accurate coincidence detectors in the brain, as they can identify acoustic information contained in microsecond timing differences, which for most neurons falls within the temporal jitter of firing. The dendritic structure and biophysical characteristics of these cells bolster their coincidence detection abilities. Octopus cells offset cochlear traveling wave delays utilizing their dendrites, while MSO cells employ dendrites to refine coincidence detection of inputs from both sides. These cells exhibit an extraordinary degree of separation between their somatodendritic and axonal compartments.

Considering the accuracy needed for proper dendritic functioning within the auditory pathway, it is crucial to recognize the significant impact of individual or combined modulation effects that might not have notable consequences in other pathways.

The axon initial segment

The axon initial segment (AIS), situated at the base of axons, plays a crucial role in generating and shaping action potentials before they propagate along the axon. The AIS composition and position significantly affect neuronal excitability, which can adapt to developmental and physiological changes. Additionally, the axon initial segment is a barrier that separates the somatodendritic and axonal compartments²³. Contemporary research has shed light on the molecular structure of the AIS and its regulation of protein trafficking^{23,24}.

Relatively recent studies demonstrated how the axon initial segment can express plasticity during development^{25,26}, changes in neuronal activity^{27,28}, sensory deprivation^{25,29}, and brain disorders. Moreover, the AIS's heterogeneity has been documented across various cell types, brain regions, and species^{28,30}. In the auditory system, researchers have examined the AIS structural features on the chick brainstem model, in the laminaris and magnocellularis nuclei^{26,29,31}, and saw similar features that were previously observed in the mouse MNTB (tonotopy differentiation of the axon initial segment and the action potential waveform)³². High-frequency (HF) neurons, with a generally smaller length of the AIS, but projecting further from the soma, fired action potentials of a lower amplitude than those neurons with low-frequency. During development, the axon initial segment of low- and high-frequency neurons shortened²⁶, while in mice, MNTB neurons with a high frequency CF specifically experienced AIS adjustments until they became adults. This AIS adjustment in HF neurons influences MNTB spike waveforms in both mice and chicks²⁶. Differences in AIS plasticity between chicks and mice could be connected to discrepancies in audiograms (2 Hz to 9 kHz, for the chick³³ and 4 kHz to 64 kHz [NO_PRINTED_FORM]for the mouse³⁴), with MNTB being capable of processing sounds of higher frequencies in mice and rats than in chicks. The NL in chicks shows a higher resemblance to the MSO found in rodents like gerbils that prefer lower frequency sounds³⁴.

Sound-induced activity shapes axon initial segment development, as seen in congenitally deaf mice with longer segments in MNTB high-frequency (HF) neurons. Absent sound input hinders AIS shortening, leaving it immature. HF neuron AIS is more adaptable, while low-frequency (LF) neuron AIS remains constant. In MNTB's lateral hindbrain (LH) neurons, AIS location adjusts in response to sound changes, shifting closer during stimulation and further during deprivation. This shift affects neuronal excitability, as seen in hippocampal and pyramidal cells. The distinct responses in various brain areas may be due to cell-type or region-specific AIS structural plasticity^{27,28,35}.

The mammalian brain's structural and functional attributes evolve over time^{36,37}. Studying axon initial segment (AIS) regulation across an individual's life can offer insights into key molecules and signaling pathways. AIS shortening is observed in the auditory brainstem of chicks, monkey prefrontal cortex, and mouse visual cortex during development, before stabilizing^{25,26,38}. In mice, AIS length increases until P15, then decreases as eyes open, continuing until P21's cortical ocular dominance plasticity onset²⁵. AIS developmental plasticity may relate to individual neuron functionality in specific regions^{25,39}. While AIS has a unique range of length and location, its structural flexibility may be lost with age, leading to alterations^{40,41}. Aging-related changes differ from homeostatic processes aimed at compensating for reduced neuronal activity^{42,43}. In older mice, AIS-associated ankyrinG, spectrin, and actin levels decrease, potentially shortening AIS and reducing NaV1.6 channel expression, thus increasing primary visual cortex neuronal activity⁴¹. Sensory input decline seems to affect AIS structural stability in the sensory system. However, the relationship between AIS morphological changes and neuronal excitability in aging brains remains uncertain. Studying molecular mechanisms targeting AIS reorganization during aging could help develop new strategies for diseases of the central auditory segment and for physiological hearing loss.

Contemporary societies with advanced technology expose individuals to heightened sensory inputs. Continuous exposure to sounds of varying intensities can influence the growth and development patterns of the neurons in the auditory pathway. During development, sound stimulation promotes axon initial segment (AIS) shortening but does not modify AIS length in

adulthood. AIS structural adaptability in response to sound inputs stays within particular boundaries, avoiding excessive shortening³². In both development and adulthood, sound stimulation causes a proximal shift of MNTB neurons' AIS. This contradicts findings from experiments using hippocampus cell cultures or brain slices where increased neuronal activity results in a distal AIS shift, suggesting that sound stimulation's impact on AIS position in the auditory system is cell-specific^{27,28}. This indicates that sound stimulation can substantially alter the auditory brain's cellular structures.

Neuronal excitability in the auditory brainstem is a significant area of interest, specifically regarding AIS plasticity's role in modulating it. MNTB neurons' AP amplitude is crucial for their rapid spiking properties⁴⁴, with ion channel location and characteristics believed to be responsible. Research indicates that sodium channel positioning in the nerve terminal influences the AP waveform⁴⁵. Computational models suggest that Na channels located nearer to the terminal could produce a larger, higher-amplitude AP. Divergent AIS responses to neuronal activity might be influenced by stimulus conditions and durations, potentially accounting for discrepancies between studies demonstrating a distal axonal shift in increased neuronal activity^{27,28,32}.

The impact of input-related adaptations in the auditory system, regardless whether it is stimulation or deprivation, that are physiological or homeostatic in nature, is significant for devising new techniques and therapies, especially in the modern approach of medicine, with targeted strategies against lasting deficits or damage, regardless of age.

The axon and the myelin around it

Action potentials (APs) represent electrical impulses conveyed by axons between neurons in a circuit as a reaction to sensory input or in communication between motor neurons and muscles. In mammals and various other vertebrates, a substantial proportion of axons are insulated by myelin, synthesized by Schwann cells in the peripheral nervous system (PNS) and oligodendrocytes in the central nervous system (CNS). Myelin consists of multiple layers of glial membrane that encase axons, enhancing transmembrane resistance while minimizing membrane capacitance. While myelinating glia were once considered passive entities in nervous system functionality, they are now recognized for their numerous active roles. These roles encompass the modulation of axon diameter, the management of axonal energy metabolism, and the organization of ion channels at intervals within the myelin sheath known as nodes of Ranvier. Myelin's active and passive influences on axons lead to higher AP conduction speeds, decreased metabolic needs, and smaller space requirements compared to their unmyelinated counterparts. As a result, the existence of myelin and the strategic arrangement of ion channels within axons have facilitated the development of sophisticated nervous systems in vertebrates.

In both the central and peripheral nervous systems, glial cells such as oligodendrocytes or Schwann cells, respectively, tightly wrap myelin around neuronal axons in a segmented pattern⁴⁶. Myelin is a substance mostly produced in the nervous system of mammals after birth⁴⁷. This process continues during the entire lifespan in order to support and maintain memory and learning as well as remyelination after injury. It is a substance rich in lipids, made primarily of proteins (PLP, MBP), phospholipids, glycolipids, and cholesterol.

Myelin plays a crucial role in the nervous system functionality by providing electrical insulation for the axon and enabling fast and reliable conduction of action potentials across myelinated axons. Furthermore, myelination creates the structural and molecular divisions within the axonal compartment: an alternation of myelinated (internodes) and unmyelinated spaces (the nodes of Ranvier, with adjacent regions called paranodes and juxtaparanodes)^{46,48}.

Myelinating glial cells interact with axons at paranodes, which flank the distal and proximal sides of a node, to form axoglial junctions that are required in forming the node and further nodal maintenance. Additionally, the regions called paranodes also play a vital role in sustaining conduction speeds in the myelinated axons, with even the slightest imbalance of the paranodal junctions having a significant slowing effect on the conduction velocities⁴⁹. The disruptions of axonal domains are an important element of several neurological diseases' pathophysiological pathways. This is yet another important argument for furthering research in neuron-glia communication and mechanisms and their corresponding pathological implications in nervous tissue diseases.

The core functionality of the nervous system, regardless if we refer to reflexes, perception, sensation, or any processing, relies on the constant interplay of action potentials, the primary means of conveying messages and thus information between neurons. This diverse information is encoded in action potential frequency as well as the organization and quantity of active neurons within neural networks. The synaptic transmission timing and the processing of signals in neural circuitry are affected by disruptions of the conduction capabilities of the axons involved. This is particularly important because when signals conveyed by different axons reach the same postsynaptic site within a very short period of time of each other (milliseconds), temporal summation amplifies the overall postsynaptic response. This concurrent input is necessary in tweaking and enhancing action potential speeds and for classical conditioning. Besides synaptic transmission, which exhibits plastic changes vital for information storage in the brain^{49,50}, the activity itself can have direct impact on the axonal conduction through dependent plasticity in neural fibers, myelinated and non-myelinated alike⁵¹⁻⁵³.

Oligodendrocytes, the central nervous system's glial cells responsible for myelination, can myelinate between 10 and 30 axons each. These cells are crucial in the plasticity of axonal conduction within myelinated fibers and contribute to the subtle temporal regulation of neuronal activities. The white matter plasticity paradigm is supported by the alterations in speed and excitability of the axons, particularly within insulated ones; this paradigm is essential in higher and advanced cognition functions and learning⁵⁴.

Oligodendrocytes play a key role in regulating conduction speed by creating myelin sheaths around axons. Myelinated axon clusters situated beneath the cortex function as connecting cables for remote cortical areas, making oligodendrocytes crucial for information processing within the central nervous system (CNS)^{55,56}. Lately, there has been growing interest in oligodendrocyte precursor cells (OPCs), which possess the capacity to multiply and generate new oligodendrocytes in the adult brain⁵⁷. Additionally, OPCs can substitute or alter the circuitry through synapse-like structures across various brain regions⁵⁸. Neural activity governs OPC proliferation and differentiation, which subsequently impacts information processing by adjusting conduction speed. The initial description and classification of oligodendrocytes in four groups was made by Pio Del Rio-Hortega. He based his work on cell morphology and distribution⁵⁹. Oligodendrocytes' primary function is to produce myelin around axons, controlling conduction velocity in the CNS. Brain white matter is composed of myelinated axon bundles that serve as connectors for distant cortical areas, contributing significantly to information processing^{55,56}. Recent research has revealed that OPCs, such as NG2 cells, are mobile cells capable of proliferating and differentiating into oligodendrocytes within the mature brain⁶⁰. Furthermore, OPCs can form synaptic-like bonds adjacent or in contact with presynaptic terminals as part of neuronal circuits⁵⁸. Studies have shown that high-activity axons are preferentially myelinated, probably via distant, localized translation of MBP at the myelinating wraps. This is suggested to happen via interactions between oligodendrocytes and axons⁶¹.

Axonal excitability is primarily determined by two factors: the ion channel activity during the action potential generating process and maintaining the proper ionic equilibrium that make the action

potential transmission possible⁶². In myelinated axons, both nodal and internodal ion channels contribute to axonal excitability. The threshold current required for evoking an action potential is a common tool for measuring axonal excitability in all axons⁶³. Impaired axonal excitability can result in suboptimal axonal conduction, leading to altered action potential timing and impaired information processing. Various mechanisms regulate axonal excitability, including activity-dependent and neurotransmitter-mediated mechanisms. Temporary alterations in axonal excitability, including supernormal and subnormal activity states that occur in response to neuronal stimulation, can be detected in myelinated and unmyelinated axons within the CNS and PNS. Bucher and Goillard described the innate regulation of the recovery cycle in 2011. In parallel with the intrinsic processes, the neurotransmitters and neuromodulators themselves also directly affect the excitability of the axons by binding to the corresponding receptors that are found on the surface of the axon^{65,66}. Various neurotransmitter receptors, such as those for GABA, acetylcholine, adenosine, serotonin and glutamate were identified on axons, further away from either the AIS or the synaptic terminal^{51,64}.

When action potentials are initiated at a specific point on the axon, they set off a depolarization that spreads much like a domino effect. In unmyelinated axons, this propagation occurs continuously, whereas in myelinated axons, it takes place through saltatory conduction. To determine conduction velocity, which refers to the rate at which the electrical impulse travels along the axon, the distance covered by the signal is divided by the time taken to cover that distance. Various factors influence conduction velocity, such as the rate at which the membrane depolarizes and reaches the threshold, as well as the physical size of the various parts of the axon (the diameter and the length of an internode or the area of a node) and the electrical characteristics (the conductance of the axon, the capacitance and the conductance of a node) in myelinated fibers⁶⁵. As spike conduction is essential for communication between distinct brain regions, regulating conduction velocity is of paramount importance.

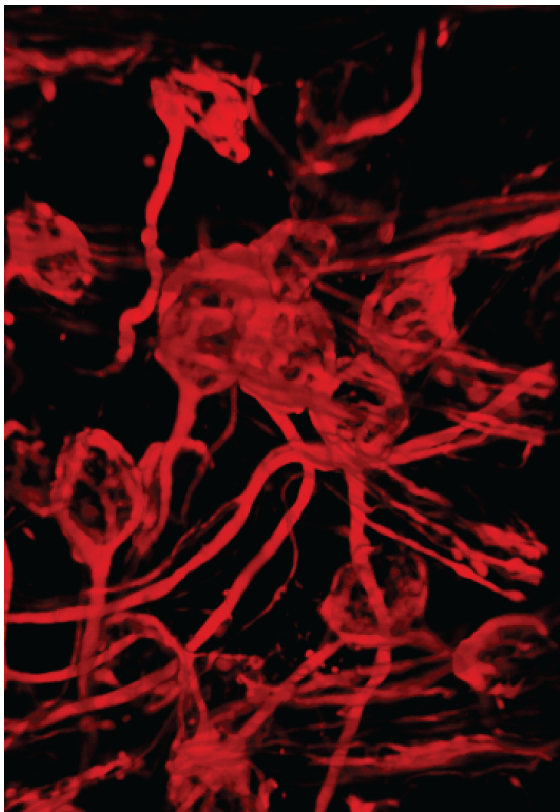
Conduction velocity can fluctuate based on the specific neural area involved. For example, in the spinal cord's sensory and motor pathways, maintaining a high conduction velocity is essential for the quick recognition of environmental stimuli and prompt motor reactions. In the auditory system, the accurate processing of sound source localization is accomplished via synchrony of the action potentials, not by having every cell firing at the highest possible speed⁶⁶. Additionally, conduction velocity, together with axon length, influences the conduction delay that coordinates the neuronal circuits timings of information exchanges and neuronal temporal coding⁶⁷.

For the avian brain, scientists have identified a disparity in conduction speeds for a fiber that splits in an ipsi- and contralateral parts. Notably, the contralateral axon branch exhibits a conduction velocity that is at least two times faster than that measured in the ipsilateral branch in the same neuron^{68,69}. This selective tuning of the velocity aids in surpassing the confinements dictated by axon length and makes the binaural coincidence detectors activity possible. Achieving appropriate conduction velocities is made possible through localized axon-glia interactions that dictate the internode length⁶⁶. Neuroactive substances can impact not only axonal excitability but also conduction velocity. Research by Chida et al.⁵² revealed that repetitive low-frequency stimulation led to a reduction of the conduction velocity in the hippocampus of rats for approximately 30 seconds. Although the inactivation of voltage-dependent Na⁺ channels might contribute to activity-dependent modulation of conduction velocity, the study also highlighted the involvement of kainate receptors on the length of the axonal surface. Repetitive axonal stimulation may result in excessive glutamate release, which then activates GluK1 glutamate receptors on neighboring axons. Moreover, increasing evidence show how glia release transmitters and modulators using different methods, and they could

these modulators and transmitters can also be released from the axonal body through vesicles or non-vesicular pathways⁷⁰⁻⁷³.

The synaptical terminal

As an action potential arrives at a neuron's terminal, it prompts the release of chemical compounds called neurotransmitters from the cell. These molecules are stored in synaptic vesicles, subcellular structures that gather at specialized release points known as active zones within axon terminals. In order to discharge the neurotransmitter into the synaptic cleft, vesicles approach and merge with the neuron's plasma membrane, leading them to rupture in a process referred to as exocytosis. Once released, the neurotransmitter acts as the neuron's graded output signal. The quantity of neurotransmitter emitted depends on the frequency and number of action potentials reaching the presynaptic terminals. The neurotransmitter then traverses the synaptic cleft and



connects with receptors on the postsynaptic neuron, creating a synaptic potential. Whether this potential is excitatory or inhibitory relies on the specific receptor in the postsynaptic cell, rather than the neurotransmitter itself. Moreover, identical neurotransmitter substances can elicit different responses at various receptors. The auditory pathway offers a remarkable model for examining synaptic transmission, known as the Calyx of Held.

Figure 2, Multiple examples of the Calyx of Held, from AG CKS

The distinct structure and substantial size of the Calyx of Held synapse are essential for conveying sound localization data through rapid and accurate synaptic transmission in the auditory system. Several changes in anatomy, morphology and physiology take place during when this structure is developing, and these transformations are vital to its functions later on. Its considerable size makes the calyx of Held an ideal place for performing presynaptic electrophysiology measurements that are inaccessible in other, smaller, regular synaptic boutons. This exceptional feature has offered invaluable insights into mechanisms of the central neuronal transmission, especially for its presynaptic part. We can take ion channels, the examination of presynaptic ion channels, neurotransmitter mechanisms, and plasticity as the fields that benefitted the most from studying the Calyx of Held.

Sound localization is a vital sensory function for many animals, depending on accurate and specialized neural networks. The calyx of Held synapse is among the various synapses with distinct properties that support this processing. Its morphological and electrophysiological features enable precise signal information transmission, drawing significant attention. The calyx of Held is made of the

distal part of a bushy cell neuron from the ventral cochlear nucleus that wraps around a single principle neuron in the medial nucleus of the trapezoid body (MNTB)^{74,75}. It experiences swift morphological and functional changes before hearing onset⁷⁶⁻⁷⁹, which occurs around postnatal day 12 (P12) in rats⁸⁰⁻⁸². These alterations guarantee rapid and reliable relay of sound localization data. Intriguingly, most developmental stages occur before hearing onset in mice, implying that inherent signaling mechanisms, rather than sensory activity, guide calyx synapse maturation^{76,83-85}. However, in mice, sensory activity may have a more significant influence the developmental process for calyx formation, and this suggests that each species' intrinsic influences of genetic- and activity-dependent elements are different^{86,87}.

This particular synapse operates in an axosomatic manner and is associated with swift and efficient synaptic transmission⁷⁴. The calyceal endzone has numerous active spots, which is precisely where neurotransmitter exchange takes place^{79,88}. When a VCN globular-bushy cell fires off a single action potential (AP), it can unleash a considerable number of synaptic vesicles that are filled with glutamate that drive fast and reliable stimulation of the target neuron from the MNTB⁸⁹. The strength and adaptability of this release mechanism are regulated through calcium influx. The number, composition, arrangement of the voltage gated calcium channels (VGCCs) that mediate the influx within the active zone have a direct impact on their function^{76,90-95}.

The calyx of Held possesses distinct structural and functional characteristics that, in conjunction with MNTB principal cell properties^{74,96}, makes the auditory information to be relayed with a very high degree of precision and accuracy towards the superior processing units⁹⁷. We can safely assume this network as fundamental to the auditory system.

The MNTB principal cell comes in contact with an unusually extended part of the upstream axon – creating a magnified synaptic terminal. The sheer size of the entire complex makes electrophysiology studies feasible in an otherwise inaccessible location – the presynaptic terminal. It is thus possible to measure calcium currents, vesicle releasing and reuptake mechanisms, and, if desired, simultaneous measurements in the principal cell of the MNTB⁹⁸⁻¹⁰². This unique situation of a giant synapse with a 1:1 input-target anatomical layout also makes calcium imaging and calcium dynamics studies possible for a single neuronal terminal¹⁰³⁻¹⁰⁶. Naturally, this also means that the Calyx of Held is suitable for studying vesicular mechanisms and molecules that manage exocytosis, like synaptotagmins¹⁰⁷⁻¹¹⁰ and the endocytosis that follows for retrieving molecules from the synaptic cleft^{101,111-115}.

The ventral cochlear nucleus (VCN) in adults contains globular bushy cells with large-diameter axons (2-3 microns in diameter¹¹⁶) that project to the MNTB on the contralateral side after passing the brainstem midline, and form the calyx-type synapses. The general rule is one principal neuron receives input from just one calyx, but there is some proof of multiple calyces converging to the same principal neuron as well^{76,117-119}. Additionally, there are both excitatory and inhibitory afferents to the MNTB neurons that come from unknown sources, with yet unelucidated functions^{76,119,120}. The inhibitory effect is thought to be generated in the ipsilateral cochlea and suffer significant changes during postnatal development¹²¹. The ventral nucleus of the trapezoid body (VNTB) was also shown to be a significant provider of glycinergic inhibition for MNTB¹²².

As the calyx of Held matures, both its morphology and physiological characteristics undergo modifications to ensure rapid and dependable synaptic transmission^{74,75}. During the initial and second postnatal weeks, the presynaptic action potential waveform becomes quicker and shorter, which decreases release probability and synaptic delays and allows the calyx to fire at high frequencies⁷⁸. These alterations are partly the result of voltage-gated Na and K channels changes during the early development stages, with higher channel density, faster K current activation as well as faster inactivation and recovery of sodium currents^{45,123,124}.

1.2 The auditory pathway

Sound is created through the vibration of an elastic medium, such as air, resulting in alternating compressions and rarefactions. In air, the process of sound propagation occurs at a speed of approximately 340m/s¹²⁵. In order to generate these pressure changes, the vibrating sound source must exert force on the conductive medium. The overarching role of the auditory system is to perceive, interpret and integrate the surrounding auditory landscape. In order to accomplish this, several components including the ear and subcortical and cortical auditory pathways with all their connections and implications having to work together¹²⁶.

Our ears are responsible for capturing the mechanical energy and transmitting it to the receptors, where it is processed into electrical signals that can be analyzed by neurons. These three functions are carried out by the external ear, middle ear, and inner ear, respectively¹²⁶.

The mammalian external ear is primarily comprised of the auricle, a cartilage cup-like structure on the lateral sides of the head. The auricle has several functions: similarly to a parabolic antenna it aids in collecting sound efficiently and focusing it into the ear canal, or external auditory meatus¹²⁷, and making use of sound features for sound source localization. This, in turn, leads to the eardrum or tympanum, with a varying dimension from species to species. The corrugated surface of the auricle is particularly adept at collecting sound from specific positions relative to the head and is thus not equally effective in capturing sound from all directions. Our ability to compute sound sources, particularly on the vertical axis, depends largely on the ability to focus sound that the external ear has¹²⁸.

The middle ear is a cavity that contains air, and is directly linked to the pharyngeal cavity through the Tube of Eustachio. The three ossicles (small bones) in the middle ear vibrate and conduct the sound from the tympanic membrane to the cochlea. A curiosity about them is that the first two are evolutionary remnants of reptilian ancestors, for whom they served as components of the jaw^{126,127}.

The inner ear is also called the cochlea and it has a coiled structure (that is approximately 9 mm in diameter in humans) and shaped like a snail's shell. A thin layer of laminar bone covers it the temporal bone (the hardest bone in the human body) surrounds it, for protection. The cochlea consists of three compartments that are filled with liquid, named *scalae*, with the *scala vestibuli* farthest from the base and the *scala tympani* nearest to the cochlear base and the *scala media*, which is positioned between the other ducts and is delimited by elastic structures, the basilar membrane and the Reissner's membrane. These structures play a crucial role in auditory transduction^{126,127,129}.

The cochlea of therian mammals is a distinctive feature not found in other vertebrates, including monotremes. While several hypotheses have been proposed about how the unique shape of the cochlea may enhance its function, none have been able to fully explain its origin, other than its ability to fit a long structure into a small space¹²⁷. The cochlea's evolution involved losing the vestibular lagenar macula and having an endolymph that is significantly less abundant in Ca²⁺. The configuration and dimensions of the cochlea in different species are influenced by a range of factors, including the creature's size, way of life, sound pinpointing, interaction, and echolocation abilities. Before the development of the spiral cochlea, bone had permeated the organ of Corti's soft tissues, and the emerging laminae probably offered improved mechanical compatibility with the mammalian middle ear, ultimately resulting in high-frequency hearing. Simultaneously, the protein prestin evolved,

acquiring high-frequency amplification capacities that were later independently enhanced in bats and toothed whales¹²⁶.

Auditory nerve fibers exit the cochlea and merge with the vestibulocochlear nerve, thus forming the eighth cranial nerve. This enters the brain and the auditory fibers relay in the cochlear nucleus, which is made of the following parts: the anteroventral cochlear nucleus (AVCN), the posteroventral cochlear nucleus (PVCN) and the dorsal cochlear nucleus (DCN). The fibers split into two branches: the ascending part towards the AVCN and the descending part towards the PVCN initially and terminates in the DCN. In each of the three CN subdivisions, the nerve fiber branches establish a multitude of connections with diverse neuron types that vary in their anatomical position, structure, cellular functioning, synaptic inputs, and their properties related to time and frequency responses^{126,130,131}.

For instance, the AVCN has spherical and globular bushy cells that form strong excitatory synapses from the auditory nerve, known as Endbulbs of Held¹⁵. The bushy cells display primary-like responses, meaning their firing patterns in response to sound are almost the same as the auditory nerve fibers' that drive them, preserving temporal firing pattern information. Another type of neuron found in the AVCN and PVCN are the stellate cells, which receive inputs from several auditory nerve fibers and other neuron types¹³². They exhibit rhythmic bursts as responses to pure tone stimuli (chopper), but are unrelated to the tone stimulus frequency. They might not maintain the precise timing of incoming spikes; however, they exhibit more refined frequency selectivity and potentially a broader dynamic scope. This makes them more apt for encoding the spectral structure of incoming signals¹³³.

The posteroventral cochlear nucleus cells fire a single AP at the beginning of a pure-tone that is presented. They are called onset cells and can come in different flavors: stellate or octopus cells. These cells receive inputs from more than one auditory fiber, making them have a broad frequency tuning. Even if they have very low latency jitter (10s of microseconds), their purpose is not solely to mark the beginning of a sound. When stimulated with complex tones, such as two tones played together, onset cells mark every beat with an action potential, not just the beginning of the complex tone. Therefore, these cells process and offer more information about the complex tones' temporal properties, not just about the onset^{128,131,133,134}.

By contrast, DCN cells have more complex response patterns (pauser-type) and can be either fusiform or pyramidal in shape. They can be inhibited by some frequencies and excited by others, indicating a role in detecting spectral contrasts. Additionally, the DCN receives somatosensory input from the skin or the outer ear, making their processing even more complex. While cells in the ventral cochlear nucleus (VCN) process the sounds' temporal properties, cells in the DCN deal with spectral contrast detection^{132,135}.

Experts on cochlear nucleus cell physiology further categorize the cells into such as chopper-transients, onset-lockers, or primary-like with notch, although this is beyond the scope of this thesis.

The primary cell types of the cochlear nucleus project to various locations within the auditory pathway. Eventually, all signals from the CN arrive at the midbrain's primary auditory processing center, the IC. Although the majority of stellate and dorsal cochlear nucleus cells project straight in the inferior colliculus, the projections coming from the anteroventral cochlear nucleus bushy cells go via the brainstem's superior olivary complex (SOC). The olivary nuclei contribute to our spatial perception of sound by converging information from both ears. The complex is a cluster of nuclei located in the mammalian brainstem that plays a critical role in sound localization in the horizontal

plane. It is mainly composed of the medial nucleus of the trapezoid body (MNTB), medial superior olive (MSO), lateral superior olive (LSO), the superior paraolivary nucleus (SPN) and the lateral lemniscus nuclei¹³⁴. Globular bushy cells of the VCN project to the MNTB, which converts an excitatory input to an inhibitory, glycinergic output targeting all the other nuclei of the SOC- MSO, LSO, SPN, VNLL¹³⁶. Spherical bushy cells provide excitatory input to the ipsilateral LSO and bilateral MSO, while octopus cells go contralaterally to the neurons of the contralateral VNLL and the SPN. Some further smaller structures like the lateral and the ventral nuclei of the trapezoid body and several periolivary nuclei complete the organization of the superior olivary complex in mammals¹³⁵⁻¹³⁷.

The superior olivary complex is an evolutionary outcome of the need to process information about the auditory environment with enough precision and reliability¹³⁸ and now plays a prominent role in auditory processing through two pathways that process horizontal sound source localization. The MSO processes interaural time differences (ITDs) and the LSO encodes interaural level differences (ILDs). According to the duplex theory, the low-frequency sounds are used for ITDs and high-frequency sounds are used for computing ILDs in mammals¹³⁹.

The MNTB provides necessary fast glycinergic input for ITD and ILD computations^{10,12}. The SPN, although the main target of MNTB inhibition in the auditory brainstem, has not been implicated in contributing to sound localization, but rather to the encoding of sounds rhythms, gaps and temporal edges¹⁴⁰⁻¹⁴².

Axonal projections from the cochlear and SOC nuclei course through the lateral lemniscus fiber tract towards the inferior colliculus (IC), potentially emitting collateral branches to the nuclei in the lateral lemniscus. These ascending fibers are almost always crossed, so that the regions in the inferior colliculi and the auditory cortices and thalami respond more robustly to sounds coming from the opposite ear¹⁴³.

The inferior colliculus structure is intricate, with a commissure connecting the right and left colliculi, which facilitates additional binaural interplay in the ascending auditory pathway. ICs contain many interneurons, which likely perform various operations that are just beginning to be understood¹⁴⁴⁻¹⁴⁷. The inferior colliculus is further split in subnuclei, with the most prominent being the central nucleus (ICC). It gets most of its inputs from the brainstem and one of the adjacent structures, the nBIC, projects to the superior colliculus (SC), a gaze control center, to facilitate eye and head movements towards novel sounds^{135,148}. The majority axons leaving the IC nuclei go through the brachium fiber bundle reaching the medial geniculate body, which is the principal relay for the auditory pathway in the thalamus. The MGB is also subdivided into ventral, dorsal, and medial nuclei¹³⁵. Notably, most auditory nuclei have a tonotopic organization, including the CN, SOC, NLL, ICC, vMGB, with neurons being anatomically arranged according to their characteristic frequency, with the exceptions of lateral, dorsal and brachium nuclei of the IC. Structures in the auditory midbrain that display a tonotopic organization are known as "lemniscal," whereas those that do not are referred to as "nonlemniscal."^{135,136,143,148,149}

Most of the fibers coming from the thalamus travel towards the temporal lobes, and reach the auditory cortex on each side. This is not exhaustive, as some MGB fibers project to the limbic system, which is considered responsible for the affective part of the overall response to sound. The auditory cortical fields on both sides are connected via the corpus callosum, by commissural connections. This allows for bidirectional informational transfer among the right and left hemispheres. In the auditory cortex, stimuli delivered to either ear can influence the discharge patterns of nearly all acoustically responsive neurons^{131,133-135}.

The auditory cortex is divided into various fields, some of which exhibit clear tonotopic organization while others do not. These fields are differentiated not only by their tonotopy but also by their anatomical connectivity patterns, physiological characteristics of their neurons, and the presence of specific cell markers such as parvalbumin^{150,151}. Up to the thalamic level, the ascending auditory pathway appears to be relatively consistent across mammalian species, with some variations such as the large intermediate NLL in rats and well-developed LSO in cats. However, the auditory cortical fields are organized differently across species, particularly in higher-order areas, leading to different names being used to describe them. Therefore, while subcortical auditory structures have similar anatomical structures across species, the naming of cortical fields may vary considerably. For instance, two primary cortex areas are present in carnivores and primates, they are situated next to each other and receive significant input from the thalamus¹⁵². However, while in carnivores these are called the primary auditory cortex (A1) and the anterior auditory field (AAF)¹⁵³, in monkeys they are known as A1 and R¹⁵⁴, but we do not know how comparable they truly are. The posterior auditory field in cats also bears certain resemblances to the CL and CM areas in monkeys, however we do not know about other species¹⁵⁵. Because the cortex is the youngest and most prone to adaptation section of the brain, it could exhibit fundamental particularities for different species. For example, echolocating bats have several specialized areas in their auditory cortex for processing echo delays and Doppler shifts^{156,157} that do not have an apparent counterpart in the monkey brain. For all mammals though, the auditory cortex has a primary area, surrounded by a second-order belt. They are responsible for communicating with other advanced cognitive structures, such as the site of short term memory and action planning, the prefrontal lobe, or the infratemporal structures that process object recognition^{158,159}. As far as we know, we wouldn't be able to recognize the sound of a Formula 1 V10 engine or recall the beginning of a spoken sentence when it ends without the involvement of these high-level cortical areas. Hence, they are also essential components of the auditory brain.

A significant number of neurons also convey information in the reverse direction (top-down or efferent), starting from the frontal cortex and moving towards the auditory cortex, and then from the auditory cortex to every station in the midbrain and thalamus, particularly the medial geniculate body and the inferior colliculus^{135,143,148,149}, but also the NLL, SOC, and CN^{131,136,143}. Following this, the information is transmitted backwards, with fibers reaching from the superior olivary complex all the way to the OHCs or IHCs. This disposition shows how auditory processing involves and requires not only feedforward but also feedback circuits at various stages, allowing the system to adapt to the unique requirements of diverse environments or circumstances¹³⁴.

1.3 Potassium channels

The neuronal excitability and signal transmission are key requirements for the proper functioning of the auditory pathway described in the previous chapter, and the neurons possess an extended machinery for achieving this. An important part of it is represented by the voltage-gated potassium channels (Kv). These channels are transmembrane proteins that enable potassium ions to pass through the cellular membrane when the membrane potential changes. Their activity is important for gauging the resting membrane potential, for action potential shaping – and consequently the firing frequencies and patterns.

Groundbreaking work in this field was first done by Hodgkin and Huxley in 1952¹⁶⁰, and they identified the basis of action potential depolarization: the delayed rectifying potassium currents, but the plethora of variants and the complexities of potassium channels were not known or even suspected at that time. We know now of about 40 subunit genes in 12 families that contribute to the assembly and formation of a wide variety of Kv channels, each with their distinct properties and functions¹⁶¹.

A functional potassium channel is usually made of four α subunits, that could be complemented by β subunits or other accessory proteins. The subunits can assemble in various combinations for achieving channels with unique properties. The selective permeability for K⁺ ions is achieved through the pore region, which, from a structural point of view, is highly conserved among the variants of Kv; this feature is combined with functional diversity that is enabled by other structural variations of the channels¹⁶².

The potassium channels classification shows several families that are based on the sequence homology and the functional characteristics. The major voltage-gated (Kv) potassium channel families that are involved in neural excitability are the Kv1 (Shaker), Kv2 (Shab), Kv3 (Shaw), and Kv4 (Shal). Each of these has their own distinct activation/inactivation kinetics, that makes them suitable for different roles in neuronal functioning¹⁶³.

The auditory brainstem (that was presented in the previous chapter) is an excellent model for studying the physiological roles of Kv channels in neurons. In the context of processing information for sound localization tasks, the medial nucleus of the trapezoid body (MNTB) receives excitatory input from the cochlear nucleus and projects inhibitory output towards several other nuclei – the medial and lateral superior olives, the superior paraolivary nucleus and the nuclei of the lateral lemniscus. The potassium channels that are involved in this circuitry can be classified as either fast or slow in terms of activation and inactivation kinetics or high- or low-voltage-activated⁹⁷.

The fast potassium channels are the Kv1 and Kv3. Kv1s are low-voltage-activated, so they begin activating at relatively low depolarizations. They exhibit fast activation, but not as fast as the Kv3 variants. Their function is to establish the AP firing threshold and to control the excitability of the neuron. Their role is to ensure one-to-one fidelity in synaptic transmission, by preventing multiple action potentials to form as a response to a single excitatory input due to their slow inactivation kinetics. This maintains precise timing and reduces temporal jitter¹⁶⁴. The Kv3 channels on the other hand are high-voltage-activated, thus requiring a significant depolarization for their activation, which occurs during the action potentials. The fast kinetics make them essential for the fast repolarization of the AP, which in turn is a requirement for high-frequency firing rates with minimal jitter^{164,165}.

The more slowly activating potassium channels are the Kv2 and Kv4. Kv2 channels are also high-voltage-activated units, but they have slower kinetics. Once they are activated, they remain open

for longer and thus contribute to the stabilization of the membrane potential during high-frequency firing. In the MNTB, Kv2.2 channels help to hyperpolarize the membrane potential between action potentials, a critical requirement for maintaining the sodium channels availability for future APs¹⁶⁶. Kv4 channels are low-voltage-activated, similar to Kv1, and they generate transient potassium currents, known as A-type currents. Their kinetics require prior hyperpolarization to remove the steady-state inactivation before they can activate once more. The Kv4 channels influence the neuronal excitability by modulating the number of action potentials during depolarization or excitatory postsynaptic potentials¹⁶⁷.

Ion channel functioning is important for understanding the various types of synapses in the brain, each with their characteristics and roles. For the auditory brainstem, the potassium channels play an important role, with Kv3.1 and Kv3.3 being crucial for proper physiological functioning. Part of the work for my thesis was to gain more insights on the role of Kv3.3 subunits in synaptic transmission in a model auditory synapse, the Calyx of Held.

1.4 Semantics, adaptation & (en)coding



As with almost every aspect of reality, the devil is in the details. To ensure an accurate portrayal of a notion, one must pay attention to the way information is conveyed. For humans (and not only!), semantics is of utmost importance. The word “semantics” comes from Ancient Greek (*sēmantikós*, "significant") and it refers to the study of meaning or truth. Even in academic environments, it can often happen, without intent, to use terms in the wrong way; This can lead to confusion and ultimately to more time and energy spent clarifying, rather than tackling a certain subject of interest. To prevent this, I will discuss in this section some of the relevant terms for this work.

Salvador Dalí, A Logician Devil, part of the Divine Comedy series. 1963

Coding & encoding

There can often be confusion surrounding the terminology used in neuroscience, particularly when discussing "coding" and "encoding." To help clarify these terms, Theunissen and Miller provided comprehensive definitions and outlined their significance in their study¹⁶⁸. Two primary encoding approaches exist: Rate encoding, where the conveyed information relates solely to the average spike count within the encoding time frame or any weighted average throughout that period, and Temporal encoding, in which extra information is associated with certain aspects of the spike pattern's timing within the encoding window. Temporal coding, on the other hand, is characterized as the application of rate or temporal encoding techniques to represent a fluctuating sensory signal. This approach establishes a direct connection between the moment a sensory event occurs and the corresponding neural response's timing. In simpler terms, temporal encoding uses time as the syllabus for transmitting information, while temporal coding represents the way time is depicted – through encoding – in neural codes.

Adaptation

When we come across the notion of “adapting”, we are referring to a biology-specific process, in which an organism becomes fitter to its environment. It is one of the evolutionary biology concepts, alongside natural selection, inclusive fitness, progress and decent¹⁶⁹. Although adaptation is mainly a process rather than a feature, for practical reasons, it refers to end results: the features that result from the process. If one desires to set apart the two notions, they can use the term “adaptive trait” for the product (i.e. function or bodily part) and “adaptation” for the process¹⁷⁰⁻¹⁷². Biologist Theodosius Dobzhansky gives the following definitions for adaptation:

1. Adaptation is the evolutionary process whereby an organism becomes better able to live in its habitat or habitats¹⁷³.
2. Adaptedness is the state of being adapted: the degree to which an organism is able to live and reproduce in a given set of habitats¹⁷⁴
3. An *adaptive trait* is an aspect of the developmental pattern of the organism, which enables or enhances the probability of that organism surviving and reproducing¹⁷⁵.

For adaptation to be feasible, it must happen in an organism that is viable while evolving and developing. This puts certain requirements on the process, the main being that any genetic or phenotypic change must be relatively small, due to the sheer size, complexity and intertwining of the developmental systems. This view has been much debated, as “relatively small” could mean rather large genetic changes as well – the polyploidy in plants¹⁷⁶.

The sets of adaptive traits keep the organisms alive in their ecological niches. These could refer to structure, behaviour or physiology. By structure we mean the bodily traits, such as size, covering, etc, while behavioural adaptive traits can be passed on specifically, like instincts, or as the inherited ability to learn. A few examples are foraging, sexual behaviours and vocalized communication. The physiological adaptive traits make specialized tasks possible: secreting certain substances, -tropisms, while also encompassing broader aspects, like body development, maturation, homeostasis (i.e. ionic balance, temperature regulation).

One must keep in mind that similar concepts to adaptation exist and they could be wrongly inter-used. Adaptation is different from learning, acclimatization and flexibility. These are changes, which are not inherited. Learning means a better behavioural performance output, acclimatization is an automatic adjustment in physiology and flexibility is the organism’s capacity to survive various environments; all of these happen during the life span of an individual (also in the physiological range!). To better illustrate the difference and link between adaptation and other terms, we can think about the situation in which a person moves to a high-altitude environment: their breathing and fitness are no longer optimal, but if they spend enough time in that environment, *acclimatization* to lowered oxygen pressures occurs, for example through an increased red blood cell production. The adaptation product is the ability to acclimatize, not the acclimatization. Some humans would have their reproductive rates decline, and they will contribute less to the later generations. In time, and by gradual natural selection, all individuals will become adapted to the new environment; it was very elegantly shown by observing the performance of high-altitude long-term communities compared to the performance of newcomers, despite them having time to acclimatize¹⁷⁷.

We must not forget about the trade-offs of this process: the adaptive traits can be destructive on other aspects of life – ostriches can run very fast, but are unable to fly, mammals hair can help temperature regulation, but provide a niche for parasites. The overarching goal is compromising, not

perfection – “It is a profound truth that Nature does not know best; that genetical evolution... is a story of waste, makeshift, compromise and blunder.”¹⁷⁸ and “Since the phenotype as a whole is the target of selection, it is impossible to improve simultaneously all aspects of the phenotype to the same degree”¹⁶⁹.

Time and the brain

According to physics, our universe has a minimum of four dimensions: three spatial dimensions and one temporal dimension. Relativity theory proposes that these dimensions are merged into a continuum, with invariants that are neither purely spatial nor purely temporal, but rather spatiotemporal measures that combine spatial and temporal coordinates (spacetime intervals). Conversely, biology reveals that space and time are experienced differently; while most of our sensory organs can directly perceive spatial distances, there is no evidence of direct sensory perception of time.

These two fields of study examine the relationship between observers and the observed from complementary perspectives. Physics focuses on the observed, while biology examines the observer. It is intriguing that physics treats space and time as nearly equivalent dimensions, whereas biology identifies fundamental differences in how biological observers perceive space and time. Therefore, a complete understanding of the observer-observed relationship regarding spacetime requires an understanding of how biological agents perceive time.

The brain constructs the perception of time without relying on dedicated receptors, unlike the direct links between spatial perception and sensory organization. Although temporal relationships can aid spatial perception, the reverse is not necessarily true. Despite this asymmetry, our abstract description of spacetime does not differentiate between temporal and spatial dimensions. A rather recent study suggests that the perception of "filled" intervals, marked by enduring events, differs from "empty" intervals, marked by isolated events¹⁷⁹.

Although the sensory organs do not function like a camera, which is based on capturing a rapid succession of still images, the brains still need to resolve temporal features of the incoming stimuli, no matter the modality. Due to the nature of our input requirements, the resolution can be either high or low. For a fair perspective, we can take smell, vision and hearing for comparison: Smell, being a chemical-based process, is on the lower side of the temporal resolution spectrum, with mice being able to achieve an up to ~40 Hz odour structure discrimination rate¹⁸⁰. The peak temporal resolution of vision, for example, is ~129 Hz for the peregrine falcon, a raptor bird that tracks fast-moving and maneuverable prey¹⁸¹, while for mice it is 15 Hz at best¹⁸². With hearing, the temporal resolution can be defined as how many changes in the perceived sound can happen each second and that rounds up to ~500 Hz, measured through gap detection thresholds^{183,184}.

The particularity of sound is the inherent nature of it: an oscillating value of the pressure in a conducting medium. The oscillation values simply translate to sound frequency, and an organism has two cutoff values, a low one and a high one, with the hearing range in between. In vertebrates, it can be from 16 Hz to more than 100 kHz, with many animals having several orders of magnitude wide capabilities (human 20Hz-19kHz, ferret 16 Hz-44kHz, mouse 900Hz-79kHz, porpoise 75Hz-150kHz). Although the thought of any kind of neuronal receptor directly being capable of picking up a mechanical oscillation of hundreds of thousands of cycles per second is appealing and exotic, the

reality is slightly different: the sound transduction is highly dependent of the intrinsic mechanical properties of a membrane with which hair cells interact (basilar membrane). Interestingly enough, there is a 1-to-1 action signal generation up until $\sim 1-2$ kHz, in which mechanical-gated ion channels in the hair cells are able to keep up with the oscillations themselves. This phenomenon is called phase locking. For the rest of the frequencies, the hair cells rely on the highly localized oscillation properties of the corresponding part of the basilar membrane.

1.5 Motivation & objectives of the thesis

The importance of neuronal adaptive traits for fast and accurate information transmission is best highlighted in the auditory system. Having a plethora of mechanisms which enable it in the mammalian brain, as illustrated in the introduction section of this thesis, could put someone in difficulty when choosing their work angle if they wanted to further the knowledge in this field. However, previous work of our department and our lab on activity modulation of myelination¹⁸⁵ provided a valuable hint for my starting point. The aim of refining the insights on the contributions of myelin to individual sets of conditions had started to take shape and was clearly defined by the accepted grant proposal of my PI, Conny Kopp-Scheinflug. Additionally, through a collaboration with Ian Forsythe's group, we also aimed at looking at how potassium channels influence the same timing accuracy in the auditory pathway.

From there, we were happy to have our objectives established:

- To assess whether physiological (non-pathological) monaural sensory alterations could be a working model for influencing the normal auditory function and establish it as our working paradigm.
- To measure electrophysiological changes induced by our paradigm
- To describe the anatomy of myelinated fibers in the auditory system, in the context of monaural sensory alteration.
- To investigate *in vivo* electrophysiological characteristics of Kv3.3 potassium channels.

2. Chapter 2 – Myelin



Ambient sound stimulation tunes axonal conduction velocity by regulating radial growth of myelin on an individual, axon-by-axon basis

Mihai Stancu^{a,b,c} , Hilde Wohlfrom^a, Martin Heß^a , Benedikt Grothe^{a,b} , Christian Leibold^{a,d} , and Conny Kopp-Scheinflug^{a,1}

Edited by Michael Shadlen, Columbia University, New York, NY; received September 22, 2023; accepted January 31, 2024

Adaptive myelination is the emerging concept of tuning axonal conduction velocity to the activity within specific neural circuits over time. Sound processing circuits exhibit structural and functional specifications to process signals with microsecond precision: a time scale that is amenable to adjustment in length and thickness of myelin. Increasing activity of auditory axons by introducing sound-evoked responses during postnatal development enhances myelin thickness, while sensory deprivation prevents such radial growth during development. When deprivation occurs during adulthood, myelin thickness was reduced. However, it is unclear whether sensory stimulation adjusts myelination in a global fashion (whole fiber bundles) or whether such adaptation occurs at the level of individual fibers. Using temporary monaural deprivation in mice provided an internal control for a) differentially tracing structural changes in active and deprived fibers and b) for monitoring neural activity in response to acoustic stimulation of the control and the deprived ear within the same animal. The data show that sound-evoked activity increased the number of myelin layers around individual active axons, even when located in mixed bundles of active and deprived fibers. Thicker myelination correlated with faster axonal conduction velocity and caused shorter auditory brainstem response wave VI-I delays, providing a physiologically relevant readout. The lack of global compensation emphasizes the importance of balanced sensory experience in both ears throughout the lifespan of an individual.

white matter | axonal conduction | sensory deprivation | myelination | hearing

The development of a bony skull combined with increased brain size during the evolution of the vertebrate nervous system required faster axonal conduction velocities than can be achieved by a simple increase in axon diameter. The role of myelin in supporting such an increase in conduction velocity was originally understood simply as a static physical insulator acting to increase resistance and reduce the time scale of membrane uncharging. However, myelinated axons are highly plastic, shaping firing rates, conduction velocity, and reducing energy consumption of axonal conduction (1, 2). Thus, myelination is now considered an integral part of neuronal processing in the vertebrate brain, but the mechanisms underlying activity-dependent myelination are still elusive.

The function of myelin in sensory processing, cognition, and demyelinating neurological disorders is predominantly addressed by structural analysis of myelination patterns created by the specific sequence of nodes and internodes, as well as by the thickness of the myelin sheaths with respect to axon diameter. While the longitudinal pattern of myelin along axons is defined by neuronal identity (3, 4) and as such, optimizes the network behavior (5, 6), myelin thickness is generally defined by the canonical “g-ratio” (axon diameter/fiber diameter) with species-specific variations between 0.6 and 0.8 (7, 8). However, both myelin thickness and g-ratio change with axonal activity. Increased axonal firing rates following sensory maturation, skill learning, or social engagement (9–11) cause thicker myelination of the involved axons, while sensory or social deprivation results in thinner myelin sheaths (11–13). The mechanisms by which axonal activity levels are communicated to myelinating oligodendrocytes and what degree of change in myelin thickness is required to achieve a physiological objective are still largely unknown.

During development, increased neural activity regulates myelination (14, 15) via the release of soluble axonal factors such as adenosine (16), GABA (17) or glutamate (18), which subsequently lead to calcium-transients in nearby myelin sheaths and in the somata of myelinating oligodendrocytes. This calcium increase triggers enhanced myelination of active axons. Later in development, when myelin sheaths have already formed around their axon, activity-dependent calcium-transients were only observed in the myelin sheaths, but not in the oligodendrocyte somata (19). Therefore, once most parts of the axon are myelinated and vesicle secretion becomes restricted to the synaptic terminal, axon-glia communication needs to take a different form.

Significance

Myelin ensures fast and reliable conduction of action potentials along axons. Once myelin in the central nervous system is lost due to disease, injury, or aging, remyelination efforts by proliferating oligodendrocyte precursor cells occur, but often remain incomplete. Therefore, reaching and maintaining optimal myelination through sensory or social experience forms a crucial equilibrium. Using the auditory system as a model, the present work shows that activity-dependent myelination occurs at the level of individual axons and that activity in one input channel, i.e., one ear, contributes to proper myelination of activated axons. However, activity in one input channel cannot compensate for activity deficits in another, thereby causing imbalanced myelination and mismatched auditory temporal processing.

Author affiliations: ^aDivision of Neurobiology, Faculty of Biology, Ludwig-Maximilians-University Munich, Planegg-Martinsried 82152, Germany; ^bMunich Cluster for Systems Neurology, Munich 81377, Germany; ^cGraduate School of Systemic Neurosciences, Planegg-Martinsried 82152, Germany; and ^dFaculty of Biology, Bernstein Center Freiburg, BrainLinks-BrainTools, University of Freiburg, Freiburg im Breisgau 79110, Germany

Author contributions: C.K.-S. designed research; M.S., H.W., M.H., C.L., and C.K.-S. performed research; M.S., C.L., and C.K.-S. analyzed data; and M.S., B.G., C.L., and C.K.-S. wrote the paper.

The authors declare no competing interest.

This article is a PNAS Direct Submission.

Copyright © 2024 the Author(s). Published by PNAS. This article is distributed under Creative Commons Attribution-NonCommercial-NoDerivatives License 4.0 (CC BY-NC-ND).

¹To whom correspondence may be addressed. Email: cks@bio.lmu.de.

Published March 5, 2024.

Release of ATP, GABA, or glutamate from synaptic terminals or the nodes of Ranvier requires a form of volume transmission to reach their receptors on the oligodendrocyte somata. While such nonspecific mechanisms would be suitable for homogenous fiber tracts where all axons that are myelinated by the same oligodendrocyte are equally active, little is known about whether adaptive myelination can occur at the level of individual axons, particularly within heterogeneous fiber tracts (20). This gap in knowledge most likely arises from the fact that axons within a fiber tract often originate from neurons of similar class-specific genetic identity, which attracts the same subpopulation of myelinating oligodendrocytes (21), conveys similar activity levels and dictates projections to similar targets. Together, this complicates the use of genetic markers for pharmaco- or optogenetics as well as input-specific neural activation. One recent study, using elegant pharmacogenetics, showed that individual active axons within a fiber tract will be preferentially myelinated during development, suggesting local axo-glia communication (22).

Here, we take advantage of the auditory system, which allows differential sensory stimulation of left- and right-side neural circuits. Two monaural fiber tracts were targeted: 1) the auditory nerve, formed by axons of spiral ganglion neurons, and 2) the trapezoid body (TB), formed by axons of globular bushy cells (GBC) which cross the midline and project to nuclei on the opposite side of the brainstem (5, 6, 11). Afferent auditory nerve fibers of the spiral ganglion neurons only contain axons arising from the same ear; however, within the TB, each bundle could contain fibers crossing in one direction only or it could contain a mixture of fibers originating from both sides of the head. An answer to this dilemma will further our understanding of how oligodendrocytes regulate myelination in two ways. First, if all fibers in a bundle arise from the same ear and possess similar activity levels, soluble factors released by active axons and distributed via volume transmission will likely reach oligodendrocyte somata and regulate myelination globally for all axons within the same bundle. Second, if axons within a bundle arise from different ears and possess different activity levels, a differential, local axon-by-axon regulation of myelin might be needed.

Neuronal firing in the auditory pathway consists of spontaneous activity and sound-evoked activity, the latter only starting at about P10 in mice. A mild and reversible (11) sensory deprivation approach was used by raising mice with monaural earplugs between P10 and P20. This allows the degree of myelination of individual axons within mixed-activity fiber bundles to be measured, while additionally creating an internal control by the nonplugged ear to assess the physiological significance of adaptive myelination.

Results

Sagittal brainstem sections show that TB fibers are organized in bundles, isolated from each other by perpendicularly arranged pyramidal tract fibers (Fig. 1C). To test the composition of TB fiber bundles, anterograde tracers of different colors (tetramethylrhodamine and biocytin) were injected into the cochlear nucleus of the control and the deprived ear (Fig. 1A). Coronal brainstem sections show that both tracers labeled TB fibers, approaching and crossing the midline from either side of the brain (Fig. 1B). Many of the fibers form giant calyx synapses upon targeting the medial nucleus of the trapezoid body (MNTB). In addition, some cell bodies are retrogradely labeled, consistent with an efferent projection of the MNTB to the ipsilateral cochlear nucleus (23). Coronal sections were counterstained with CC1, a marker commonly used for detecting mature oligodendrocytes (24). An 800- μm \times 400- μm region of interest was defined left

and right of the midline in coronal sections and the number of CC1-positive cells was counted. The side receiving active input contained 778 ± 57 oligodendrocytes/ mm^2 ($n = 3$ mice), which was not significantly different from the deprived side with 751 ± 77 oligodendrocytes/ mm^2 ($n = 3$ mice; paired t test: $P = 0.174$). There were no signs of membrane blebbing or nuclear fragmentation in the CC1-positive cells on either side, suggesting that the deprivation did not cause oligodendrocyte death (Fig. 1B, Inset).

Sagittal sections were taken at three positions: near the midline, ~ 200 μm lateral to the midline and ~ 600 μm lateral to the midline and the two colors of the tracers were then used to identify control or deprived fibers (Fig. 1D and E). Inspection of eleven monaurally deprived, bilaterally traced brains revealed active and deprived fibers to form interspersed, salt-and-pepper like patterns within each fiber bundle (Fig. 1D). Counterstaining with antibodies against myelin basic protein (MBP) showed that not all TB fibers were traced via the cochlear nucleus injections (Fig. 1E). Based on the circular MBP labeling, axon diameter and myelin thickness were assessed by fitting two ellipses to each axon as previously described (11). To minimize bias, all axon and myelin measures were taken from monochromatic images showing only the MBP staining. Each axon was numbered so that it could be identified as active, deprived, or nonlabeled upon overlaying the tracing colors. Since nonlabeled fibers could potentially originate from the active or deprived side, they were disregarded for further analysis.

In agreement with Sinclair et al. (11), auditory deprivation instigated fewer large-caliber axons in the trapezoid body, particularly at locations further away from the midline (Fig. 1F). GBC axons undergo an increase in axon diameter as they approach the calyx synapse in the MNTB (6, 11). Sagittal sections taken at ~ 200 μm and ~ 600 μm from the midline at either side, include the MNTB and therefore contain axons that are close to forming calyx synapses. Our data revealed more large-caliber axons in the 200- μm and 600- μm sections for the control fibers, but not for the deprived fibers, resulting in significantly decreased overall axon diameters. Sagittal sections near the midline did not show a difference in axon diameter (near midline_{control}: 1.30 ± 0.45 μm vs. near midline_{deprived}: 1.29 ± 0.50 μm , $P \geq 1.000$; 200 μm _{control}: 1.61 ± 0.59 μm vs. 200 μm _{deprived}: 1.37 ± 0.39 μm , $P \leq 0.001$; 600 μm _{control}: 1.73 ± 0.86 μm vs. 600 μm _{deprived}: 1.27 ± 0.54 μm , $P \leq 0.001$; $n = 1,565$ fibers; 11 mice; one-way repeated measures ANOVA followed by the Bonferroni t test; Fig. 1F). In addition to the changes in axon diameter, the present data show significantly thicker myelin in control compared to deprived fibers at all three locations (near midline_{control}: 0.61 ± 0.19 μm vs. near midline_{deprived}: 0.52 ± 0.16 μm , $P \leq 0.001$; 200 μm _{control}: 1.04 ± 0.26 μm vs. 200 μm _{deprived}: 0.95 ± 0.16 μm , $P \leq 0.001$; 600 μm _{control}: 1.04 ± 0.24 μm vs. 600 μm _{deprived}: 0.87 ± 0.17 μm , $P \leq 0.001$; $n = 1,565$ fibers; 11 mice; one-way repeated measures ANOVA followed by the Bonferroni t test; Fig. 1G). Similar statistical results were achieved when differences in axon diameter and myelin thickness were analyzed within animals (gray lines in Fig. 1F and G) or within fiber bundles (black lines in Fig. 1F and G). The within bundle analysis was restricted to bundles containing more than 10 traced fibers of both colors to ensure statistical power (axon diameter_{control}: 1.43 ± 0.23 μm , axon diameter_{deprived}: 1.23 ± 0.18 μm , paired t test: $P = 0.002$; myelin_{control}: 0.95 ± 0.10 μm , myelin_{deprived}: 0.87 ± 0.08 μm , paired t test: $P = 0.005$). Together, these data suggest that activity-dependent adaptive myelination occurs on an individual fiber basis, even when they arise from neurons of an identical cell type, possessing the same target and run within the same fiber bundle.

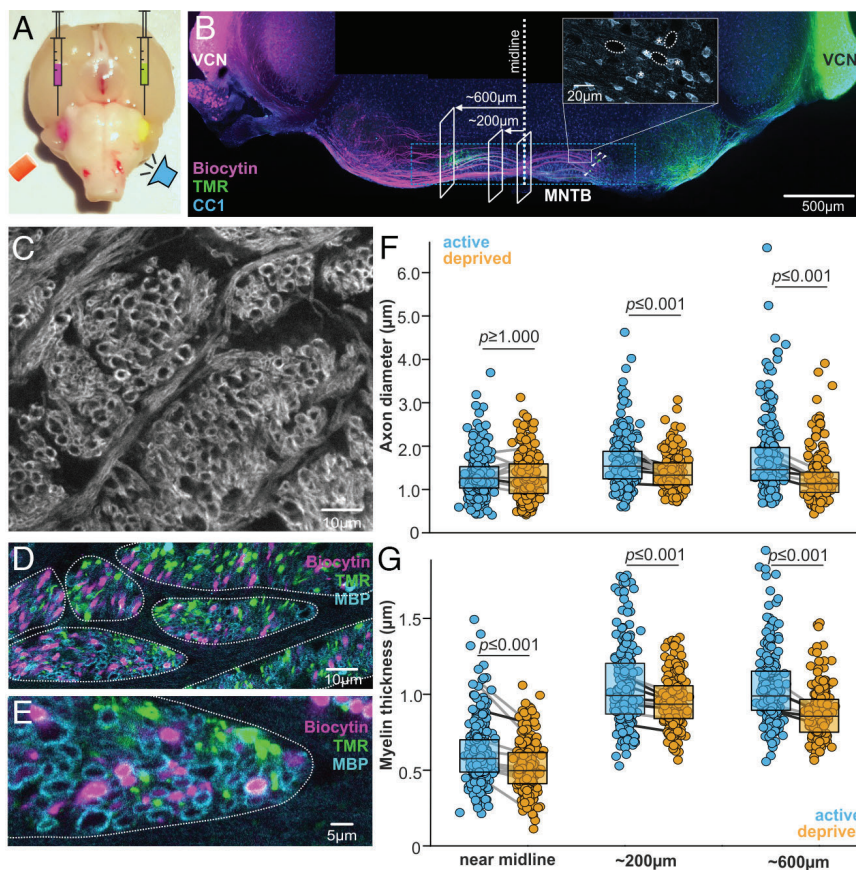


Fig. 1. Radial growth of myelin occurs on an axon-by-axon basis. (A) Ventral view of a mouse brain illustrating the injection of different colored tracers into both cochlear nuclei to differentially trace fibers originating from either the deprived or the control ear. (B) Coronal brainstem section (reassembled) showing traced TB fibers from both sides approaching and crossing the midline, most of them terminating in calyx synapses in the contralateral MNTB. White arrow heads mark retrogradely labeled green MNTB cells that project to the cochlear nucleus. *Inset:* CC1-labeled oligodendrocytes are marked by the asterisks and are smaller than MNTB principal neurons (white dashed outlines). Oligodendrocyte numbers were counted in $800 \times 400\text{-}\mu\text{m}$ areas (blue dashed boxes) left and right from the midline. Sagittal sections were taken near the midline, at $\sim 200\text{-}\mu\text{m}$ and $\sim 600\text{-}\mu\text{m}$ away from the midline on either side (white perpendicular boxes shown on one side only). (C) Sagittal section of the TB fiber tract shows cross-sections of auditory fiber bundles separated by perpendicularly oriented pyramidal tract fibers. (D) Sagittal TB section shows that fiber bundles contain fibers of both colors. White dotted lines indicate the boundaries of each bundle. (E) Magnification of the section shown in D also reveals fiber cross-sections lacking either tracer (blue MBP circles only). (F) Individual axon diameters (minimum diameter of the inner ellipse; $n = 1,565$ fibers) were measured for fibers at three lateral locations. Boxes show medians and interquartiles. Gray solid lines indicate the within mouse ($n = 11$) comparisons and black solid lines, the within bundle comparisons. (G) Same design as in F. Myelin thickness [(minimum outer diameter - minimum inner diameter)/2] is significantly larger in control compared to deprived fibers in all three locations.

Radial growth of myelin is achieved by adding new myelin layers starting from the inner tongue. High-magnification electron microscopy was used to measure the exact number of myelin layers in control and deprived fibers and to test for possible differences in individual myelin layer thickness. Since the injected tracers were not electron-dense, we measured these parameters in the auditory nerve, which contains fibers solely from one ear. Cross-sections of the proximal auditory nerve from the control and the deprived ear were investigated using electron microscopy. Electron micrographs revealed individual auditory nerve axons, with inner tongues and myelin sheaths (Fig. 2A). Scans of rectangular sections were performed across the myelin sheaths to assess the overall myelin thickness, the number of myelin layers and the thickness of individual myelin layers. The regular peaks and troughs of the resulting histogram represent the extracellular intraperiod line (IPL, lighter shade) and the major dense line (MDL, darker shade), respectively (Fig. 2B–D). Similar to the findings in TB fibers, auditory nerve fibers of the active, control ear had significantly thicker myelin sheaths (median: $0.205\text{ }\mu\text{m}$; IQR: $0.175\text{--}0.244\text{ }\mu\text{m}$; $n = 42$) compared to fibers arising from the deprived ear (median: $0.175\text{ }\mu\text{m}$; IQR: $0.156\text{--}0.203\text{ }\mu\text{m}$; $n = 48$; Mann–Whitney rank-sum test: $P = 0.003$; Fig. 2E). Recognizing the peak-to-peak distance of the scan histograms as one myelin layer, the average number of layers

was significantly larger on the control side (30.24 ± 7.02 ; $n = 42$) compared to the deprived side (25.48 ± 6.53 ; $n = 48$; two-tailed t test: $P = 0.001$; Fig. 2F). Using the distance between two IPLs as a measure of layer thickness, no significant difference was found between active and sound-deprived fibers (control median: 4.81 nm , control IQR: $4.64\text{--}5.35\text{ nm}$; $n = 42$; deprived median: 4.82 nm , control IQR: $4.59\text{--}5.16\text{ nm}$; $n = 48$; Mann–Whitney rank-sum test: $P = 0.389$; Fig. 2D and G). These results show that sound-evoked activity increases the number of myelin layers at active auditory axons. There were no signs of myelin swelling or degradation on the sound-deprived side, consistent with the increase in myelination on the active side being physiological rather than representing pathological degradation on the deprived side.

It is conceivable that the earplug caused a developmental delay in downstream auditory neurons, so four established neurophysiological markers of maturation were tested for active and sound-deprived neurons (Fig. 3): 1) synaptic delay, 2) pre-, and 3) postsynaptic action potential (AP) half-width (25) and 4) lack of regular bursting of spontaneous activity (26, 27). With respect to the monaural earplug, cochlear nucleus neurons activated by the control ear send sound-evoked activity through TB fibers, across the midline toward their targets in the contralateral superior

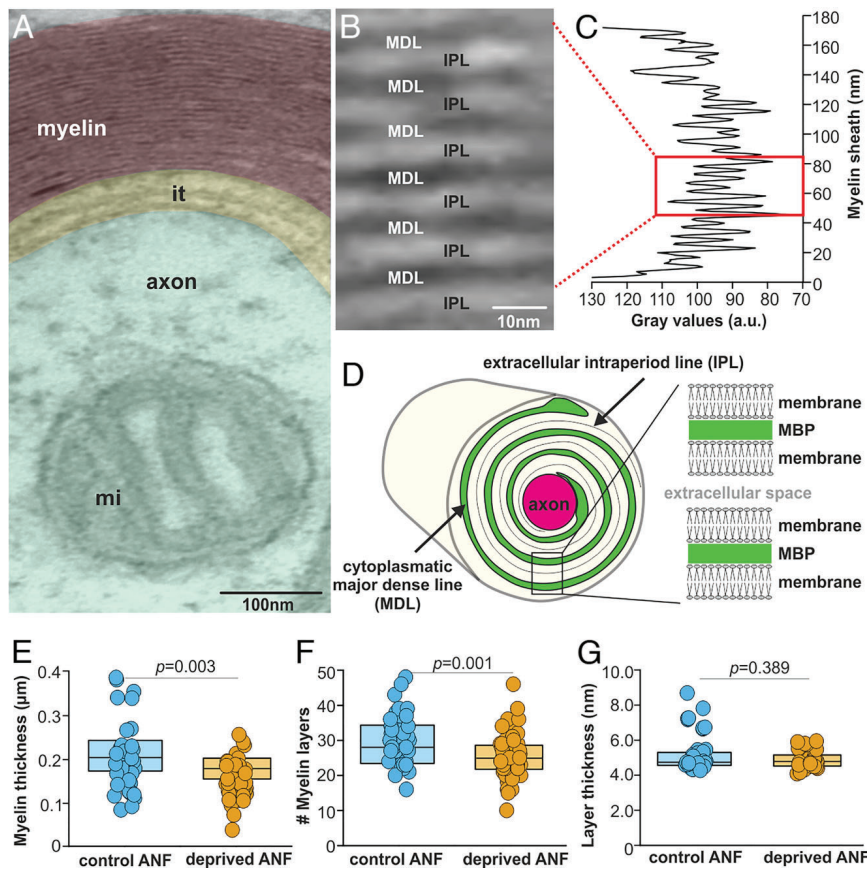


Fig. 2. Ambient sound increases the number of myelin layers, not their thickness. (A) Electron micrograph of an auditory nerve fiber (ANF) visualizes the axon (green), mitochondria (mi), myelin sheath (red), and the inner tongue of myelin (it; yellow). (B) Section of myelin sheath showing only 6 (out of >20) individual myelin layers with the cytoplasmic major dense line (MDL, dark lines) and the extracellular intraperiod line (IPL, lighter lines). (C) Histogram of all the peaks and troughs through the whole myelin sheath acquired by a line scan using ImageJ. (D) Schematic of MDL and IPL in a myelin sheath. (E) Thickness of ANF myelin excluding the inner tongue. (F) Number of myelin layers assessed from peaks in histograms such as shown in C. (G) Thickness of individual myelin layers calculated by trough-to-trough distances in histograms as in C.

olivary complex (SOC). In contrast, cochlear nucleus neurons receiving input from the ear-plugged ear transmit only spontaneous APs along the TB fiber toward their SOC targets. In the SOC, neurons of the MNTB receive exclusive excitatory input from contralateral cochlear nucleus neurons and as such serve as an ideal within-subject control of activity changes following the monaural sensory deprivation. Due to the crossed inputs, we refer to MNTB neurons contralateral to the control ear as active and vice versa, MNTB neurons contralateral to the ear-plugged ear as deprived (Fig. 3A). Single-unit activity was recorded from the active and deprived MNTB within the same mice immediately following earplug removal. MNTB neurons were identified by their excitatory response to contralateral sound and the typical complex waveform comprising both presynaptic and postsynaptic components (28). This was used to obtain the half-width of the pre- and postsynaptic APs as well as the synaptic delay (Fig. 3B). The time between the peak and trough of extracellular APs is a recognized marker for AP half-width (29, 30). Presynaptic AP half-widths, synaptic delays and postsynaptic AP half-widths did not differ significantly between active and deprived MNTB neurons (preAP-HW_{active}: median: 0.18 ms; IQR: 0.14–0.19; n = 28; preAP-HW_{deprived}: median: 0.16 ms; IQR: 0.14–0.19 ms; n = 22; Mann-Whitney rank-sum test: $P = 0.501$; Fig. 3C, synaptic delay, SD_{active}: 0.45 ± 0.06 ms; n = 28; SD_{deprived}: 0.42 ± 0.04 ms; n = 22; two-tailed t test: $P = 0.091$; Fig. 3D and postsynaptic AP half-width, postAP-HW_{active}: median = 0.43 ms, IQR = 0.39–0.47, n = 28; postAP-HW_{deprived}: median: 0.45 ms, IQR: 0.37–0.49 ms, n = 22; Mann-Whitney rank-sum test: $P = 0.672$;

Fig. 3E). Regularity of spontaneous firing was quantified by the coefficient of variation, which is high (~2) for prehearing activity and ~1 for firing activity in post-hearing-onset animals (27). Spontaneous activity of MNTB neurons from neither control nor deprived side showed any signs of bursting activity (Fig. 3F and G) and their coefficients of correlation clustered around 1 with no significant difference between the groups (CV_{active}: median: 0.76; IQR: 0.66–0.83; n = 28; CV_{deprived}: median: 0.79, IQR: 0.72–0.87; n = 22; Mann-Whitney rank-sum test: $P = 0.233$; Fig. 3H).

Together, the similarity in synaptic delay, AP half-width and patterns of spontaneous activity supports the notion that cellular and circuit development has not been delayed during the 10-d deprivation period. However, thicker myelin of active auditory nerve and TB fibers could lead to temporal mismatches in downstream binaural processing centers.

Latency differences between auditory brainstem responses (ABR) wave IV and wave I serve as a compelling marker for signal conduction speed through the auditory brainstem and are known to correlate with the extent of myelination of auditory axons in rodents (11, 31) and humans (32, 33). Auditory thresholds were measured in response to brief broadband sounds (clicks) and were compared between the control ear, the closed ear with the earplug still in place, and the deprived ear immediately following earplug removal (Fig. 4A). Thresholds were elevated by about 47 dB due to the earplug, yielding a significant difference in auditory thresholds between the control ear (median: 24 dB SPL, IQR: 22–26 dB SPL) and the closed ear (median: 68 dB SPL, IQR: 61–80 dB

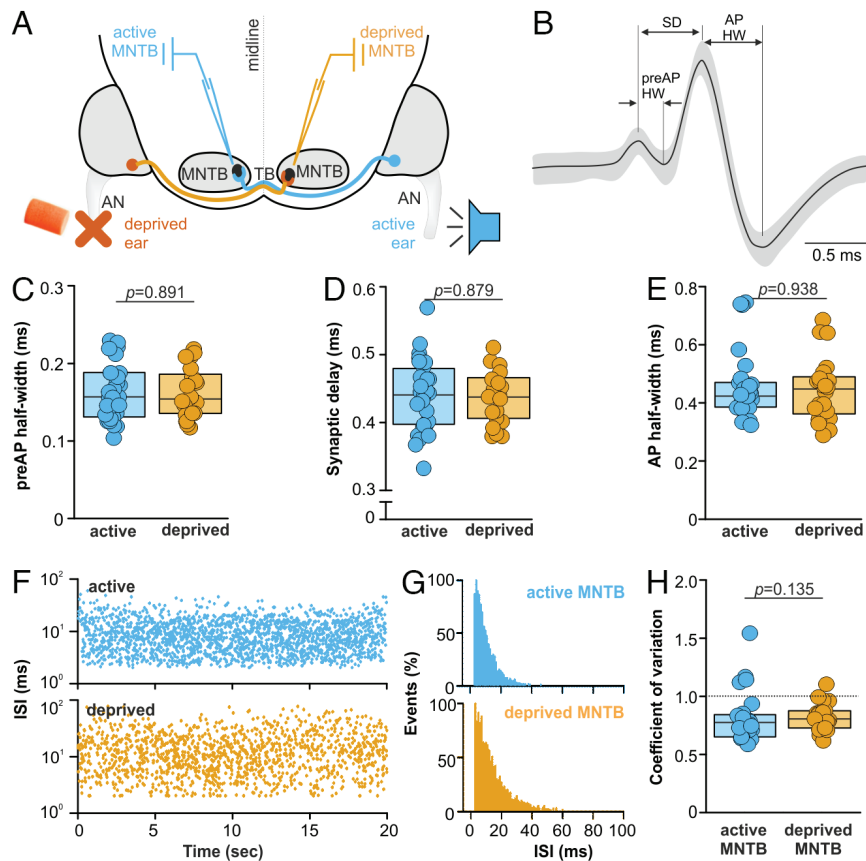


Fig. 3. Normal development of basic physiological properties of active and deprived MNTB neurons. (A) Schematic showing the monaural innervation pathway to the MNTB and semantics used with respect to the active and deprived ear. (B) Extracellularly recorded MNTB neuron, consisting of the presynaptic calyx of Held AP (preAP) and the postsynaptic AP (postAP), separated by the synaptic delay (SD). (C–E) Average data for (C) preAP half-width, (D) synaptic delay, and (E) postAP half-width show no significant differences between the control and the deprived group. (F) Patterns of spontaneous firing activity for an active (Top, blue plot) and a deprived (Lower, orange plot) neuron for 20 s. No regularity of interspike intervals (ISIs) was observed, which was corroborated by the absence of (G) multiplexed ISI histograms. (H) Regularity of spontaneous activity was quantified by the coefficient of variation (CV = SDISI/meanISI). CVs around 1 (dashed line) indicate a near-Poisson distribution of the spontaneous rates.

SPL; $P \leq 0.001$). Immediately after earplug removal, thresholds partially recovered (median: 52 dB SPL, IQR: 46–62 dB SPL; $P = 0.127$; Kruskal–Wallis one-way ANOVA on ranks; $n = 22$ ears/11 mice, Fig. 4A–C). Full recovery of thresholds was observed about 25 d after earplug removal in a previous study (11). In the present study, ABR measurements were used to assess latency differences and relate them to changes in myelination. Since latencies of neural responses are negatively correlated to stimulus intensities, we corrected for the observed differences in auditory thresholds after earplug removal by assessing the latencies 20 dB above the respective thresholds of either ear (Fig. 4D). This correction resulted in an alignment of ABR waves I, but the latency for ABR wave IV was still longer when the deprived ear was stimulated (Fig. 4E). The average latency difference (Δ IV–I) revealed a neuronal processing delay of about 458 μ s for the sound-deprived ear (median_{control}: 2.82 ms, IQR: 2.62–2.97 ms; median_{deprived}: 3.08 ms, IQR: 3.86–3.62 ms; $n = 30$ ears; 15 mice; Wilcoxon signed-rank test: $P \leq 0.001$; Fig. 4F).

Together, these data suggest that the neuronal processing delay observed in the ABR recordings following 10 d of sound deprivation was caused by an additive change in myelination of fibers along the auditory pathway.

There is a broad agreement that ABR wave I corresponds to activity entering the cochlear nucleus (CN) and wave IV to activity of the inferior colliculus (IC). The path length between those two nuclei in mice was estimated from coronal brain sections to be 9.82 mm. Including these data on adaptive myelination along

the TB fibers into our reported computational model (11) provides estimates for the conduction velocity of active and sound-deprived fibers (Fig. 4G). The distribution of conduction velocity was narrower in the control population, and the median conduction velocity of the controls was significantly faster (velocity_{active}: median = 4.46 m/s, IQR = 3.78–5.30 m/s, $n = 314$) compared to the deprived ear (velocity_{deprived}: median = 4.39 m/s, IQR = 3.42–5.28, $n = 257$; Mann–Whitney rank-sum test: $P = 0.047$; Fig. 4H). This result was then used to predict how ABR latencies would change based on adaptive myelination alone. The model shows that the wave Δ IV–I latency in controls was around 2.5 ms (gray curve in Fig. 4I), assuming each action potential would make an alpha function-shaped contribution to the ABR with the filter length a of the alpha function taken as 2 ms (approximating synaptic currents in the inferior colliculus; ref. 34). This wave Δ IV–I latency is in accordance with the actual ABR measurements (Fig. 4F), validating the model. Assigning the peak of wave I as time point zero and using a filter length of $a = 2$ ms (Fig. 4E), the model predicts the peak of wave IV to occur 0.355 ms earlier when stimulating the control ear (blue curve in Fig. 4I) compared to stimulating the sound-deprived ear (orange curve in Fig. 4I). Since the filter length a is not well constrained, increasing it to 2.5 ms gave an upper boundary of 0.45 ms for the wave IV latency-changes (Fig. 4I, Inset). This delay closely approximates the mean wave IV–I differences between both ears seen in the ABR measurements of 0.45 ± 0.10 ms ($n = 14$), consistent with the temporal mismatch measured at

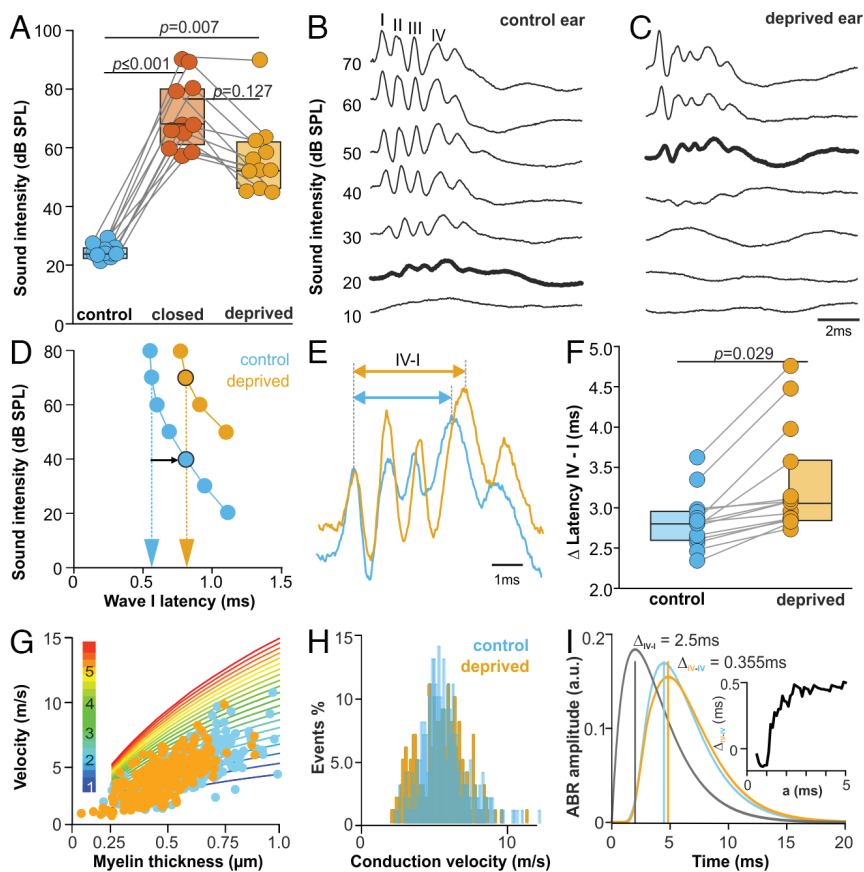


Fig. 4. Monaural deprivation leads to a mismatch in neuronal processing speed. (A) ABR thresholds in response to click stimulation of the control ear, the deprived ear with the earplug in place (“closed ear”) and the deprived ear immediately after earplug removal. (B) ABR waveform examples of one mouse stimulating either the control or the deprived ear. (C) Both datasets show four characteristic ABR peaks and enhanced thresholds (bold trace) of the deprived ear. (D) Latency-intensity functions depict the typical increase of latencies with decreasing intensities by example of wave I stimulated by either control or deprived ear. The black arrow indicates the correction of wave I latencies with respect to thresholds. At 20 dB above threshold (black circled symbols), wave I latencies are the same. (E) Following latency correction for wave I, the time to wave IV was still longer when stimulating the deprived ear. (F) Average data comparing within animal differences of wave IV-I latencies. (G) The Sinclair et al. (11) model was used to acquire the conduction velocity of the active (blue circles) and deprived (orange circles) fibers. Different velocities according to axon diameter (μm on the vertical color scale) are shown in the background. (H) Histogram of conduction velocities (bin width 0.1 m/s) shows active dataset to have no slow fibers. (I) Model ABRs. Black: Wave I assuming synchronous spiking in the brainstem. Blue/orange: Wave IV derived from the velocity distributions in H, for an ABR filter constant $a = 2.5$ ms. Inset: IV-I latency difference only slightly increases for filter constants $a > 2$ ms.

the level of the inferior colliculus after monaural sensory deprivation being fully attributed to adaptive myelination.

Discussion

The present study reveals that radial growth of myelin is driven by axonal activity rather than being an exclusive product of the neuron’s (or oligodendrocyte’s) genetic identity. We show that fiber bundles carrying axons originating from the same neuronal cell type on either side of the brain form a mosaic of interspersed active and passive axons. This raises the question of how individual myelinating oligodendrocytes can identify active from passive axons in such a mixed population.

One of the main fiber types in the trapezoid body are GBC axons. In early postnatal development (long before earplugs were inserted in the present study), GBC axons are guided across the midline to find their targets in the contralateral MNTB by the expression of the receptor tyrosine kinases Ephs and their ephrin ligands, a large family of contact-mediated guidance molecules (35). Particularly ephrin-A5 is strongly expressed in the MNTB and may cause the concentration of axons into bundles within 600 μm left and right of the midline (36, 37). One might imagine that axons growing in the same direction are facilitated in reaching their targets by being in bundles. However, as our salt and pepper patterns of traced fibers show, each fiber crosses the midline

without the support of “like-minded neighbors.” The precise temporal pattern of initial myelination at newly formed axons and the rate at which myelin sheaths are generated will vary with the identity of the neuron and the brain region, with the brainstem typically being myelinated earlier than the cortex (38). On initiation, the wrapping of individual axonal segments might be completed within only a few hours (39), and this process mainly determines internodal patterns. In the TB, myelinated axons were found as early as postnatal day eight (P8), based on the expression of myelin basic protein and electron microscopic visualization of myelin sheaths in axonal cross-sections (11, 40).

The ear canal of rodents is still closed with connective tissue at P8, preventing the passage of airborne sound. Over this developmental period until the onset of hearing at P10, the cochlea generates spontaneous activity, which occurs in bursts and propagates throughout the auditory system (27, 41). Interestingly, MNTB neurons that develop without sound-evoked activity for 10 d also change their spontaneous activity from developmental burst-firing to mature Poisson-distributed firing, suggesting that the change is triggered intrinsically and independently of hearing onset. Therefore, the large increase in the number of action potentials due to sound stimulation rather than the change in firing pattern likely underlies the rapid radial growth of myelin following hearing onset (11).

Earplugs are a widely established method to mimic mild and reversible conductive hearing loss (11, 42–46). It is important to

point out that reversibility of this hearing loss relates to the removal of earplugs and the subsequent restoration of peripheral conductive hearing, rather than to central auditory processing, which can show persistent adaptations in temporal and spatial processing (42, 43, 45, 46). We have employed monaural earplugs to prevent the typical increase in neuronal activity that occurs with the onset of hearing (27). Blocking the sound-evoked activity while maintaining spontaneous firing enables titration of firing rates required for normal development of axonal conduction.

Neuronal activity triggers high-frequency calcium transients in individual myelin sheaths which subsequently promotes myelin sheath elongation (19, 47). Although it is unclear whether radial growth of myelin is also promoted by these high-frequency calcium transients, both processes depend on axonal activity and require local translation of myelin basic protein. The activity-dependent local increase in calcium can be caused by either calcium influx through calcium channels or by calcium release from intracellular stores. To our knowledge, voltage-gated calcium channels have not been described in the membrane of myelin sheaths. Therefore, an intracellular calcium release via voltage-induced second messenger activation, which has been described in neurons, could act as an alternative origin of activity-dependent calcium transients (48). One mechanism by which axons could communicate their activity levels directly to their myelin sheaths would be for action potentials to provide the depolarization required to increase intracellular calcium and initiate MBP synthesis. The depolarization can be achieved by the efflux of potassium ions from highly active axons into the inner tongue of myelin via composite channels consisting of a low-voltage activated Kv1 channel on the axonal surface and a connexin 29 hemichannel on the inner tongue of myelin (49). The subsequent depolarization of the myelin sheath could then trigger calcium-transients and the translation of MBP at the inner tongue of individual myelin sheaths. Remote translation of MBP, directly at the active axon–myelin sheath interface (50, 51) and away from the oligodendrocyte soma, is well recognized and provides the basis for an axon-by-axon adaptive myelination process. It is likely that such a potassium flux mechanism enables activity-dependent fine-tuning of axonal conduction velocity, but is not required for general myelination. Connexin-29 null mutants show no major myelination deficits and inconspicuous ABRs (52). As suggested by our current results, activity-dependent myelin plasticity taking place after the initial myelin formation may lead only to small temporal mismatches of about half a millisecond. However, since the time window during which spiking activity in the lateral superior olive is suppressed by MNTB inhibition only lasts a few hundreds of microseconds (53, 54), a ~500- μ s delay of the inhibitory input will most certainly cause a deficit in the sound localization ability. Indeed, deficits in sound localization performance and the effects on neural plasticity following temporary monaural occlusion by either earplugs or Otis media have been investigated for many decades (55, 56). These studies agree that monaural occlusion causes an initial deficit in sound localization, which over time is followed by adaptive neural plasticity. Our present results add to this body of work by showing that the change in myelination is an additional factor which contributes to these adaptive processes.

In the present study, we observed increased myelination and faster overall processing speed through the auditory brainstem for the controls compared to sound-deprived ears. However, the earplug-induced delay at each processing stage was small, suggesting compensatory mechanisms. In rats that received earplugs at 30 d of age, a lasting change in AMPA receptor composition toward GluA3 subunits in cochlear nucleus neurons was described, a subunit known to be responsible for ultrafast excitatory synaptic transmission also at the calyx of Held (42, 57, 58). Even though

we corrected for earplug-induced differences in auditory thresholds, additional changes or compensations could occur at different levels of the auditory pathway. However, the observation that the ABR wave IV-I difference between plugged and control sides was still nearly 500 μ s suggest a large influence of myelination. The computational model only considered changes in conduction velocity and could still predict at least 75% of the temporal mismatch based on stronger myelination in the control side. Such a temporal mismatch during early days after hearing onset is likely to disturb the experience-dependent refinement of the sound localization circuit (59).

Materials and Methods

Experiments were approved in accordance with the stipulations of the German animal welfare law (Tierschutzgesetz) (ROB-55.2-2532.Vet_02-18-118). Male and female CBA/Ca mice born at the LMU Faculty of Biology vivarium to breeders acquired from Charles River laboratories were housed with 12-h light/dark cycles and food and water ad libitum.

Depending on normality of the distribution, population average data are given by the mean \pm SD, or the median and 25 and 75% interquartile ranges (IQR) as box edges with full data ranges depicted by individual data points. Accordingly, parametric or nonparametric tests were used to determine statistical significance.

Ear Plugging. Small pieces of an “E.A.R Classic II” human foam earplug were compressed and inserted into the external auditory meatus before being sealed with dental cement (Paladur; Heraeus-Kulzer) at P10 under MMF anesthesia (Medetomidin: 0.5 mg/kg BW, Midazolam: 5.0 mg/kg BW, Fentanyl: 0.05 mg/kg BW). Earplugs were examined daily and replaced every third day to avoid uncontrolled loss as the mice grew.

ABRs were recorded in MMF-anesthetized mice, placed on a temperature-controlled heating pad (ATC1000, WPI) in a soundproof chamber (Industrial Acoustics). Subdermal needle electrodes (Rochester Electro-Medical, Inc.) were placed at the vertex of the mouse’s head (reference), ventral to the pinna (active), and near the base of the tail (ground). Electrodes were attached to a low-impedance headstage (RA4LI, Tucker Davis Technologies: TDT), and a preamplifier (RA16PA, TDT; amplification factor: 250) and connected to the auditory processor (RZ6, TDT) via optical cables. SPIKE software (Brandon Warren, UW) was used for speaker calibration (MF1, TDT), stimulus (100 μ s clicks; 10 to 90 dB SPL) generation and waveforms recording. Thresholds were determined as the sound intensity at which at least two peaks could be distinguished in the average (1,000 \times) ABR waveform. When switching between control ear and ear-plugged ear, only the active electrode was swapped to the other ear. All other electrodes were kept in place during earplug removal. At the end of ABR experiments, animals were either kept in anesthesia for subsequent *in vivo* single-unit recordings or killed with an overdose of MMF for tracing and histology experiments.

In Vivo Physiology. MMF-anesthetized mice were placed on a heating pad in a soundproof chamber and stabilized in a custom stereotaxic device. A craniotomy was performed just anterior to the lambda suture and glass microelectrodes (3M KCl; 5 to 20 M Ω) were lowered into the brainstem. A ground electrode was placed in the muscle at the base of the neck. Signals were amplified (AM Systems, Neuroprobe 1600), filtered (300 to 3,000 Hz; TDT PC1), and sampled (50 kHz) with a Fireface UFX audio interface (RME). AudioSpike software (HoerrTech) was used to calibrate the multifield magnetic speakers, generate stimuli, and record action potentials. Search stimuli to identify auditory nuclei consisted of pure tones (50 to 100 ms duration, 5 ms rise/fall time) at varying intensity (0 to 90 dB SPL) and were presented through short hollow ear bars directly connected to the speakers.

Axon Tracing. P20 mice were killed with an overdose of MMF and intracardially perfused with Ringer’s solution containing heparin. Brains were removed from the skull into ice-cold ACSF. Crystals of tetramethylrhodamine (TMR, Invitrogen D3308) were grown from a 50 to 100% TMR in H₂O solution on fine tungsten needle tips and stored until used (24 h maximum). Small incisions were made in the meninges corresponding to the ventral cochlear nucleus on each side and TMR crystals or correspondingly small biocytin (TOCRIS, 3349/ Sigma B4261) crystals were inserted. The brains were then incubated for 2 h in carbogenated ACSF at room temperature before being fixed in 4% PFA overnight.

Immunohistochemistry and Confocal Microscopy. Sagittal brainstem sections (50 μm) including the TB were taken using a vibratome (Leica, VT1200S). Immunostaining was carried out as previously described (11) using primary MBP antibodies (ab7349 abcam; 1:150) and corresponding secondary antibodies (Alexa-647 donkey anti-rat, Dianova 712-605-150, 1:140; biocytin-targeted streptavidin Alexa-488, Dianova, 016-540-084, 1:250). Optical sections were acquired with a confocal laser-scanning microscope (TCS SP5-2, Leica Microsystems, Mannheim, Germany) equipped with HCX PLAPO CS 20 \times /NAO.7 and HCX PLAPO Lambda Blue 63 \times /NA1.4 immersion oil objectives. For each optical section, images were collected sequentially for the different fluorophores. 8-bit grayscale images were obtained with ABC pixel sizes of 120 to 1,520 nm depending on the selected zoom factor and objective. To improve the signal-to-noise ratio, images were averaged from three successive scans.

Electron Microscopy. P20 mice were killed with an overdose of MMF and intracardially perfused with Ringer's solution, followed by 2.5% glutaraldehyde plus 2% PFA in 0.1% cacodylate buffer (CB) pH 7.0. Brains were removed from the skull and postfixed in the same fixative overnight at 4 $^{\circ}\text{C}$. After washing (3 \times) in CB, control and deprived auditory nerves were dissected and sectioned perpendicular to the fiber direction. The tissue blocks were washed (4 \times) in CB and postfixed in 1% OsO_4 in CB for 1 to 2 h. After washing and dehydrating in graded series of acetone, the tissue was embedded in Spurr's resin (60). Before ultrathin (70 nm) sectioning, several semithin (1 μm) sections were cut for light microscopic investigation. The ultra-thin sections were collected on formvar-coated copper

slot grids and stained with uranyl acetate and lead citrate. EM images were taken using a FEI Morgagni transmission electron microscope (80 kV, SIS Mega view III camera, 1,375 \times 1,032 pixels).

Computational Modeling. We used the multicompartmental model of an axon developed in previous publications (9, 11) to assess the conduction velocity of control vs deprived fibers for the dataset collected in the present study. Conduction velocities were obtained for measured fibers (Fig. 1 F and G) using the geometrically determined pair of parameters, axon radius and myelin thickness, and leaving all other parameters unchanged. The ABR was modeled by replacing each spike time t_n (at the CN for wave I and at the IC for wave IV) by an alpha function with parameter a :

$$\text{ABR}(t) = \sum_n (t - t_n) / (a^2) \exp[-(t - t_n)/a] * (t < t_n).$$

Spike times at the CN are assumed to be fully coincident; spike times at the IC are derived from the distribution of simulated conduction speeds (Fig. 4H).

Data, Materials, and Software Availability. All study data are included in the main text.

ACKNOWLEDGMENTS. This research was funded by the Deutsche Forschungsgemeinschaft (KO2207/3-1, SFB870-A10, SFB870-B01), the Munich Cluster for Systems Neurology (Synergy) and the Graduate School of Systemic Neuroscience. We thank Prof. Ian D. Forsythe for critical comments on our manuscript as well as Heidemarie Gensler for technical support with electron microscopy.

- R. J. Franklin, C. French-Constant, Remyelination in the CNS: From biology to therapy. *Nat. Rev. Neurosci.* **9**, 839–855 (2008).
- D. E. Bergles, W. D. Richardson, Oligodendrocyte development and plasticity. *Cold Spring Harb. Perspect. Biol.* **8**, a020453 (2015).
- G. S. Tomassy *et al.*, Distinct profiles of myelin distribution along single axons of pyramidal neurons in the neocortex. *Science* **344**, 319–324 (2014).
- C. L. Call, D. E. Bergles, Cortical neurons exhibit diverse myelination patterns that scale between mouse brain regions and regenerate after demyelination. *Nat. Commun.* **12**, 4767 (2021).
- A. Stange-Marten *et al.*, Input timing for spatial processing is precisely tuned via constant synaptic delays and myelination patterns in the auditory brainstem. *Proc. Natl. Acad. Sci. U.S.A.* **114**, E4851–E4858 (2017).
- M. C. Ford *et al.*, Tuning of Ranvier node and internode properties in myelinated axons to adjust action potential timing. *Nat. Commun.* **6**, 8073 (2015).
- W. A. Rushton, A theory of the effects of fibre size in medullated nerve. *J. Physiol.* **115**, 101–122 (1951).
- J. Guy, E. A. Ellis, K. Kelley, G. M. Hope, Spectra of G ratio, myelin sheath thickness, and axon and fiber diameter in the guinea pig optic nerve. *J. Comp. Neurol.* **287**, 446–454 (1989).
- E. G. Hughes, J. L. Orthmann-Murphy, A. J. Langseth, D. E. Bergles, Myelin remodeling through experience-dependent oligodendrogenesis in the adult somatosensory cortex. *Nat. Neurosci.* **21**, 696–706 (2018).
- C. Sampaio-Baptista, H. Johansen-Berg, White matter plasticity in the adult brain. *Neuron* **96**, 1239–1251 (2017).
- J. L. Sinclair *et al.*, Sound-evoked activity influences myelination of brainstem axons in the trapezoid body. *J. Neurosci.* **37**, 8239–8255 (2017).
- L. N. Collins, D. L. Hill, P. C. Brunjes, Myelination of the developing lateral olfactory tract and anterior commissure. *J. Comp. Neurol.* **526**, 1843–1858 (2018).
- M. Makinodan, K. M. Rosen, S. Ito, G. Corfas, A critical period for social experience-dependent oligodendrocyte maturation and myelination. *Science* **337**, 1357–1360 (2012).
- C. Demerens *et al.*, Induction of myelination in the central nervous system by electrical activity. *Proc. Natl. Acad. Sci. U.S.A.* **93**, 9887–9892 (1996).
- E. M. Gibson *et al.*, Neuronal activity promotes oligodendrogenesis and adaptive myelination in the mammalian brain. *Science* **344**, 1252304 (2014).
- B. Stevens, S. Porta, L. L. Haak, V. Gallo, R. D. Fields, Adenosine: A neuron-glia transmitter promoting myelination in the CNS in response to action potentials. *Neuron* **36**, 855–868 (2002).
- N. B. Hamilton *et al.*, Endogenous GABA controls oligodendrocyte lineage cell number, myelination, and CNS internode length. *Glia* **65**, 309–321 (2017).
- H. Wake, P. R. Lee, R. D. Fields, Control of local protein synthesis and initial events in myelination by action potentials. *Science* **333**, 1647–1651 (2011).
- A. M. Krasnow, M. C. Ford, L. E. Valdivia, S. W. Wilson, D. Attwell, Regulation of developing myelin sheath elongation by oligodendrocyte calcium transients in vivo. *Nat. Neurosci.* **21**, 24–28 (2018).
- A. Y. Foster, H. Bujalka, B. Emery, Axoglial interactions in myelin plasticity: Evaluating the relationship between neuronal activity and oligodendrocyte dynamics. *Glia* **67**, 2038–2049 (2019).
- M. Zonouzi *et al.*, Individual oligodendrocytes show bias for inhibitory axons in the neocortex. *Cell Rep.* **27**, 2799–2808.e3 (2019).
- S. Mitew *et al.*, Pharmacogenetic stimulation of neuronal activity increases myelination in an axon-specific manner. *Nat. Commun.* **9**, 306 (2018).
- B. R. Schofield, Projections to the cochlear nuclei from principal cells in the medial nucleus of the trapezoid body in guinea pigs. *J. Comp. Neurol.* **344**, 83–100 (1994).
- B. Emery, Regulation of oligodendrocyte differentiation and myelination. *Science* **330**, 779–782 (2010).
- H. Taschenberger, H. von Gersdorff, Fine-tuning an auditory synapse for speed and fidelity: Developmental changes in presynaptic waveform, EPSC kinetics, and synaptic plasticity. *J. Neurosci.* **20**, 9162–9173 (2000).
- W. R. Lippe, Rhythmic spontaneous activity in the developing avian auditory system. *J. Neurosci.* **14**, 1486–1495 (1994).
- M. Sonntag, B. Englitz, C. Kopp-Scheinpflug, R. Rubsam, Early postnatal development of spontaneous and acoustically evoked discharge activity of principal cells of the medial nucleus of the trapezoid body: An in vivo study in mice. *J. Neurosci.* **29**, 9510–9520 (2009).
- C. Kopp-Scheinpflug, W. R. Lippe, G. J. Dorrscheidt, R. Rubsam, The medial nucleus of the trapezoid body in the gerbil is more than a relay: Comparison of pre- and postsynaptic activity. *J. Assoc. Res. Otolaryngol.* **4**, 1–23 (2003).
- A. Ritzau-Jost *et al.*, Large, stable spikes exhibit differential broadening in excitatory and inhibitory neocortical boutons. *Cell Rep.* **34**, 108612 (2021).
- A. Richardson *et al.*, Kv3.3 subunits control presynaptic action potential waveform and neurotransmitter release at a central excitatory synapse. *Elife* **11**, e75219 (2022).
- S. E. Kim, K. Turkington, C. Kushmerick, J. H. Kim, Central dysmyelination reduces the temporal fidelity of synaptic transmission and the reliability of postsynaptic firing during high-frequency stimulation. *J. Neurophysiol.* **110**, 1621–1630 (2013).
- S. B. Amin, D. Vogler-Elias, M. Orlando, H. Wang, Auditory neural myelination is associated with early childhood language development in premature infants. *Early Hum. Dev.* **90**, 673–678 (2014).
- J. K. Moore, L. M. Perazzo, A. Braun, Time course of axonal myelination in the human brainstem auditory pathway. *Hear Res.* **87**, 21–31 (1995).
- P. C. Nelson, L. H. Carney, A phenomenological model of peripheral and central neural responses to amplitude-modulated tones. *J. Acoust. Soc. Am.* **116**, 2173–2186 (2004).
- A. A. Sitko, L. V. Goodrich, Making sense of neural development by comparing wiring strategies for seeing and hearing. *Science* **371**, eaaz6317 (2021).
- K. S. Cramer, M. L. Gabriele, Axon guidance in the auditory system: Multiple functions of Eph receptors. *Neuroscience* **277**, 152–162 (2014).
- M. L. Abdul-Latif, J. A. Salazar, S. Marshak, M. L. Dinh, K. S. Cramer, Ephrin-A2 and ephrin-A5 guide contralateral targeting but not topographic mapping of ventral cochlear nucleus axons. *Neural Dev.* **10**, 27 (2015).
- M. Simons, K. A. Nave, Oligodendrocytes: Myelination and axonal support. *Cold Spring Harb. Perspect. Biol.* **8**, a020479 (2015).
- T. Czopka, C. French-Constant, D. A. Lyons, Individual oligodendrocytes have only a few hours in which to generate new myelin sheaths in vivo. *Dev. Cell* **25**, 599–609 (2013).
- A. L. Nabel *et al.*, Development of myelination and axon diameter for fast and precise action potential conduction. *Glia* **72**, 794–808 (2024).
- N. X. Tritsch *et al.*, Calcium action potentials in hair cells pattern auditory neuron activity before hearing onset. *Nat. Neurosci.* **13**, 1050–1052 (2010).
- C. Clarkson, F. M. Antunes, M. E. Rubio, Conductive hearing loss has long-lasting structural and molecular effects on presynaptic and postsynaptic structures of auditory nerve synapses in the cochlear nucleus. *J. Neurosci.* **36**, 10214–10227 (2016).
- M. L. Caras, D. H. Sanes, Sustained perceptual deficits from transient sensory deprivation. *J. Neurosci.* **35**, 10831–10842 (2015).
- C. E. Carr *et al.*, Experience-dependent plasticity in nucleus laminaris of the barn owl. *J. Neurosci.* **44**, e0940232023 (2024).
- D. P. Kumpik, A. J. King, A review of the effects of unilateral hearing loss on spatial hearing. *Hear. Res.* **372**, 17–28 (2019).
- M. V. Popescu, D. B. Polley, Monaural deprivation disrupts development of binaural selectivity in auditory midbrain and cortex. *Neuron* **65**, 718–731 (2010).
- M. Baraban, S. Koudelka, D. A. Lyons, Ca²⁺ activity signatures of myelin sheath formation and growth in vivo. *Nat. Neurosci.* **21**, 19–23 (2018).
- S. Ryglewski, H. J. Pflueger, C. Duch, Expanding the neuron's calcium signaling repertoire: Intracellular calcium release via voltage-induced PLC and IP3R activation. *PLoS Biol.* **5**, e66 (2007).
- J. E. Rash *et al.*, KV1 channels identified in rodent myelinated axons, linked to Cx29 in innermost myelin: Support for electrically active myelin in mammalian saltatory conduction. *J. Neurophysiol.* **115**, 1836–1859 (2016).

50. C. Muller, N. M. Bauer, I. Schafer, R. White, Making myelin basic protein—from mRNA transport to localized translation. *Front. Cell Neurosci.* **7**, 169 (2013).
51. L. S. Laursen, C. W. Chan, C. Ffrench-Constant, Translation of myelin basic protein mRNA in oligodendrocytes is regulated by integrin activation and hnRNP-K. *J. Cell Biol.* **192**, 797–811 (2011).
52. J. Eiberger *et al.*, Expression pattern and functional characterization of connexin29 in transgenic mice. *Glia* **53**, 601–611 (2006).
53. D. R. Irvine, V. N. Park, L. McCormick, Mechanisms underlying the sensitivity of neurons in the lateral superior olive to interaural intensity differences. *J. Neurophysiol.* **86**, 2647–2666 (2001).
54. D. J. Tollin, T. C. Yin, Interaural phase and level difference sensitivity in low-frequency neurons in the lateral superior olive. *J. Neurosci.* **25**, 10648–10657 (2005).
55. E. I. Knudsen, Experience alters the spatial tuning of auditory units in the optic tectum during a sensitive period in the barn owl. *J. Neurosci.* **5**, 3094–3109 (1985).
56. A. J. King, C. H. Parsons, D. R. Moore, Plasticity in the neural coding of auditory space in the mammalian brain. *Proc. Natl. Acad. Sci. U.S.A.* **97**, 11821–11828 (2000).
57. F. M. Antunes, M. E. Rubio, K. Kandler, Role of GluA3 AMPA receptor subunits in the presynaptic and postsynaptic maturation of synaptic transmission and plasticity of endbulb-bushy cell synapses in the cochlear nucleus. *J. Neurosci.* **40**, 2471–2484 (2020).
58. I. Joshi, S. Shokralla, P. Titis, L. Y. Wang, The role of AMPA receptor gating in the development of high-fidelity neurotransmission at the calyx of Held synapse. *J. Neurosci.* **24**, 183–196 (2004).
59. A. H. Seidl, B. Grothe, Development of sound localization mechanisms in the mongolian gerbil is shaped by early acoustic experience. *J. Neurophysiol.* **94**, 1028–1036 (2005).
60. A. R. Spurr, A low-viscosity epoxy resin embedding medium for electron microscopy. *J. Ultrastruct. Res.* **26**, 31–43 (1969).

3. Chapter 3 – Potassium channels

Kv3.3 subunits control presynaptic action potential waveform and neurotransmitter release at a central excitatory synapse

Amy Richardson^{1†}, Victoria Ciampani¹, Mihai Stancu², Kseniia Bondarenko^{1‡}, Sherylanne Newton^{1§}, Joern R Steinert^{1#}, Nadia Pilati³, Bruce P Graham⁴, Conny Kopp-Scheinflug², Ian D Forsythe^{1*}

¹Auditory Neurophysiology Laboratory, Department of Neuroscience, Psychology and Behaviour, College of Life Sciences, University of Leicester, Leicester, United Kingdom; ²Division of Neurobiology, Faculty of Biology, Ludwig-Maximilians-University, Munich, Germany; ³Autifony S.r.l., Istituto di Ricerca Pediatrica Citta' della Speranza, Corso Stati Uniti, Padova, Italy; ⁴Computing Science and Mathematics, Faculty of Natural Sciences, University of Stirling, Stirling, United Kingdom

*For correspondence:
idf@le.ac.uk

Present address: [†]Department of Clinical and Experimental Epilepsy, Institute of Neurology, University College London, London, United Kingdom; [‡]Institute of Immunology and Infection Research, University of Edinburgh, Edinburgh, United Kingdom; [§]UCL Ear Institute, University College London, London, United Kingdom; [#]School of Life Sciences, Medical School, University of Nottingham, Nottingham, United Kingdom

Competing interest: See page 27

Funding: See page 28

Received: 02 November 2021

Preprinted: 03 November 2021

Accepted: 29 April 2022

Published: 05 May 2022

Reviewing Editor: Henrique von Gersdorff, Oregon Health and Science University, United States

© Copyright Richardson et al. This article is distributed under the terms of the [Creative Commons Attribution License](https://creativecommons.org/licenses/by/4.0/), which permits unrestricted use and redistribution provided that the original author and source are credited.

Summary: Kv3 potassium currents mediate rapid repolarisation of action potentials (APs), supporting fast spikes and high repetition rates. Of the four Kv3 gene family members, Kv3.1 and Kv3.3 are highly expressed in the auditory brainstem and we exploited this to test for subunit-specific roles at the calyx of Held presynaptic terminal in the mouse. Deletion of Kv3.3 (but not Kv3.1) reduced presynaptic Kv3 channel immunolabelling, increased presynaptic AP duration and facilitated excitatory transmitter release; which in turn enhanced short-term depression during high-frequency transmission. The response to sound was delayed in the Kv3.3KO, with higher spontaneous and lower evoked firing, thereby reducing signal-to-noise ratio. Computational modelling showed that the enhanced EPSC and short-term depression in the Kv3.3KO reflected increased vesicle release probability and accelerated activity-dependent vesicle replenishment. We conclude that Kv3.3 mediates fast repolarisation for short precise APs, conserving transmission during sustained high-frequency activity at this glutamatergic excitatory synapse.

Editor's evaluation

This work shows that Kv3.3 potassium channels play a major role in shaping the presynaptic action potential waveform of calyx-type auditory synapses. Mice that lack Kv3.3 showed auditory response deficits, including increases of spike latency and jitter. Overall, the study shows the uniquely important role for Kv3.3 channels in the fast synaptic transmission between the neurons that compute sound localization in mammals.

Introduction

Kv3 voltage-gated potassium currents rapidly repolarise APs and underlie fast-spiking neuronal phenotypes, enabling high-frequency firing with temporal precision (*Rudy and McBain, 2001; Kaczmarek and Zhang, 2017*). Kv3 channels are expressed throughout the brain including the hippocampus, cortex, cerebellum, and auditory brainstem (*Weiser et al., 1994; Du et al., 2000; Lien and Jonas, 2003*). They influence dendritic integration (*Zagha et al., 2010*) and somatic AP waveform (*Espinosa et al., 2008; Rowan et al., 2014; Choudhury et al., 2020*), but Kv3 channels are also located in

particular axons, including nodes of Ranvier (*Devaux et al., 2003*) and synaptic terminals (*Schneggenburger and Forsythe, 2006*).

There are four Kv3 genes (*kcnc1-4*) specifying alpha subunits (Kv3.1–3.4) that assemble as tetramers (*Coetzee et al., 1999; Rudy et al., 1999*). The transmembrane domains are generally well conserved across subunits, but both the N- and C-terminal domains have diverse sequences, creating distinct inactivation kinetics, interaction with cytoskeletal proteins (*Blosa et al., 2015; Stevens et al., 2021*) and regulation by phosphorylation (*Macica et al., 2003; Song et al., 2005; Desai et al., 2008*). Kv3 channels display ultra-fast kinetics (*Grissmer et al., 1994; Labro et al., 2015*) with half-activation at positive voltages, making them particularly effective in AP repolarisation (*Brew and Forsythe, 1995*). N-type inactivation is a powerful means of regulating K⁺ channel activity (*Hoshi et al., 1990*) and inactivation in the Kv3 family is influenced by the subunit(s) expressed and their regulation by protein phosphorylation (see *Kaczmarek and Zhang, 2017*).

Transgenic knockouts of one subunit generally show mild phenotypes, consistent with heterogeneous composition of native channels and functional redundancy (*Joho et al., 1999; Espinosa et al., 2001; Joho et al., 2006*). Co-expression of Kv3.1 and Kv3.3 has been widely observed in different brain regions (*Chang et al., 2007*) and we recently showed that principal neurons of the medial nucleus of the trapezoid body (MNTB) within the auditory brainstem, have Kv3 channels composed of Kv3.1 and Kv3.3 subunits. In the MNTB, in contrast to the lateral superior olive, each subunit type can compensate for deletion of the other (*Choudhury et al., 2020*).

Changes in AP waveform at the synaptic terminal critically control calcium influx and neurotransmitter release (*Borst and Sakmann, 1998; Forsythe et al., 1998; Yang et al., 2014*), this in turn influences short-term plasticity (*Sakaba and Neher, 2003; Hennig et al., 2008; Neher and Sakaba, 2008; Neher, 2017; Lipstein et al., 2021*) and presynaptic forms of long term potentiation at mossy fiber terminals (*Geiger and Jonas, 2000*). Indeed, tuning of voltage-gated sodium and potassium channel kinetics not only enhances fast signaling, but also increases metabolic efficiency (*Hu et al., 2018*). In the present study, we took advantage of the calyx of Held giant synapse in the MNTB to investigate the role of Kv3 subunits at that presynaptic terminal. These binaural auditory nuclei must rapidly integrate AP trains transmitted from left and right cochlea with microsecond accuracy (*Beiderbeck et al., 2018; Joris and Trussell, 2018; Karcz et al., 2011*). The region expresses Kv3.1 and Kv3.3 subunits, with little or no Kv3.2 and Kv3.4 (*Choudhury et al., 2020*). This synapse is optimised for speed and fidelity (*Taschenberger et al., 2002*) and is operating at the 'biophysical limit' of information processing, in that fast conducting axons and giant synapses with nano-domain localisation of P/Q Ca²⁺ channels, combine with postsynaptic expression of fast AMPARs, short postsynaptic membrane time-constants and exceptionally rapid APs to enable binaural sound localisation (*Schneggenburger and Forsythe, 2006; Neher and Sakaba, 2008; Joris and Trussell, 2018; Young and Veeraraghavan, 2021*).

In this study, we test whether Kv3.1 or Kv3.3 subunits have a specific presynaptic role by examining the calyx of Held AP waveform and transmitter release on deletion of either subunit. We show that Kv3.3 subunits are localised to the presynaptic terminal and that their deletion increases transmitter release. We demonstrate the role of Kv3.3 in enhancing the speed and reliability of brainstem binaural auditory processing and conclude that presynaptic Kv3.3 subunits are essential for fast AP repolarisation at this excitatory synapse.

Results

The experiments reported here were conducted using CBA/CrL wildtype mice or transgenic mice backcrossed onto CBA/CrL that lacked either Kv3.3 or Kv3.1 (the genotypes are referred to as WT, Kv3.3KO and Kv3.1KO). We previously reported that Kv3.1 and Kv3.3 mRNAs are highly expressed in the MNTB, and no compensation for either subunit in the respective knockouts was observed (*Choudhury et al., 2020*). The influence of these deletions was assessed in vivo using extracellular recording from the MNTB and in vitro using whole cell patch clamp from the calyx of Held and MNTB principal neurons. Additionally, immunohistochemical localisation of Kv3.1 and Kv3.3 was determined using expansion microscopy. Together, these methods were applied to determine the contribution of Kv3 subunits to the presynaptic AP waveform, to assess the impact on transmitter release and determine how this impacts the response to sound. As an additional control, we confirmed that both Kv3.1 and Kv3.3 mRNA are present in the cochlear nucleus where globular bushy cells give rise to the calyx of Held synaptic terminal. The percent contribution of each subunit gene to the cochlear

nucleus Kv3 mRNA was $30.3\% \pm 9.1\%$ (Kv3.1), $7.7\% \pm 2.8\%$ (Kv3.2), $52.0\% \pm 6.0\%$ (Kv3.3), and $10.0\% \pm 1.6\%$ (Kv3.4; for data see **Figure 1—figure supplement 1** and summary statistics). These values are similar to those measured in the MNTB (**Choudhury et al., 2020**). Additionally, immunohistochemistry confirmed that both spiral ganglion neurons and cochlear nucleus have broad neuronal staining for Kv3.1 and Kv3.3 and as validated using tissue from knockout mice (**Figure 1—figure supplements 2 and 3**).

Kv3 channels contribute to action potential repolarisation at the calyx of Held terminal

Previous reports have employed potassium channel blockers (4-aminopyridine or tetraethylammonium) to show that Kv3 currents contribute to fast repolarisation of APs in the MNTB (**Forsythe, 1994; Brew and Forsythe, 1995; Wang et al., 1998**). Low concentrations of extracellular TEA (1 mM) give a relatively selective block of Kv3 potassium channels (**Johnston et al., 2010**). Whole terminal voltage-clamp recordings of the calyx terminal revealed an outward current, as shown in the current-voltage relations in **Figure 1A**, with 1 mM TEA blocking 28.7% of the total outward current at a command voltage of +10 mV (current amplitude in WT = 9.37 ± 2.6 nA, $n=7$ calyces; WT+TEA = 6.68 ± 0.9 nA, $n=6$; unpaired t-test, $p=0.037$; mean \pm SD). Injection of depolarising current steps (100 pA, 50ms) under current-clamp triggered a single AP in the presynaptic terminal, (**Figure 1B**) which increased in duration on perfusion of 1 mM TEA (**Figure 1C**; with inset showing \pm TEA overlay). In tissue from WT mice the mean AP half-width increased from 0.28 ± 0.02 ms (control; $n=9$) to 0.51 ± 0.1 ms ($n=7$) in the presence of 1 mM TEA (**Figure 1E**), supporting the hypothesis that presynaptic Kv3 channels are present and contribute to AP repolarisation at the calyx of Held.

AP duration increased in terminals from Kv3.3KO mice, similar to that from WT mice in the presence of TEA. In contrast, the AP duration recorded from terminals of Kv3.1KOs was comparable to WT APs (see **Figure 1D and E**). AP half-widths increased from 0.28 ± 0.02 ms in WT ($n=9$) and 0.32 ± 0.02 ms Kv3.1KOs ($n=5$) to 0.43 ± 0.03 ms in Kv3.3KO mice ($n=6$) and 0.51 ± 0.1 ms in WT+TEA ($n=7$). This increase in duration at 50% amplitude was accompanied by a slowed rate of AP decay in both Kv3.3KO terminals and WT terminals upon perfusion of TEA (**Figure 1G**, one-way ANOVA, Tukey's post hoc, Kv3.3KO vs WT $p=0.0042$; TEA vs WT $p=0.0016$) with no changes in the rising phase of the AP (one-way ANOVA, $p=0.50$; **Figure 1H**), nor in the resting (input) membrane conductance (one-way ANOVA, $p=0.56$; **Figure 1I**) or AP threshold (one-way ANOVA, $p=0.96$; see statistics table). Similar significant changes in AP duration were observed at 25% and 75% amplitudes for deletion of Kv3.3, but deletion of Kv3.1 did not significantly change AP duration at 25%, 50%, or 75% amplitude (see **Figure 1—figure supplement 4**). This suggests that Kv3.3 subunits are of most importance for presynaptic Kv3 channels and fast AP repolarisation. Despite the lack of a significant increase in action potential duration measured in Kv3.1KOs, the rate of decay was significantly slowed from 99 ± 20 mV/ms ($n=10$) to 66 ± 16 mV/ms ($n=5$; one-way ANOVA, Tukey's post hoc, $p=0.02$), consistent with Kv3.1 having a secondary role in presynaptic AP repolarisation, as might be expected from their localisation at axonal nodes of Ranvier (**Devaux et al., 2003**) and potential to form heteromers with Kv3.3 subunits.

Immunohistochemical localisation shows that presynaptic Kv3 channels require the presence of a Kv3.3 subunit

Since Kv3 channels are present in both the presynaptic calyx of Held and the postsynaptic MNTB neuron, conventional fluorescence immunohistochemistry fails to resolve any differential localisation of particular subunits in the presynaptic or postsynaptic membranes. An additional complication is that few studies have localised both Kv3.1 and Kv3.3 subunits, most focus on imaging one subunit (usually Kv3.1). Electron microscopic studies demonstrated that Kv3.1b is present in the membrane of the non-release face of the calyx of Held (**Elezgarai et al., 2003**), while **Wu et al., 2021** show that Kv3.3 is present at the release face of the calyx. Kv3.3 has also been demonstrated at terminals in the medial vestibular nucleus (**Brooke et al., 2010**) at the neuromuscular junction (**Brooke et al., 2004**) and in hippocampal mossy fibers (**Chang et al., 2007**). Hence, there is histological evidence for Kv3.1 and Kv3.3 at specific presynaptic terminals, but they are not universally expressed at all synaptic terminals.

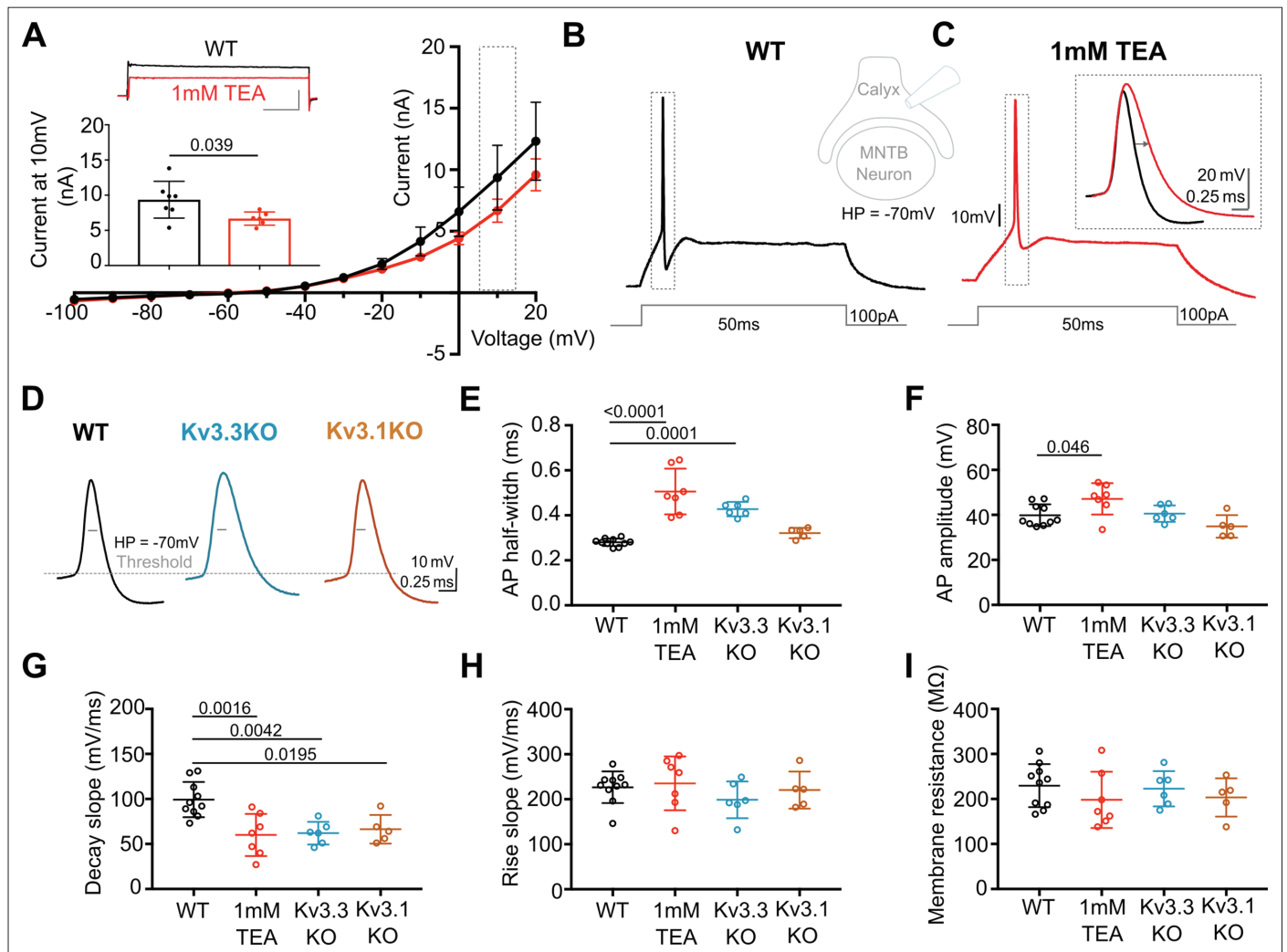


Figure 1. Presynaptic AP duration is increased by TEA or Kv3.3 deletion. **(A)** Current-Voltage (I–V) relationship for potassium currents in the calyx of Held terminal of WT mice (P10–P12) in control (black; n=7 terminals, 4 mice) and TEA, 1 mM (red, n=6 terminals, 5 mice; HP = –70 mV). **Inset (top):** Example current traces in response to voltage command of +10 mV step (grey box in IV) in WT (black) and WT +1 mM TEA (red). Scale bars = 5 nA and 20ms. **Inset (lower):** Bar graph of mean currents ± SD, measured on step depolarisation to +10 mV (from HP –70 mV) ±1 mM TEA. Outward currents are significantly reduced by TEA (student’s t-test, unpaired, P=0.0386). **(B)** WT calyx AP (black trace) evoked by 100 pA step current injection; **inset** - diagram of recording configuration. **(C)** WT calyx AP in the presence of TEA (1 mM, red trace); **inset** - overlaid WT APs ±TEA (red) as indicated by dotted box (grey) around APs in B and C. **(D)** Representative AP traces from calyx terminals of WT (black), Kv3.3KO (blue), and Kv3.1KO (orange); double arrows indicate the half-width of WT AP. AP threshold is indicated by the grey dashed line. **(E)** AP half-width measured as time difference between rise and decay phases at 50% maximal amplitude. Half-width is significantly increased in TEA and in Kv3.3KO; N is individual terminals: WT N=9 from 6 animals; TEA = 7 from 5 mice; Kv3.3KO = 6 from 3 mice and Kv3.1KO = 5 from 3 mice. **(F)** AP amplitude, **(G)** AP Decay slope, **(H)** AP rise slope (10–90%) and **(I)** membrane resistance for calyceal recordings. Average data presented as mean ± SD. Statistical test (parts E–I) were one-way ANOVAs and Tukey’s post hoc for multiple comparisons, with significant Ps indicated on the graph.

The online version of this article includes the following source data and figure supplement(s) for figure 1:

Source data 1. Relates to **Figure 1**.

Figure supplement 1. WT mRNA Levels for *Kcnc* family genes in the cochlear nucleus which show a similar pattern of expression to those measured previously for the MNTB (Choudhury et al., 2020).

Figure supplement 1—source data 1. Relates to **Figure 1—figure supplement 1**.

Figure supplement 2. Kv3.1 and Kv3.3 immunoreactivity in the cochlear nucleus of CBA WT mice.

Figure supplement 3. Kv3.1 and Kv3.3 are present in spiral ganglion neurons of CBA WT mice.

Figure 1 continued on next page

Figure 1 continued

Figure supplement 4. Repolarisation of the presynaptic AP is slowed during the entire length of the downstroke in the presence of 1 mM TEA and in Kv3.3KOs.

Figure supplement 4—source data 1. Relates to **Figure 1—figure supplement 4**.

Capitalising on using KO-validated antibodies (*Choudhury et al., 2020 Figure 1—figure supplement 3*), we have employed protein-retention expansion microscopy (*Asano et al., 2018*) to increase resolution and gain more precision in localising Kv3.1 and Kv3.3 subunits at the calyx of Held synaptic terminal. The technique employs a hydrogel to expand the tissue by ~4.5 x prior to confocal imaging. We compared the location of Kv3 subunits in the three genotypes: antibodies targeting Kv3.3 were employed in the Kv3.1KO, antibodies against Kv3.1 were used in tissues from the Kv3.3KO and both Kv3.1 and Kv3.3 antibodies were employed in WT tissue. This experiment asks whether either Kv3.1 or Kv3.3 subunits are necessary and sufficient to enable presynaptic localisation of Kv3 channels. Synaptic release sites were identified using bassoon antibodies (*Chen et al., 2013*) to label the presynaptic specialisation and the results are shown in **Figure 2**.

In **Figure 2**, the two quadrants on the left show Kv3.3 staining (in the Kv3.1KO above, and WT, below) and the two right quadrants show Kv3.1 staining (in the Kv3.3KO above, and WT, below) in yellow. All sections are co-stained with bassoon (purple). Each quadrant shows single optical sections from three different MNTB neuron/calyx pairs shown at lower magnification in the respective top row. Kv3.3 staining was clearly present in the presynaptic terminal profiles surrounding each of the 3 MNTB neurons which lacked Kv3.1 (**Figure 2A1–C1**). In contrast, Kv3.1 labelling (from the Kv3.3KO tissue) showed little evidence of presynaptic labelling (**Figure 2D1–F1**). As a positive control, Kv3.1 labelling was robust in the postsynaptic membrane; and indeed Kv3.3 is also clearly present in the postsynaptic membrane. Each neuron in rows 1 and 4 has two synaptic profiles indicated by the orange and green arrowheads, each of these synapses are shown enlarged below their neuron of origin in rows 2 and 3 and rows 5 and 6, respectively. Similar labelling profiles are observed in the WT tissue (lower quadrants of **Figure 2A4–F4**). As for the KO tissue, two examples of WT presynaptic profiles are indicated by the coloured arrows and their enlargement shown below each principal neuron. The Kv3.3 antibody staining was clearly observed in the presynaptic membrane on the non-release face of the WT synapse (for example see **Figure 2B2 and C3, A6**) and in some image sections the release face of the synapse, between bassoon labelling (see **Figure 2C3, B5 and A6**) was clear. It was hard to visualise presynaptic membrane staining with the Kv3.1 antibody in the Kv3.3KO tissue (**Figure 2D2, E3 and F2**); but some Kv3.1-stained membrane profiles were observed on the non-release face in the WT tissue (**Figure 2E5, E6 and F6**).

While the calyceal Kv3.3 staining in the WT is similar to that in the Kv3.1KO, the levels of Kv3.1 staining in the WT are higher (than in the Kv3.3KO) consistent with the hypothesis that Kv3.1 may gain access to the presynaptic compartment through heteromeric assembly with Kv3.3 subunits. This data shows that while both Kv3.1 and Kv3.3 subunits are present in the postsynaptic soma membrane, only Kv3.3 subunits are required to achieve trafficking of Kv3 channels to the presynaptic terminal; and there is some evidence that the presence of Kv3.3 permits access of Kv3.1 subunits to the terminal, while both Kv3.1 and Kv3.3 were localised to the postsynaptic plasma membrane in the WT tissue.

Deletion of Kv3.3 subunits increases calyceal-evoked EPSC amplitude

Transmitter release crucially depends on depolarisation of the presynaptic membrane and consequent calcium influx. Since Kv3 channels are present and involved in calyceal AP repolarisation, we assessed the physiological impact of each Kv3 subunit on transmitter release, and compared this to WT and to transmitter release following pharmacological block of presynaptic Kv3 channels using 1 mM TEA.

Whole cell patch recordings under voltage-clamp (HP = -40 mV, to inactivate voltage-gated Na⁺ channels) were made from MNTB neurons possessing an intact calyx, in tissue from mice of each genotype and in the presence of 1 mM TEA. This allows comparison of the EPSC amplitude in four conditions: where Kv3 channels are intact (WT) and where they lack Kv3.1 or Kv3.3, and finally with all presynaptic Kv3 channels blocked (TEA). Unitary calyceal EPSCs were evoked in MNTB principal neurons as shown in **Figure 3A and F**. The global average for each condition and the unitary mean evoked EPSCs are overlaid from each genotype in **Figure 3F**. The dashed grey line shows the WT mean amplitude for comparison. The calyceal EPSCs recorded from Kv3.3KO mice were of larger peak

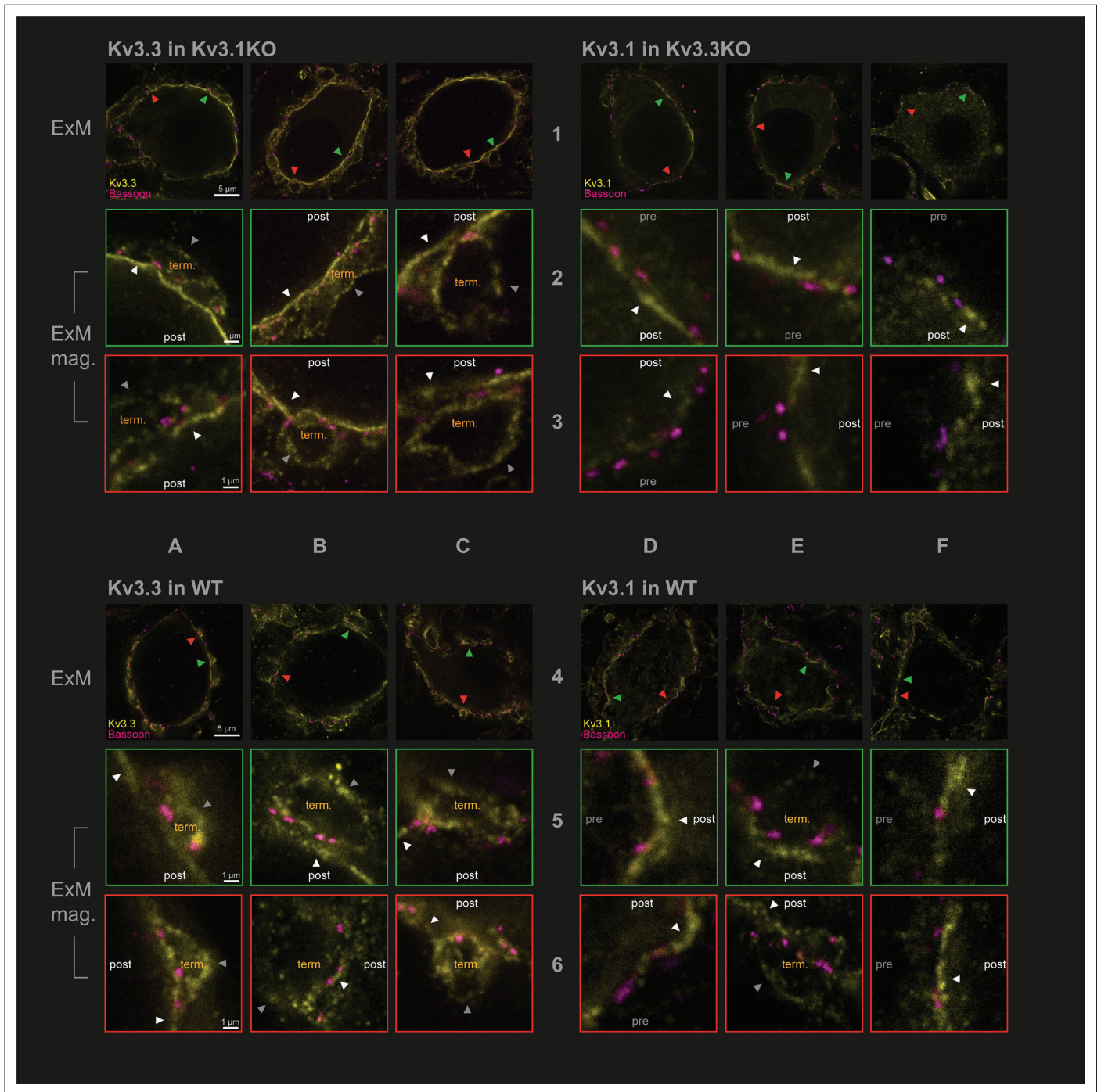


Figure 2. Protein-retention Expansion Microscopy (proExM) with confocal fluorescence imaging shows that Kv3.3 subunits are present in calyx of Held presynaptic terminal membrane. Individual images are identified in rows 1–6 and columns A–F, as indicated by the central labels. Four quadrants of 9 images are shown, each 3 × 3 matrix is from the named genotype and stained as specified in the title of each quadrant. The top row of each quadrant (rows 1 and 4) are single optical sections from 3 different MNTB neurons, in which their calyceal synaptic profiles are labelled with bassoon (purple) and co-labelled with either Kv3.1 or Kv3.3 antibodies (yellow): from Kv3.1KO and stained for Kv3.3 (**A1–C1**); the Kv3.3KO stained for Kv3.1 (**D1–F1**); WT stained for Kv3.3 (**A4–C4**); WT stained for Kv3.1 (**D4–F4**). In each MNTB neuron (rows 1 & 4) two synaptic regions of interest (ROI) containing bassoon are indicated by the red and green arrowheads. These magnified ROIs are displayed below (in rows 2+3 or 5+6) bordered by the same colour, respectively. The neuronal compartments are labelled: ‘post’ – postsynaptic; ‘pre’ – presynaptic; ‘term.’ – synaptic terminal. In each image, the dark grey arrows point to presynaptic Kv3 labelling, and the white arrows point to postsynaptic Kv3 labelling. Scale bars are indicated for each row in column A (5 μm in rows 1 and 4; 1 μm in rows 2,3,5, and 6). Tissue was used from mice aged P28–P30.

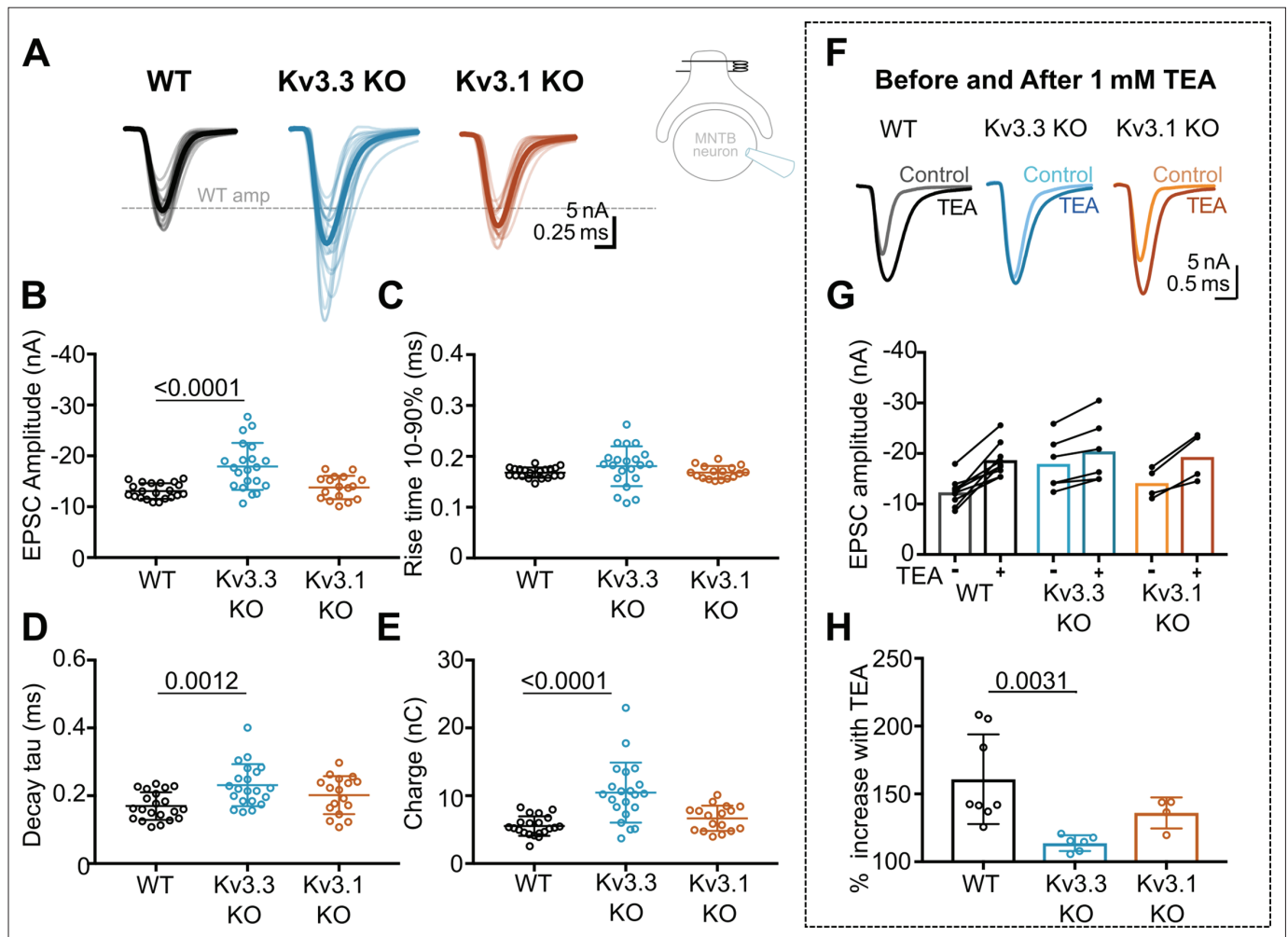


Figure 3. Kv3.3 deletion increases EPSC amplitude and occludes block by TEA. **(A)** Superimposed calyceal EPSCs generated from each genotype (age P21-P25): wildtype (WT; black), Kv3.3KO (blue), and Kv3.1KO mice (orange). Thin lines show traces from individual neurons (each is mean of 5 EPSCs) with thick line showing the population mean for each genotype. Grey dashed line indicates the average WT amplitude; N=WT, 22 neurons (11 mice); Kv3.3KO, 22 neurons (10 mice); Kv3.1KO, 17 neurons (8 mice). Inset shows recording and stimulation configuration. **(B)** EPSC amplitude increased in the Kv3.3KO. **(C)** EPSC rise time (10–90%) no difference was found between groups (one-way ANOVA, $p=0.1576$). **(D)** EPSC decay tau and **(E)** EPSC total charge were increased in the Kv3.3KO relative to WT. **(F)** EPSC traces from WT, Kv3.3KO, and Kv3.1KO mice, before and after the addition of 1 mM TEA. **(Centre):** EPSC amplitudes recorded before and after perfusion of TEA (1 mM); n=WT, 9 neurons (7 mice); Kv3.3KO, 6 neurons (3 mice); Kv3.1KO, 5 neurons (3 mice). **(G)** Increase in EPSC amplitude by 1 mM TEA. **(H)**. The amplitude increase induced by TEA was significantly reduced in Kv3.3KO mice compared to WT. Average data presented as mean \pm SD; statistics was using one-way ANOVA with Tukey's post hoc for multiple comparisons. Kruskal-Wallis ANOVA with Dunn's multiple corrections was used to compare change to EPSC amplitude in TEA due to a non-gaussian distribution in WT.

The online version of this article includes the following source data and figure supplement(s) for figure 3:

Source data 1. Relates to **Figure 3**.

Figure supplement 1. mEPSCs recorded from Kv3.3KO mice have a decreased amplitude.

Figure supplement 1—source data 1. Relates to **Figure 3—figure supplement 1**.

amplitude and longer lasting compared to WT or Kv3.1KOs, consistent with increased transmitter release from the calyx of Held in the Kv3.3KO.

The data for EPSC peak amplitude, rise-time, decay tau and charge are plotted in **Figure 3B–E**, respectively, for each genotype. EPSC amplitudes were similar in WT and Kv3.1KO, -13 ± 2 nA ($n=21$) and -14 ± 2 nA ($n=17$), respectively; but increased significantly in the Kv3.3KO to -18 ± 5 nA ($n=21$); one-way ANOVA, Tukey's post hoc, Kv3.3KO vs WT, $p=0.0001$; Kv3.3KO vs Kv3.1KO $p=0.0005$). The decay tau for the EPSCs in the Kv3.3KO slowed to 0.23 ± 0.06 ms ($n=21$) compared to 0.17 ± 0.04 ms

in WT ($n=21$; one-way ANOVA, Tukey's post hoc, $p=0.0012$). The total charge of EPSCs in Kv3.3KOs increased to -10 ± 4 nC ($n=21$) compared to -6 ± 1 nC and -7 ± 2 nC in WT ($n=21$) and Kv3.1KOs ($n=17$), respectively (one-way ANOVA, Tukey's post hoc; Kv3.3KO vs WT, $p=0.0001$; Kv3.3KO vs Kv3.1KO $p=0.0007$). No change of EPSC rise time was observed in either KO (one-way ANOVA, $p=0.1918$). Examination of miniature EPSCs in postsynaptic MNTB neurons from each genotype (**Figure 3—figure supplement 1**) showed no difference in the mEPSC frequency, rise-time or decay tau. There was a small significant decrease in quantal amplitude in the Kv3.3KO relative to WT, but no change in the Kv3.1KO. This contrasts with the increased amplitude of the evoked EPSCs in the Kv3.3KO measured here, and perhaps reflects an opposing change in synaptic scaling due to the larger transmitter release induced in the Kv3.3KO (Tatavarty et al., 2013).

The increased EPSC amplitude observed in Kv3.3KOs suggests that Kv3.3 subunits are major contributors to repolarisation of the presynaptic terminal. If Kv3.3 subunits dominate presynaptic Kv3 channels, then blocking presynaptic Kv3 channels with TEA will have a lesser effect on EPSCs from the Kv3.3KO. To test this hypothesis, we compared the effect of 1 mM TEA on EPSC amplitude from each of the three genotypes (**Figure 3F–H**). Indeed, blocking Kv3 channels with TEA had a much smaller effect on EPSC amplitude in the Kv3.3 KO compared to WT and Kv3.1 KO. TEA increased EPSC amplitude to $160\% \pm 33\%$ ($n=8$) in WT, compared to $114\% \pm 6\%$ ($n=6$) in Kv3.3KO (Kruskal-Wallis, Dunn's multiple comparison, $p=0.0031$). The EPSC amplitude in the Kv3.1KO ($136\% \pm 11\%$, $n=4$) was not significantly different from WT (Kruskal-Wallis, Dunn's multiple comparison $p=0.99$). This result is consistent with dominance of presynaptic repolarisation by channels containing Kv3.3.

Enhanced short-term depression in Kv3.3KO

The calyx of Held/MNTB synapse is capable of sustained transmission at firing frequencies of around 300 Hz in vivo (Kopp-Scheinflug et al., 2008) (also see Figure 8), encoding information about sound stimuli for binaural integration with high temporal precision. Indeed, the calyx of Held giant synapse can sustain short AP bursts with peak firing rates of up to 1000 Hz, in vitro (Kim et al., 2013) for a few milliseconds. Clearly, the increased transmitter release observed in the Kv3.3KO (**Figure 3**) has consequences for maintenance of EPSC amplitude during repetitive firing, in that vesicle recycling and priming must rapidly replace docked vesicles if transmitter release is to be maintained for the duration of the high frequency train. Repetitive stimulation shows that the evoked EPSC amplitude declines during a stimulus train until rates of vesicle priming are in equilibrium with the rate of transmitter release for a given stimulus frequency. To assess repetitive transmitter release in each of the genotypes we evoked EPSCs over a range of frequencies from 100 to 600 Hz (with each stimulus train lasting 800ms).

Whole-cell patch recordings from voltage-clamped MNTB neurons ($HP = -40$ mV) were conducted in which calyceal EPSC trains were evoked at 100 Hz, 200 Hz, or 600 Hz. Each train was repeated three times, with a resting interval of 30 s between repetitions of stimuli trains. The EPSC amplitudes during the trains were compared in MNTB neurons of each genotype: WT (black), Kv3.3KO (blue) and Kv3.1KO (orange) mice. The first EPSC amplitude in trains delivered to the calyx/MNTB from the Kv3.3KO mouse was of larger amplitude than observed in WT or in the Kv3.1KO and subsequent EPSCs showed a larger short-term depression. In **Figure 4A–C** a matrix of EPSC trains are plotted with the same stimulus frequency in each row for each genotype. The inset traces show the first 3 EPSCs and the last 3 EPSCs in each train, with the black arrow heads indicating the WT amplitude for comparison across genotypes.

Paired pulse ratio (PPR) was significantly decreased in the Kv3.3KO compared to both WT and Kv3.1KO at 100 Hz, 200 Hz, and 600 Hz, with mean PPR ($EPSC_2/EPSC_1$) plotted in **Figure 4D** (left column). This enhanced depression of EPSC amplitude was maintained for the duration of the train shown in comparison with the 80th EPSC in the train ($EPSC_{80}/EPSC_1$; **Figure 4D**, right column; **Table 1**).

The mean data, normalized to the amplitude of the first EPSC, is plotted for each genotype at the stated stimulus frequency: **Figure 4E–G** (100–600 Hz). There are two key parameters plotted below each depression curve: first, the short-term depression decay time-constant (Decay Tau, defined as the rate at which the EPSC amplitude equilibrates to the new steady-state amplitude at each stimulus frequency); and second, amplitude at steady-state (the amplitude of the new steady-state EPSC during the train, relative to $EPSC_1$). The Kv3.3KO consistently showed the fastest rate of short-term depression, compared to WT and Kv3.1KOs; this was highly significant at 100 Hz and 200 Hz (**Table 1**).

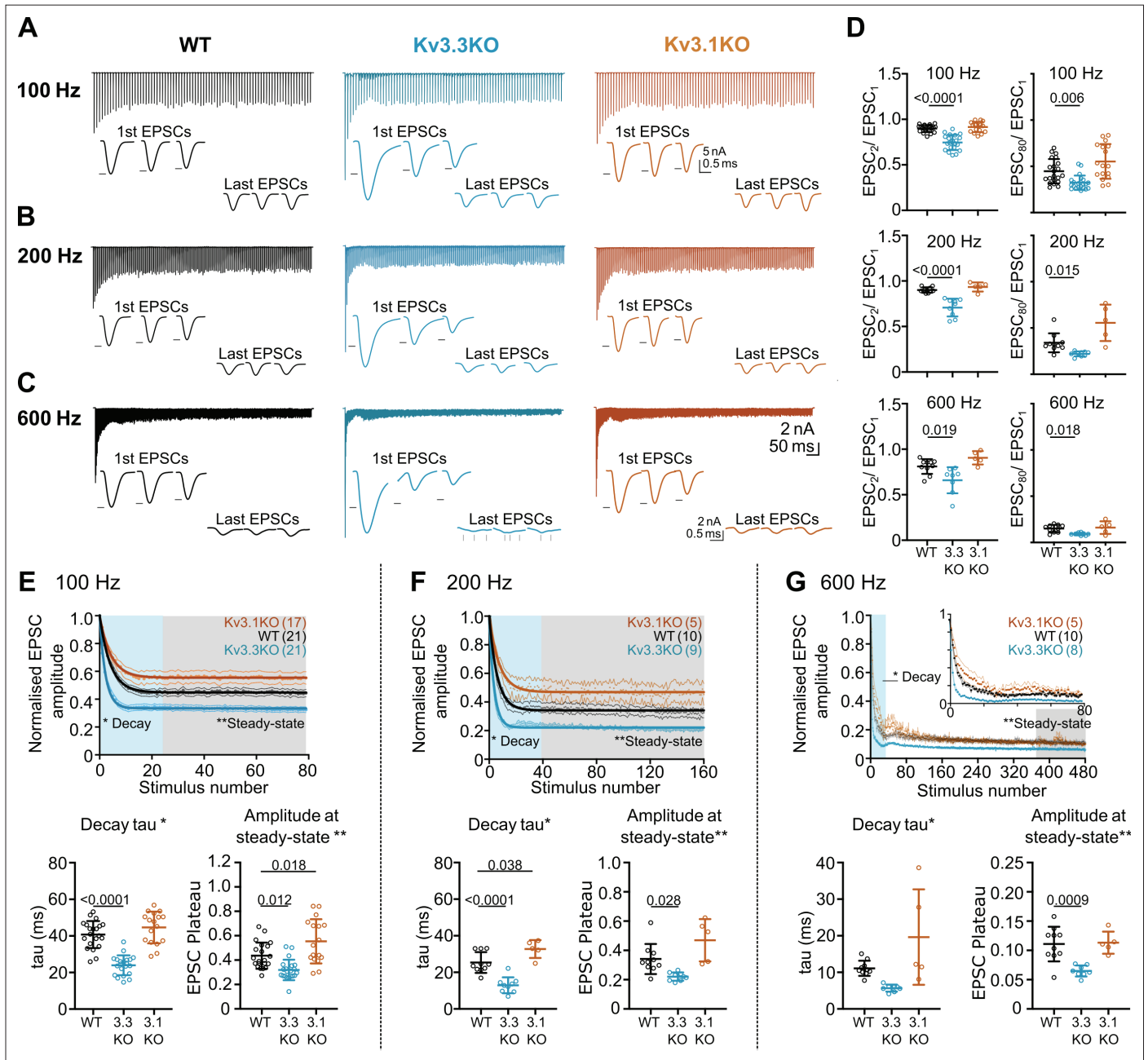


Figure 4. Evoked EPSC short-term depression is faster and more pronounced in the Kv3.3KO. **(A,B,C)** Example MNTB EPSC trains (800ms) on stimulation at **(A)** 100, **(B)** 200 or **(C)** 600 Hz for WT (left, black), Kv3.3KO (middle, blue), and Kv3.1KO (right, orange) mice (aged P21-P25). Each trace shows an average of 5 trials from a single neuron with stimulus artefacts removed for clarity. Lower insets: The first and last three EPSC traces are shown below each train. Black arrows show EPSC amplitudes from the WT mouse (left). Vertical grey arrows indicate multiple, asynchronous responses in the final EPSCs of Kv3.3KO traces. **(D)** Paired-pulse ratios for EPSC₂/EPSC₁ (left) and EPSC₈₀/EPSC₁ (right) generated in response to 100 Hz (top), 200 Hz (middle), and 600 Hz (bottom); in each case the ratio is significantly decreased in Kv3.3KO with respect to WT. For 100 Hz - WT: N=21 cells (11 mice); Kv3.3KO: N=21 (10 mice); Kv3.1KO: N=17 (8 mice); for 200 and 600 Hz - WT: N=10 (6 mice); Kv3.3KO: N=9 (4 mice); Kv3.1KO: N=5 (3 mice). Data shows mean ± SD and statistical significance estimated by one-way ANOVAs with Tukey's post hoc for multiple comparisons or Kruskal-Wallis with Dunn's multiple comparison (EPSC₈₀/EPSC₁ at 100 and 200 Hz due to non-gaussian data distributions), significant P values given on the respective graphs. **(E, F, G)** Normalised EPSCs, short-term depression is faster and larger in Kv3.3KO mice (compared to WT and Kv3.1KO mice) **(E)** 100 Hz **F:** 200 Hz **G:** 600 Hz. The rate of EPSC depression is plotted as a single exponential tau (lower left) and normalised EPSC amplitudes at steady-state are plotted (lower right) for each genotype and stimulus frequency. N numbers are presented in brackets on normalised EPSC amplitude graphs (and are the same neurons as Figure 4 continued on next page

Figure 4 continued

used in D). One-way ANOVAs with Tukey's post hoc for multiple comparison correction were used to test significance, p values reported on graphs. All data plotted as mean ± SD, except in graphs of normalised EPSC amplitudes (E, F, and G, top) where data is plotted as mean ± SEM for clarity.

The online version of this article includes the following source data for figure 4:

Source data 1. Relates to **Figure 4**.

This trend continued so that during stimuli at 600 Hz (**Figure 4G**), a further increase in the rate of short-term depression was observed; again, this was most marked in EPSC trains from the Kv3.3KO compared to both WT and Kv3.1KO. The decay time-constant for short-term depression was 6 ± 1 ms for Kv3.3KOs (n=8), 11 ± 2 ms for WT (n=10) and 20 ± 13 ms for Kv3.1KOs (n=5; **Table 1**).

Following short-term depression, the 'steady-state' EPSC amplitude was achieved after 20–40 evoked responses (**Figure 4E, F and G**; lower right graph). This reflects the net equilibrium achieved under control of four key presynaptic parameters: probability of transmitter release, the rate of AP stimulation, the rate of vesicle replenishment at the release sites and the size of the vesicle pool (see modelling section below). In young animals, postsynaptic AMPAR desensitisation can also play a role in short-term depression, but this is a minor contribution at mature synapses and physiological temperatures, as employed here (**Taschenberger et al., 2002; Wong et al., 2003**). At all frequencies, EPSCs from the Kv3.3KO mice showed lower amplitude steady-state values in comparison to WT; while the Kv3.1KO data was either the same or greater than WT (**Figure 4E, Table 1**).

Table 1. Short-term depression was accelerated and enhanced in mice lacking Kv3.3.

Values shown are for parameters measured from data presented in **Figure 3** for WT, Kv3.3KO and Kv3.1KO genotypes at 100 Hz to 600 Hz range. Paired pulse depression of EPSC responses recorded in MNTB neurons ($EPSC_2/EPSC_1$) was increased in Kv3.3 KO animals during high frequency stimulation of the calyx. The increased depression was maintained throughout the stimulation train ($EPSC_{80}/EPSC_1$) across all frequencies. The rate of short term-depression in EPSC amplitudes during EPSC trains (duration 800ms), measured as short-term depression (STD) decay tau was significantly increased in Kv3.3 KOs at 100 and 200 Hz compared to WT. This STD was more severe in mice lacking Kv3.3, as shown by decreased normalized steady-state EPSC amplitudes compared to WT. STD tau and steady state amplitudes were measured using a single exponential fit to normalized EPSC amplitudes throughout the 800ms stimulation trains. n=number of neurons. Values in bold are significantly different to WT (see statistics table for more detail). Data represented as mean ± SD.

		WT	Kv3.3KO	Kv3.1KO
100 Hz	EPSC ₂ /EPSC ₁ Ratio	0.90±0.04 (n=21)	0.75±0.08 (n=21)	0.92±0.06 (n=17)
	EPSC ₈₀ /EPSC ₁ Ratio	0.45±0.13 (n=21)	0.32±0.08 (n=21)	0.55±0.19 (n=17)
	STD tau (ms)	41±7 (n=21)	24±5 (n=21)	45±2 (n=17)
	Norm. steady-state amp	0.4±0.1 (n=21)	0.3±0.08 (n=21)	0.6±0.2 (n=17)
	EPSC ₂ /EPSC ₁ Ratio	0.90±0.03 (n=10)	0.71±0.1 (n=9)	0.93±0.05 (n=5)
	EPSC ₈₀ /EPSC ₁ Ratio	0.34±0.10 (n=10)	0.22±0.03 (n=9)	0.56±0.20 (n=5)
	STD tau (ms)	25±6 (n=10)	13±4 (n=9)	33±5 (n=5)
200 Hz	Norm. steady-state amp	0.3±0.10 (n=10)	0.2±0.03 (n=9)	0.5±0.1 (n=5)
	EPSC ₂ /EPSC ₁ Ratio	0.91±0.06 (n=8)	0.68±0.10 (n=9)	0.91±0.15 (n=6)
	EPSC ₈₀ /EPSC ₁ Ratio	0.25±0.19 (n=8)	0.1±0.02 (n=9)	0.18±0.042 (n=6)
	STD tau (ms)	7±5 (n=7)	3±1 (n=6)	5±2 (n=4)
400 Hz	Norm. steady-state amp	0.26±0.12 (n=6)	0.12±0.04 (n=7)	0.12±0.04 (n=3)
	EPSC ₂ /EPSC ₁ Ratio	0.8±0.08 (n=10)	0.7±0.1 (n=8)	0.9±0.07 (n=5)
	EPSC ₈₀ /EPSC ₁ Ratio	0.15±0.04 (n=10)	0.09±0.01 (n=8)	0.16±0.07 (n=5)
	STD tau (ms)	11±2 (n=10)	6±1 (n=8)	20±13 (n=5)
600 Hz	Norm. steady-state amp	0.11±0.03 (n=10)	0.07±0.01 (n=8)	0.11±0.02 (n=5)

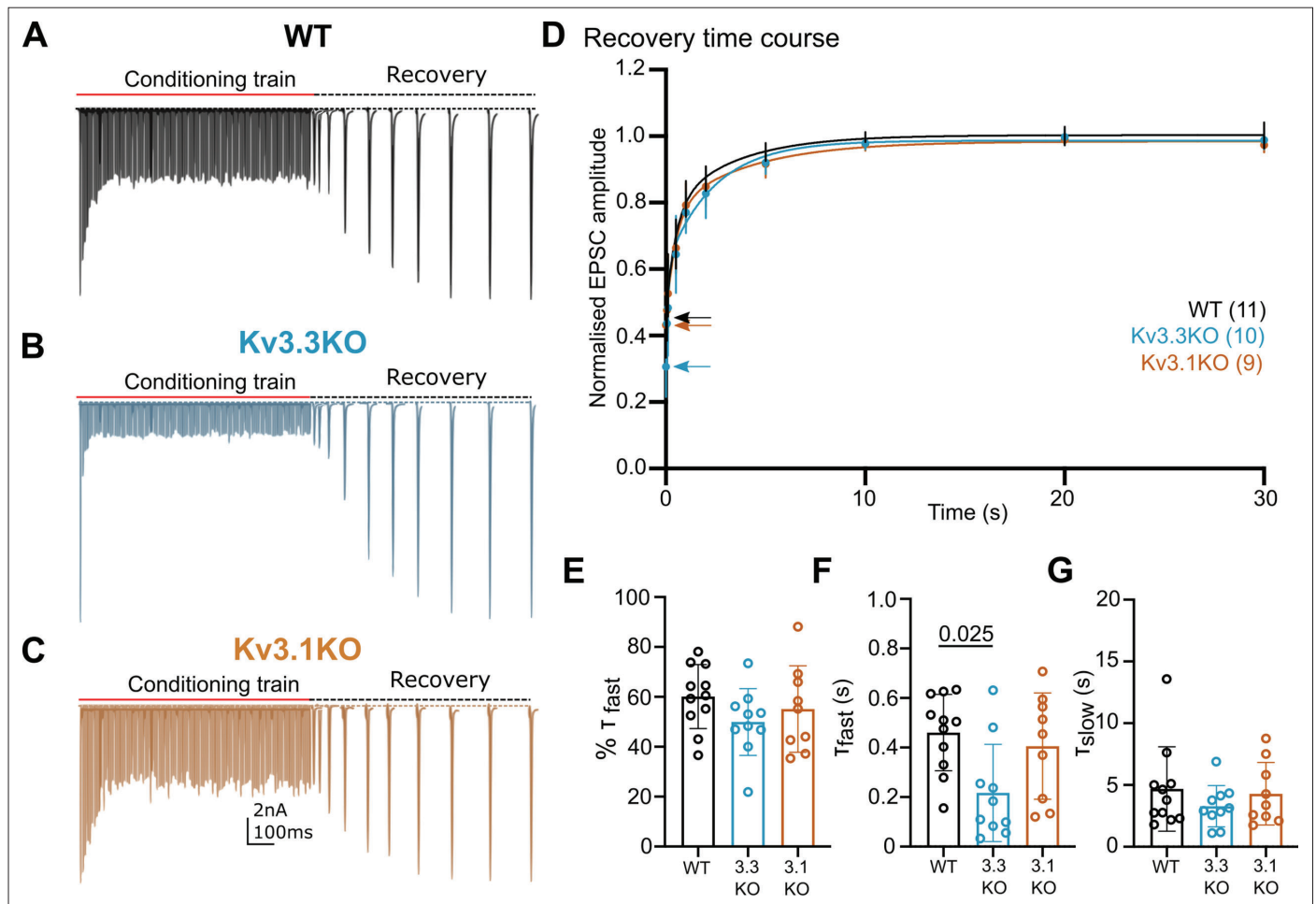


Figure 5. Recovery from short-term depression is accelerated on deletion of Kv3.3. (A) WT (black), (B) Kv3.3KO (blue), (C) Kv3.1KO (orange). A representative example is shown for each genotype. A conditioning train of 100 Hz (800ms duration) evoked EPSCs displaying short-term depression. The recovery was estimated by delivery of single stimuli at intervals following the conditioning train (50ms, 100ms, 500ms, 1 s, 2 s, 5 s, 10 s, 20 s, and 30 s. Recovery intervals not to scale). (D) The mean EPSC amplitude during the recovery is plotted for each genotype (mean \pm SD. WT, black; Kv3.3KO, blue; Kv3.1KO, orange) over the 30 s recovery period. The mean amplitude at the end of the conditioning train, from which the recovery starts, is shown by the respective coloured arrow. A double exponential was fit to each individual recovery curve and the mean curve is plotted for the respective genotype. Values are plotted as raw data and mean \pm SD in E-G; N values from part D also apply here. (E) The percent contribution of the fast component is similar between genotypes. (F) The fast time-constant significantly accelerated from 0.4 s in WT to 0.2 s in the Kv3.3KO. (G) The slow time-constant at around 5 s was unchanged between genotypes.

The online version of this article includes the following source data for figure 5:

Source data 1. ,Relates to **Figure 5**.

Kv3.3 deletion accelerated a fast component of recovery from short-term depression

Presynaptic spike broadening has previously been shown to enhance vesicle recycling during repetitive stimulation trains (Wang and Kaczmarek, 1998) due to enhanced calcium-dependent recovery. An increase in the rate of recovery of the evoked EPSC following short-term depression (Figure 5) could indicate changes in vesicle recycling. In WT animals the EPSC was depressed to around 40% on stimulation at 100 Hz (Figure 4E), increasing to 90% depression for 600 Hz (Figure 4G). Three example conditioning traces are shown in Figure 5A–C for each genotype. On ceasing stimulation, the depressed EPSC recovered back to control amplitudes over a time-course of 30 s (Figure 5A–C, recovery). The recovery phase was measured by presenting stimuli at intervals of: 50, 100, 200, 500 ms, and 1, 2, 5, 10, 20, and 30 s after the end of the conditioning train. Each recovery curve was

repeated 3 times and the mean EPSC amplitudes plotted over the 30 s period (**Figure 5D**) and fit with a double exponential. The fast time-constant contributed around half of the recovery amplitude and this did not differ significantly between the three genotypes (**Figure 5E**). The fast time-constant was significantly accelerated in the Kv3.3KO compared to WT and Kv3.1KO (0.2 ± 0.2 s in Kv3.3KO; 0.45 ± 0.2 s in WT and 0.4 ± 0.2 s in the Kv3.1KO; **Figure 5F**, $p=0.025$). The slow time-constant was 5 ± 3 s in WT, and was similar to both Kv3.1KO and Kv3.3KO (**Figure 5G**). The enhanced fast recovery rate is consistent with an activity-dependent component of vesicle recycling as observed previously on blocking presynaptic Kv3 channels at the calyx of Held (**Wang and Kaczmarek, 1998**) and as recently attributed to Ca^{2+} -phospholipid-dependent vesicle priming (**Lipstein et al., 2021**) via Munc13-1.

Computational model of transmitter release

The magnitudes and rates of EPSC depression and recovery following synaptic train stimulation provided constraints in refining a computational model of transmitter release and vesicle recycling at the calyx of Held (**Graham et al., 2004**). A simple model of transmission at the calyx of Held, based on transmitter release and recycling was employed as set out in **Figure 6A**, equations 1-3. It included activity-dependent vesicle recycling (**Graham et al., 2004; Billups et al., 2005; Lucas et al., 2018**) and parameters were fit across the range of stimulus frequencies (100–600 Hz) for the WT and the Kv3.3KO mouse. The model possessed a readily releasable pool (RRP; normalized size n), from which vesicles undergo evoked exocytosis with a release probability (P_v), following each AP and are recycled with a time-constant τ_r . A basal rate of recycling (large time-constant τ_b) is accelerated to an activity-dependent rate (smaller time-constant τ_h) on invasion of an AP, and relaxed back to τ_b with a time-constant of τ_d . The table in **Figure 6B** shows that the dominant change in the model parameters between WT and Kv3.3KO, was an increase in the probability of vesicular release (P_v) from 0.13 in WT to 0.266 in the Kv3.3KO. There was also evidence for an increase in activity-dependent recycling, with a 20% acceleration of the replenishment rate (smaller τ_h in Kv3.3KO). The fit of the model to the mean experimental data (\pm SEM) is shown for the short-term depression and the recovery curves (WT: **Figure 6C–D**; Kv3.3KO: **Figure 6E–F**). This model showed that the physiologically observed changes in short-term depression and recycling could be fit across the range of stimuli rates with only two parameter changes in the Kv3.3KO: a dramatically increased P_v and a modest decrease in the activity-dependent vesicle recycling time-constant τ_h (higher recycling rate), both of which are attributable to the raised calcium influx during the presynaptic AP (see **Neher and Sakaba, 2008; Young and Veeraraghavan, 2021**).

Integration of EPSCs in generating APs in the postsynaptic MNTB neuron

A key physiological question is the extent to which presynaptic Kv3.3 influences AP firing of the MNTB neuron in response to trains of synaptic stimuli, since most auditory stimuli will be trains rather than single APs. This was addressed in two experiments: first in an in vitro slice study comparing the AP firing of MNTB neurons in response to synaptic stimulation over a range of frequencies and across the genotypes (**Figure 7**) and then through an in vivo study of the response of MNTB neurons to sound-evoked inputs, focusing on the Kv3.3KO and WT genotypes (**Figure 8**).

The first question was how does MNTB AP firing in response to a train of synaptic inputs change on deletion of Kv3.1 and Kv3.3? The initial observation was that MNTB AP output in response to high frequency calyceal EPSC input, declines with both Kv3.1 and Kv3.3 deletion (**Figure 7A**) when measured over the whole train (WT: $52.49\% \pm 8.15\%$, $n=5$; Kv3.3KO: $29.8\% \pm 10.43\%$, $n=7$; Kv3.1KO: $36.29\% \pm 11.12\%$, $n=6$; Kv3.3KO vs WT $p=0.0044$, Kv3.1KO vs WT $p=0.046$, one-way ANOVA, Tukey's post hoc). But closer inspection reveals three phases of AP firing to evoked trains of calyceal synaptic responses as illustrated in **Figure 7B**. This shows MNTB EPSPs/APs during an 800ms 600 Hz train in a WT mouse. In Phase I (green trace, **Figure 7B**) which predominates at the start of each train, every evoked EPSP triggered one MNTB AP: so the MNTB output matched the calyx input. Firing then transitioned to Phase II (blue trace, **Figure 7B**) after around 6–9 stimuli, where EPSPs often failed to evoke an AP, and the MNTB AP firing becomes chaotic, unpredictable and poorly transmits the timing information contained within the presynaptic AP train. In Phase III (black trace, **Figure 7B**): the EPSP had undergone short-term depression and approached a 'steady-state' amplitude; now the MNTB neuron fired APs to alternate EPSPs. At frequencies up to 200 Hz the duration of Phase I was essentially

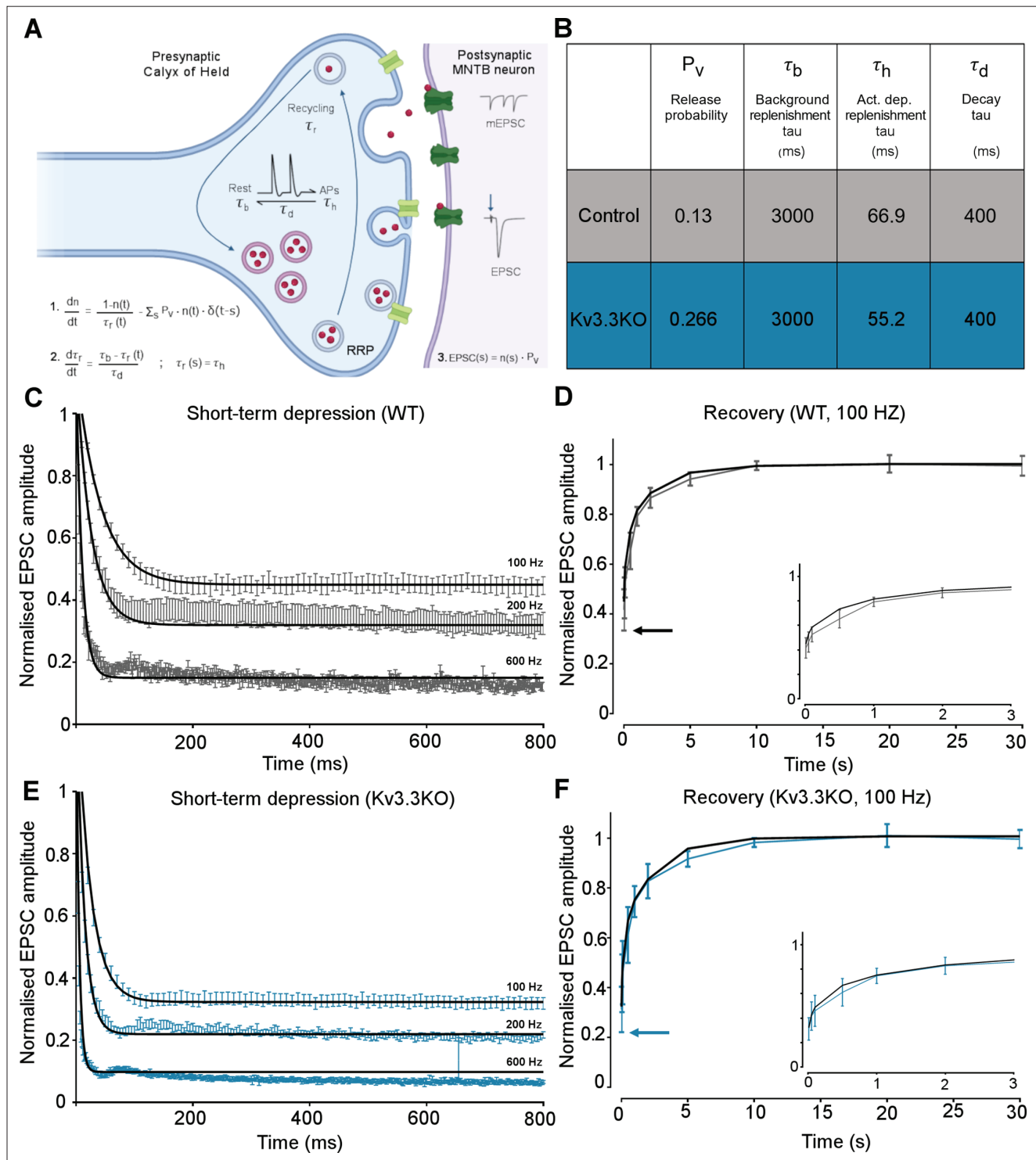


Figure 6. Kv3.3 deletion increases release probability and speeds a fast component of vesicle recycling, based on computational modelling. **(A)** Model illustration: Vesicles are released from the readily releasable pool (RRP; normalized size n) with a probability P_v ; the RRP is replenished with the recycling time-constant τ_r . In the absence of APs $\tau_r = \tau_b$ – the background replenishment time-constant, which decreases (accelerates) to τ_h following a presynaptic AP, and decays back to τ_b with a time-constant τ_d . Model parameters were fit to WT data for evoked EPSC trains (100–600 Hz) and their 100 Hz recovery curves. Schematic created with [BioRender.com](https://www.biorender.com). **(B)** Table showing the model parameters for fitting WT and Kv3.3KO data. Increasing P_v from 0.13 to 0.266 and accelerating τ_h from 66.9 to 55.2 were sufficient to fit the changes observed on Kv3.3 deletion. **(C)** WT - EPSC amplitude data (mean \pm SEM) during the conditioning train (100, 200, and 600 Hz, grey) are plotted with superimposed model prediction curves (black). **(D)** WT

Figure 6 continued on next page

Figure 6 continued

100 Hz: Recovery of the EPSC (mean \pm SEM) over 30 s. Inset shows data and fit for the first 3 s. Model fit is the superimposed black line. Horizontal arrow indicates EPSC amplitude at the end of the conditioning train. (E) Kv3.3KO: EPSC amplitude data (mean \pm SEM) during the conditioning trains are plotted (blue) with superimposed model prediction curves (black). (F) Kv3.3KO 100 Hz: Recovery of the EPSC amplitude (mean \pm SEM) over 30 s. Inset shows data and fit for the first 3 s. Model fit is the superimposed line. Horizontal arrow indicates EPSC amplitude at the end of the conditioning train.

The online version of this article includes the following source data for figure 6:

Source data 1. Relates to **Figure 6.**

identical across the three genotypes (**Figure 7C**), all showed 100% firing throughout the train; then from 300 Hz and above, the Phase I duration declined dramatically for all genotypes. Genotype-specific limitations were observed at the highest frequencies. **Figure 7D** shows the relative duration of each phase for 600 Hz EPSP trains (as a % of the train duration). There were no differences in the duration of Phase I, while Phase II and III were of variable duration. At 600 Hz stimulation frequency, the latency to the start of Phase II was 34.3 ± 12.3 ms for WT (n=10), 25 ± 8 ms for Kv3.3KO (n=6) and 26 ± 14 ms for Kv3.1KO (n=5). The latency for Phase III was similar in WT and Kv3.1KO (510 ± 224 ms and 597 ± 251 ms, respectively) but in the Kv3.3KO only 1 out of 6 calyx/MNTB pairs briefly entered Phase III firing (Kv3.3KO vs WT Phase II $p=0.0135$, Phase III $p=0.02$, two-way ANOVA, Tukey's post hoc). This is consistent with the idea that presynaptic Kv3.3 and hence fast presynaptic APs, serve a role in maintaining information transmission across the synapse during high frequency firing, when short APs conserve resources, and slow the rate of short-term depression.

Large magnitude Kv3 currents in postsynaptic MNTB neurons demonstrably assists in transmission of timing information (**Song et al., 2005**). Kv3 has little impact on the resting MNTB neuron membrane time-constant or AP firing threshold (induced by current injection through the pipette) and these are essentially identical in the three genotypes (**Choudhury et al., 2020**), which was also confirmed here (**Figure 7i**). However, in the Kv3.1KO, calyceal stimulation evoked a sustained depolarisation (in addition to EPSPs) at frequencies above 100 Hz (**Figure 7E**). The mean amplitude of this depolarising plateau potential during the train is plotted against stimulus frequency for each genotype (**Figure 7F**). Although all genotypes exhibited this plateau depolarisation at 600 Hz, it was significantly larger for the Kv3.1KO at frequencies above 100 Hz (**Figure 7F**). In contrast, Kv3.3KOs showed a reduced plateau potential at frequencies above 300 Hz, reaching significance only at 600 Hz (**Figure 7F**; two-way ANOVA, Tukey's post hoc). This was also observed as a decaying depolarisation at the end of the train (**Figure 7G**), with the time to half-decay plotted in **Figure 7H** (WT: 2.79 ± 1.73 ms, n=7; Kv3.3KO: 1.89 ± 0.92 ms, n=6; Kv3.1KO: 15.96 ± 8.59 ms, n=8; Kv3.1KO vs WT $p=0.000553$, one-way ANOVA, Tukey's post hoc). In WT and Kv3.3KO genotypes, this decay was similar to the postsynaptic membrane time-constant, but in the Kv3.1KO, non-synchronous spontaneous EPSPs were observed. The EPSC decay time constants for all genotypes were essentially identical, consistent with no change in glutamate receptor expression (WT: 2.74 ± 1.26 ms, n=8; Kv3.3KO: 3.1 ± 0.87 ms, n=8; Kv3.1KO: 3.54 ± 0.9 ms, n=6). This plateau depolarisation caused increased depolarisation block of APs and thereby undermined our ability to examine AP firing physiology in the Kv3.1KO. Therefore, in vivo experiments focused on comparison of the WT and Kv3.3KO genotypes, which did not exhibit this postsynaptic epi-phenomenon.

Kv3.3 increases precision and signal-to-noise ratios in MNTB response to sound

The prolonged presynaptic AP duration and increased transmitter release observed here in the Kv3.3KO, shows that the calyx has a specific need for Kv3.3 channels. So, what is the impact of presynaptic Kv3.3 on brainstem auditory processing in the MNTB?

Behaviourally, the Kv3.3KO mouse is as sensitive to sound as the WT in that Auditory Brainstem Response (ABR) thresholds were similar in 6-month-old WT and Kv3.3KO mice, with no statistical difference across a wide frequency range (see summary statistics, unpaired t-test with Holm-Šidák's test for multiple comparisons). However, further analysis of the ABR waveform showed significant deficits in Wave IV at 6 months which were not apparent in recordings taken at 1 month of age. We have previously demonstrated that a developmental 'knockout' of the MNTB impacts ABR Wave III (**Jalabi et al., 2013**), so the decrease in Wave IV reflects changes in downstream areas of the auditory

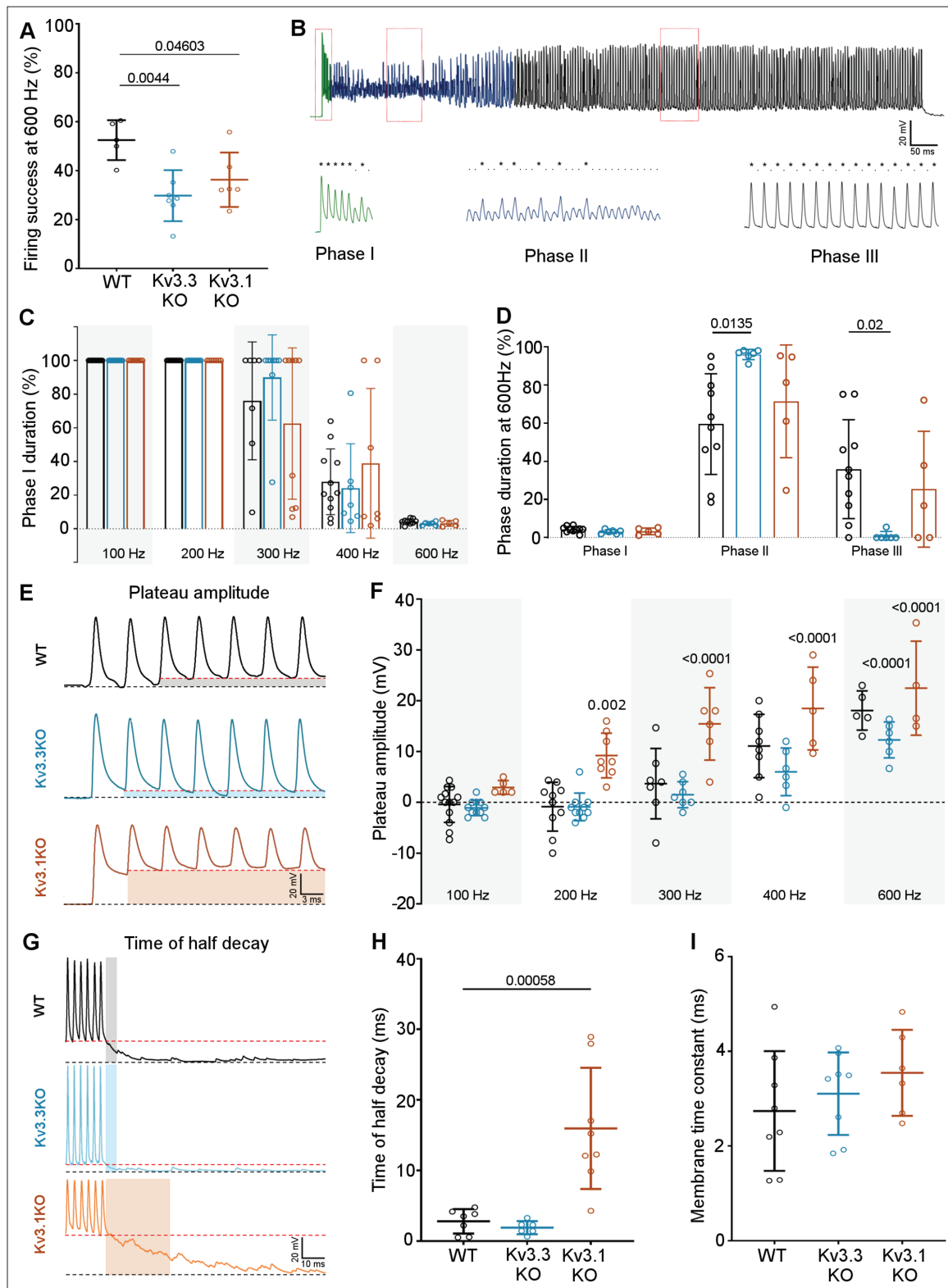


Figure 7. Kv3.3 deletion reduced ability to sustain MNTB AP firing at high frequencies. **(A)** Percent firing success of MNTB neurons for 600 Hz calyceal stimulation is reduced for both Kv3.3KO and Kv3.1KO. **(B)** A representative AP train recorded for an MNTB neuron in response to 600 Hz synaptic stimulation lasting 800ms. Three phases of input:output firing defined: Phase I (green) 1:1 AP firing calyx:MNTB for each EPSC is prevalent early in the train. Phase II (dark blue) follows phase I where some EPSCs drop below threshold, and AP firing becomes less probable and chaotic. Phase III (black) shows a transition to a more regular firing pattern. **(C)** Phase I duration is reduced for Kv3.3KO and Kv3.1KO at 300 Hz, 400 Hz, and 600 Hz. **(D)** Phase II duration is reduced for Kv3.3KO and Kv3.1KO at 300 Hz, 400 Hz, and 600 Hz. **(E)** Plateau amplitude is reduced for Kv3.3KO and Kv3.1KO. **(F)** Plateau amplitude is reduced for Kv3.3KO and Kv3.1KO at 300 Hz, 400 Hz, and 600 Hz. **(G)** Time of half decay is increased for Kv3.3KO and Kv3.1KO. **(H)** Time of half decay is increased for Kv3.1KO. **(I)** Membrane time constant is not significantly different between genotypes. *Figure 7 continued on next page*

Figure 7 continued

MNTB AP firing becomes regular again but is now firing to alternate input EPSCs, restoring information transmission. Expanded sections (boxed) of each phase of AP firing are shown below the full trace, APs are indicated by '*' and EPSPs that are below threshold are indicated by '.'. (C) Phase I duration across stimulation frequencies (100–600 Hz) for each genotype (WT, black; Kv3.3KO, blue; Kv3.1KO, orange): Phase I firing lasts throughout the train at frequencies up to 300 Hz but declines to only a few milliseconds at 600 Hz synaptic stimulation, but there were no significant differences between the genotypes. (D) The time spent in each phase for 600 Hz stimulation train (with each genotype indicated by the same colours as in C). The MNTB neuron is unable to maintain Phase I and Phase II dominates for each genotype. However, Phase III is only achieved briefly on 1 of 6 observations in the Kv3.3KO. (E) A sustained depolarized plateau was also observed, in the MNTB AP trains, as indicated by the shaded regions in this data from 300 Hz, and was particularly large the Kv3.1KO. (F) The amplitude of the depolarisation plateau increased in magnitude with stimulation frequency for each genotype, but was significantly larger in the Kv3.1KO at all frequencies above 100 Hz. (G) A slowly decaying depolarisation following the end of the synaptic train, as shown for representative traces from each genotype. (H) This decaying depolarisation is quantified as the time to half-decay and was significantly longer in the Kv3.1KO compared to WT in a 300 Hz AP train. (I) The postsynaptic MNTB neuron membrane time constant was unchanged across all genotypes (genotype: WT, black; Kv3.3KO, blue; Kv3.1KO, orange).

The online version of this article includes the following source data for figure 7:

Source data 1. Relates to **Figure 7**.

brainstem and is being characterized as part of another study. Here, we used the opportunity to examine auditory processing in the MNTB in vivo using extracellular recordings from WT and Kv3.3KO mice during sound stimulation. This data was non-gaussian and summary statistics are presented as median, and quartile values (in square brackets).

Extracellular MNTB single unit recordings exhibited a typical complex waveform, comprised of a presynaptic and a postsynaptic component (**Figure 8A**; **Kopp-Scheinflug et al., 2003**). The time between the peak and trough of extracellular APs is a compelling marker for AP halfwidth (**Ritzau-Jost et al., 2021**) and confirmed our results of the presynaptic patch clamp recordings. AP halfwidth of the presynaptic AP (preAP) was significantly longer in Kv3.3KOs (0.25ms [0.16; 0.31]; n=13) compared to WT recordings (0.17ms [0.16; 0.19]; n=20; **Figure 8B**; Mann-Whitney Rank Sum Test: p=0.036). Synaptic delays as measured by peak-to-peak times in the complex waveform were also significantly prolonged in Kv3.3KOs (0.56ms [0.45; 0.70]; n=13) compared to WT controls (0.44ms [0.41; 0.49]; n=20; **Figure 8C**; n=13; Mann-Whitney Rank Sum Test: p=0.013). While changes in presynaptic AP duration and synaptic delay may predominantly affect temporal processing, the prolonged postsynaptic AP duration observed in the Kv3.3KOs (0.64ms [0.29; 0.46]; n=13; **Figure 8D**) might influence high-frequency firing abilities (WT: 0.36ms [0.48; 0.82]; n=20; Mann-Whitney Rank Sum Test: p<0.001).

Temporal processing was tested by presenting suprathreshold sound stimuli at the neurons' characteristic frequency in 6–8 months old mice and comparing WT and Kv3.3KO strains. MNTB neurons in WT responded with a phasic-tonic firing pattern (**Figure 8E and F**) with short latencies (3.44ms [3.01; 4.21]; n=25; **Figure 8I and J**) and minimal jitter (0.18ms [0.09; 0.51]; n=18; **Figure 8I and K**). In contrast, Kv3.3KO neurons were slower to respond to sound with first spike latencies of 4.06ms [3.01; 4.21] (n=25; Mann-Whitney Rank Sum Test: p=0.015; **Figure 8I and J**) and showed larger temporal variability (0.92ms [0.56; 1.50]; n=18; Mann-Whitney Rank Sum Test: p=0.001; **Figure 8I and K**). This increased onset jitter contributed to the reduced magnitude of the phasic component in the peri-stimulus time histogram in Kv3.3KO neurons (**Figure 8F** arrows). The inability to fire high instantaneous rates at sound onset was accompanied by a shift in the average inter-spike intervals from 2.16ms [1.48; 3.57] (n=22) in the WT to 3.10ms [2.49; 4.19] (n=18) in the Kv3.3KO (Mann-Whitney Rank Sum Test: p<0.001; **Figure 8G**). Indeed, comparing peak firing rates during the first 10ms of the sound-evoked response revealed significantly lower rates in Kv3.3KOs (240 Hz [180; 280]; n=18) compared to WTs (350 Hz [200; 425]; n=22; Mann-Whitney Rank Sum Test: p=0.003; **Figure 8H**). In contrast to the reduced sound-evoked firing rates, an increase in spontaneous firing was observed in the Kv3.3KOs (Kv3.3KO: 40 Hz [19.3; 62.0]; n=19) compared to WT controls (16.5 Hz [4.5; 42.8]; n=24; Mann-Whitney Rank Sum Test: p=0.044; **Figure 8L**). Together, these combined changes caused a significant reduction in signal-to-noise ratio in the Kv3.3KO (2.77 [2.04; 3.99]; n=14) compared to WT controls (9.70 [4.38; 40.95]; n=18; Mann-Whitney Rank Sum Test: p=0.001; **Figure 8M**).

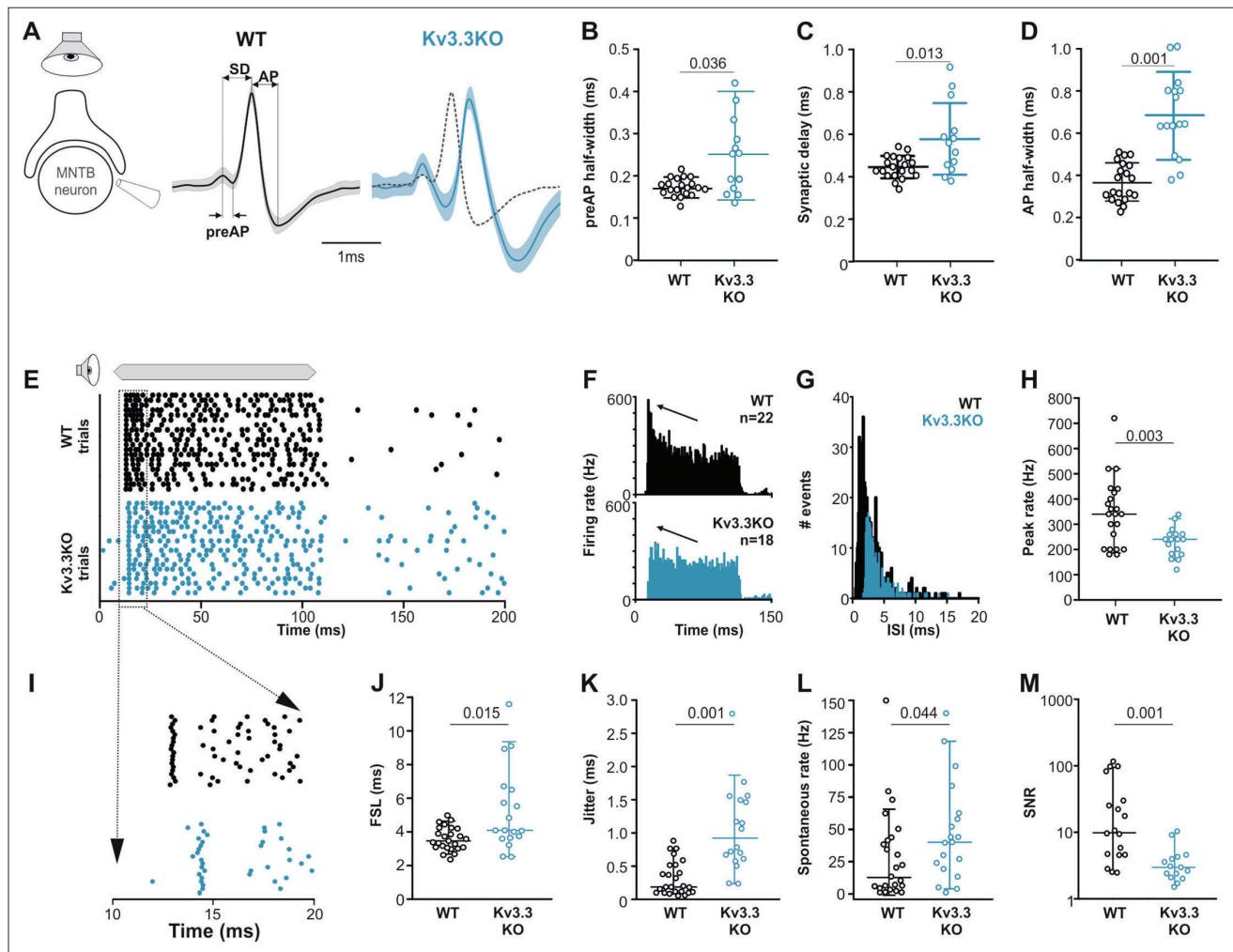


Figure 8. Presynaptic Kv3.3 accelerates the brainstem response to sound and improves timing and signal-to-noise ratio. **(A)** Extracellular recording from Calyx/MNTB *in vivo* shows complex APs (presynaptic and postsynaptic) from WT (black) and Kv3.3KO (blue) mice in response to sound; overlay of APs (right) shows delayed and longer APs in the KO. **(B, C, D)** Presynaptic AP half-width, synaptic delay and postsynaptic AP half-width are all longer in the Kv3.3KO (blue) than WT (black). **(E)** Raster display of MNTB AP response to sound (20 trials, 100ms duration) and spontaneous firing for both WT (black, upper) and Kv3.3KO (blue, lower). **(F, G, H)** Peri Stimulus Time Histogram (PSTH) of the evoked APs (grand avg. over all neurons, 1ms bins) show reduced peak firing rates (F, black arrow) due to longer interspike intervals (ISIs) and increased jitter (I, K) in the Kv3.3KO (blue) and the peak (0–10ms of the response) firing rate is significantly reduced. **(I, J, K)** Expansion of first 20ms of the Raster plot shows increased first spike latency and jitter (latency SD) in the Kv3.3KO (blue). **(L, M)** The mean spontaneous firing rate was higher in the Kv3.3KO (blue) and overall, these changes degraded signal-to-noise ratio in Kv3.3KO (blue) relative to WT (black). Data is presented as median and inter-quartiles. p Values calculated using Mann-Whitney Rank Sum Test and statistically significant values displayed on each graph.

The online version of this article includes the following source data for figure 8:

Source data 1. Relates to **Figure 8**.

Discussion

Neurotransmitter release is triggered by calcium influx through voltage-gated calcium channels and is highly influenced by the presynaptic AP waveform. Deletion of Kv3.3 subunits increased presynaptic AP duration and transmitter release, enhancing short-term depression on repetitive stimulation. In contrast, deletion of Kv3.1 had little effect on the presynaptic AP or transmitter release. Expansion microscopy was used to enhance resolution in imaging presynaptic compartments and showed localisation of Kv3.3 subunits to the presynaptic membrane. These observations are consistent with a computational model of transmitter release in which Kv3.3 deletion increased vesicle release probability by twofold and to a lesser degree accelerated fast vesicle replenishment. This is consistent with

increased calcium influx and activity-dependent facilitation of recycling. The enhanced short-term depression of synaptic responses increased latency jitter and reduced postsynaptic AP firing (output) at high frequencies in the Kv3.3KO. In vivo this manifests as reduced temporal fidelity and firing rates in the binaural auditory circuit in response to sound, whilst spontaneous AP firing increased in the Kv3.3KO. We conclude that presynaptic Kv3 channels require one (or more) Kv3.3 subunits to achieve presynaptic targeting for fast and temporally precise transmitter release at this excitatory synapse.

On deletion of Kv3.3, synaptic transmission at the calyx of Held showed accelerated recovery from short-term depression, along with increased presynaptic AP duration and increased transmitter release from WT mice of a similar age. The magnitude and fast kinetics of Kv3 channels guarantee fast repolarisation and generate a fast afterhyperpolarisation (**Brew and Forsythe, 1995; Figure 1B**, here) which in concert with a resurgent Na⁺ current (**Kim et al., 2010; Lewis and Raman, 2014**) maximizes the availability of voltage-gated Na⁺ channels to maintain short APs during sustained firing, as also observed in vivo (**Sierksma and Borst, 2017**). Our results on transmitter release are consistent with enhanced activity-dependent vesicle recycling in the absence of Kv3.3, as a consequence of the increased AP duration and calcium influx (**Neher and Sakaba, 2008; Yang et al., 2014; Lipstein et al., 2021**). Our modelling indicates that the increase in transmitter release is primarily an increase in vesicle release probability (and subsequent short-term depression) but an acceleration of vesicle recycling also contributes.

Changes in auditory processing over development

A key design element of this study was that each experiment compared mice of similar age against the three genotypes (WT, Kv3.3KO, and Kv3.1KO) all of which were on the same CBA background strain. Thus, variance contributed by the developmental stage was minimized within each experiment and the significant changes therefore related to the absence or presence of the Kv3 subunits under study. The range of animal ages used in this study (in different experiments) shows that Kv3.3 is relevant across development. Nevertheless, auditory responses are maturing, particularly around the onset of acoustically evoked activity (P12) in the mouse. The calyx of Held undergoes a range of developmental changes that foster temporally accurate transmission (**Borst and Soria van Hoeve, 2012**). Presynaptic calcium channels shift from N to P/Q type (**Iwasaki et al., 2000**), myelination induces developmental and activity-dependent changes (**Kim et al., 2013; Sinclair et al., 2017**) and similar adaptations favouring high-frequency firing are occurring in neonatal rat pups (**Sierksma and Borst, 2017**). The AP time-course accelerates (**Taschenberger and von Gersdorff, 2000**) with increased expression of Nav1.6 (**Leão et al., 2005**) which in turn influences activation of the voltage-gated calcium channels (**Borst and Sakmann, 1998**) and hence the efficacy of transmitter release (**Yang and Wang, 2006**). Presynaptic Kv currents also increase (**Nakamura and Takahashi, 2007**) with the major change being before hearing onset (and little change from P13 to P20). At the post-synaptic membrane, a concurrent switch to fast time-course GluA4-flop dominated AMPAR-mediated EPSCs (**Barnes-Davies and Forsythe, 1995; Geiger et al., 1995; Yang et al., 2011**) with developmental refinement in GluA2, reducing calcium permeability (**Lujan et al., 2019**) and a decrease in AMPAR desensitisation, further enhance transmission fidelity (**Taschenberger et al., 2002; Wong et al., 2003**). The present study interrogates the role of Kv3 subunits over a wide age range, from a relatively immature calyx (P10-P12) to mature adult (6 months old) and despite the inevitable developmental changes during this period, Kv3.3 remains crucial in shaping the presynaptic AP waveform and neurotransmitter release at the calyx. An increase in Kv3 expression with age may actually amplify the deficits observed in Kv3.3KOs at later developmental stages however this study shows that even with a small deficiency in Kv3.3 expression in young Kv3.3KO animals, there are drastic consequences at the synapse.

Kv3 channel subunit composition

Knowledge of Kv channel subunit composition, interactions and precise location within identified neurons is key to understanding their extensive physiological roles in controlling neuronal excitability (**Trimmer, 2015**). Kv channel building is regulated by the N-terminal tetramerisation domain (T1) (**Li et al., 1992**) to favour assembly of 'dimers of dimers' (**Tu and Deutsch, 1999**) usually from subunits within the same Kv family. Although early studies suggested otherwise, Kv3 subunits do not co-assemble with the accessory subunit gene families (Kv5, Kv6, Kv8, and Kv9) (**Bocksteins et al., 2014**), so Kv3 channels are likely composed of four Kv3 alpha subunits. Frequent co-expression of Kv3

subunits in the same neurons suggest functional channels could exist as heteromers, indeed coimmunoprecipitation has revealed interactions of Kv3.1b with Kv3.4a and Kv3.2 in globus pallidus neurons (Baranauskas *et al.*, 2003; Hernández-Pineda *et al.*, 1999), and with Kv3.3 in the cerebellum (Chang *et al.*, 2007) but homomeric assemblies of Kv3.3 subunits could also form presynaptic Kv3 channels. The data reported here suggests that presynaptic Kv3 channels at the calyx of Held require an obligatory Kv3.3 subunit, since TEA (which will block all Kv3 heteromers) showed little effect on transmission in the Kv3.3KO. This result also implies that Kv3.1 does not have a directive or independent role in the terminal and while heteromers with Kv3.3 may occur, Kv3.1 is certainly not required for Kv3.3 localisation to the presynaptic membrane.

Could other Kv3 subunits contribute to presynaptic Kv3 channels here at the calyx or at other synapses?

Excitatory synaptic boutons, including hippocampal mossy fiber terminals (Alle *et al.*, 2011), cerebellar mossy fiber terminals (Ritzau-Jost *et al.*, 2014) and small neocortical boutons (Ritzau-Jost *et al.*, 2021) show pharmacological evidence for presynaptic Kv3. Inhibitory interneurons also possess presynaptic Kv3 channels, including cerebellar basket cell terminals (Southan and Robertson, 2000) and stellate cell axons (Rowan *et al.*, 2016), with the latter being identified as Kv3.4. However, it is difficult to exclude a role for Kv3.3 at this site since the Kv3 antagonist BDS is not specific for Kv3.4, having similar actions on Kv3.1 and Kv3.2; and should also block Kv3.3 subunits on the basis of sequence homology in the putative BDS binding site (Yeung *et al.*, 2005). It seems unlikely that Kv3.4 (or Kv3.2) subunits have a directive (or independent) role in trafficking Kv3 channels to the calyx terminal, since the mRNA levels for these subunits was very low in the MNTB and VCN. However, if there were effective translation and assembly of Kv3.4 (or Kv3.2) into calyx Kv3 channels, then TEA should have enhanced transmitter release in the Kv3.3KO, but TEA potentiation of transmission was occluded in the Kv3.3KO.

In contrast to Kv3.1 and Kv3.2, early studies of recombinant Kv3.3 showed N-type (ball-peptide) inactivation, as originally described for Kv1 potassium channels (Hoshi *et al.*, 1990). We conclude here that Kv3.3 is a principal component of presynaptic Kv3 channels but we observe little or no inactivation of the presynaptic Kv3 current. There are multiple explanations for this lack of inactivation. The degree of Kv3 inactivation varies between different expression systems (Rudy *et al.*, 1999), perhaps due to there being two methionine start codons. Mammals lack a well-defined Kozak consensus sequence for the first, favouring initiation at the second methionine, thereby excluding the N-terminal peptide (Fernandez *et al.*, 2003). Alternatively, endogenous PKC phosphorylation of N-terminal Kv3.3 could occlude the N-type inactivation (Desai *et al.*, 2008). Also, little or no inactivation was observed in the postsynaptic Kv3.3 channel (Choudhury *et al.*, 2020). Given this lack of inactivating current observed at the calyx, it is unlikely that Kv3.4 subunits are present in this terminal. Further to this, in recombinant co-expression studies, Kv3.3 and Kv3.4 did not readily form heteromers, but instead formed distinct currents with differing kinetics in the same cells (Richardson, Forsythe and Pilati, unpublished observations) suggesting that heteromeric channels composed of these subunits are unlikely.

In terminals that exhibit inactivation of presynaptic potassium currents, this has important physiological implications for transmitter release, especially during sustained high-frequency AP firing. Repetitive activation during AP trains would cause cumulative Kv3 inactivation and progressively slows AP repolarisation. This can generate a form of activity-dependent short-term potentiation where increasing AP duration potentiates transmitter release, as occurs at mossy fiber terminals (Geiger and Jonas, 2000). During sustained high-frequency AP firing at the calyx, the longer AP duration induced by an inactivating Kv3 would risk earlier transmission failure, with faster depletion of vesicles and inactivation of the presynaptic sodium channels. The physiological end-point for an inactivating Kv3 would be similar to that measured for the Kv3.3KO. Hence, the minimal inactivation of the presynaptic Kv3 current at the calyx of Held enables transmission to be sustained for longer, at higher firing rates and greater accuracy.

Do interactions with the cytoskeleton dictate Kv3 localisation or function?

Proximity of K⁺ channels have powerful influences on the local voltage and therefore in control of other voltage-gated ion channels. The data reported here demonstrates an ionic role for Kv3.3 in

the presynaptic terminal but stabilisation in any compartment will require non-ionic interactions with components of the cytoskeleton. The permutations and complexity of channel subunit assembly optimize function through subunit-specific localisation (Trimmer, 2015) involving trafficking, insertion, phosphorylation, and stabilisation of channel complexes. Indeed, a general scaffolding interaction is essential for intrinsic plasticity where insertion into key sites of excitability (axon initial segments, nodes of Ranvier, heminodes and synaptic terminals) will control hyper-excitability (Steinert et al., 2011) and calcium overload. There is a well-established role for ankyrin-G in axonal targeting of Kv3.1b (Xu et al., 2007) and for clustering of sodium and potassium channels at the initial segment (Pan et al., 2006). Ankyrin-R binds and stabilizes Kv3.1b in fast spiking interneuron somatic membranes and nodes of Ranvier; and crosslinks Kv3.3 via spectrin to the cytoskeleton in Purkinje neurons, which aids their survival (Stevens et al., 2021; Stevens et al., 2022). This interaction of both subunits with ankyrin-R would explain the inability of the MNTB neuron soma to differentiate or partition channels composed of Kv3.1b or Kv3.3 subunits (Choudhury et al., 2020) so that each subunit type could largely compensate for the absence of the other within the soma. Presynaptic stabilisation of Kv3.3 however, is unlikely to be through ankyrin-R alone, as this mechanism would not discriminate between the subunits.

Another possibility is that Kv3.3 inactivation is suppressed by the C-terminus associating with Hax1 (Blosa et al., 2015) to bind the Kv3.3 N-Terminal ball peptide and modulate the actin network. However, as in the WT, the calyceal outward currents reported in Zhang et al., 2016 were an order of magnitude smaller than observed here or elsewhere. Additionally, the presynaptic K⁺ currents from a Kv3.3KO calyx were similar magnitude to WT (Figure S4: Zhang et al., 2016). Based on association with the actin cytoskeleton, deletion of Kv3.3 was proposed to inhibit endocytosis in the calyx synaptic terminal by this non-ionic mechanism (Wu et al., 2021). However, the Wu et al., 2021 study does not test for the possibility of a simultaneous ionic mechanism or for a change in the presynaptic AP waveform on deletion or mutation of Kv3.3. With the evidence reported here, it is clear that Kv3.3 does have an ionic role at the calyx of Held. Our observations on EPSCs and modelling of short-term depression show that Kv3.3 deletion increases transmitter release and accelerates a fast sub-second component of activity-dependent recycling (Figure 5F, inset) following conditioning stimulation. Although this contrasts with the slowing of endocytosis observed in Wu et al., 2021 our observations are over a much shorter time-course and measure EPSC amplitude, rather than presynaptic capacitance. Future experiments will determine what part of the endocytosis capacitive changes result from direct or indirect ionic mechanisms versus non-ionic mechanisms.

Relevance of Kv3.3 to mechanisms of sound localisation

The kinetics of Kv3 channels is fast enough to generate a rapid afterhyperpolarisation following the AP, which maximises the driving force for calcium influx and promotes recovery of voltage-gated sodium and calcium channels from inactivation. Short duration APs permit high firing rates by minimising the absolute refractory period, thus Kv3 enables well-timed high-frequency AP trains and when input firing rates exceed the refractory limit, neurons expressing Kv3 readily switch to firing on alternate input spikes (Song et al., 2005). In this study, we evoked MNTB neuron AP firing in response to presynaptic stimulation and asked how effective was the input/output relationship across a range of firing frequencies from 100 to 600 Hz in each genotype. Although there was little difference at low firing frequencies, at the highest frequencies only the first few presynaptic APs generate postsynaptic APs with 1:1 fidelity (Phase I) before entering a chaotic phase (Phase II) with many failures, which resolves later in the train into precise firing but to alternate stimuli (Phase III). In the absence of Kv3.3 the MNTB firing passed into Phase II but did not converge into Phase III firing, consistent with the idea that presynaptic Kv3.3 improved stability of synaptic transmission.

Integration of information from both ears for the purpose of sound localisation requires high temporal accuracy for bilateral transmission of auditory APs from each cochlea to the superior olivary complex (Tollin, 2003; Joris and Trussell, 2018). This is facilitated by Kv3 channels within specific neurons, from cell bodies, axons, synaptic terminals and across the neural network. In vivo extracellular recording from the MNTB measures simultaneously the presynaptic calyx and postsynaptic MNTB single unit APs. Accurate transmission of AP timing was compromised in the Kv3.3KO, and the peak firing rate was reduced. Additionally, spontaneous AP firing was elevated (with respect to WT animals), likely reflecting hyper-excitability upstream in the auditory pathway, with Kv3.3 being

expressed in spiral ganglion (Kim et al., 2020) and the globular bushy cells (Li et al., 2001; Cao et al., 2007) which give rise to the calyx of Held. The use of anesthetic for our in vivo study may affect auditory processing, but comparison with multiple other studies in mice and gerbil and using a range of different anesthetics showed that the synaptic delay measured in this study was favourably comparable to these other studies: ketamine/xylazine in mouse: 0.40ms (Blosa et al., 2015), 0.46ms (Kopp-Scheinflug et al., 2003), 0.50ms (Lorteije et al., 2009) ketamine/xylazine in gerbil: 0.44ms (Tolnai et al., 2009). This narrow distribution of synaptic delays with different anesthesia suggests that the effect of anesthesia on synaptic delay is negligible compared to the effect of deleting Kv3.3.

Kv3.3 physiology, dysfunction, and disease

Immunohistochemical studies have localized Kv3.3 subunits to many different synaptic terminals across the brain, from spiral ganglion afferent processes (Kim et al., 2020), medial vestibular nuclei (Brooke et al., 2010), cerebellar dentate nucleus (Alonso-Espinaco et al., 2008), parallel fiber synapses (Puente et al., 2010), posterior thalamic nucleus (Chang et al., 2007), and the neuromuscular junction (Brooke et al., 2004). It is interesting to consider why Kv3.3 is present at some synaptic terminals, but not all. One hypothesis is that presynaptic Kv3.3 would enhance resource and energy conservation during high frequency firing, but more importantly it will support the physiological mechanisms as a synapse evolves from a microdomain to a nanodomain architecture for exocytosis (Meinrenken et al., 2003; Young and Veeraraghavan, 2021) by constraining presynaptic calcium influx.

Disease mutations associated with Kv3.3, such as spinocerebellar ataxia type 13 (SCA13) cause multiple neurological defects, which from the evidence reported here could include aberrant neurotransmitter release in addition to postsynaptic excitability changes. In the case of the SCA13 mutation R420H (Middlebrooks et al., 2013), the observations made here support the hypothesis that SCA13 disrupts the physiological process of interaural level discrimination by reducing the gain and signal to noise ratio, thereby undermining sound source localisation (Tollin, 2003). The current study suggests several areas for further investigation of presynaptic potassium conductances: First, the contribution of ionic and non-ionic mechanisms is now recognized for Kv3 and their relative contribution to cytoskeleton and physiology can be elucidated. Second, it is necessary to determine which spliced-variants or potassium channel beta subunits/accessory proteins are expressed and how subunit phosphorylation contributes to the physiology. Third, while Kv3.3 can be clearly resolved on the non-release face of the terminal, the resolution on the release face is not sufficient to unambiguously distinguish between the pre- and post-synaptic membranes, but in order to avoid depolarisation by $[K^+]_o$ accumulation, one would predict minimal potassium efflux into the synaptic cleft. Fourth, Kv3 currents do not mediate all the presynaptic potassium current and other Kvs operating at more negative voltage activation ranges, such as Kv1 (Geiger and Jonas, 2000; Dodson et al., 2003) or Kv7 (Zhang et al., 2022) are likely to contribute to terminal threshold, excitability and AP waveform.

The combinatorial potential of Kv3 channel subunits gives rise to a spectrum of physiological roles in fast-spiking neurons (Choudhury et al., 2020) and interneurons (Chang et al., 2007). The pre- and postsynaptic studies conducted here at the calyx of Held/MNTB neuron clearly show that Kv3.3 subunits are critical for presynaptic localisation of Kv3 channels mediating fast AP repolarisation. They contribute to improved temporal accuracy and conservation of presynaptic resources during high-frequency firing. Together these results suggest a general role for Kv3.3 in raising the biophysical 'speed limit' for information transmission at fast synapses, especially during intense synaptic activity.

Materials and methods

Key resources table

Reagent type (species) or resource

Designation	Source or reference	Identifiers	Additional information
Genetic reagent (<i>M. musculus</i>) CBA/Crl	Charles River	Strain code: 609	Leicester breeding colony

Continued on next page

Continued

Reagent type (species) or resource

Reagent type (species) or resource	Designation	Source or reference	Identifiers	Additional information
Genetic reagent (<i>M. musculus</i>)	Kv3.1 knockout mouse on CBA back-ground (Kv3.1KO)	Ho et al, PNAS 94, 1533–1,538. 1997.	CBA/CaCrI.Kcnc1 ^{tm1Joho} /UoL	Strain originally created on 129/SV background and backcrossed onto CBA for >10 generations at the Preclinical Research Facility – University of Leicester
Genetic reagent (<i>M. musculus</i>)	Kv3.3 knockout mouse on CBA back-ground (Kv3.3KO)	Espinosa et al., J Neurosci 21, 6657–6,665. 2001	CBA/CaCrI. Kcnc3 ^{tm1Echa} /UoL	Strain was originally created on C57BL/6 background and backcrossed onto CBA for >10 generations at the Preclinical Research Facility – University of Leicester
Commercial assay or kit	Illumina NextSeq500 High Output	Illumina	FC-404–2002	Used for Cochlear Nucleus
Chemical compound, drug	Strychnine hydrochloride	Sigma Aldrich (MERCK)	S8753-25G	(0.5 µM)
Chemical compound, drug	Tetraethylammonium	Sigma Aldrich (MERCK)	86614–25 G	(1 mM)
Chemical compound, drug	Fentanyl	Janssen	6,001	(0.05 mg/kg)
Chemical compound, drug	Midazolam	B Braun	17206034	(5.0 mg/kg)
Chemical compound, drug	Medetomidine	Vetoquil GmbH	Domitor	(0.5 mg/kg)
Antibody	Anti-Kv3.1b (rabbit polyclonal)	Alomone	APC-014	(1:1000)
Antibody	Anti-Kv3.3 (mouse monoclonal)	Neuromab	75–354	(1:3000)
Antibody	Alexafluor488 Goat anti-rabbit (Goat polyclonal)	Thermofisher	A-11008	(1:1000)
Antibody	Alexafluor546 Goat anti-mouse (Goat polyclonal)	Thermofisher	A-11003	(1:1000)
Antibody	Anti-Kv3.1b (rabbit polyclonal)	Synaptic systems	242 003 (Lot# 1–2)	(1:300)
Antibody	Anti-Kv3.3 (rabbit polyclonal)	Alomone	APC-102 (Lot# APC 102AN0502)	(1:300)
Antibody	Anti-Bassoon (mouse monoclonal)	Synaptic systems	141 111 (Lot# 1–2)	(1:300)
Antibody	Alexafluor488 Goat anti-mouse (goat polyclonal)	Invitrogen	A11001 (Lot# 21 40660)	(1:300)
Antibody	Alexafluor546 Goat anti-rabbit (goat polyclonal)	Invitrogen	A11010 (Lot# 21 89179)	(1:300)
Software, algorithm	Graphpad Prism 9.0.2	Graphpad	RRID:SCR_002798	
Software, algorithm	pClamp 10 software suite	Molecular Devices	RRID:SCR_011323	
Software, algorithm	Zen Blue, 3.1	Zeiss	RRID:SCR_013672	
Software, algorithm	ABR Averager (Custom)	Wellcome Trust Sanger Institute		
Software, algorithm	AudioSpike	HoerrTech	https://audiospike.hz-ol.de/	
Software, algorithm	MATLAB R2010a	Mathworks	RRID:SCR_001622	

Continued on next page

Continued

**Reagent type
(species) or
resource**

Reagent type (species) or resource	Designation	Source or reference	Identifiers	Additional information
Software, algorithm	Fiji	NIH ImageJ	RRID:SCR_002285	
Other	Custom concentric bipolar stimulating electrodes	FHC	CBASD75	
Other	Borosilicate glass capillaries	WPI	GC150F-7.5	

Experiments were conducted in accordance with the Animals (Scientific Procedures) Act UK 1986 and as revised by the European Directive 2010/63/EU on the protection of animals used for scientific purposes. All procedures were approved by national oversight bodies (UK Home Office, or Bavarian district government, ROB-55.2–2532.Vet_02-18-1183) and the local animal research ethics review committees.

Experiments were conducted on CBA/Crl mice (wildtype, WT) and knockouts were backcrossed for 10 generations onto this CBA/Crl background ([Choudhury et al., 2020](#)). PCR genotyping was done from ear notch samples made at P10. Mice were housed and breeding colonies maintained at the preclinical research facility (PRF) at the University of Leicester, subject to a normal 12 hr light/dark cycle and with free access to food and water (ad libitum). Both male and female animals were used in experiments with ages ranging from P10-25 for electrophysiology to 6 months of age for in vivo and auditory brainstem response (ABR) recordings.

mRNA sequencing

Mice were killed by decapitation and brainstems were removed into 'RNA Later' stabilisation solution (Invitrogen, Cat# AM7020), before dissection to isolate both cochlear nuclei. Tissue from 3 CBA/Crl mice were pooled into 9 individual samples (27 mice total) before phenol extraction to isolate RNA. RNA purity, integrity, and concentration was assessed by UV-Vis spectroscopy (Nanodrop 8000) and capillary electrophoresis (Agilent Bioanalyzer 2000). Samples with RIN (RNA integrity) <7 were discarded. cDNA libraries were constructed using the NEBNext Ultra Directional RNA Library Prep Kit for Illumina sequencing performed using the Illumina NextSeq500 High Output (v2, 150 cycles) kit and the Illumina NextSeq500. Analysis of sequencing data was performed using Illumina Basespace. Using FastQC toolkit (Babraham Bioinformatics) total reads were trimmed of low-quality reads (Q<20), poly-A/T tails >10 bp, and adapter sequences before alignment to the mm10 (GRCM387) mouse genome (Ensembl) using TopHat2. Output values represented as Fragments per kilobase of transcript per million mapped reads (FPKM).

Electrophysiology**In vitro brain slice preparation**

Mice were killed by decapitation, the brainstem removed and placed into ice-cold artificial cerebrospinal fluid aCSF, oxygenated with 95%O₂/5%CO₂, containing (in mM): sucrose (250), KCl (2.5), NaHCO₃ (26), NaH₂PO₄ (1.25), D-Glucose (10), ascorbic acid (0.5) MgCl₂ (4), and CaCl₂ (0.1). For presynaptic recordings, 100-µm-thick transverse slices or 250-µm-thick slices for postsynaptic recordings were prepared in a pre-cooled chamber using a Leica VT1200S vibratome. Slices were allowed to recover for 1 hr at 37 °C in normal aCSF ([Choudhury et al., 2020](#)), continually bubbled with 95%O₂/5%CO₂ and subsequently allowed to passively cool to room temperature. The aCSF (310 mOsm) contained (in mM): NaCl (125), NaHCO₃ (26), D-Glucose (10), KCl (2.5), myo-inositol (3), NaH₂PO₄ (1.25), sodium pyruvate (1), ascorbic acid (0.5), MgCl₂ (1), and CaCl₂ (2). Recordings from brain slices were conducted at a temperature of 35±1°C.

Presynaptic recordings

Mice aged P10-P12 were used for presynaptic calyx recordings. For each experiment, slices were placed in a recording chamber of a Nikon E600FN upright microscope and cells visualized with a 60 x DIC water-immersion objective ([Lucas et al., 2018](#)). Slices were continuously perfused with normal aCSF saturated with 95%O₂/5%CO₂, (as above), heated to 35 °C±1, at a rate of 1 ml/min. Whole-cell patch recordings were made using thick-walled borosilicate capillaries (1.5 mm OD, 0.86 mm ID) with

a resistance of 4–6 M Ω , filled with an internal solution composed of (in mM): KGluconate (97.5), KCl (32.5), HEPES (40), EGTA (0.2), MgCl₂ (1), K₂ATP (2.2), Na₂GTP (0.3), pH adjusted to 7.2 with KOH (295 mOsm). Calyces were identified visually, appearing as a second membrane profile around an MNTB principal neuron (*Billups and Forsythe, 2002a; Billups et al., 2002b*) using Differential Interference Contrast (DIC) optics. Presynaptic recordings were confirmed here through the total absence of spontaneous miniature synaptic events. (In 40 terminals 0 miniature synaptic events were observed in each 16 s calyceal recording (n=40) vs 10 \pm 7 events per second when recording from MNTB principal neuron; n=9, mice aged P10-P12). If any single spontaneous synaptic event was observed in a presynaptic recording, this data set was excluded. Additional criteria for calyceal recordings were that APs had a pronounced depolarising after-depolarisation potential (DAP, *Borst et al., 1995; Dodson et al., 2003; Kim et al., 2010*), a high membrane input resistance, a fast I_H current (*Cuttle et al., 2001*) as opposed to a slow I_H in the postsynaptic MNTB neuron (*Kopp-Scheinflug et al., 2015*) and a resting membrane potential of around –70 mV, compared to –60 mV for postsynaptic neurons.

Recordings were made with a Multiclamp 700A amplifier (Molecular Devices), 1322A digidata (Axon Instruments) and pClamp 10 software (Molecular Devices) for acquisition and analysis. Electrode and cell capacitance were compensated and series resistances were corrected, with recordings discarded when series resistances reached >20 M Ω before compensation. All recordings were compensated by 70%. Signals were digitized at 100 kHz and filtered at 10 kHz. The stated voltages were not corrected for a liquid junction potential of 11 mV.

Current-voltage relationships were generated in voltage-clamp over a range of command voltages from –110 mV to +30 mV in 10 mV incremental steps. Steps were 150 ms in duration and separated by 1 s intervals. Action potentials measured in current-clamp were generated using short depolarising current steps (50 pA increments) of 50 ms duration, the first (threshold) evoked action potential was analyzed. Pipette capacitance was neutralized and the bridge balanced. Hyperpolarising current steps (–50 pA, 150 ms) were used to determine membrane resistance. For both voltage and current clamp experiments, voltage or current commands were from –70 mV.

Postsynaptic recordings

The same experimental setup as described above was used for postsynaptic recordings. Borosilicate glass pipettes (2.5–3.5 M Ω resistance) were filled with a solution containing (in mM) KGluconate (120), KCl (10), HEPES (40), EGTA (0.2), MgCl₂ (1), K₂ATP (2.2). Electrode and cell capacitance were compensated and series resistances were corrected, with recordings discarded when series resistances reached >10 M Ω (before compensation) or changed by >10% during the recording. All recordings were compensated by 70%, signals were digitized at 100 kHz and filtered at 10 kHz.

Mice aged P20-P27 were used for studying synaptic physiology. Axons giving rise to the calyx terminal were stimulated using a concentric bipolar electrode (FHC, inc #CBAD75S) placed at the midline of a brainstem slice, controlled by a constant voltage stimulator box (DS2A, Digitimer) triggered by the pClamp 10 software. Axons were subjected to low-frequency stimulation (0.3 Hz) in order to determine the threshold for generating evoked excitatory postsynaptic currents (EPSCs) after which stimulation trains of 5 \times 100, (separated by 20 s intervals), 200 and 600 Hz for 800ms separated by 30 s intervals were applied. Time was allowed for the internal patch solution to equilibrate (5 min) before stimulation trains were applied. EPSC recordings were conducted from a holding potential of –40 mV (to inactivate voltage-gated sodium channels) and inhibitory transmission blocked by adding 0.5 μ M strychnine hydrochloride to external aCSF.

Postsynaptic recordings of action potential trains at high frequencies

Current clamp recordings were made from MNTB neurons stimulated presynaptically with a bipolar concentric electrode (FHC, inc #CBAD75S). Trains of 0.1 ms stimuli of variable voltages (3–15 V) were delivered to the presynaptic axon at 100, 200, 300, 400, and 600 Hz using a constant voltage stimulation box (DS2A, Digitimer) triggered by the pClamp10 software. Evoked responses were recorded from the postsynaptic neuron under current clamp, with resting membrane potentials adjusted to –60 mV. Stimulation trains of the duration of 800 ms at the different frequencies were repeated 3 times and separated by 20 s intervals to allow for recovery.

Voltage and current-clamp analysis

Electrophysiology analysis was conducted using Clampfit 10 software (Molecular Devices). Current amplitudes were measured as the steady-state current towards the end of the 150 ms voltage step. Presynaptic action potentials were analyzed using the threshold detection function. The threshold was set to the voltage of action potential activation and the relative amplitude defined as the difference between voltage at the peak and voltage at the threshold. Half-width is defined as the time delay between upstroke and downstroke at half-maximal amplitude. Rise and decay slopes were measured from 10% to 90% of peak amplitude.

Single excitatory postsynaptic currents were analyzed using the threshold detection function in pClamp. Baseline was defined as the resting current before stimulation. The threshold for detection was set to twice the standard deviation of the noise level. Peak amplitudes were defined as the difference between the current at the peak and the current at the baseline. Rise times were measured from 10% to 90% of the peak and decay taus were measured by fitting an exponential curve on the decay phase from 90% of the peak value. Charge was measured as the area under the curve, between the peak and baseline.

EPSC trains were analyzed by normalising each response to the first response in the train then fitting a single exponential to normalized amplitudes of responses and extracting the decay tau and steady-state amplitudes of the exponential fit to define the rate at which responses underwent short-term depression and the extent to which they depressed. mEPSCs were analyzed using template detection. A template of mEPSC kinetics was created by manually selecting 20 mEPSCs. This was then used for automatic detection of mEPSCs in all files.

Immunofluorescence

Immunohistochemistry was conducted using similar methods to those reported in *Choudhury et al., 2020*. Briefly, mice aged 28 days were killed by decapitation and the brainstem dissected and immediately snap frozen in OCT before cutting at 12 μ m transverse slices on a cryostat. Sections were mounted on poly-L-Lysine (Sigma Aldrich P8920) coated glass slides. For brainstem sections, tissues were removed and post-fixed with 4% PFA for 10 min at 4 °C. Antigen retrieval was achieved by incubating fixed tissues in a 10 mM Citrate buffer for 20 min at 85–90°C. For the cochlea both inner ears were dissected and fixed by perfusion at the round and oval window with 4% PFA in 1xPBS + 0.1% TritonX-100 (PBST), followed by overnight submersion in fixative at 4 °C. Cochlea sections were cut from whole tissues decalcified for 72 hr at 4 °C in 4% EDTA, cryoprotected with 30% sucrose, then embedded in OCT before sectioning at 12 μ m on a cryostat and mounted on poly-L-Lysine (Sigma Aldrich P8920) glass slides. Antigen retrieval was achieved by 5 min incubation in 1% SDS prior to staining. Low-affinity binding was blocked using 10% Normal Goat Serum +1% BSA in PBST ('blocking solution') for 1 hr at room temperature. Afterwards primary antibodies for Kv3.1b (Rabbit, Alomone APC-014, 1:1000) and Kv3.3 (Mouse, Neuromab 75–354, 1:3000) were diluted in blocking solution and incubated overnight at 4 °C. Following 3 \times 10 min washes in PBST, sections were incubated for 2 hours at room temperature with the appropriate secondary antibodies diluted 1:1000 in blocking solution (AF488 Goat Anti-Rabbit, A-11008; AF546, Goat Anti-Mouse, A-11003, Thermo Fisher). Slides were washed 3 \times 20 min in PBST before cover slipping with hard-set mounting medium (Vectashield, H-1400) and stored at 4 °C. Slides were imaged using Leica DM 2500 and image analysis performed using Fiji software. The same observations were made in at least 3 animals for WT and 2 animals for each KOs.

Protein retention expansion microscopy (proExM)

Mice aged P28-P30 were killed by decapitation, their brain dissected and brainstem sectioned to obtain transverse slices of 100 μ m thickness. Tissue from three animals per genotype was used for each investigation. Free-floating brain slices underwent fixation (PBST, 4% PFA, 4 °C, 15 min), and then washed in PBST (3 \times 10 min). A tissue blocking stage (RT, 1 h) was used to minimize low affinity binding with 1% BSA +10% Normal Goat Serum (Vector Laboratories S-1000) in PBST ('blocking solution'). Free floating slices were incubated with the primary antibodies in a petri dish: Anti-Kv3.1b rabbit (Synaptic Systems 242 003 Lot# 1–2, polyclonal), or Anti-Kv3.3 rabbit (Alomone APC-102 Lot# APC102AN0502, polyclonal), and Bassoon mouse C1179H11 (Synaptic Systems 141 111 Lot# 1–2, monoclonal), diluted in blocking solution (1:300 for all primary Abs) and incubated overnight at room

temperature on a shaker. The slices were washed 3×10 min in PBST, and incubated with the respective secondary antibodies (AF488 goat anti-mouse IgG, 1:300 Invitrogen A11001, Lot# 2140660; AF546 goat anti-rabbit IgG, 1:300 Invitrogen A11010, Lot# 2189179) for 2 hr at room temperature on a shaker. Slices were washed 3×10 min in PBST and incubated with 0.1 mg/ml 6-((acryloyl)amino) hexanoic acid (AcX) solution in PBS overnight with no shaking, followed by 2×15 min wash in PBS. The slices were then 'gelled' and the gels digested according to the proExM protocol for intact tissues (basic protocol 2, [Asano et al., 2018](#)). The digested gels were expanded in ddH₂O water for 3×20 min for same-day imaging or stored at 4 °C in the dark in PBS for later use. For imaging, gels were transferred to 35 mm glass-bottom petri dishes with a sealed lid, previously coated with poly-L-Lysine (Sigma Aldrich P8920). Fluorescence imaging was conducted using a Zeiss LSM 980 Airyscan 2 microscope and images were processed using ZEN 3.1 (blue edition) and Fiji software. Controls for non-specific immunostaining of the secondary antibodies (incubations without the primary antibody, data not shown), and pre-incubation of each primary antibody with the corresponding antigenic peptide (blocking peptide) were conducted as part of the antibody validation procedure. Immunostaining with Kv3.1b and Kv3.3 primary antibodies was confirmed as absent in the corresponding knockout tissues.

In vivo physiology

Adult (6–8 month) Kv3.3 knockout mice of either sex ($n=5$) and five age-matched CBA wild type mice were anesthetized with a subcutaneous injection of 0.01 ml/g MMF (0.5 mg/kg body weight Medetomidine, 5.0 mg/kg body weight Midazolam and 0.05 mg/kg body weight Fentanyl). They were placed on a temperature-controlled heating pad (WPI: ATC 1000) in a soundproof chamber (Industrial Acoustics). Depth of anesthesia was measured using the toe pinch reflex and animals responding were given supplemental MMF at 1/3 the initial dose. The mice were stabilized in a custom stereotaxic device. An incision was made at the top of the skull, followed by a craniotomy just anterior to the lambda suture intersection. The skull was tilted to provide access to the auditory brainstem. A ground electrode was placed in the muscle at the base of the neck. Glass microelectrodes were pulled from glass capillaries so that the resistance was 5–20 M Ω when filled with 3 M KCl solution. Signals were amplified (AM Systems, Neuroprobe 1600), filtered (300–3000 Hz; Tucker-Davis-Technologies PC1) and recorded (~50 kHz sampling rate) with a Fireface UFX audio interface (RME). AudioSpike software (HoerrTech) was used to calibrate the multi-field magnetic speakers, generate stimuli and record action potentials. Stimuli consisted of pure tones (50–100 ms duration, 5ms rise/fall time) at varying intensity (0–90 dB SPL) and were presented through hollow ear bars connected to the speakers with Tygon tubing. PSTHs were assessed at characteristic frequency (CF) and 80 dB SPL. MNTB neurons were identified by their excitatory response to contralateral sound stimulation and their typical complex waveform ([Kopp-Scheinflug et al., 2003](#)), consisting of a presynaptic potential (preAP), a synaptic delay (SD) and a postsynaptic potential (AP).

Auditory-evoked brainstem response

ABR equipment set-up and recordings have previously been described in detail in [Ingham et al., 2011](#). Briefly, mice were anesthetized with fentanyl (0.04 mg/kg), midazolam (4 mg/kg), and medetomidine (0.4 mg/kg) by intraperitoneal injection. Animals were placed on a heated mat inside a sound-attenuated chamber, and electrodes were inserted sub-dermally; below the right pinnae, into the muscle mass below the left ear, and at the cranial vertex. ABR responses were collected, amplified, and averaged using the TDT System3 (Tucker Davies Technology) in conjunction with custom 'Averager' software, provided by the Wellcome Trust Sanger Institute. Binaural stimuli were delivered in the form of a 0.1ms broadband click. All stimuli were presented in 5 dB SPL rising steps to 95 dB SPL, and responses were averaged 512 times per step. Recordings were averaged over a 20ms period with a 300–3000 Hz bandwidth filter and a gain of 25,000 x. Wave amplitude and latencies were analyzed using the Auditory Wave Analysis Python script developed by Bradley Buran (Eaton-Peabody Laboratory), and calculated as the difference between peak and valley (μ V) and time to wave peak (s), respectively.

Computation model

A simple model with activity-dependent vesicle recycling ([Graham et al., 2004](#); [Billups et al., 2005](#); [Lucas et al., 2018](#)) was used. In the model, vesicles in a releasable pool of normalized size n may

release with a fixed probability $P=P_v$ on the arrival of a presynaptic action potential at time s to give an EPSC amplitude proportional to np (equ. 3). Vesicles in this releasable pool are replenished up to the maximum normalised pool size of $n=1$ at a rate τ_r from an infinite reserve pool (equ. 1). In the absence of presynaptic action potentials, replenishment proceeds at a constant background rate (time constant τ_b). Following a presynaptic action potential, the replenishment rate is instantaneously raised to a higher rate, τ_h (equ. 2b) which then decays back to the background rate with time constant τ_d (equ. 2 a). The model equations are:

$$\frac{dn}{dt} = \frac{1-n(t)}{\tau_r(t)} - \sum_s P_v \cdot n(t) \cdot \delta(t-s) \quad (1)$$

$$\frac{d\tau_r}{dt} = \frac{\tau_b - \tau_r(t)}{\tau_d} \quad (2a)$$

$$\tau_r(s) = \tau_h \quad (2b)$$

$$EPSC(s) = n(s) \cdot P_v \quad (3)$$

The model is implemented in Matlab. Differential equations are solved by simple forward Euler integration.

Statistics

Statistical analysis of the in vitro data was performed in Graphpad Prism V7 unless otherwise specified. Data were tested for a normal gaussian distribution using a Shapiro-Wilk normality test and parametric (one-way ANOVA) or non-parametric tests (Kruskal-Wallis ANOVA) applied as appropriate. Multiple comparisons were corrected for using Tukey's multiple comparisons test or Dunn's multiple comparison test post-hoc and a p value of <0.05 was taken as significant. The statistical tests applied are noted in the figure legends and corresponding text. Data is represented as mean \pm SD unless otherwise stated. In vivo data are presented as medians and inter-quartiles in text numbers and figures in addition to individual data points. Statistical analyses of the in vivo data were performed with SigmaStat/SigmaPlot. Normality was tested by the Shapiro-Wilk Test. Comparisons between data sets were made using parametric tests for normally distributed data (two-tailed Student's t-test for comparing two groups) and when the normality assumption was violated, a non-parametric test (Mann-Whitney Rank Sum Test) was used.

Acknowledgements

We are grateful to the Preclinical Research Facility at the University of Leicester for the animal care, husbandry and expert assistance provided, also to Neil Ingram for assistance and advice in setting up the ABR recording system. We thank the Advanced Imaging Facility (RRID:SCR_020967) at the University of Leicester for their support, including BBSRC funding (BB/S019510/1). This research was funded by a BBSRC project grant (R001154/1: VC, IDF) and a BBSRC Case PhD Studentship (M016501: AR, NP, IDF) including support from Autifony Therapeutics Ltd, and an EU H2020 LISTEN (722098) International Training Network postgraduate funding supporting KB (IDF). Further funding was provided by DFG SFB870 A-10 (CKS) supporting MS. Thanks also for the support provided to IDF by Benedikt Grothe during a sabbatical in the Division of Neurobiology, Faculty of Biology Ludwig Maximilian University, Munich, Germany.

Additional information

Competing interests

Nadia Pilati: This author is employed by Autifony Therapeutics Ltd. The other authors declare that no competing interests exist.

Funding

Funder	Grant reference number	Author
Biotechnology and Biological Sciences Research Council	R001154/1	Ian Forsythe
Biotechnology and Biological Sciences Research Council	Case Award M016501	Ian Forsythe
H2020 Health	ITN LISTEN 722098	Ian Forsythe
Deutsche Forschungsgemeinschaft	DFG SFB870 A-10	Conny Kopp-Scheinflug

The funders had no role in study design, data collection and interpretation, or the decision to submit the work for publication.


Author contributions

Amy Richardson, Formal analysis, Investigation, Methodology, Writing – original draft, Writing – review and editing; Victoria Ciampani, Mihai Stancu, Sherylanne Newton, Bruce P Graham, Formal analysis, Investigation, Writing – review and editing; Kseniia Bondarenko, Formal analysis, Investigation, Methodology, Writing – review and editing; Joern R Steinert, Formal analysis, Investigation, Supervision, Writing – review and editing; Nadia Pilati, Funding acquisition, Investigation, Supervision, Writing – review and editing; Conny Kopp-Scheinflug, Formal analysis, Funding acquisition, Investigation, Project administration, Supervision, Writing – review and editing; Ian D Forsythe, Conceptualization, Formal analysis, Funding acquisition, Investigation, Methodology, Project administration, Supervision, Writing – original draft, Writing – review and editing

Author ORCIDs

Amy Richardson  <http://orcid.org/0000-0002-1552-2915>

Victoria Ciampani  <http://orcid.org/0000-0002-4154-1562>

Kseniia Bondarenko  <http://orcid.org/0000-0003-3321-9423>

Sherylanne Newton  <http://orcid.org/0000-0002-8210-3526>

Joern R Steinert  <http://orcid.org/0000-0003-1640-0845>

Ian D Forsythe  <http://orcid.org/0000-0001-8216-0419>

Ethics

Experiments were conducted in accordance with the Animals (Scientific Procedures) Act UK 1986 and as revised by the European Directive 2010/63/EU on the protection of animals used for scientific purposes. All procedures were approved by national oversight bodies (UK Home Office, or Bavarian district government, ROB-55.2-2532.Vet_02-18-1183) and the local animal research ethics review committees. In vivo experiments were conducted under anaesthesia: with a subcutaneous injection of 0.01ml/g MMF (0.5mg/kg body weight Medetomidine, 5.0mg/kg body weight Midazolam and 0.05mg/kg body weight Fentanyl). Every effort was made to minimise suffering and at the end of each procedure the animal was humanely killed using an approved method.

Decision letter and Author response

Decision letter <https://doi.org/10.7554/eLife.75219.sa1>

Author response <https://doi.org/10.7554/eLife.75219.sa2>

Additional files

Supplementary files

- Supplementary file 1. Summary table of averaged data and statistical tests presented in the figures, including significant (red) and non-significant values (black). Data are presented in the same order as figures appear in the article. Details are provided about the number of animals, number of cells, statistical test used and calculated p values.
- Transparent reporting form

Data availability

Data generated in this study are included in the manuscript and supporting files. Source data files for each figure has been uploaded onto FigShare. Datasets Generated for the Ms "Kv3.3 subunits control presynaptic action potential waveform and neurotransmitter release at a central excitatory synapse" Authors: Ian D. Forsythe, Amy Richardson, Victoria Ciampani, Mihai Stancu, Kseniia Bondarenko, Sherylanne Newton, Joern Steinert, Nadia Pilati, Bruce Graham, Conny Kopp-Scheinflug, 2022, <https://figshare.com/s/9c0a07ed2fe5761cc281>. The model code and associated data files are available at: Bruce Graham, 2021, <https://github.com/bpgraham/CoH-Models>, (copy archived at swh:1:rev:6ae468a42fc94dec2cf3f7c5490593ee321c8321).

The following datasets were generated:

Author(s)	Year	Dataset title	Dataset URL	Database and Identifier
Forsythe ID, Richardson A, Ciampani V, Stancu M, Bondarenko K, Newton S, Steinert J, Pilati N, Graham B, Kopp-Scheinflug C	2022	Kv3.3 subunits control presynaptic action potential waveform and neurotransmitter release at a central excitatory synapse	https://doi.org/10.25392/leicester.data.19322864.v1	figshare, 10.25392/leicester.data.19322864.v1
Graham B	2021	The model code and associated data files	https://github.com/bpgraham/CoH-Models	GitHub, bpgraham/CoH-Models

References

- Alle H, Kubota H, Geiger JRP. 2011. Sparse but highly efficient Kv3 outpace BKCa channels in action potential repolarization at hippocampal mossy fiber boutons. *The Journal of Neuroscience* **31**:8001–8012. DOI: <https://doi.org/10.1523/JNEUROSCI.0972-11.2011>, PMID: 21632922
- Alonso-Espinaco V, Elezgarai I, Díez-García J, Puente N, Knöpfel T, Grandes P. 2008. Subcellular localization of the voltage-gated potassium channels Kv3.1b and Kv3.3 in the cerebellar dentate nucleus of glutamic acid decarboxylase 67-green fluorescent protein transgenic mice. *Neuroscience* **155**:1059–1069. DOI: <https://doi.org/10.1016/j.neuroscience.2008.07.014>, PMID: 18682278
- Asano SM, Gao R, Wassie AT, Tillberg PW, Chen F, Boyden ES. 2018. Expansion Microscopy: Protocols for Imaging Proteins and RNA in Cells and Tissues. *Current Protocols in Cell Biology* **80**:e56. DOI: <https://doi.org/10.1002/cpcb.56>, PMID: 30070431
- Baranauskas G, Tkatch T, Nagata K, Yeh JZ, Surmeier DJ. 2003. Kv3.4 subunits enhance the repolarizing efficiency of Kv3.1 channels in fast-spiking neurons. *Nature Neuroscience* **6**:258–266. DOI: <https://doi.org/10.1038/nn1019>, PMID: 12592408
- Barnes-Davies M, Forsythe ID. 1995. Pre- and postsynaptic glutamate receptors at a giant excitatory synapse in rat auditory brainstem slices. *The Journal of Physiology* **488**:387–406. DOI: <https://doi.org/10.1113/jphysiol.1995.sp020974>, PMID: 8568678
- Beiderbeck B, Myoga MH, Müller NIC, Callan AR, Friauf E, Grothe B, Pecka M. 2018. Precisely timed inhibition facilitates action potential firing for spatial coding in the auditory brainstem. *Nature Communications* **9**:1771. DOI: <https://doi.org/10.1038/s41467-018-04210-y>, PMID: 29720589
- Billups B, Forsythe ID. 2002a. Presynaptic mitochondrial calcium sequestration influences transmission at mammalian central synapses. *The Journal of Neuroscience* **22**:5840–5847. DOI: <https://doi.org/20026597>, PMID: 12122046
- Billups B, Wong AYC, Forsythe ID. 2002b. Detecting synaptic connections in the medial nucleus of the trapezoid body using calcium imaging. *Pflügers Archiv* **444**:663–669. DOI: <https://doi.org/10.1007/s00424-002-0861-6>, PMID: 12194020
- Billups B, Graham BP, Wong AYC, Forsythe ID. 2005. Unmasking group III metabotropic glutamate autoreceptor function at excitatory synapses in the rat CNS. *The Journal of Physiology* **565**:885–896. DOI: <https://doi.org/10.1113/jphysiol.2005.086736>, PMID: 15845577
- Blosa M, Sonntag M, Jäger C, Weigel S, Seeger J, Frischknecht R, Seidenbecher CI, Matthews RT, Arendt T, Rübsamen R, Morawski M. 2015. The extracellular matrix molecule brevican is an integral component of the machinery mediating fast synaptic transmission at the calyx of Held. *The Journal of Physiology* **593**:4341–4360. DOI: <https://doi.org/10.1113/JP270840>, PMID: 26223835
- Bocksteins E, Mayeur E, Van Tilborg A, Regnier G, Timmermans JP, Snijders DJ. 2014. The subfamily-specific interaction between Kv2.1 and Kv6.4 subunits is determined by interactions between the N- and C-termini. *PLOS ONE* **9**:e98960. DOI: <https://doi.org/10.1371/journal.pone.0098960>, PMID: 24901643
- Borst JGG, Helmchen F, Sakmann B. 1995. Pre- and postsynaptic whole-cell recordings in the medial nucleus of the trapezoid body of the rat. *The Journal of Physiology* **489**:825–840. DOI: <https://doi.org/10.1113/jphysiol.1995.sp021095>, PMID: 8788946

- Borst JGG**, Sakmann B. 1998. Calcium current during a single action potential in a large presynaptic terminal of the rat brainstem. *The Journal of Physiology* **506**:143–157. DOI: <https://doi.org/10.1111/j.1469-7793.1998.143bx.x>, PMID: 9481678
- Borst JGG**, Soria van Hoeve J. 2012. The calyx of Held synapse: from model synapse to auditory relay. *Annual Review of Physiology* **74**:199–224. DOI: <https://doi.org/10.1146/annurev-physiol-020911-153236>, PMID: 22035348
- Brew HM**, Forsythe ID. 1995. Two voltage-dependent K⁺ conductances with complementary functions in postsynaptic integration at a central auditory synapse. *The Journal of Neuroscience* **15**:8011–8022 PMID: 8613738.
- Brooke RE**, Moores TS, Morris NP, Parson SH, Deuchars J. 2004. Kv3 voltage-gated potassium channels regulate neurotransmitter release from mouse motor nerve terminals. *The European Journal of Neuroscience* **20**:3313–3321. DOI: <https://doi.org/10.1111/j.1460-9568.2004.03730.x>, PMID: 15610163
- Brooke RE**, Corns L, Edwards IJ, Deuchars J. 2010. Kv3.3 immunoreactivity in the vestibular nuclear complex of the rat with focus on the medial vestibular nucleus: Targeting of Kv3.3 neurones by terminals positive for vesicular glutamate transporter 1. *Brain Research* **1345**:45–58. DOI: <https://doi.org/10.1016/j.brainres.2010.05.020>
- Cao XJ**, Shatadal S, Oertel D. 2007. Voltage-sensitive conductances of bushy cells of the Mammalian ventral cochlear nucleus. *Journal of Neurophysiology* **97**:3961–3975. DOI: <https://doi.org/10.1152/jn.00052.2007>, PMID: 17428908
- Chang SY**, Zagha E, Kwon ES, Ozaita A, Bobik M, Martone ME, Ellisman MH, Heintz N, Rudy B. 2007. Distribution of Kv3.3 potassium channel subunits in distinct neuronal populations of mouse brain. *The Journal of Comparative Neurology* **502**:953–972. DOI: <https://doi.org/10.1002/cne.21353>, PMID: 17444489
- Chen Z**, Cooper B, Kalla S, Varoqueaux F, Young SM. 2013. The Munc13 proteins differentially regulate readily releasable pool dynamics and calcium-dependent recovery at a central synapse. *The Journal of Neuroscience* **33**:8336–8351. DOI: <https://doi.org/10.1523/JNEUROSCI.5128-12.2013>, PMID: 23658173
- Choudhury N**, Linley D, Richardson A, Anderson M, Robinson SW, Marra V, Ciampani V, Walter SM, Kopp-Scheinflug C, Steinert JR, Forsythe ID. 2020. Kv3.1 and Kv3.3 subunits differentially contribute to Kv3 channels and action potential repolarization in principal neurons of the auditory brainstem. *The Journal of Physiology* **598**:2199–2222. DOI: <https://doi.org/10.1113/JP279668>
- Coetzee WA**, Amarillo Y, Chiu J, Chow A, Lau D, McCormack T, Moreno H, Nadal MS, Ozaita A, Pountney D, Saganich M, Vega-Saenz de Miera E, Rudy B. 1999. Molecular diversity of K⁺ channels. *Annals of the New York Academy of Sciences* **868**:233–285. DOI: <https://doi.org/10.1111/j.1749-6632.1999.tb11293.x>, PMID: 10414301
- Cuttle MF**, Rusznák Z, Wong AY, Owens S, Forsythe ID. 2001. Modulation of a presynaptic hyperpolarization-activated cationic current I(h) at an excitatory synaptic terminal in the rat auditory brainstem. *The Journal of Physiology* **534**:733–744. DOI: <https://doi.org/10.1111/j.1469-7793.2001.00733.x>, PMID: 11483704
- Desai RR**, Kronengold JJ, Mei JJ, Forman SAS, Kaczmarek LKL. 2008. Protein kinase C modulates inactivation of Kv3.3 channels. *The Journal of Biological Chemistry* **283**:22283–22294. DOI: <https://doi.org/10.1074/jbc.M801663200>, PMID: 18539595
- Devaux J**, Alcaraz G, Grinspan J, Bennett V, Joho R, Crest M, Scherer SS. 2003. Kv3.1b is a novel component of CNS nodes. *The Journal of Neuroscience* **23**:4509–4518. DOI: <https://doi.org/10.1523/JNEUROSCI.23-11-04509.2003>, PMID: 12805291
- Dodson PD**, Billups B, Rusznák Z, Szûcs G, Barker MC, Forsythe ID. 2003. Presynaptic rat Kv1.2 channels suppress synaptic terminal hyperexcitability following action potential invasion. *The Journal of Physiology* **550**:27–33. DOI: <https://doi.org/10.1113/jphysiol.2003.046250>, PMID: 12777451
- Du J**, Haak LL, Phillips-Tansey E, Russell JT, McBain CJ. 2000. Frequency-dependent regulation of rat hippocampal somato-dendritic excitability by the K⁺ channel subunit Kv2.1. *The Journal of Physiology* **522**:19–31. DOI: <https://doi.org/10.1111/j.1469-7793.2000.t01-2-00019.xm>, PMID: 10618149
- Elezgarai I**, Díez J, Puente N, Azkue JJ, Benítez R, Bilbao A, Knöpfel T, Doñate-Oliver F, Grandes P. 2003. Subcellular localization of the voltage-dependent potassium channel Kv3.1b in postnatal and adult rat medial nucleus of the trapezoid body. *Neuroscience* **118**:889–898. DOI: [https://doi.org/10.1016/s0306-4522\(03\)00068-x](https://doi.org/10.1016/s0306-4522(03)00068-x), PMID: 12732235
- Espinosa F**, McMahon A, Chan E, Wang S, Ho CS, Heintz N, Joho RH. 2001. Alcohol hypersensitivity, increased locomotion, and spontaneous myoclonus in mice lacking the potassium channels Kv3.1 and Kv3.3. *The Journal of Neuroscience* **21**:6657–6665 PMID: 11517255.
- Espinosa F**, Torres-Vega MA, Marks GA, Joho RH. 2008. Ablation of Kv3.1 and Kv3.3 potassium channels disrupts thalamocortical oscillations in vitro and in vivo. *The Journal of Neuroscience* **28**:5570–5581. DOI: <https://doi.org/10.1523/JNEUROSCI.0747-08.2008>, PMID: 18495891
- Fernandez FR**, Morales E, Rashid AJ, Dunn RJ, Turner RW. 2003. Inactivation of Kv3.3 potassium channels in heterologous expression systems. *The Journal of Biological Chemistry* **278**:40890–40898. DOI: <https://doi.org/10.1074/jbc.M304235200>, PMID: 12923191
- Forsythe ID**. 1994. Direct patch recording from identified presynaptic terminals mediating glutamatergic EPSCs in the rat CNS, in vitro. *The Journal of Physiology* **479**:381–387. DOI: <https://doi.org/10.1113/jphysiol.1994.sp020303>, PMID: 7837096
- Forsythe ID**, Tsujimoto T, Barnes-Davies M, Cuttle MF, Takahashi T. 1998. Inactivation of presynaptic calcium current contributes to synaptic depression at a fast central synapse. *Neuron* **20**:797–807. DOI: [https://doi.org/10.1016/S0896-6273\(00\)81017-X](https://doi.org/10.1016/S0896-6273(00)81017-X)

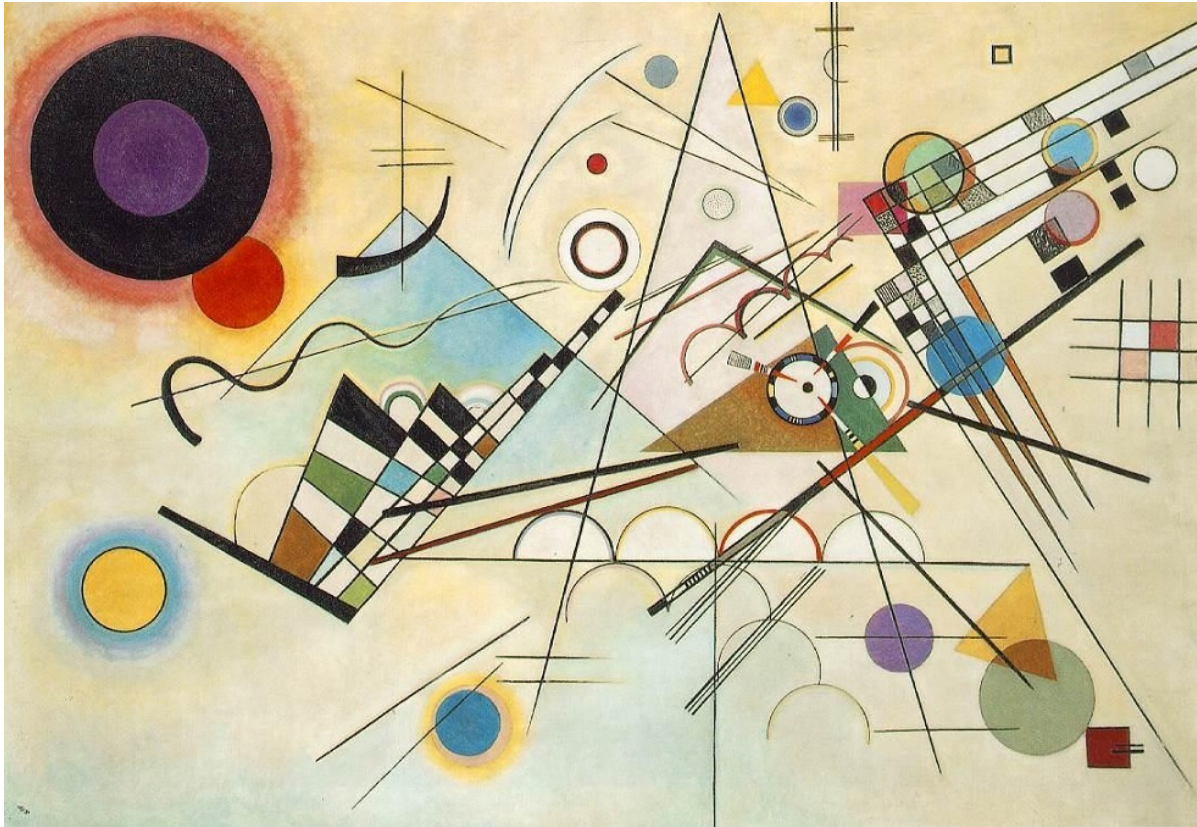
- Geiger JR**, Melcher T, Koh DS, Sakmann B, Seeburg PH, Jonas P, Monyer H. 1995. Relative abundance of subunit mRNAs determines gating and Ca²⁺ permeability of AMPA receptors in principal neurons and interneurons in rat CNS. *Neuron* **15**:193–204. DOI: [https://doi.org/10.1016/0896-6273\(95\)90076-4](https://doi.org/10.1016/0896-6273(95)90076-4), PMID: 7619522
- Geiger JR**, Jonas P. 2000. Dynamic control of presynaptic Ca⁽²⁺⁾ inflow by fast-inactivating K⁽⁺⁾ channels in hippocampal mossy fiber boutons. *Neuron* **28**:927–939. DOI: [https://doi.org/10.1016/s0896-6273\(00\)00164-1](https://doi.org/10.1016/s0896-6273(00)00164-1), PMID: 11163277
- Graham BP**, Wong AYC, Forsythe ID. 2004. A multi-component model of depression at the calyx of Held. *Neurocomputing* **58–60**:449–454. DOI: <https://doi.org/10.1016/j.neucom.2004.01.080>
- Grissmer S**, Nguyen AN, Aiyar J, Hanson DC, Mather RJ, Gutman GA, Karmilowicz MJ, Auperin DD, Chandy KG. 1994. Pharmacological characterization of five cloned voltage-gated K⁺ channels, types Kv1.1, 1.2, 1.3, 1.5, and 3.1, stably expressed in mammalian cell lines. *Molecular Pharmacology* **45**:1227–1234 PMID: 7517498.,
- Hennig MH**, Postlethwaite M, Forsythe ID, Graham BP. 2008. Interactions between multiple sources of short-term plasticity during evoked and spontaneous activity at the rat calyx of Held. *The Journal of Physiology* **586**:3129–3146. DOI: <https://doi.org/10.1113/jphysiol.2008.152124>
- Hernández-Pineda R**, Chow A, Amarillo Y, Moreno H, Saganich M, Vega-Saenz de Miera EC, Hernández-Cruz A, Rudy B. 1999. Kv3.1-Kv3.2 channels underlie a high-voltage-activating component of the delayed rectifier K⁺ current in projecting neurons from the globus pallidus. *Journal of Neurophysiology* **82**:1512–1528. DOI: <https://doi.org/10.1152/jn.1999.82.3.1512>, PMID: 10482766
- Hoshi T**, Zagotta WN, Aldrich RW. 1990. Biophysical and molecular mechanisms of Shaker potassium channel inactivation. *Science (New York, N.Y.)* **250**:533–538. DOI: <https://doi.org/10.1126/science.2122519>, PMID: 2122519
- Hu H**, Roth FC, Vandael D, Jonas P. 2018. Complementary tuning of Na⁺ and K⁺ channel gating underlies fast and energy-efficient action potentials in GABAergic interneuron axons. *Neuron* **98**:156–165. DOI: <https://doi.org/10.1016/j.neuron.2018.02.024>, PMID: 29621485
- Ingham NJ**, Pearson S, Steel KP. 2011. Using the auditory brainstem response (ABR) to determine sensitivity of hearing in mutant mice. *Current Protocols in Mouse Biology* **1**:279–287. DOI: <https://doi.org/10.1002/9780470942390.mo110059>, PMID: 26069055
- Iwasaki S**, Momiyama A, Uchitel OD, Takahashi T. 2000. Developmental changes in calcium channel types mediating central synaptic transmission. *The Journal of Neuroscience* **20**:59–65 PMID: 10627581.,
- Jalabi W**, Kopp-Scheinpflug C, Allen PD, Schiavon E, DiGiacomo RR, Forsythe ID, Maricich SM. 2013. Sound localization ability and glycinergic innervation of the superior olivary complex persist after genetic deletion of the medial nucleus of the trapezoid body. *The Journal of Neuroscience* **33**:15044–15049. DOI: <https://doi.org/10.1523/JNEUROSCI.2604-13.2013>, PMID: 24048834
- Johnston J**, Forsythe ID, Kopp-Scheinpflug C. 2010. Going native: voltage-gated potassium channels controlling neuronal excitability. *The Journal of Physiology* **588**:3187–3200. DOI: <https://doi.org/10.1113/jphysiol.2010.191973>
- Joho RH**, Ho CS, Marks GA. 1999. Increased gamma- and decreased delta-oscillations in a mouse deficient for a potassium channel expressed in fast-spiking interneurons. *Journal of Neurophysiology* **82**:1855–1864. DOI: <https://doi.org/10.1152/jn.1999.82.4.1855>, PMID: 10515974
- Joho RH**, Street C, Matsushita S, Knöpfel T. 2006. Behavioral motor dysfunction in Kv3-type potassium channel-deficient mice. *Genes, Brain, and Behavior* **5**:472–482. DOI: <https://doi.org/10.1111/j.1601-183X.2005.00184.x>, PMID: 16923152
- Joris PX**, Trussell LO. 2018. The Calyx of Held: A Hypothesis on the need for reliable timing in an intensity-difference encoder. *Neuron* **100**:534–549. DOI: <https://doi.org/10.1016/j.neuron.2018.10.026>, PMID: 30408442
- Kaczmarek LK**, Zhang Y. 2017. Kv3 Channels: Enablers of rapid firing, neurotransmitter release, and neuronal endurance. *Physiological Reviews* **97**:1431–1468. DOI: <https://doi.org/10.1152/physrev.00002.2017>, PMID: 28904001
- Karcz A**, Hennig MH, Robbins CA, Tempel BL, Rübsamen R, Kopp-Scheinpflug C. 2011. Low-voltage activated Kv1.1 subunits are crucial for the processing of sound source location in the lateral superior olive in mice. *The Journal of Physiology* **589**:1143–1157. DOI: <https://doi.org/10.1113/jphysiol.2010.203331>, PMID: 21224222
- Kim JH**, Kushmerick C, von Gersdorff H. 2010. Presynaptic resurgent Na⁺ currents sculpt the action potential waveform and increase firing reliability at a CNS nerve terminal. *The Journal of Neuroscience* **30**:15479–15490. DOI: <https://doi.org/10.1523/JNEUROSCI.3982-10.2010>, PMID: 21084604
- Kim JH**, Renden R, von Gersdorff H. 2013. Demyelination of auditory afferent axons increases the jitter of action potential timing during high-frequency firing. *The Journal of Neuroscience* **33**:9402–9407. DOI: <https://doi.org/10.1523/JNEUROSCI.3389-12.2013>, PMID: 23719808
- Kim WB**, Kang KW, Sharma K, Yi E. 2020. Distribution of Kv3 Subunits in Cochlear Afferent and Efferent Nerve Fibers Implies Distinct Role in Auditory Processing. *Experimental Neurobiology* **29**:344–355. DOI: <https://doi.org/10.5607/en20043>, PMID: 33154197
- Kopp-Scheinpflug C**, Lippe WR, Dörrscheidt GJ, Rübsamen R. 2003. The medial nucleus of the trapezoid body in the gerbil is more than a relay: comparison of pre- and postsynaptic activity. *Journal of the Association for Research in Otolaryngology* **4**:1–23. DOI: <https://doi.org/10.1007/s10162-002-2010-5>, PMID: 12098017
- Kopp-Scheinpflug C**, Tolnai S, Malmierca MS, Rübsamen R. 2008. The medial nucleus of the trapezoid body: comparative physiology. *Neuroscience* **154**:160–170. DOI: <https://doi.org/10.1016/j.neuroscience.2008.01.088>, PMID: 18436383

- Kopp-Scheinflug C**, Pigott BM, Forsythe ID. 2015. Nitric oxide selectively suppresses IH currents mediated by HCN1-containing channels. *The Journal of Physiology* **593**:1685–1700. DOI: <https://doi.org/10.1113/jphysiol.2014.282194>, PMID: 25605440
- Labro AJ**, Priest MF, Lacroix JJ, Snyders DJ, Bezanilla F. 2015. Kv3.1 uses a timely resurgent K⁺ current to secure action potential repolarization. *Nature Communications* **6**:10173. DOI: <https://doi.org/10.1038/ncomms10173>, PMID: 26673941
- Leão RM**, Kushmerick C, Pinaud R, Renden R, Li G-L, Taschenberger H, Spirou G, Levinson SR, von Gersdorff H. 2005. Presynaptic Na⁺ channels: locus, development, and recovery from inactivation at a high-fidelity synapse. *The Journal of Neuroscience* **25**:3724–3738. DOI: <https://doi.org/10.1523/JNEUROSCI.3983-04.2005>, PMID: 15814803
- Lewis AH**, Raman IM. 2014. Resurgent current of voltage-gated Na⁺ channels. *The Journal of Physiology* **592**:4825–4838. DOI: <https://doi.org/10.1113/jphysiol.2014.277582>, PMID: 25172941
- Li M**, Jan YN, Jan LY. 1992. Specification of subunit assembly by the hydrophilic amino-terminal domain of the Shaker potassium channel. *Science (New York, N.Y.)* **257**:1225–1230. DOI: <https://doi.org/10.1126/science.1519059>, PMID: 1519059
- Li W**, Kaczmarek LK, Perney TM. 2001. Localization of two high-threshold potassium channel subunits in the rat central auditory system. *The Journal of Comparative Neurology* **437**:196–218. DOI: <https://doi.org/10.1002/cne.1279>, PMID: 11494252
- Lien CC**, Jonas P. 2003. Kv3 potassium conductance is necessary and kinetically optimized for high-frequency action potential generation in hippocampal interneurons. *The Journal of Neuroscience* **23**:2058–2068. PMID: 12657664.
- Lipstein N**, Chang S, Lin KH, López-Murcia FJ, Neher E, Taschenberger H, Brose N. 2021. Munc13-1 is a Ca²⁺-phospholipid-dependent vesicle priming hub that shapes synaptic short-term plasticity and enables sustained neurotransmission. *Neuron* **109**:3980–4000. DOI: <https://doi.org/10.1016/j.neuron.2021.09.054>, PMID: 34706220
- Lorteije JAM**, Rusu SI, Kushmerick C, Borst JGG. 2009. Reliability and precision of the mouse calyx of Held synapse. *The Journal of Neuroscience* **29**:13770–13784. DOI: <https://doi.org/10.1523/JNEUROSCI.3285-09.2009>, PMID: 19889989
- Lucas SJ**, Michel CB, Marra V, Smalley JL, Hennig MH, Graham BP, Forsythe ID. 2018. Glucose and lactate as metabolic constraints on presynaptic transmission at an excitatory synapse. *The Journal of Physiology* **596**:1699–1721. DOI: <https://doi.org/10.1113/JP275107>, PMID: 29430661
- Lujan B**, Dagostin A, von Gersdorff H. 2019. Presynaptic diversity revealed by Ca²⁺-permeable AMPA receptors at the calyx of Held synapse. *The Journal of Neuroscience* **39**:2981–2994. DOI: <https://doi.org/10.1523/JNEUROSCI.2565-18.2019>, PMID: 30679394
- Macica CM**, von Hehn C, Wang LY, Ho CS, Yokoyama S, Joho RH, Kaczmarek LK. 2003. Modulation of the Kv3.1b potassium channel isoform adjusts the fidelity of the firing pattern of auditory neurons. *The Journal of Neuroscience* **23**:1133–1141. DOI: <https://doi.org/10.1523/JNEUROSCI.23-04-01133.2003>
- Meinrenken CJ**, Borst JGG, Sakmann B. 2003. Local routes revisited: the space and time dependence of the Ca²⁺ signal for phasic transmitter release at the rat calyx of Held. *The Journal of Physiology* **547**:665–689. DOI: <https://doi.org/10.1113/jphysiol.2002.032714>, PMID: 12562955
- Middlebrooks JC**, Nick HS, Subramony SH, Advincula J, Rosales RL, Lee LV, Ashizawa T, Waters MF. 2013. Mutation in the kv3.3 voltage-gated potassium channel causing spinocerebellar ataxia 13 disrupts sound-localization mechanisms. *PLOS ONE* **8**:e76749. DOI: <https://doi.org/10.1371/journal.pone.0076749>, PMID: 24116147
- Nakamura Y**, Takahashi T. 2007. Developmental changes in potassium currents at the rat calyx of Held presynaptic terminal. *The Journal of Physiology* **581**:1101–1112. DOI: <https://doi.org/10.1113/jphysiol.2007.128702>, PMID: 17331991
- Neher E**, Sakaba T. 2008. Multiple roles of calcium ions in the regulation of neurotransmitter release. *Neuron* **59**:861–872. DOI: <https://doi.org/10.1016/j.neuron.2008.08.019>, PMID: 18817727
- Neher E**. 2017. Some subtle lessons from the calyx of Held synapse. *Biophysical Journal* **112**:215–223. DOI: <https://doi.org/10.1016/j.bpj.2016.12.017>, PMID: 28122210
- Pan Z**, Kao T, Horvath Z, Lemos J, Sul JY, Cranstoun SD, Bennett V, Scherer SS, Cooper EC. 2006. A common ankyrin-G-based mechanism retains KCNQ and NaV channels at electrically active domains of the axon. *The Journal of Neuroscience* **26**:2599–2613. DOI: <https://doi.org/10.1523/JNEUROSCI.4314-05.2006>, PMID: 16525039
- Puente N**, Mendizabal-Zubiaga J, Elezgarai I, Reguero L, Buceta I, Grandes P. 2010. Precise localization of the voltage-gated potassium channel subunits Kv3.1b and Kv3.3 revealed in the molecular layer of the rat cerebellar cortex by a pre-embedding immunogold method. *Histochemistry and Cell Biology* **134**:403–409. DOI: <https://doi.org/10.1007/s00418-010-0742-6>, PMID: 20857303
- Ritzau-Jost A**, Delvendahl I, Rings A, Byczkovicz N, Harada H, Shigemoto R, Hirrlinger J, Eilers J, Hallermann S. 2014. Ultrafast action potentials mediate kilohertz signaling at a central synapse. *Neuron* **84**:152–163. DOI: <https://doi.org/10.1016/j.neuron.2014.08.036>, PMID: 25220814
- Ritzau-Jost A**, Tsintsadze T, Krueger M, Ader J, Bechmann I, Eilers J, Barbour B, Smith SM, Hallermann S. 2021. Large, stable spikes exhibit differential broadening in excitatory and inhibitory neocortical boutons. *Cell Reports* **34**:108612. DOI: <https://doi.org/10.1016/j.celrep.2020.108612>, PMID: 33440142
- Rowan MJM**, Tranquil E, Christie JM. 2014. Distinct Kv channel subtypes contribute to differences in spike signaling properties in the axon initial segment and presynaptic boutons of cerebellar interneurons. *The*

- Journal of Neuroscience* **34**:6611–6623. DOI: <https://doi.org/10.1523/JNEUROSCI.4208-13.2014>, PMID: 24806686
- Rowan MJM**, DelCanto G, Yu JJ, Kamasawa N, Christie JM. 2016. Synapse-level determination of action potential duration by K⁺ channel clustering in axons. *Neuron* **91**:370–383. DOI: <https://doi.org/10.1016/j.neuron.2016.05.035>, PMID: 27346528
- Rudy B**, Chow A, Lau D, Amarillo Y, Ozaita A, Saganich M, Moreno H, Nadal MS, Hernandez-Pineda R, Hernandez-Cruz A, Erisir A, Leonard C, Vega-Saenz de Miera E. 1999. Contributions of Kv3 channels to neuronal excitability. *Annals of the New York Academy of Sciences* **868**:304–343. DOI: <https://doi.org/10.1111/j.1749-6632.1999.tb11295.x>, PMID: 10414303
- Rudy B**, McBain CJ. 2001. Kv3 channels: voltage-gated K⁺ channels designed for high-frequency repetitive firing. *Trends in Neurosciences* **24**:517–526. DOI: [https://doi.org/10.1016/s0166-2236\(00\)01892-0](https://doi.org/10.1016/s0166-2236(00)01892-0), PMID: 11506885
- Sakaba T**, Neher E. 2003. Involvement of actin polymerization in vesicle recruitment at the calyx of Held synapse. *The Journal of Neuroscience* **23**:837–846. DOI: <https://doi.org/10.1523/JNEUROSCI.23-03-00837.2003>, PMID: 12574412
- Schneggenburger R**, Forsythe ID. 2006. The calyx of Held. *Cell and Tissue Research* **326**:311–337. DOI: <https://doi.org/10.1007/s00441-006-0272-7>, PMID: 16896951
- Sierksma MC**, Borst JGG. 2017. Resistance to action potential depression of a rat axon terminal in vivo. *PNAS* **114**:4249–4254. DOI: <https://doi.org/10.1073/pnas.1619433114>, PMID: 28373550
- Sinclair JL**, Fischl MJ, Alexandrova O, Heß M, Grothe B, Leibold C, Kopp-Scheinflug C. 2017. Sound-Evoked Activity Influences Myelination of Brainstem Axons in the Trapezoid Body. *The Journal of Neuroscience* **37**:8239–8255. DOI: <https://doi.org/10.1523/JNEUROSCI.3728-16.2017>, PMID: 28760859
- Song P**, Yang Y, Barnes-Davies M, Bhattacharjee A, Hamann M, Forsythe ID, Oliver DL, Kaczmarek LK. 2005. Acoustic environment determines phosphorylation state of the Kv3.1 potassium channel in auditory neurons. *Nature Neuroscience* **8**:1335–1342. DOI: <https://doi.org/10.1038/nn1533>, PMID: 16136041
- Southan AP**, Robertson B. 2000. Electrophysiological characterization of voltage-gated K⁺ currents in cerebellar basket and Purkinje cells: Kv1 and Kv3 channel subfamilies are present in basket cell nerve terminals. *The Journal of Neuroscience* **20**:114–122. DOI: <https://doi.org/10.1523/JNEUROSCI.20-01-00114.2000>
- Steinert JR**, Robinson SW, Tong H, Hausteiner MD, Kopp-Scheinflug C, Forsythe ID. 2011. Nitric oxide is an activity-dependent regulator of target neuron intrinsic excitability. *Neuron* **71**:291–305. DOI: <https://doi.org/10.1016/j.neuron.2011.05.037>, PMID: 21791288
- Stevens SR**, Longley CM, Ogawa Y, Teliska LH, Arumanayagam AS, Nair S, Osés-Prieto JA, Burlingame AL, Cykowski MD, Xue M, Rasband MN. 2021. Ankyrin-R regulates fast-spiking interneuron excitability through perineuronal nets and Kv3.1b K⁺ channels. *eLife* **10**:e66491. DOI: <https://doi.org/10.7554/eLife.66491>, PMID: 34180393
- Stevens SR**, van der Heijden ME, Ogawa Y, Lin T, Sillitoe RV, Rasband MN. 2022. Ankyrin-R Links Kv3.3 to the Spectrin Cytoskeleton and Is Required for Purkinje Neuron Survival. *The Journal of Neuroscience* **42**:2–15. DOI: <https://doi.org/10.1523/JNEUROSCI.1132-21.2021>, PMID: 34785580
- Taschenberger H**, von Gersdorff H. 2000. Fine-tuning an auditory synapse for speed and fidelity: developmental changes in presynaptic waveform, EPSC kinetics, and synaptic plasticity. *The Journal of Neuroscience* **20**:9162–9173. DOI: <https://doi.org/10.1523/JNEUROSCI.20-24-09162.2000>, PMID: 11124994
- Taschenberger H**, Leão RM, Rowland KC, Spirou GA, von Gersdorff H. 2002. Optimizing synaptic architecture and efficiency for high-frequency transmission. *Neuron* **36**:1127–1143. DOI: [https://doi.org/10.1016/s0896-6273\(02\)01137-6](https://doi.org/10.1016/s0896-6273(02)01137-6), PMID: 12495627
- Tatavarty V**, Sun Q, Turrigiano GG. 2013. How to scale down postsynaptic strength. *The Journal of Neuroscience* **33**:13179–13189. DOI: <https://doi.org/10.1523/JNEUROSCI.1676-13.2013>, PMID: 23926271
- Tollin DJ**. 2003. The lateral superior olive: a functional role in sound source localization. *The Neuroscientist* **9**:127–143. DOI: <https://doi.org/10.1177/1073858403252228>, PMID: 12708617
- Tolnai S**, Englitz B, Scholbach J, Jost J, Rübsamen R. 2009. Spike transmission delay at the calyx of Held in vivo: rate dependence, phenomenological modeling, and relevance for sound localization. *Journal of Neurophysiology* **102**:1206–1217. DOI: <https://doi.org/10.1152/jn.00275.2009>, PMID: 19515955
- Trimmer JS**. 2015. Subcellular localization of K⁺ channels in mammalian brain neurons: remarkable precision in the midst of extraordinary complexity. *Neuron* **85**:238–256. DOI: <https://doi.org/10.1016/j.neuron.2014.12.042>, PMID: 25611506
- Tu LW**, Deutsch C. 1999. Evidence for dimerization of dimers in K⁺ channel assembly. *Biophysical Journal* **76**:2004–2017. DOI: [https://doi.org/10.1016/S0006-3495\(99\)77358-3](https://doi.org/10.1016/S0006-3495(99)77358-3), PMID: 10096897
- Wang LY**, Gan L, Forsythe ID, Kaczmarek LK. 1998. Contribution of the Kv3.1 potassium channel to high-frequency firing in mouse auditory neurones. *The Journal of Physiology* **509**:183–194. DOI: <https://doi.org/10.1111/j.1469-7793.1998.183bo.x>, PMID: 9547392
- Wang LY**, Kaczmarek LK. 1998. High-frequency firing helps replenish the readily releasable pool of synaptic vesicles. *Nature* **394**:384–388. DOI: <https://doi.org/10.1038/28645>, PMID: 9690475
- Weiser M**, Vega-Saenz de Miera E, Kentros C, Moreno H, Franzen L, Hillman D, Baker H, Rudy B. 1994. Differential expression of Shaw-related K⁺ channels in the rat central nervous system. *The Journal of Neuroscience* **14**:949–972. PMID: 8120636.
- Wong AYC**, Graham BP, Billups B, Forsythe ID. 2003. Distinguishing between presynaptic and postsynaptic mechanisms of short-term depression during action potential trains. *The Journal of Neuroscience* **23**:4868–4877. PMID: 12832509.

- Wu XS**, Subramanian S, Zhang Y, Shi B, Xia J, Li T, Guo X, El-Hassar L, Szigeti-Buck K, Henao-Mejia J, Flavell RA, Horvath TL, Jonas EA, Kaczmarek LK, Wu LG. 2021. Presynaptic Kv3 channels are required for fast and slow endocytosis of synaptic vesicles. *Neuron* **109**:938–946. DOI: <https://doi.org/10.1016/j.neuron.2021.01.006>, PMID: 33508244
- Xu M**, Cao R, Xiao R, Zhu MX, Gu C. 2007. The axon-dendrite targeting of Kv3 (Shaw) channels is determined by a targeting motif that associates with the T1 domain and ankyrin G. *The Journal of Neuroscience* **27**:14158–14170. DOI: <https://doi.org/10.1523/JNEUROSCI.3675-07.2007>, PMID: 18094255
- Yang YM**, Wang LY. 2006. Amplitude and kinetics of action potential-evoked Ca²⁺ current and its efficacy in triggering transmitter release at the developing calyx of Held synapse. *Journal of Neuroscience* **26**:5698–5708. DOI: <https://doi.org/10.1523/JNEUROSCI.4889-05.2006>, PMID: 16723526
- Yang YM**, Aitoubah J, Lauer AM, Nuriya M, Takamiya K, Jia Z, May BJ, Huganir RL, Wang LY. 2011. GluA4 is indispensable for driving fast neurotransmission across a high-fidelity central synapse. *The Journal of Physiology* **589**:4209–4227. DOI: <https://doi.org/10.1113/jphysiol.2011.208066>, PMID: 21690196
- Yang YM**, Wang W, Fedchyshyn MJ, Zhou Z, Ding J, Wang LY. 2014. Enhancing the fidelity of neurotransmission by activity-dependent facilitation of presynaptic potassium currents. *Nature Communications* **5**:4564. DOI: <https://doi.org/10.1038/ncomms5564>, PMID: 25078759
- Yeung SYM**, Thompson D, Wang Z, Fedida D, Robertson B. 2005. Modulation of Kv3 subfamily potassium currents by the sea anemone toxin BDS: significance for CNS and biophysical studies. *Journal of Neuroscience* **25**:8735–8745. DOI: <https://doi.org/10.1523/JNEUROSCI.2119-05.2005>, PMID: 16177043
- Young SM**, Veeraraghavan P. 2021. Presynaptic voltage-gated calcium channels in the auditory brainstem. *Molecular and Cellular Neurosciences* **112**:103609. DOI: <https://doi.org/10.1016/j.mcn.2021.103609>, PMID: 33662542
- Zagha E**, Manita S, Ross WN, Rudy B. 2010. Dendritic Kv3.3 potassium channels in cerebellar purkinje cells regulate generation and spatial dynamics of dendritic Ca²⁺ spikes. *Journal of Neurophysiology* **103**:3516–3525. DOI: <https://doi.org/10.1152/jn.00982.2009>, PMID: 20357073
- Zhang Y**, Zhang XF, Fleming MR, Amiri A, El-Hassar L, Surguchev AA, Hyland C, Jenkins DP, Desai R, Brown MR, Gazula VR, Waters MF, Large CH, Horvath TL, Navaratnam D, Vaccarino FM, Forscher P, Kaczmarek LK. 2016. Kv3.3 channels bind Hax-1 and Arp2/3 to assemble a stable local actin network that regulates channel gating. *Cell* **165**:434–448. DOI: <https://doi.org/10.1016/j.cell.2016.02.009>, PMID: 26997484
- Zhang Y**, Li D, Darwish Y, Fu X, Trussell LO, Huang H. 2022. KCNQ channels enable reliable presynaptic spiking and synaptic transmission at high frequency. *The Journal of Neuroscience* **42**:3305–3315. DOI: <https://doi.org/10.1523/JNEUROSCI.0363-20.2022>, PMID: 35256530

4. Discussion & further directions



Kandinsky, Composition 8, 1923

The main findings of this thesis directly address mechanisms of neuronal processing in the lower auditory pathway, in the mammalian brainstem. The Stancu et al. paper demonstrates how auditory activity directly influences myelination on an individual axonal basis, which could yield significant meaning for future research in neuroplasticity and sensorial processing. The discrete myelination points towards an adaptive response to the environment, so future effort could be directed towards exploring the potential of sensory stimulation in treating demyelinating diseases when combined with conventional therapies. Another key point of the study is the importance of well-balanced sensorial experience for the development and optimal neuronal functioning. It opens the gate to the question whether altered sensory input has a long-lasting effect on cognitive and sensory processing capabilities of the central nervous system. Further investigation of molecular and signaling pathways that are involved in the activity-dependent myelination could further shed more light on potential therapeutic targets for pharmacological targeting and could further advance our understanding of the dynamic nature of myelin plasticity.

The Richardson et al. paper offers perspectives on the roles of the Kv3.3 potassium channels in auditory processing. It clearly shows how these are essential for maintaining a precise synchronization and for a high-fidelity signal transmission at the Calyx of Held synapse. This has major implications in

temporal auditory processing and sound localization mechanisms. Future research on these potassium channels could yield further results in other sensory and neuronal circuits, which would point towards common mechanisms that form the basis precise encoding in different modalities. Furthermore, understanding the developmental timeline and the factors that influence the expression of Kv3.3 channels could help building therapeutic strategies for auditory processing or sound localization disorders, with potential applications also for neurodevelopment studies and auditory rehabilitation.

Both papers show the importance of speed, accuracy and fidelity in auditory processing. While the adaptive traits that make very fast and reliable neuronal signal generation and transmission possible are intricate, interesting and can be fascinating on their own, we should put another step forward and try to question the overall framework in which the entire ensemble takes place. The overarching purpose of the nervous system, as previously mentioned, is to deal with information, regardless of its type, origin or final destination or purpose. At the same time, we must keep in mind that any individual neural system is, by nature, a limited-resource setup. For the living organisms, efficient energy use is found everywhere, from molecular mechanisms to whole organ assemblies.

The auditory pathway is an exceptional model to study these limitations and their consequences, because it functions at the very limit of physical neuronal AP generation and conduction speeds, in a sustained and reliable manner.

4.1 Efficient coding

The signals the neurons generate and use for conveying information were strongly proposed to be part of an elegant *modus operandi* of the brain called Efficient Coding, where the adaptive traits for temporal coding play a crucial role.

Efficient coding, a concept in information theory, pertains to the transmission or storage of data while minimizing the use of resources, energy, and time. This notion was first developed at the Bell Telephone Labs, from the 1920s to the 1950s. The key people involved were Ralph Hartley, Harry Nyquist, and Claude Shannon¹⁸⁶. Information theory aided their company in reducing telegram and telephone transmission expenses by offering a quantitative framework for assessing emerging telecommunications technology. The objective was to devise a system that guaranteed dependable message transmission and storage.

According to the source coding theorem, efficient encoding schemes are characterized by the average number of bits employed to transmit messages, approaching the entropy of the source^{187–190}. Efficient codes aim to use the least number of bits by eliminating predictable information, minimizing redundancy, adapting to environmental statistics and maximizing information transmission. The efficient coding hypothesis posits that the brain's sensory processing should adapt to stimuli coming from the environment, with neural cells from the visual and auditory systems finely-tuned to encode images or sounds found in nature. Research has revealed if you compile filters that are optimal for representing naturalistic images, they would be highly similar the V1 cells' receptive fields. Similarly, optimizing a network for encoding natural sounds yields filters analogous to the inner ear's cochlear filtering. This principle suggests that activity in the neurons would mirror the environment's statistical structure of inputs and optimize representational abilities. In achieving these requirements, the neuronal code should be sparse and non-redundant, capturing the full spectrum of variability in signal structure while remaining as concise as possible along pertinent dimensions.

To test this principle, researchers developed artificial codes optimized based on specific limitations for optimal naturalistic sound representation. The resulting codes were compared to experimental neuron spiking data in the auditory pathway and, assuming sparse responses and examining a library of sounds, researchers created spectro-temporal filters exhibiting diverse spectro-temporal relations that aligned with the observed diversity in the auditory pathway¹⁹¹. Further looking at speech sounds and other naturalistic examples and analyzing their independent components identified a link between tuning center frequency and bandwidth, predicting overrepresentation when overexposing a tone's frequency. Experiments found this was found to be true for neurons in the A1¹⁹². The need for restraining the code used for representing naturalistic sounds led to having neurons that respond to a single or multiple frequencies, similar to the ones found in the primate auditory cortex¹⁹³. Having the restraint (sparseness) and scaling down the input (divisive normalization in a neuron network) led to observing highly similar firing patterns to the ones found in the auditory pathway¹⁹⁴. If there is an additional set of neural connectivity added to the pipeline, the result is the non-uniform distribution of spatial tuning experimentally observed for mammals¹⁹⁵.

Vocalizations represent a fascinating subject in auditory neuroscience, with con-specific vocalizations being especially pertinent to auditory communication. The natural vocalizations are a special target for auditory processing in many species, with neurons in the cortex having elevated tuning capabilities for them^{196–200}. Encoding vocalizations at a higher information rate is achievable when their statistical properties remain constant²⁰¹. Predictive models for auditory processing have

shown improved accuracy in forecasting activity in the primary auditory cortex when stimuli consist of sounds exhibiting the statistical structure of con-specific vocalizations²⁰².

The principles for efficient coding could be applied for speech perception as well. Listeners are better at discriminating speech when this is done through vocoders with filters that follow the efficient coding principles in comparison with simple linear or cochleotopic filtering²⁰³. Another very important finding is the scale-invariance property of speech perception that was observed in adults^{204–208}, children^{209,210}, and newborn babies²¹¹ because it shows that despite the ongoing changes caused by aging, the system is capable of maintaining the same level of output. It is to be noted however that the amount of compression that the system can tolerate is about a third of the original duration; with this being regarded as evidence for a multi-level time scale framework for processing speech, that is made to represent the building blocks of verbalizations – phrase/syllable/phoneme^{212–214}.

A further development and more refined iteration of the Efficient Coding paradigm is the *Active Efficient Coding* or *Adaptive Efficient Coding*, depending on various authors and slight variations in the definition^{215,216}. To maintain the general line of this work, I will choose and use the term *Active Efficient Coding*, to keep any overlap at bay.

4.2 Active efficient coding

In the realm of perception, the primary goal of sensory processing within the brain is to facilitate precise judgments and behavioral reactions based on neural mechanisms. However, due to the ever-changing nature of sensory environments, the brain must possess the capability to analyze signals in an adaptable and appropriate fashion. A significant challenge arises when the statistics of natural environments undergo rapid and extensive shifts. For example, transitioning from a boisterous, crowded bar to a tranquil restroom or from a well-lit area to a dimly lit room may involve considerable changes in loudness, brightness, and other statistical properties that represent each environment's distinct features. To manage these fluctuations, which may surpass the range of stimulus values that can be encoded through firing rate variations, sensory neurons modify their sensitivity or tuning characteristics in a compensatory fashion^{217,218}. This process, referred to as active coding, permits these neurons to convey information to downstream targets more effectively, thereby enhancing our capacity to identify faces, understand speech, and execute other tasks across a broad array of environmental conditions.

Neural circuits involved in sound localization exemplify experience-dependent plasticity. The physical separation of ears results in interaural disparities in sound intensity and arrival time, while monaural spectral cues are produced as sounds enter the visible external ear on the head's side. These cues vary with the sound source's orientation relative to the head, and this association alters as the head expands during development^{219–223}. Obstructing one ear in young animals can also provoke compensatory changes in auditory spatial processing within the brain, preserving normal localization accuracy^{224–229}. Furthermore, spatially incongruent visual information can elicit corresponding changes in the spatial tuning in the barn owl optic tectum²³⁰ and its mammalian equivalent, the superior colliculus²³¹. This cross-modal plasticity culminates in the emergence of topographically aligned maps of auditory and visual space during development^{230,231}. Although this feature can be advantageous, it may also give rise to systematic errors in auditory localization²³².

These findings underscore the functional importance of experience-dependent plasticity during early development, allowing the brain to calibrate itself and optimize sensory inputs varying

based on individual anatomical disparities. The ability to adapt to altered sensory cues is not confined to early development but persists into adulthood. In the context of spatial hearing, adults can rapidly learn to localize sounds accurately despite atypical binaural cues^{233–238}.

Over shorter timeframes, auditory neurons' tuning characteristics are influenced by the behavioral context in which sounds are introduced. They emphasize specific stimulus attributes pertinent to the task at hand^{191,239–241}. This implies that auditory processing is constantly fine-tuned during active listening to optimize the processing of attention-capturing features, thus enhancing sound detection and discrimination²⁴². Neuronal stimulus selectivity also flexibly shifts during the acquisition and reversal of conditioned behavioral responses^{243–245} and is frequently linked to training-induced enhancements in discrimination that facilitate perceptual learning^{246–248}. Adjustable and plastic processes in the brain are essential for successful auditory rehabilitation in individuals using hearing aids and cochlear implants. The brain's adaptability to the unique inputs provided by these devices enables users to incorporate and maximize their hearing aids^{249–253}. Similarly, the brain's reactive plasticity plays a critical role in recuperating from other types of central nervous system damage or illness²⁵⁰.

Grasping the mechanisms of neural plasticity in flexible, healthy, and maladaptive scenarios is crucial for devising efficient interventions for auditory rehabilitation and managing conditions such as tinnitus and hyperacusis^{253,254}. A variable firing rate is a fundamental aspect of sensory neurons, where they react to a steady stimulus by reducing impulses over time. This occurrence was first documented in studies on cat plantar digital nerves responding to tactile stimuli on the toe²⁵⁵, and was later recognized in a variety of sensory systems. Sensory neurons usually possess a limited scope of stimulus intensities they can encode, referred to as their dynamic range. Proactive firing-rate adaptations protect these neurons from being overloaded and their responses from reaching saturation upon encountering a novel stimulus within their dynamic range. This adaptability indicates that neurons are more receptive to new or short-lived stimuli than to continuous background stimulation. At the perceptual level, modifying firing rates can lead to decreased sensitivity to an ongoing stimulus. For instance, in vision, this happens when a bright light is observed for a prolonged duration, followed by a brief aftereffect once the light is removed²⁵⁶. Physiologically suitable adjustments and flexibility are vital for sensory processing, ensuring the brain can efficiently discern between significant sensory input alterations and trivial background noise.

A modifiable firing rate can also be found in auditory nerve fibers, which are crucial for relaying auditory information from the inner ear to the auditory brainstem²⁵⁷. Within the cochlea, the basilar membrane's mechanical properties distinguish various sound frequency components, with higher frequency tones causing maximum vibration at the cochlea's base and lower frequencies at its apex. The basilar membrane supports the organ of Corti, which houses two types of mechanosensory receptor cells, inner and outer hair cells, organized in rows along the cochlea. The majority of auditory nerve fibers each connects to a single inner hair cell and display comparable frequency tuning, mirroring their placement along the cochlea. An adjustable firing rate initially emerges in these auditory nerve fibers, averting their responses from reaching saturation by decreasing the impulses generated by a constant stimulus over time^{257–259}. As a result, neurons exhibit greater sensitivity to novel or fleeting stimuli than constant background stimuli. It is crucial to recognize that the adjustment observed in auditory nerve fibers represents only the initial phase of intricate auditory information processing taking place in the brain. As auditory signals traverse the auditory pathway, they experience more complex processing involving higher-order neurons, culminating in the perception of intricate auditory stimuli, such as speech and music.

Based on electrophysiological observations across diverse animal species, a continuous tone within an auditory nerve fiber's responsive frequency range prompts a swift surge in action potential firing rates, peaking shortly after stimulus onset. This is then followed by a rapid decrease within the initial milliseconds, eventually stabilizing. Upon sound cessation, spike frequency momentarily dips below the baseline or innate firing rate. This firing pattern adeptly conveys rapid fluctuations in sound intensity, characteristic of many natural sounds, while filtering out superfluous information. In the avian auditory nerve, noise increases in rate coding as the response wanes during adaptation, yet spike timing precision is maintained, highlighting the potential significance of conveying neural signals to the brain with high temporal fidelity via afferent auditory fibers ²⁶⁰.

Adaptive firing-rates can result from various factors: neuronal intrinsic ion channel properties, modifications in its synaptic inputs, or upstream property changes of neurons²¹⁷. Sensitivity to change is crucial for the conversion process executed by hair cells within the auditory and vestibular systems of the inner ear²⁶⁰. In these sensory cells, external stimuli like sound waves or head movements/tilts shift stereocilia or hair bundles, leading to fluctuations in the tension of tip links connecting neighboring stereocilia rows. This regulates the opening of mechano-electrical transduction channels, subsequently causing graduated shifts in membrane potential, primarily through potassium ion influx.

Numerous studies have shown that when the hair bundle is persistently deflected toward the tallest stereocilia, mechano-electrical transduction channels open and then close, resulting in a decreasing initial inward current. Low-frequency hair cells, such as those in the vestibular regions of the inner ear or the basilar papilla, exhibit both fast and slow mechanisms for this type of responsiveness. However, transducer activity in mammalian auditory hair cells differs from that in nonmammalian species^{260,261}. Sound-evoked receptor potentials recorded from mammalian inner hair cells are too sustained to account for the responsive change in the auditory nerve^{262,263}. Instead, synaptic depression occurs at ribbon synapses that link hair cells and afferent nerve fibers, suggesting this change primarily results from synaptic fatigue²⁶⁴⁻²⁶⁶. Although differences in the time constants of firing-rate changes have been reported in the auditory higher processing levels, these differences likely reflect the added contribution of intrinsic and network properties²⁶⁷⁻²⁶⁹.

To process ever-changing real-world stimuli, sensory systems have evolved various forms of responsiveness to shifting stimulus statistics. Initially studied in the visual system²⁷⁰, this phenomenon is now acknowledged as a fundamental aspect of general sensory information processing. Comprehending these mechanisms holds significant theoretical implications for the efficient and robust representation of sensory information in the brain. In the auditory system, responsiveness to changing stimulus statistics has been extensively studied, especially at early sensory processing levels. One example is adjusting to the mean sound level, demonstrated in the auditory nerve and other levels of the auditory pathway^{271,272}. However, more complex forms of responsive change to stimulus statistics are also present at higher processing levels.

In summary, these distinct forms of continuous fine-tuning in the auditory system are believed to serve various functions in sound perception and contribute to the efficient representation of auditory information in the brain. By adjusting firing activity to the changing statistical properties of sounds, the auditory system can process complex sounds more effectively, which may be particularly crucial in natural environments where sounds can be highly variable.

4.3 Predictive coding

Another branching of the efficient coding theory deals with an extra refinement in the overall efficiency of the computational system. It is intuitive to assume that if predictions can be made through detecting certain patterns, then the energy performance and final outcome would be improved.

The predictive coding theory stands as a broad and influential model for comprehending neural function, aiming to shed light on the brain's interpretation of the world²⁷³. Though it has recently garnered more attention, various foundational notions have their roots in earlier academic literature. For example, Neisser²⁷⁴ presented the perceptual cycle concept during cognitive psychology's infancy, which can be considered a forerunner to predictive coding. This in turn provides persuasive justifications for a range of subjects, such as neuroanatomy²⁷⁵, electrophysiology²⁷⁶ and psychology²⁷⁷ when it is used as a physical support for Bayesian theories of higher brain functions. Initially implemented in the visual system, the predictive coding's application has broadened to encompass auditory system investigations^{273,278–281}.

Predictive coding naturally arises from efficient coding principles, especially regarding the processing of sequential or autocorrelated data. This insinuates that the brain's neural codes are configured to minimize the information needed to represent a specific dataset while preserving its essential aspects. This feat is accomplished by taking advantage of correlations and patterns within the data, allowing the brain to encode information efficiently without omitting crucial details. Nevertheless, a neural code's efficiency relies on the statistical distribution of the data being encoded. For instance, the statistical distribution differences could render a code efficient for one situation, but completely crippled for another. This points towards an optimization of the codes to the surroundings, with a continuous adaptation for keeping up with changes in the environment. These adjustments can occur at multiple levels of neural processing, from singular neurons to intricate networks. Efficient encoding of sequential data mandates that the brain learns the sequence's order and the timing between events. This is essential because the brain needs to predict upcoming events to encode the data accurately. Indeed, the ability to forecast future occurrences is thus a byproduct of efficient coding in the circuitry, without a specific framework for representational purposes¹⁸⁶. In summary, predictive coding is an intrinsic result of efficient coding principles, specifically in relation to processing sequential or autocorrelated data.

The theory posits that substantial energy savings are achievable, but reaching these savings demands an understanding of sensory input distributions, even including the layout of inputs and outputs. However, learning these relevant distributions often surpasses conventional efficient coding theory's scope. While neural structures facilitating efficient coding can develop over generations²⁸², or over the course of a life, through specific learning algorithms (self- or un-supervised)^{283–286}, the phrase "predictive coding" introduces some semantic uncertainty, as it might refer to particular unsupervised learning algorithms that don't necessarily align with Shannon's efficient coding formalism^{275,276,287–291}. Furthermore, the general agreement is that the predictive functions are cortical, throughout developmental stages, learning processes, and efficient coding performed by the neurons^{285,292–296}. In this framework, predictive coding refers to a method for encoding and compressing data from specific distributions and modalities to promote energy efficiency.

Mismatch negativity (MMN) is an event-related potential (ERP) automatically initiated by a noticeable change in auditory stimulation. As a widely studied marker of auditory deviance detection, MMN can be measured from the human scalp. Generated using the classic oddball paradigm, MMN

involves rare acoustic events (deviant stimuli) randomly mixed with frequently repeating sounds (standard stimuli²⁹⁷). This deviance-specific auditory ERP component persists during sleep²⁹⁸, anesthesia^{299,300}, coma³⁰¹, and is detectable in newborns^{302,303}. MMN has evolved to identify deviances within complex sequences governed by abstract rules^{304–308} and is believed to support higher-order cognitive functions³⁰⁹ like attention^{310,311} and memory^{312,313}. MMN disruptions are found in various conditions such as schizophrenia^{314–319}, Parkinson's and Alzheimer's diseases^{320–325}, autism spectrum disorders^{326–328}, and language impairments^{329,330}, making it a vital tool in cognitive and clinical neuroscience with potential diagnostic applications^{312,331–336}.

Many animal species display deviance-detection processes similar to human MMN. Certain neurons in auditory pathways exhibit reduced responses to repetitive standard sounds but react to unexpected deviant sounds. This adaptation is a subtype of plasticity and is called stimulus-specific adaptation or SSA. The SSA index measures the change in a neuron's firing rate responding to a deviant stimulus. SSA neurons are present in non-lemniscal sections of the auditory midbrain^{337–343} and thalamus^{344–347}, and primary^{348–352} and secondary^{353,354} auditory cortex areas. SSA is proposed as a neural correlate for the deviance-detection mechanism³⁵⁵, with population activity summation leading to an MMN signal on the scalp³⁵⁶. This has encouraged research that aimed to connect microscopic (SSA) and macroscopic (MMN) aspects of deviance detection by studying anatomy, internal biochemical clockwork and stimulus-specific adaptation dynamics^{356–359}.

The predictive coding theory posits that perception results from merging environmental sensory input with internal model predictions^{275,360,361}. The system anticipates input based on previous events, minimizing errors by consistently updating the model. Recurrent interactions among processing levels in individual volumes or clusters reduce errors. These levels in turn create their characteristic model that would represent the input and transmit top-down predictions to account for input without reprocessing³⁶². The merging of inputs and predictions forms a multilevel sensory representation, allowing for perception with minimal resources. However, if predictions don't align with input, first-level neuronal populations signal prediction errors to higher levels, prioritizing processing of unpredicted features, similar to true deviance detection. The levels therefore communicate back and forth for silencing the erroneous signal, signifying optimized perceptual encoding³⁶².

Optimal perceptual representation across increasingly complex processing levels necessitates a balance between expectations and predictions of the neural circuits and this balance would involve short-term synaptic plasticity. Neuronal input mechanisms like synaptic depression, facilitation, and inhibition have varying effects on different parts of a neuron's dendritic tree, boosting postsynaptic sensitivity in deviance-detection neurons exhibiting SSA³⁶³. As a result, when repetitive stimuli align with top-down inputs, bottom-up influences are weakened due to reduced postsynaptic responsiveness to recurring sensory inputs, as suggested by the adaptation hypothesis. However, adaptation primarily accounts for repetition suppression in deviance detection^{360,364–367}, which refers to a diminished representation of a certain characteristic, such as frequency or intensity in auditory stimulation³⁴¹.

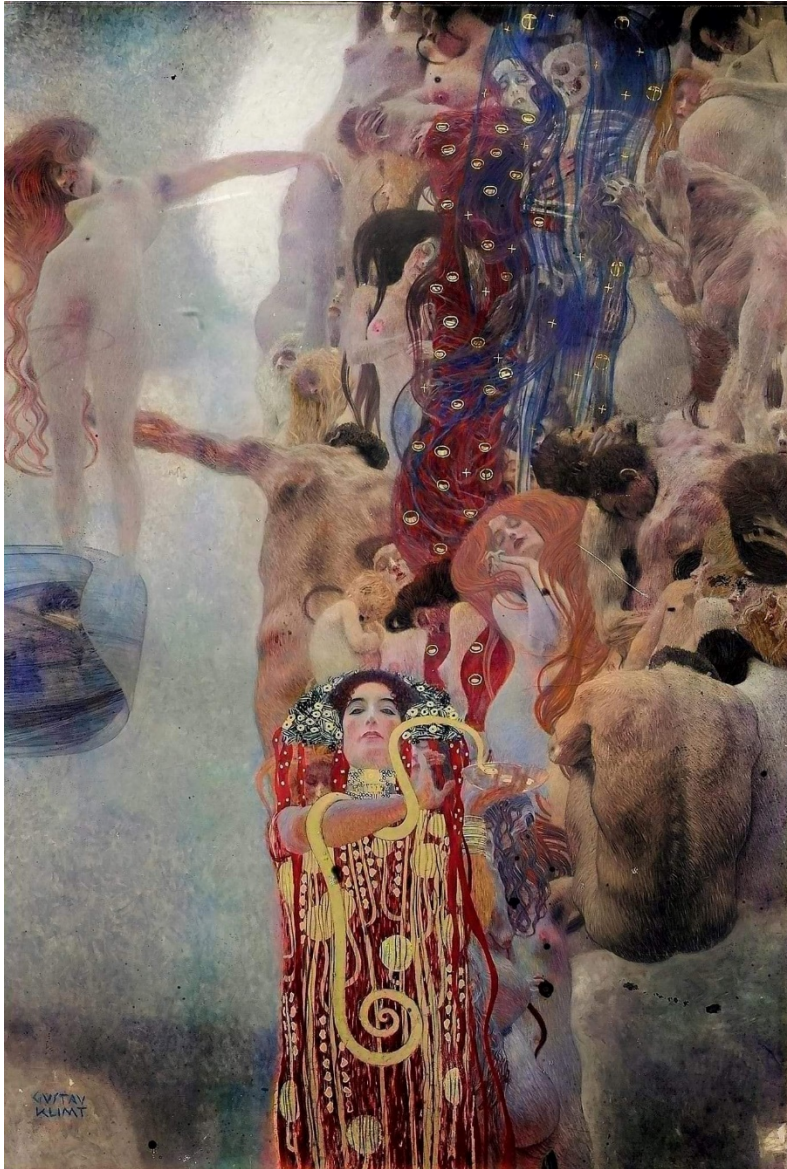
This theory states that the brain encodes regularities of varying complexity across multiple processing levels, so when a stimulus adheres to a recognized regularity, it doesn't require new representation, resulting in dampened responses and conserved processing resources. This automatic expectation suppression^{368–372} serves as a functional characteristic of perceptual representations upheld by a neuronal population's processing network. Automatic expectation suppression operates as a series of filters for redundant information throughout hierarchical processing levels. Repetition suppression, the most basic form of expectation suppression, can be attributed to adaptation. Lower

levels of the processing hierarchy can locally represent less resource-demanding regularities, like the repetition of a physical attribute, through suppression. However, as processing levels accumulate iteratively, higher regions may extract increasingly intricate stimulus patterns and abstract relationships, as demonstrated in MMN studies.

The act of interpreting stimuli involves recognizing patterns and identifying deviations from those patterns. Predictive coding theory posits that as more input aligns with established representations, the reliability and potency of the perceptual model increase, resulting in a more robust suppression of responses triggered by conforming inputs. However, when input strays away from the recognized pattern, the predictive expectation will fail. Both output intensity and delay of the signal responsible for detecting discrepancies should correspond to the level of deviation and the certainty linked to the perceptual model. This idea is backed by studies on mismatch negativity (MMN) in humans³³² and stimulus-specific adaptation (SSA) in animals³⁵⁵.

To identify deviations, a standard for consistency is required²⁸¹. This benchmark is the overarching signal produced by an input which breaches the pattern produced within a specific processing pathway segment. Deviance detection encompasses two procedures: aligning afferent information with the circuit's pattern, resulting in expectation suppression, and the liberation of neuronal responses from suppression and the transmission of prediction errors to subsequent processing stages when a divergent event does not align with expectations. Interaction between hierarchical processing levels enables distinct predictive responses from varying circuits, primarily reliant on how these networks encode information.

Research on MMN and SSA supports the notion that predictive coding can explain and connect the three fundamental concepts of deviance detection, expectation suppression, and prediction error. The brain can be conceptualized as a prediction mechanism, and this framework has successfully integrated perception and cognitive neuroscience. Numerous research teams have embraced the predictive coding approach and integrated it into their investigations, leading to enhanced comprehension of auditory scene analysis, deviance detection, and sound attention^{279–281,364,373,374}. The stimulus firing train model adjusts in response to changing stimuli, with synaptic connectivity's plastic alterations and conduction velocity changes facilitating the adaptation process.³⁶⁴



Gustav Klimt, Medizin, 1897; Colorized photo;
 Painting was destroyed in a fire at Schloss Immendorf caused by retreating troops on 8 May 1945.

My core training as a medical doctor makes it natural to try and have an overview of the impact that my work could have for helping patients. I will provide an outline of two medical subjects of particular interest, in which temporal coding mechanisms are crucial for positive outcomes.

4.4 Cochlear implants

Cochlear implants (CIs) represent a groundbreaking development in neural prosthetics, enabling those with severe hearing impairments to regain their sense of sound. CIs function by electrically stimulating the cochlear nerve, where the health of spiral ganglion neurons (SGNs) significantly influences their effectiveness. Factors such as the duration and cause of hearing loss^{375–378}, which are associated with neural integrity, play a crucial role in predicting CI

outcomes. However, establishing a direct connection between these factors and SGN integrity in humans has been challenging. Post-mortem examinations have disclosed a substantial decrease in SGN cell bodies in older individuals, mainly in the cochlea's base. This reduction is more pronounced when both inner and outer hair cells are missing. Further indirect evidence supports the notion that SGN integrity is vital for CI outcomes³⁷⁹. Patients with non-syndromic deafness that leaves SGNs intact typically experience better CI outcomes than those with genetic or infectious origins that result in nerve damage³⁸⁰.

Studies have indicated that sensorineural deafness can prompt sudden and progressive alterations in the structure and functionality of SGNs in both humans and animals^{381,382}. These changes encompass axonal demyelination and a reduction in the number of myelin lamellae³⁸³, which may deteriorate over time. The myelin loss occurs first in the SGN periphery, which is then followed by central segment and ends with the complete cell destruction³⁸¹. Recent research observed a decrease in myelin sheath count and an altered myelin thickness arrangement in rats exposed to deafening acoustic levels, suggesting that SGN structural integrity is negatively impacted by deafness. Although

no studies have directly explored the relationship between SGN myelination and human auditory behavior, some cases have documented temporary hearing impairments in patients with autoimmune demyelinating disorders who suffer from fever-related deafness due to elevated core body temperatures. These instances underscore the critical function of myelination in the auditory nerve system³⁸⁴.

The majority of individuals with bilateral, post-lingual deafness who receive cochlear implants experience some enhancement in speech recognition and quality of life. However, the degree of improvement varies significantly among individuals. Some achieve nearly flawless performance on speech recognition tasks, while others show less progress.^{375,376,385} Binaural hearing tasks, such as localizing sound sources, can be particularly challenging for those with bilateral implants, even when incorporating advanced techniques like temporal fine structure information coding, electrode pitch-matching, and device synchronization^{386,387}. Pre- and peri-operative factors only partially account for this variability in cochlear implant outcomes³⁷⁵.

To better comprehend the connection between anatomical and electrophysiological neural changes in hearing loss, computational models of the cochlear implant electrode-neuron interface can be employed. These could shed light on the variability that was seen in how humans benefit from cochlear implants, as not every patient has the same level of improvement. While previous studies have utilized analytical models to investigate myelination and current spread through fibers³⁸⁸⁻³⁹⁰, these models are limited as they can only reveal electrotonic effects and cannot predict suprathreshold fiber behavior or account for stochasticity introduced by small ion channel populations³⁹¹⁻³⁹³. Recently, point-process models that are empirically derived are increasingly employed for studying the activity elicited by stimuli from outside the cell. They can mimic the electrophysiology of individual neuronal units from real life organisms and also carry the information needed for the modulation of the action potential amplitude³⁹⁴. Moreover, they have been expanded to create the initiation of action potentials from the central nervous system as well as the peripheral one. This allows the duplication of what is seen in cat neurons, namely the activity evoked by monophasic stimuli that have opposing polarities^{395,396}. However, these models are difficult to interpret due to their empirical nature, making it challenging to predict the way different variables change in disease paradigms. Additionally, the current data scarcity on rheobase exploration in chronic deafness models in animals makes it difficult to construct such phenomenological models. Accurate delivery of neural responses to individual pulses from cochlear implants is essential for encoding fine temporal information, especially temporal pitch coding and interaural time differences. However, pathologies that cause changes in the latency of single-pulse responses can hinder the quality of conveyed information. Even minor changes in myelin integrity can substantially alter the timing of stimulus-induced action potentials, significantly affecting behavior. Although phonetically relevant temporal information in speech usually exceeds 20 milliseconds^{397,398}, the auditory system can detect disparities of tens of microseconds between the left and right ears to localize sounds^{399,400}.

When demyelination impacts a minimum of first ten peripheral nodes, the AP initiation delay increases when elicited through polarized electric pulses. This increase in latency is proportional to how much the axon was impacted as well as to how much myelin was lost, causing a drop in conduction capabilities for the affected axons. The links between the responses characteristics and myelination states are different throughout various pulse polarities, with special implications for bi-phasic pulses. In healthy fibers and those with limited demyelination, both cathodic-first (CF) and anodic-first (AF) stimulations elicits comparable thresholding and latency with respect to cathodic monophasic stimuli⁴⁰¹. However, for axons experiencing more severe and extensive demyelination, the response properties turn more like the anodic monophasic stimuli and it happens because of the

demyelination of the fiber area typically activated by cathodic polarity pulses, with the central part that is depolarized by anodic pulses being left untouched. This causes sharp alterations at the location of action potential generation⁴⁰¹. Consequently, the shift in relative phase sensitivity notably alters response timing⁴⁰².

To ensure cochlear implant users have access to the interaural time differences (ITDs) needed for precise lateralization judgments, it is critical to accurately encode the timing of individual pulses. Individuals with normal hearing can quickly utilize ITDs, with onset ITDs being especially significant for this purpose^{403–405}. However, the employment of biphasic pulses in contemporary implants might lead to diminished temporal precision, with latency effects more pronounced for AF pulses than CF pulses. Despite the necessity for precise timing in transmitting accurate timing details, the modern CI technologies rely on high rates of sampling and pulses to enhance verbalization acquisition. As a result, it is crucial to explore various myelin patterns in both single units and circuits that are involved in processing speech input.

Post-deafness, several structural changes in auditory nerve fibers have been identified, such as increased internodes, altered axonal and paranodal diameters and the length of juxtaparanodes³⁸³. However, it remains unclear whether changes in internode length occur and whether these changes occur independently or in a coordinated manner due to a common underlying mechanism. Recent studies have suggested the possibility of complex interactions between structural changes, as focal axonal swelling was found to change the transmission speeds with intact myelination patterns⁴⁰⁶. Nonetheless, it remains uncertain whether internode length changes occur, and if they arise independently or in coordination due to a shared underlying mechanism. Recent research has indicated the potential for intricate interactions between structural changes, as even without internodal myelination loss, focal axonal swelling was discovered to affect conduction velocity⁴⁰⁷. Furthermore, submyelin vacuolization has been observed in deafened guinea pigs that occur quicker than myelin thinning seen in other species, implying species-specific pathological progression⁴⁰⁷. It is also plausible that ion channel alterations (distribution patterns, expression), either compensatory or pathological, could alter the electrical properties of spiral ganglion neurons, significantly impacting action potential initiation and propagation. These are comparable to alterations seen in the visual system in monocular deficiencies models⁴⁰⁸.

Temporal auditory processing deficits can significantly impact patients with cochlear implants, this being proof of the critical role of temporal processing in auditory perception. These deficiencies can then develop into full-blown impairments in rapid sound changes, such as the ones present in speech – the basis of an efficient communication system in the modern society.

4.5 Dyslexia

The implications however extend beyond the auditory perception and are especially relevant in understanding dyslexia as a multi-sensory disease. Although traditionally regarded through the framework of phonological processing deficits, recent research has shown adjacent impact in other modalities as well, with visual processing being the best example – a proof of more complex, multimodal disease. Some individuals struggle with visual attention and processing, which impact reading and language acquisition and use.

Developmental dyslexia embodies a complex neurodevelopmental disorder influenced by an array of factors. This condition emerges from the interplay of phonological processing difficulties and

subtle sensory impairments, primarily in the auditory domain, leading to the challenges experienced by those with dyslexia. Present-day research aims to unravel the intricate relationships between these factors and their impact on reading ability. A notable area of investigation concerns the link between auditory processing deficits and the development of phonological awareness^{409–411}. As a crucial precursor to learning to read, it involves the capability of manipulating sound structures inherent to language^{412–414}. Auditory processing deficits can impede the growth of phonological awareness, resulting in the reading difficulties characteristic of dyslexia.

A focal point for research is the neuroanatomical basis of dyslexia. Employing structural and functional neuroimaging techniques, scientists have consistently observed alterations, which include atypical activation in left temporoparietal and occipitotemporal regions, which are vital for reading and phonological processing, as well as irregularities in the structure and function of white matter tracts connecting these areas^{415,416}. The specific nature of these alterations and their influence on the complex processes underlying reading abilities are still under investigation. It is likely that a combination of factors, rather than a single deficit, contributes to the development of dyslexia.

Emerging research suggests that ion channel function abnormalities may be involved in dyslexia, leading to disrupted neuronal communication. This disruption could impair cognitive processing, affecting language and reading skills^{417,418}. Potassium channels, in particular, have garnered attention in dyslexia research. Genetic variations in potassium channel-encoding genes, such as *KCNJ2* and *KCNQ2*, have been linked to dyslexia^{419,420}. These potassium channels are crucial for maintaining resting membrane potential and repolarizing cells after an action potential. Dysfunction in these channels can result in abnormal firing patterns of neurons, which might explain the atypical brain activity observed in individuals with dyslexia⁴²¹. Voltage-gated calcium channels have also been implicated in dyslexia. Variations in the *CACNA1C* gene, which encodes a subunit of a voltage-gated calcium channel, have been associated with dyslexia in specific populations⁴²². Further research is essential to delineate the mechanisms and roles of ion channels in the pathophysiology of this disorder.

Recent studies in the field of dyslexia have revealed that changes in myelination could be a contributing factor to the neural mechanisms associated with this condition^{416,423}. Diffusion tensor imaging has been employed in studying axon tract organization in dyslexic brains. Findings consistently demonstrate a decrease in fractional anisotropy (FA), indicating abnormal myelination or axonal reorganization in crucial language and reading networks^{415,424,425}. Notably, decreased FA has been detected in the left temporo-parietal and occipito-temporal regions, which are vital for phonological processing and reading^{426,427}. Such white matter changes may interfere with the connectivity between different brain areas, resulting in phonological processing difficulties and subsequent reading problems. One study suggested that targeted interventions could potentially repair white matter disruptions: after an intensive reading session, children with dyslexia showed increased FA in the left hemisphere white matter tracts related to reading.

In another study, children with dyslexia who underwent a 6-month reading intervention demonstrated improvements in reading and phonological skills, along with increased FA in the left arcuate fasciculus, a white matter tract connecting language-related cortical regions⁴²⁸. These results emphasize the potential for brain plasticity in dyslexia and stress the importance of early identification and targeted intervention to encourage more typical myelination and connectivity patterns, ultimately enhancing reading outcomes for individuals with dyslexia.

Besides auditory and phonological aspects, attentional deficits have been suggested to play a role in dyslexia^{429–431}. Individuals with dyslexia often exhibit impaired visual attention, which can

obstruct the development of effective reading techniques^{432,433}. Attentional deficits may also aggravate auditory processing difficulties, as the ability to selectively focus on relevant speech sounds amidst background noise is crucial for developing phonological awareness and reading abilities^{434,435}. Consequently, understanding the relationship between attention, auditory processing, and phonological awareness is essential for devising targeted interventions for those with dyslexia.

A further review shows how dyslexic people have problems with the visual attention span (VAS), showing a decreased visual attention, rather than a short-term memory verbal deficit. Dyslexic individuals rate poorer than average readers in tasks that require parallel processing of multiple visual elements, regardless of the stimuli being verbal or non-verbal. This points towards a deficit in the endogenous attention system, which is linked to the dorsal attentional area of the brain⁴³⁶.

Considering the complex nature of dyslexia, intervention strategies should be comprehensive and adapted to each individual's specific strengths and weaknesses. Successful interventions typically involve phonics-based instruction, multisensory teaching approaches, and targeted training in auditory processing and attentional skills^{437,438}. Early identification and intervention are vital, as they can lead to significant improvements in reading competency and overall academic achievement^{439,440}. Continued research into the neuropsychological, neuroanatomical, and attentional mechanisms of dyslexia will aid in developing more effective assessment tools and therapeutic strategies, ultimately improving the quality of life and educational outcomes for those affected by this condition.

4.6 Hearing loss and tinnitus

As an experiment, and to show limitations, these paragraphs were generated using ChatGPT. There are no references available except for a few in the last paragraph, which I modified.

The prompt that was used was "Write in scientific review style, 4-5 of paragraphs on the mechanisms of hearing loss and tinnitus". The information provided was correct (impressive!), after being verified on an individual basis. Naturally, it does not have profound, in-depth information or analysis, but it suffices as an overview of the matter.

Hearing loss is a widespread issue affecting individuals of all ages, from infants to the elderly. This impairment has extensive effects on multiple aspects of life, including children's speech and language development and the social and professional challenges faced by adults. The auditory system consists of a complex network of elements that cooperate to enable hearing. Hearing loss can stem from problems in any part of this auditory circuit. While much emphasis has been placed on the peripheral part of the auditory pathway, particularly the cochlea, recent research has broadened its scope to examine central network issues as well.

Numerous studies on mice, rats, and guinea pigs have shown that moderate noise exposure can lead to hidden hearing loss (HHL). These investigations indicate that moderate noise exposures, such as 100 dB sound pressure level (SPL) for two hours in mice, result in acute yet temporary changes in auditory thresholds (ABR, CAP, and DPOAE) that recover within days or weeks. Notably, these temporary threshold shifts (TTSs) happen without hair cell loss. However, even after threshold recovery, cochlear responses to suprathreshold sound levels are significantly modified. For instance, the first peak's amplitude in the ABR waveform (ABR peak I) is reduced, in line with a decrease in the number of auditory nerve (AN) fibers activated by the sound and/or a decline in their firing rate or synchrony.

While earlier studies primarily focused on the effects of continuous noise, recent discoveries suggest that a single blast exposure might also cause HHL in animals and humans. The diminished neural responses linked to noise-induced HHL are expected to influence the encoding of temporal and intensity characteristics of suprathreshold sounds and impair the ability to perceive sounds in complex listening situations, such as those with background noise. This hypothesis was examined in rats with HHL after being exposed to 109-dB SPL octave band noise, resulting in TTS and lasting reductions in ABR peak I amplitudes. Although thresholds recuperated within two weeks, behavioral tests of the exposed rats displayed poorer performance in a hearing test involving background noise.

Comprehending the effects of HHL and its association with various factors, including noise exposure and auditory system components, is essential for devising efficient prevention and treatment methods. As research on central network issues progresses, scientists will develop a more holistic understanding of hearing loss and its impact on the lives of those affected. This knowledge will contribute to the formation of public health policies, workplace rules, and personal practices aimed at safeguarding hearing and minimizing hearing loss consequences on speech, language, and social interactions. Several recent papers have not found significant correlations between prior noise exposure, electrophysiological measures associated with HHL, and perceptual hearing ability^{441–446}. Moreover, investigations in which small negative correlations were identified between reported noise exposure and ABR peak I amplitudes often failed to establish a clear relationship with expected perceptual dysfunction^{447,448}. This lack of correlation may indicate the necessity to study synaptic and transmission models in higher auditory pathway stations, beginning with the brainstem and reaching all the way to the cortex. Numerous factors may underlie the discordant studies relating noise and HHL, including inaccuracies in self-reporting of lifetime noise exposure, potential confounding effects of age and central auditory system compensation mechanisms, and the impact of different underlying mechanisms on physiological and behavioral measures of hearing.

5. Conclusion

The two papers that constitute the main body of my thesis (Richardson et al. and Stancu et al.) study the auditory system's capacity to process sound with high fidelity and efficiency. This is essential, as described above, for the correct communication and perception. The findings offer critical insights about the mechanisms that improve and make auditory processing possible. They both adhere to the efficient coding theorem, which states that sensory systems optimise the encoding of environmental information using minimal resources, while maximising information transfer.

If we look at optimizing the neuronal resources, the adaptive myelination study shows how auditory input during critical developmental periods contributes to the myelination of individual axons in the lower auditory pathway. This myelination process makes high conduction velocity possible and therefore reduces neuronal AP latencies to an absolute minimum for the mammalian brain, which in turn leads to higher temporal precision – a prerequisite of efficient coding. Furthermore, differential myelination, in which oligodendrocytes selectively myelinate axons according to their levels of activity proves that the auditory system efficiently allocates resources for information conduction.

The synaptic transmission is another location in which resources are used efficiently. The Richardson et al. study shows how the lack of Kv3.3 channels in the presynaptic terminal in auditory brainstem neurons causes an elevated neurotransmitter release that not only doesn't improve the system performance, but on the contrary, it causes a loss in the rapid and accurate firing abilities. This role is

also in line with the principle of efficient coding theorem of using minimal resources for obtaining maximal performance.

Redundancy is another major concern in efficient and predictive coding. The myelination attributes that are proven in the PNAS paper show that resources in the system are not wasted on less active or inactive pathways, thereby reducing redundancy. By doing this, the system ensures that each neuronal signaling transmits unique and significant information about the auditory environment. Similarly, the precise signaling at the synapse reduces or abolishes the need for redundant firing when conveying auditory information.

A particularly compelling argument the two papers make is regarding the maximization of information transmission. By definition, the higher the conduction velocity, the more room there is for information. Discrete myelination was shown to contribute to this directly, without losing the temporal resolution of auditory signals. This trait is exceptionally important for processing complex sounds, such as speech and music, where precise synchronization is essential for correct perception and interpretation. An analog of appropriate myelination is the role of Kv3.3 channels, without which the system would be flooded with delayed synaptic transmissions and reduced signal-to-noise ratios.

Adapting to the informational statistics of the environment is particularly showed through the discrete manner of myelination of more or less active axons, on an individual basis. Should the environment be auditory rich or less so, the myelination patterns would follow. High levels of activity cause thicker myelin, which ensures the system remains highly receptive in auditory rich scenarios while sensory deprivation leads to thinner myelin sheaths, conserving resources in less demanding environments. Similarly, the auditory rich environment demands the presence of Kv3.3 for processing, although further studies would have to be conducted in order to determine whether altering the level of input in Kv3.3 deficient models changes the response capabilities of the system.

Energy efficiency is a linked consequence of proper myelination and synaptic mechanisms integrity. By ensuring proper insulation and high-fidelity synaptic transmission, the system is overall conserving energy resources, which we need to keep in mind are already stretched to the physiological capabilities in the auditory system.

The brain manages to process a vast array of diverse inputs for generating output with as little functional loss as possible. The neurons are the core entities that make this possible by playing a critical role in performing complex computational tasks. This requires integrating synaptic inputs in a non-linear manner and generating electrical action potentials or spikes⁴⁴⁹. This process is driven through a multitude of entities and properties - passive membrane properties, geometrical distribution, and neurons' currents. Still, this would not be the case if only the individual properties would be taken into account. An equivalent of this would be an orchestra of musicians each playing a different composition or severely out of pace and tempo. This would render higher functions like memory retrieval, strategic planning and taking decisions impossible⁴⁴⁹. This would result in noise and a lack of meaningful information, making it difficult for the brain to process and understand the information. Instead, the brain employs a complex network of interconnected neurons that work in concert to generate coherent outputs. These circuits function by integrating and processing information from various sources and using this information to modulate the activity of individual neurons. Additionally, these circuits exhibit plasticity, which allows them to reorganize and adjust to changes in the environment or in response to learning. Thus, the ability of the brain to process an array of different types of inputs with as little functional failure, in order to produce relevant outputs is a result of the coordinated and adjustable functioning of interconnected neural circuits. This allows

for the efficient processing and interpretation of information, enabling complex cognitive processes to occur.

My thesis' line of work shows that the brain's operational capacity is supported by the timely coincident and cooperative activity of neuronal ensembles, which are in a continuous reshaping and adjusting process. This is achieved through a variety of mechanisms, which I called adaptive traits, that impact all stages of signal generation and processing.

6. Bibliography

1. Ramon y Cajal, S. Inducciones fisiológicas de la morfología y conexiones de las neuronas. *Barc. Acad.* (1891).
2. Ramón y Cajal S. Leyes de la morfología y dinamismo de las células nerviosas. *Revista Trimestral Micrográfica* 1–28 (1897).
3. Dendrites. *Dendrites* (2016) doi:10.1093/ACPROF:OSO/9780198745273.001.0001.
4. Harris, K. M. & Stevens, J. K. Dendritic spines of rat cerebellar Purkinje cells: serial electron microscopy with reference to their biophysical characteristics. *J Neurosci* **8**, 4455–4469 (1988).
5. Harris, K. M. & Stevens, J. K. Dendritic spines of CA 1 pyramidal cells in the rat hippocampus: serial electron microscopy with reference to their biophysical characteristics. *J Neurosci* **9**, 2982–2997 (1989).
6. Mishchenko, Y. *et al.* Ultrastructural analysis of hippocampal neuropil from the connectomics perspective. *Neuron* **67**, 1009–1020 (2010).
7. Peters, A. & Kaiserman-Abramof, I. R. The small pyramidal neuron of the rat cerebral cortex. The perikaryon, dendrites and spines. *Am J Anat* **127**, 321–355 (1970).
8. Gray, L., Smith, Z. & Rubel, E. W. Developmental and experimental changes in dendritic symmetry in n. laminaris of the chick. *Brain Res* **244**, 360–364 (1982).
9. Swindale, N. V. Patches in monkey visual cortex. *Nature* **293**, 509–510 (1981).
10. Brand, A., Behrend, O., Marquardt, T., McAlpine, D. & Grothe, B. Precise inhibition is essential for microsecond interaural time difference coding. *Nature* **417**, 543–547 (2002).
11. Chirila, F. V., Rowland, K. C., Thompson, J. M. & Spirou, G. A. Development of gerbil medial superior olive: integration of temporally delayed excitation and inhibition at physiological temperature. *J Physiol* **584**, 167 (2007).
12. Pecka, M., Brand, A., Behrend, O. & Grothe, B. Interaural Time Difference Processing in the Mammalian Medial Superior Olive: The Role of Glycinergic Inhibition. *The Journal of Neuroscience* **28**, 6914 (2008).
13. McGinley, M. J., Charles Liberman, M., Bal, R. M. & Oertel, D. Generating Synchrony from the Asynchronous: Compensation for Cochlear Traveling Wave Delays by the Dendrites of Individual Brainstem Neurons. *The Journal of Neuroscience* **32**, 9301 (2012).
14. Agmon-Snir, H., Carr, C. E. & Rinzel, J. The role of dendrites in auditory coincidence detection. *Nature* **393**, 268–272 (1998).
15. Cao, X. J. & Oertel, D. Auditory Nerve Fibers Excite Targets Through Synapses That Vary in Convergence, Strength, and Short-Term Plasticity. *J Neurophysiol* **104**, 2308 (2010).
16. Cao, X. J., McGinley, M. J. & Oertel, D. Connections and synaptic function in the posteroventral cochlear nucleus of deaf jerker mice. *J Comp Neurol* **510**, 297 (2008).
17. Couchman, K., Grothe, B. & Felmy, F. Medial Superior Olivary Neurons Receive Surprisingly Few Excitatory and Inhibitory Inputs with Balanced Strength and Short-Term Dynamics. *The Journal of Neuroscience* **30**, 17111 (2010).
18. Oertel, D., Bal, R., Gardner, S. M., Smith, P. H. & Joris, P. X. Detection of synchrony in the activity of auditory nerve fibers by octopus cells of the mammalian cochlear nucleus. *Proc Natl Acad Sci U S A* **97**, 11773 (2000).
19. Couchman, K., Grothe, B. & Felmy, F. Functional localization of neurotransmitter receptors and synaptic inputs to mature neurons of the medial superior olive. *J Neurophysiol* **107**, 1186–1198 (2012).

20. Magnusson, A. K., Kapfer, C., Grothe, B. & Koch, U. Maturation of glycinergic inhibition in the gerbil medial superior olive after hearing onset. *J Physiol* **568**, 497 (2005).
21. Couchman, K., Grothe, B. & Felmy, F. Medial Superior Olivary Neurons Receive Surprisingly Few Excitatory and Inhibitory Inputs with Balanced Strength and Short-Term Dynamics. *The Journal of Neuroscience* **30**, 17111 (2010).
22. König, P., Engel, A. K. & Singer, W. Integrator or coincidence detector? The role of the cortical neuron revisited. *Trends Neurosci* **19**, 130–137 (1996).
23. Rasband, M. N. The axon initial segment and the maintenance of neuronal polarity. *Nature Reviews Neuroscience* **2010 11:8 11**, 552–562 (2010).
24. Yamada, R. & Kuba, H. Structural and Functional Plasticity at the Axon Initial Segment. *Front Cell Neurosci* **10**, (2016).
25. Gutzmann, A. *et al.* A period of structural plasticity at the axon initial segment in developing visual cortex. *Front Neuroanat* **8**, (2014).
26. Kuba, H., Adachi, R. & Ohmori, H. Activity-Dependent and Activity-Independent Development of the Axon Initial Segment. *The Journal of Neuroscience* **34**, 3443 (2014).
27. Grubb, M. S. & Burrone, J. Activity-dependent relocation of the axon initial segment fine-tunes neuronal excitability. *Nature* **465**, 1070 (2010).
28. Wefelmeyer, W., Cattaert, D. & Burrone, J. Activity-dependent mismatch between axo-axonic synapses and the axon initial segment controls neuronal output. *Proc Natl Acad Sci U S A* **112**, 9757–9762 (2015).
29. Kuba, H., Oichi, Y. & Ohmori, H. Presynaptic activity regulates Na(+) channel distribution at the axon initial segment. *Nature* **465**, 1075–1078 (2010).
30. Höfflin, F. *et al.* Heterogeneity of the axon initial segment in interneurons and pyramidal cells of rodent visual cortex. *Front Cell Neurosci* **11**, 332 (2017).
31. Kuba, H., Ishii, T. M. & Ohmori, H. Axonal site of spike initiation enhances auditory coincidence detection. *Nature* **444**, 1069–1072 (2006).
32. Kim, E. J., Feng, C., Santamaria, F. & Kim, J. H. Impact of Auditory Experience on the Structural Plasticity of the AIS in the Mouse Brainstem Throughout the Lifespan. *Front Cell Neurosci* **13**, (2019).
33. Hill, E. M., Koay, G., Heffner, R. S. & Heffner, H. E. Audiogram of the chicken (*Gallus gallus domesticus*) from 2 Hz to 9 kHz. *J Comp Physiol A Neuroethol Sens Neural Behav Physiol* **200**, 863–870 (2014).
34. Gleich, O. & Strutz, J. The Mongolian Gerbil as a Model for the Analysis of Peripheral and Central Age-Dependent Hearing Loss. *Hearing Loss* (2012) doi:10.5772/33569.
35. Chand, A. N., Galliano, E., Chesters, R. A. & Grubb, M. S. A Distinct Subtype of Dopaminergic Interneuron Displays Inverted Structural Plasticity at the Axon Initial Segment. *The Journal of Neuroscience* **35**, 1573 (2015).
36. Freitas, C., Farzan, F. & Pascual-Leone, A. Assessing brain plasticity across the lifespan with transcranial magnetic stimulation: why, how, and what is the ultimate goal? *Front Neurosci* **7**, (2013).
37. Yeatman, J. D., Wandell, B. A. & Mezer, A. A. Lifespan maturation and degeneration of human brain white matter. *Nat Commun* **5**, 4932 (2014).
38. Cruz, D. A., Lovallo, E. M., Stockton, S., Rasband, M. & Lewis, D. A. Postnatal Development of Synaptic Structure Proteins in Pyramidal Neuron Axon Initial Segments in Monkey Prefrontal Cortex. *J Comp Neurol* **514**, 353 (2009).
39. Schlüter, A. *et al.* Structural Plasticity of Synaptopodin in the Axon Initial Segment during Visual Cortex Development. *Cereb Cortex* **27**, 4662–4675 (2017).

40. Bahr, B. A., Lam, N. & Lynch, G. Changes in the concentrations of tau and other structural proteins in the brains of aged mice. *Neurosci Lett* **175**, 49–52 (1994).
41. Ding, Y., Chen, T., Wang, Q., Yuan, Y. & Hua, T. Axon initial segment plasticity accompanies enhanced excitation of visual cortical neurons in aged rats. *Neuroreport* **29**, 1537 (2018).
42. Gründemann, J. & Häusser, M. Neuroscience: A plastic axonal hotspot. *Nature* **465**, 1022–1023 (2010).
43. Wefelmeyer, W., Puhl, C. J. & Burrone, J. Homeostatic Plasticity of Subcellular Neuronal Structures: From Inputs to Outputs. *Trends Neurosci* **39**, 656 (2016).
44. Kim, J. H. & von Gersdorff, H. Suppression of spikes during posttetanic hyperpolarization in auditory neurons: the role of temperature, Ih currents, and the Na⁺-K⁺-ATPase pump. *J Neurophysiol* **108**, 1924 (2012).
45. Leão, R. M. *et al.* Presynaptic Na⁺ Channels: Locus, Development, and Recovery from Inactivation at a High-Fidelity Synapse. *The Journal of Neuroscience* **25**, 3724 (2005).
46. Sherman, D. L. & Brophy, P. J. Mechanisms of axon ensheathment and myelin growth. *Nat Rev Neurosci* **6**, 683–690 (2005).
47. From, R. *et al.* Oligodendrogenesis and myelinogenesis during postnatal development effect of glatiramer acetate. *Glia* **62**, 649–665 (2014).
48. Rasband, M. N. & Peles, E. The Nodes of Ranvier: Molecular Assembly and Maintenance. *Cold Spring Harb Perspect Biol* **8**, (2015).
49. Bliss, T. V. P. & Collingridge, G. L. A synaptic model of memory: long-term potentiation in the hippocampus. *Nature* **361**, 31–39 (1993).
50. Malenka, R. C. & Bear, M. F. LTP and LTD: An embarrassment of riches. *Neuron* **44**, 5–21 (2004).
51. Debanne, D., Campanac, E., Bialowas, A., Carrier, E. & Alcaraz, G. Axon physiology. *Physiol Rev* **91**, 555–602 (2011).
52. Chida, K., Kaneko, K., Fujii, S. & Yamazaki, Y. Activity-dependent modulation of the axonal conduction of action potentials along rat hippocampal mossy fibers. *European Journal of Neuroscience* **41**, 45–54 (2015).
53. Yamazaki, R., Ishibashi, T., Baba, H. & Yamaguchi, Y. Unconventional myosin ID is expressed in myelinating oligodendrocytes. *J Neurosci Res* **92**, 1286–1294 (2014).
54. Fields, R. D. Neuroscience. Change in the brain's white matter. *Science* **330**, 768–769 (2010).
55. Nave, K. A. Myelination and support of axonal integrity by glia. *Nature* **468**, 244–252 (2010).
56. Nave, K. A. & Werner, H. B. Myelination of the nervous system: mechanisms and functions. *Annu Rev Cell Dev Biol* **30**, 503–533 (2014).
57. Hill, R. A. & Nishiyama, A. NG2 cells (polydendrocytes): listeners to the neural network with diverse properties. *Glia* **62**, 1195–1210 (2014).
58. Bergles, D. E., Roberts, J. D. B., Somogyi, P. & Jahr, C. E. Glutamatergic synapses on oligodendrocyte precursor cells in the hippocampus. *Nature* **405**, 187–191 (2000).
59. García-Marín, V., García-López, P. & Freire, M. Cajal's contributions to glia research. *Trends Neurosci* **30**, 479–487 (2007).
60. Hughes, E. G., Kang, S. H., Fukaya, M. & Bergles, D. E. Oligodendrocyte progenitors balance growth with self-repulsion to achieve homeostasis in the adult brain. *Nat Neurosci* **16**, 668–676 (2013).
61. Wake, H., Lee, P. R. & Fields, R. D. Control of local protein synthesis and initial events in myelination by action potentials. *Science* **333**, 1647–1651 (2011).
62. Kiernan, M. C. & Kaji, R. Physiology and pathophysiology of myelinated nerve fibers. *Handb Clin Neurol* **115**, 43–53 (2013).

63. McFarlan, A. R. *et al.* The plasticome of cortical interneurons. *Nature Reviews Neuroscience* 2022 24:2 **24**, 80–97 (2022).
64. Bucher, D. & Goillard, J. M. Beyond faithful conduction: Short-term dynamics, neuromodulation, and long-term regulation of spike propagation in the axon. *Prog Neurobiol* **94**, 307–346 (2011).
65. Ritchie, J. M. The Neurobiology of Disease: Ion channels in normal and pathophysiological mammalian peripheral myelinated nerve. *The Neurobiology of Disease* 3–12 (1996) doi:10.1017/CBO9780511570193.003.
66. Myelin. **1190**, (2019).
67. Bucher, D. Contribution of Axons to Short-Term Dynamics of Neuronal Communication. *Axons and Brain Architecture* 245–263 (2016) doi:10.1016/B978-0-12-801393-9.00012-8.
68. Seidl, A. H. Regulation of Conduction Time along Axons. *Neuroscience* **0**, 126 (2014).
69. Seidl, A. H. & Rubel, E. W. Systematic and differential myelination of axon collaterals in the mammalian auditory brainstem. *Glia* **64**, 487 (2016).
70. Kukley, M., Capetillo-Zarate, E. & Dietrich, D. Vesicular glutamate release from axons in white matter. *Nature Neuroscience* 2007 10:3 **10**, 311–320 (2007).
71. Micu, I. *et al.* The molecular physiology of the axo-myelinic synapse. *Exp Neurol* **276**, 41–50 (2016).
72. Ziskin, J. L., Nishiyama, A., Rubio, M., Fukaya, M. & Bergles, D. E. Vesicular release of glutamate from unmyelinated axons in white matter. *Nat Neurosci* **10**, 321–330 (2007).
73. Fields, R. D. Nonsynaptic and nonvesicular ATP release from neurons and relevance to neuron-glia signaling. *Semin Cell Dev Biol* **22**, 214–219 (2011).
74. Borst, J. G. G. & Soria Van Hoeve, J. The calyx of Held synapse: from model synapse to auditory relay. *Annu Rev Physiol* **74**, 199–224 (2012).
75. Schneggenburger, R. & Forsythe, I. D. The calyx of Held. *Cell Tissue Res* **326**, 311–337 (2006).
76. Hoffpauir, B. K., Grimes, J. L., Mathers, P. H. & Spirou, G. A. Synaptogenesis of the Calyx of Held: Rapid Onset of Function and One-to-One Morphological Innervation. *The Journal of Neuroscience* **26**, 5511 (2006).
77. Iwasaki, S. & Takahashi, T. Developmental regulation of transmitter release at the calyx of Held in rat auditory brainstem. *J Physiol* **534**, 861 (2001).
78. Taschenberger, H. & Von Gersdorff, H. Fine-tuning an auditory synapse for speed and fidelity: developmental changes in presynaptic waveform, EPSC kinetics, and synaptic plasticity. *J Neurosci* **20**, 9162–9173 (2000).
79. Taschenberger, H., Leão, R. M., Rowland, K. C., Spirou, G. A. & Von Gersdorff, H. Optimizing synaptic architecture and efficiency for high-frequency transmission. *Neuron* **36**, 1127–1143 (2002).
80. Blatchley, B. J., Cooper, W. A. & Coleman, J. R. Development of auditory brainstem response to tone pip stimuli in the rat. *Brain Res* **429**, 75–84 (1987).
81. Geal-Dor, M., Freeman, S., Li, G. & Sohmer, H. Development of hearing in neonatal rats: air and bone conducted ABR thresholds. *Hear Res* **69**, 236–242 (1993).
82. Kamiya, K., Takahashi, K., Kitamura, K., Momoi, T. & Yoshikawa, Y. Mitosis and apoptosis in postnatal auditory system of the C3H/He strain. *Brain Res* **901**, 296–302 (2001).
83. Erazo-Fischer, E., Striessnig, J. & Taschenberger, H. The Role of Physiological Afferent Nerve Activity during In Vivo Maturation of the Calyx of Held Synapse. *The Journal of Neuroscience* **27**, 1725 (2007).
84. Rodríguez-Contreras, A., Van Hoeve, J. S. S., Habets, R. L. P., Locher, H. & Borst, J. G. G. Dynamic development of the calyx of Held synapse. *Proc Natl Acad Sci U S A* **105**, 5603 (2008).

85. Youssoufian, M., Couchman, K., Shivdasani, M. N., Paolini, A. G. & Walmsley, B. Maturation of auditory brainstem projections and calyces in the congenitally deaf (dn/dn) mouse. *J Comp Neurol* **506**, 442–451 (2008).
86. Felmy, F. & Schneggenburger, R. Developmental expression of the Ca²⁺-binding proteins calretinin and parvalbumin at the calyx of Held of rats and mice. *Eur J Neurosci* **20**, 1473–1482 (2004).
87. Ford, M. C., Grothe, B. & Klug, A. Fenestration of the calyx of Held occurs sequentially along the tonotopic axis, is influenced by afferent activity, and facilitates glutamate clearance. *J Comp Neurol* **514**, 92–106 (2009).
88. Sätzler, K. *et al.* Three-Dimensional Reconstruction of a Calyx of Held and Its Postsynaptic Principal Neuron in the Medial Nucleus of the Trapezoid Body. *The Journal of Neuroscience* **22**, 10567 (2002).
89. Borst, J. G. G. & Sakmann, B. Calcium influx and transmitter release in a fast CNS synapse. *Nature* **383**, 431–434 (1996).
90. Iwasaki, S. & Takahashi, T. Developmental changes in calcium channel types mediating synaptic transmission in rat auditory brainstem. *J Physiol* **509**, 419 (1998).
91. Meinrenken, C. J., Borst, J. G. G. & Sakmann, B. Calcium Secretion Coupling at Calyx of Held Governed by Nonuniform Channel–Vesicle Topography. *The Journal of Neuroscience* **22**, 1648 (2002).
92. Nakamura, Y. *et al.* Nanoscale Distribution of Presynaptic Ca²⁺ Channels and Its Impact on Vesicular Release during Development. *Neuron* **85**, 145 (2015).
93. Sheng, J. *et al.* Calcium-channel number critically influences synaptic strength and plasticity at the active zone. *Nat Neurosci* **15**, 998 (2012).
94. Wu, L. G., Borst, J. G. G. & Sakmann, B. R-type Ca²⁺ currents evoke transmitter release at a rat central synapse. *Proc Natl Acad Sci U S A* **95**, 4720 (1998).
95. Wu, L. G., Westenbroek, R. E., Borst, J. G. G., Catterall, W. A. & Sakmann, B. Calcium Channel Types with Distinct Presynaptic Localization Couple Differentially to Transmitter Release in Single Calyx-Type Synapses. *The Journal of Neuroscience* **19**, 726 (1999).
96. Kopp-Scheinflug, C., Steinert, J. R. & Forsythe, I. D. Modulation and control of synaptic transmission across the MNTB. *Hear Res* **279**, 22–31 (2011).
97. Trussell, L. O. Synaptic mechanisms for coding timing in auditory neurons. *Annu Rev Physiol* **61**, 477–496 (1999).
98. Borst, J. G., Helmchen, F. & Sakmann, B. Pre- and postsynaptic whole-cell recordings in the medial nucleus of the trapezoid body of the rat. *J Physiol* **489**, 825 (1995).
99. Chuhma, N. & Ohmori, H. Postnatal Development of Phase-Locked High-Fidelity Synaptic Transmission in the Medial Nucleus of the Trapezoid Body of the Rat. *The Journal of Neuroscience* **18**, 512 (1998).
100. Forsythe, I. D. Direct patch recording from identified presynaptic terminals mediating glutamatergic EPSCs in the rat CNS, in vitro. *J Physiol* **479**, 381 (1994).
101. Sun, J. Y. & Wu, L. G. Fast kinetics of exocytosis revealed by simultaneous measurements of presynaptic capacitance and postsynaptic currents at a central synapse. *Neuron* **30**, 171–182 (2001).
102. Wong, A. Y. C., Graham, B. P., Billups, B. & Forsythe, I. D. Distinguishing between Presynaptic and Postsynaptic Mechanisms of Short-Term Depression during Action Potential Trains. *The Journal of Neuroscience* **23**, 4868 (2003).
103. Bollmann, J. H., Sakmann, B. & Borst, J. G. G. Calcium sensitivity of glutamate release in a calyx-type terminal. *Science* **289**, 953–957 (2000).

104. Bollmann, J. H., Helmchen, F., Gerard G Borst, J. & Sakmann, B. Postsynaptic Ca²⁺ Influx Mediated by Three Different Pathways during Synaptic Transmission at a Calyx-Type Synapse. *The Journal of Neuroscience* **18**, 10409 (1998).
105. Schneggenburger, R. & Neher, E. Intracellular calcium dependence of transmitter release rates at a fast central synapse. *Nature* **406**, 889–993 (2000).
106. Xu, J. & Wu, L. G. The decrease in the presynaptic calcium current is a major cause of short-term depression at a calyx-type synapse. *Neuron* **46**, 633–645 (2005).
107. Kochubey, O. & Schneggenburger, R. Synaptotagmin increases the dynamic range of synapses by driving Ca²⁺-evoked release and by clamping a near-linear remaining Ca²⁺ sensor. *Neuron* **69**, 736–748 (2011).
108. Kochubey, O., Lou, X. & Schneggenburger, R. Regulation of transmitter release by Ca(2+) and synaptotagmin: insights from a large CNS synapse. *Trends Neurosci* **34**, 237–246 (2011).
109. Lou, X., Scheuss, V. & Schneggenburger, R. Allosteric modulation of the presynaptic Ca²⁺ sensor for vesicle fusion. *Nature* **435**, 497–501 (2005).
110. Sun, J. *et al.* A Two Ca²⁺-Sensor Model for Neurotransmitter Release in a Central Synapse. *Nature* **450**, 676 (2007).
111. Renden, R. & Von Gersdorff, H. Synaptic vesicle endocytosis at a CNS nerve terminal: faster kinetics at physiological temperatures and increased endocytotic capacity during maturation. *J Neurophysiol* **98**, 3349–3359 (2007).
112. Sun, J. Y., Wu, X. S. & Wu, L. G. Single and multiple vesicle fusion induce different rates of endocytosis at a central synapse. *Nature* **417**, 555–559 (2002).
113. Wu, L. G., Hamid, E., Shin, W. & Chiang, H. C. Exocytosis and Endocytosis: Modes, Functions, and Coupling Mechanisms. *Annu Rev Physiol* **76**, 301 (2014).
114. Wu, X. S. *et al.* Ca²⁺ and calmodulin initiate all forms of endocytosis during depolarization at a nerve terminal. *Nat Neurosci* **12**, 1003 (2009).
115. Yamashita, T., Hige, T. & Takahashi, T. Vesicle endocytosis requires dynamin-dependent GTP hydrolysis at a fast CNS synapse. *Science* **307**, 124–127 (2005).
116. Ford, M. C. *et al.* Tuning of Ranvier node and internode properties in myelinated axons to adjust action potential timing. *Nat Commun* **6**, (2015).
117. Bergsman, J. B., De Camilli, P. & McCormick, D. A. Multiple large inputs to principal cells in the mouse medial nucleus of the trapezoid body. *J Neurophysiol* **92**, 545–552 (2004).
118. Kuwabara, N., DiCaprio, R. A. & Zook, J. M. Afferents to the medial nucleus of the trapezoid body and their collateral projections. *J Comp Neurol* **314**, 684–706 (1991).
119. Rodríguez-Contreeas, A., De Lange, R. P. J., Lucassen, P. J. & Borst, J. G. G. Branching of calyceal afferents during postnatal development in the rat auditory brainstem. *J Comp Neurol* **496**, 214–228 (2006).
120. Smith, P. H., Joris, P. X., Carney, L. H. & Yin, T. C. T. Projections of physiologically characterized globular bushy cell axons from the cochlear nucleus of the cat. *J Comp Neurol* **304**, 387–407 (1991).
121. Green, J. S. & Sanes, D. H. Early appearance of inhibitory input to the MNTB supports binaural processing during development. *J Neurophysiol* **94**, 3826–3835 (2005).
122. Albrecht, O., Dondzillo, A., Mayer, F., Thompson, J. A. & Klug, A. Inhibitory projections from the ventral nucleus of the trapezoid body to the medial nucleus of the trapezoid body in the mouse. *Front Neural Circuits* **8**, (2014).
123. Elezgarai, I. *et al.* Subcellular localization of the voltage-dependent potassium channel Kv3.1b in postnatal and adult rat medial nucleus of the trapezoid body. *Neuroscience* **118**, 889–898 (2003).

124. Nakamura, Y. & Takahashi, T. Developmental changes in potassium currents at the rat calyx of Held presynaptic terminal. *J Physiol* **581**, 1101 (2007).
125. US Department of Commerce, N. N. W. S. Speed of Sound Calculator.
126. Auditory Processing by the Cochlea | Principles of Neural Science, 6e | AccessNeurology | McGraw Hill Medical.
<https://neurology.mhmedical.com/content.aspx?bookid=3024§ionid=254330809>.
127. Driver, E. C. & Kelley, M. W. Development of the cochlea. *Development* **147**, (2020).
128. Hudspeth, A. J. How the ear's works work. *Nature* **341**, 397–404 (1989).
129. Hudspeth, A. J. Making an effort to listen: mechanical amplification in the ear. *Neuron* **59**, 530–545 (2008).
130. Eliades, S. J. & Tsunada, J. Marmosets in auditory research. *The Common Marmoset in Captivity and Biomedical Research* 451–475 (2018) doi:10.1016/B978-0-12-811829-0.00025-X.
131. Pannese, A., Grandjean, D. & Frühholz, S. Subcortical processing in auditory communication. *Hear Res* **328**, 67–77 (2015).
132. Farago, A. F., Awatramani, R. B. & Dymecki, S. M. Assembly of the brainstem cochlear nuclear complex is revealed by intersectional and subtractive genetic fate maps. *Neuron* **50**, 205–218 (2006).
133. Schnupp, J., Nelken, I. & King, A. J. Auditory Neuroscience. *Audit Neurosci* (2019) doi:10.7551/MITPRESS/7942.001.0001.
134. Principles of Neural Science, 6e | AccessNeurology | McGraw Hill Medical.
<https://neurology.mhmedical.com/book.aspx?bookID=3024>.
135. Pickles, J. O. Auditory pathways: anatomy and physiology. *Handb Clin Neurol* **129**, 3–25 (2015).
136. Cant, N. B. & Benson, C. G. Parallel auditory pathways: Projection patterns of the different neuronal populations in the dorsal and ventral cochlear nuclei. *Brain Res Bull* **60**, 457–474 (2003).
137. Nakamura, P. A. & Cramer, K. S. Formation and maturation of the calyx of Held. *Hear Res* **276**, 70–78 (2011).
138. Grothe, B. & Pecka, M. The natural history of sound localization in mammals – a story of neuronal inhibition. *Front Neural Circuits* **8**, (2014).
139. Tollin, D. J. The lateral superior olive: a functional role in sound source localization. *Neuroscientist* **9**, 127–143 (2003).
140. Felix, R. A., Fridberger, A., Leijon, S., Berrebi, A. S. & Magnusson, A. K. Sound Rhythms Are Encoded by Postinhibitory Rebound Spiking in the Superior Paraolivary Nucleus. *The Journal of Neuroscience* **31**, 12566 (2011).
141. Kopp-Scheinpflug, C., Sinclair, J. L. & Linden, J. F. When Sound Stops: Offset Responses in the Auditory System. *Trends Neurosci* **41**, 712–728 (2018).
142. Kopp-Scheinpflug, C. *et al.* The sound of silence: ionic mechanisms encoding sound termination. *Neuron* **71**, 911–925 (2011).
143. Nieuwenhuys, R. Anatomy of the auditory pathways, with emphasis on the brain stem. *Adv Otorhinolaryngol* **34**, 25–38 (1984).
144. Loftus, W. C., Bishop, D. C., Saint Marie, R. L. & Oliver, D. L. Organization of binaural excitatory and inhibitory inputs to the inferior colliculus from the superior olive. *J Comp Neurol* **472**, 330–344 (2004).
145. Krishna, B. S. & Semple, M. N. Auditory temporal processing: responses to sinusoidally amplitude-modulated tones in the inferior colliculus. *J Neurophysiol* **84**, 255–273 (2000).

146. Jiang, D., McAlpine, D. & Palmer, A. R. Responses of neurons in the inferior colliculus to binaural masking level difference stimuli measured by rate-versus-level functions. *J Neurophysiol* **77**, 3085–3106 (1997).
147. Chase, S. M. & Young, E. D. Cues for sound localization are encoded in multiple aspects of spike trains in the inferior colliculus. *J Neurophysiol* **99**, 1672–1682 (2008).
148. Pollak, G. D., Xie, R., Gittelman Joshua X., J. X., Andoni, S. & Li, N. The dominance of inhibition in the inferior colliculus. *Hear Res* **274**, 27 (2011).
149. Almasabi, F. *et al.* The role of the medial geniculate body of the thalamus in the pathophysiology of tinnitus and implications for treatment. *Brain Res* **1779**, (2022).
150. Bertero, A., Zurita, H., Normandin, M. & Apicella, A. J. Auditory Long-Range Parvalbumin Cortico-Striatal Neurons. *Front Neural Circuits* **14**, 45 (2020).
151. Moore, A. K. & Wehr, M. Parvalbumin-expressing inhibitory interneurons in auditory cortex are well-tuned for frequency. *J Neurosci* **33**, 13713–13723 (2013).
152. Bartlett, E. L. The organization and physiology of the auditory thalamus and its role in processing acoustic features important for speech perception. *Brain Lang* **126**, 29 (2013).
153. Imaizumi, K. *et al.* Modular functional organization of cat anterior auditory field. *J Neurophysiol* **92**, 444–457 (2004).
154. Baumann, S., Petkov, C. I. & Griffiths, T. D. A unified framework for the organisation of the primate auditory cortex. *Front Syst Neurosci* 1–19 (2013) doi:10.3389/FNSYS.2013.00011.
155. Bizley, J. K. & Walker, K. M. M. Sensitivity and selectivity of neurons in auditory cortex to the pitch, timbre, and location of sounds. *Neuroscientist* **16**, 453–469 (2010).
156. Kössl, M. *et al.* Auditory cortex of newborn bats is prewired for echolocation. *Nat Commun* **3**, (2012).
157. Xiao, Z. & Suga, N. Reorganization of the auditory cortex specialized for echo-delay processing in the mustached bat. *Proc Natl Acad Sci U S A* **101**, 1769–1774 (2004).
158. Kaas, J. H. The evolution of brains from early mammals to humans. *Wiley Interdiscip Rev Cogn Sci* **4**, 33–45 (2013).
159. Merzenich, M. M. & Schreiner, C. E. Mammalian Auditory Cortex—Some Comparative Observations. *The Evolutionary Biology of Hearing* 673–688 (1992) doi:10.1007/978-1-4612-2784-7_42.
160. Hodgkin, A. L. & Huxley, A. F. A quantitative description of membrane current and its application to conduction and excitation in nerve. *J Physiol* **117**, 500–544 (1952).
161. Johnston, J., Forsythe, I. D. & Kopp-Scheinflug, C. Going native: voltage-gated potassium channels controlling neuronal excitability. *J Physiol* **588**, 3187–3200 (2010).
162. Doyle, D. A. *et al.* The structure of the potassium channel: molecular basis of K⁺ conduction and selectivity. *Science* **280**, 69–77 (1998).
163. Gutman, G. A. *et al.* International Union of Pharmacology. XLI. Compendium of voltage-gated ion channels: potassium channels. *Pharmacol Rev* **55**, 583–586 (2003).
164. Brew, H. M. & Forsythe, I. D. Two voltage-dependent K⁺ conductances with complementary functions in postsynaptic integration at a central auditory synapse. *J Neurosci* **15**, 8011–8022 (1995).
165. Jan, L. Y. & Jan, Y. N. Voltage-gated potassium channels and the diversity of electrical signalling. *Journal of Physiology* **590**, 2591–2599 (2012).
166. Johnston, J. *et al.* Initial segment Kv2.2 channels mediate a slow delayed rectifier and maintain high frequency action potential firing in medial nucleus of the trapezoid body neurons. *J Physiol* **586**, 3493–3509 (2008).
167. Johnston, J., Griffin, S. J., Baker, C. & Forsythe, I. D. Kv4 (A-type) potassium currents in the mouse medial nucleus of the trapezoid body. *Eur J Neurosci* **27**, 1391–1399 (2008).

168. Theunissen, F. & Miller, J. P. Temporal encoding in nervous systems: a rigorous definition. *J Comput Neurosci* **2**, 149–162 (1995).
169. Mayr, E. The growth of biological thought : diversity, evolution, and inheritance. 974 (1982).
170. John Daintith & Elizabeth Martin. *Oxford DICTIONARY OF SCIENCE*. (2010).
171. Williams, G. C. (George C. *Adaptation and Natural Selection: A Critique of Some Current Evolutionary Thought*. (Princeton University Press, 1966).
172. Bowler, P. J. Evolution: the history of an idea. 464.
173. Dobzhansky, T. On Some Fundamental Concepts of Darwinian Biology. *Evol Biol* 1–34 (1968) doi:10.1007/978-1-4684-8094-8_1.
174. Dobzhansky, T. Genetics of the evolutionary process. 505 (1970).
175. Dobzhansky, T. Genetics of Natural Populations. XXV. Genetic Changes in Populations of *Drosophila pseudoobscura* and *Drosophila persimilis* in Some Localities in California. *Evolution (N Y)* **10**, 82 (1956).
176. G. Ledyard Stebbins. *Variation and Evolution in Plants and Microorganisms*. (National Academy Press, 1950).
177. Moore, L. G. & Regensteiner, J. G. Adaptation to High Altitude. <https://doi.org/10.1146/annurev.an.12.100183.001441> 285–304 (2003) doi:10.1146/ANNUREV.AN.12.100183.001441.
178. P. B. Medawar. The future of man. <https://www.worldcat.org/title/1374615> (1960).
179. Toso, A., Reinartz, S., Pulecchi, F. & Diamond, M. E. Time coding in rat dorsolateral striatum. *Neuron* **109**, 3663–3673.e6 (2021).
180. Erskine, A., Ackels, T., Dasgupta, D., Fukunaga, I. & Schaefer, A. T. Mammalian olfaction is a high temporal bandwidth sense. *bioRxiv* 570689 (2019) doi:10.1101/570689.
181. Potier, S., Lieuvin, M., Pfaff, M. & Kelber, A. How fast can raptors see? *J Exp Biol* **223**, (2020).
182. Nomura, Y. *et al.* Evaluation of critical flicker-fusion frequency measurement methods using a touchscreen-based visual temporal discrimination task in the behaving mouse. *Neurosci Res* **148**, 28–33 (2019).
183. Kopp-Scheinflug, C., Sinclair, J. L. & Linden, J. F. When Sound Stops: Offset Responses in the Auditory System. *Trends Neurosci* **41**, 712–728 (2018).
184. Radziwon, K. E. *et al.* Behaviorally Measured Audiograms and Gap Detection Thresholds in CBA/CaJ Mice. *J Comp Physiol A Neuroethol Sens Neural Behav Physiol* **195**, 961 (2009).
185. Sinclair, J. L. *et al.* Sound-Evoked Activity Influences Myelination of Brainstem Axons in the Trapezoid Body. *J Neurosci* **37**, 8239–8255 (2017).
186. Price, B. H. & Gavornik, J. P. Efficient Temporal Coding in the Early Visual System: Existing Evidence and Future Directions. *Front Comput Neurosci* **16**, (2022).
187. Shannon, C. E. A Mathematical Theory of Communication. *Bell System Technical Journal* **27**, 623–656 (1948).
188. Barlow, H. B. Possible Principles Underlying the Transformations of Sensory Messages. (1961).
189. Cover, T. M. & Thomas, J. A. Elements of Information Theory. *Elements of Information Theory* 1–748 (2005) doi:10.1002/047174882X.
190. Sterling Peter & Laughlin Simon. *Principles of Neural Design*. (2017).
191. Fritz, J., Shamma, S., Elhilali, M. & Klein, D. Rapid task-related plasticity of spectrotemporal receptive fields in primary auditory cortex. *Nat Neurosci* **6**, 1216–1223 (2003).
192. Saxe, A., Bhand, M., Mudur, R., Suresh, B. & Ng, A. Supplementary Material: Unsupervised learning models of primary cortical receptive fields and receptive field plasticity. *stanford.edu* (2011).

193. Kadia, S. C. & Wang, X. Spectral integration in A1 of awake primates: neurons with single- and multi-peaked tuning characteristics. *J Neurophysiol* **89**, 1603–1622 (2003).
194. Kozlov, A. S. & Gentner, T. Q. Central auditory neurons have composite receptive fields. *Proc Natl Acad Sci U S A* **113**, 1441 (2016).
195. Młynarski, W. The Opponent Channel Population Code of Sound Location Is an Efficient Representation of Natural Binaural Sounds. *PLoS Comput Biol* **11**, (2015).
196. Huetz, C., Philibert, B. & Edeline, J. M. A Spike-Timing Code for Discriminating Conspecific Vocalizations in the Thalamocortical System of Anesthetized and Awake Guinea Pigs. *The Journal of Neuroscience* **29**, 334 (2009).
197. Wang, X., Merzenich, M. M., Beitel, R. & Schreiner, C. E. Representation of a species-specific vocalization in the primary auditory cortex of the common marmoset: temporal and spectral characteristics. *J Neurophysiol* **74**, 2685–2706 (1995).
198. Galindo-Leon, E. E., Lin, F. G. & Liu, R. C. Inhibitory Plasticity in a Lateral Band Improves Cortical Detection of Natural Vocalizations. *Neuron* **62**, 705 (2009).
199. Liu, R. C. & Schreiner, C. E. Auditory Cortical Detection and Discrimination Correlates with Communicative Significance. *PLoS Biol* **5**, 1426–1439 (2007).
200. Gehr, D. D., Komiya, H. & Eggermont, J. J. Neuronal responses in cat primary auditory cortex to natural and altered species-specific calls. *Hear Res* **150**, 27–42 (2000).
201. Holmstrom, L. A., Eeuwes, L. B. M., Roberts, P. D. & Portfors, C. V. Efficient Encoding of Vocalizations in the Auditory Midbrain. *The Journal of Neuroscience* **30**, 802 (2010).
202. Carruthers, I. M. *et al.* Emergence of invariant representation of vocalizations in the auditory cortex. *J Neurophysiol* **114**, 2726 (2015).
203. Ming, V. L. & Holt, L. L. Efficient coding in human auditory perception. *J Acoust Soc Am* **126**, 1312 (2009).
204. Banai, K. & Lavner, Y. Perceptual Learning of Time-Compressed Speech: More than Rapid Adaptation. *PLoS One* **7**, (2012).
205. Nourski, K. V. *et al.* Temporal Envelope of Time-Compressed Speech Represented in the Human Auditory Cortex. *The Journal of Neuroscience* **29**, 15564 (2009).
206. Sebastián-Gallés, N., Dupoux, E., Costa, A. & Mehler, J. Adaptation to time-compressed speech: phonological determinants. *Percept Psychophys* **62**, 834–842 (2000).
207. Pallier, C., Sebastián-Gallés, N., Dupoux, E., Christophe, A. & Mehler, J. Perceptual adjustment to time-compressed speech: a cross-linguistic study. *Mem Cognit* **26**, 844–851 (1998).
208. Dupoux, E. & Green, K. Perceptual adjustment to highly compressed speech: effects of talker and rate changes. *J Exp Psychol Hum Percept Perform* **23**, 914–927 (1997).
209. Guiraud, H., Ferragne, E., Bedoin, N., Interspeech, V. B.- & 2013, undefined. Adaptation to natural fast speech and time-compressed speech in children. *isca-speech.org* (2013).
210. Orchik D J & Oelschlaeger M L. Time-compressed speech discrimination in children and its relationship to articulation. *J Am Audiol Soc* . (1977).
211. Issard, C. & Gervain, J. Adult-like processing of time-compressed speech by newborns: A NIRS study. *Dev Cogn Neurosci* **25**, 176 (2017).
212. Giraud, A. L. & Poeppel, D. Cortical oscillations and speech processing: emerging computational principles and operations. *Nat Neurosci* **15**, 511 (2012).
213. Ghitza, O., Giraud, A. L. & Poeppel, D. Neuronal oscillations and speech perception: critical-band temporal envelopes are the essence. *Front Hum Neurosci* **6**, (2012).
214. Poeppel D. The analysis of speech in different temporal integration windows: cerebral lateralization as ‘asymmetric sampling in time’. *Speech Commun* (2003) doi:10.1016/S0167-6393(02)00107-3.

215. Eckmann, S., Klimmasch, L., Shi, B. E. & Triesch, J. Active efficient coding explains the development of binocular vision and its failure in amblyopia. *Proc Natl Acad Sci U S A* **117**, 6156–6162 (2020).
216. Lu, K. *et al.* Adaptive Efficient Coding of Correlated Acoustic Properties. *The Journal of Neuroscience* **39**, 8664 (2019).
217. Whitmire, C. J. & Stanley, G. B. Rapid sensory adaptation redux: A circuit perspective. *Neuron* **92**, 298 (2016).
218. Weber, A. I., Krishnamurthy, K. & Fairhall, A. L. Coding Principles in Adaptation. *Annu Rev Vis Sci* **5**, 427–449 (2019).
219. Clifton, R. K., Gwiazda, J., Bauer, J. A., Clarkson, M. G. & Held, R. M. Growth in Head Size During Infancy: Implications for Sound Localization. *Dev Psychol* **24**, 477–483 (1988).
220. Carlile, S. The auditory periphery of the ferret: postnatal development of acoustic properties. *Hear Res* **51**, 265–277 (1991).
221. Mrsic-Flogel, T. D., Schnupp, J. W. H. & King, A. J. Acoustic factors govern developmental sharpening of spatial tuning in the auditory cortex. *Nat Neurosci* **6**, 981–988 (2003).
222. Campbell, R. A. A. *et al.* Virtual Adult Ears Reveal the Roles of Acoustical Factors and Experience in Auditory Space Map Development. *The Journal of Neuroscience* **28**, 11557 (2008).
223. Tollin, D. J. & Koka, K. Postnatal development of sound pressure transformations by the head and pinnae of the cat: Monaural characteristics. *J Acoust Soc Am* **125**, 980 (2009).
224. Knudsen, E. I., Esterly, S. D. & Knudsen, P. F. Monaural occlusion alters sound localization during a sensitive period in the barn owl. *The Journal of Neuroscience* **4**, 1001 (1984).
225. Knudsen, E. I. Experience alters the spatial tuning of auditory units in the optic tectum during a sensitive period in the barn owl. *The Journal of Neuroscience* **5**, 3094 (1985).
226. Gold, J. I. & Knudsen, E. I. Abnormal Auditory Experience Induces Frequency-Specific Adjustments in Unit Tuning for Binaural Localization Cues in the Optic Tectum of Juvenile Owls. *The Journal of Neuroscience* **20**, 862 (2000).
227. King, A. J., Parsons, C. H. & Moore, D. R. Plasticity in the neural coding of auditory space in the mammalian brain. *Proc Natl Acad Sci U S A* **97**, 11821 (2000).
228. Keating, P., Dahmen, J. C. & King, A. J. Context-Specific Reweighting of Auditory Spatial Cues following Altered Experience during Development. *Current Biology* **23**, 1291 (2013).
229. Keating, P., Dahmen, J. C. & King, A. J. Complementary adaptive processes contribute to the developmental plasticity of spatial hearing. *Nat Neurosci* **18**, 185 (2015).
230. Knudsen, E. I. & Brainard, M. S. Visual instruction of the neural map of auditory space in the developing optic tectum. *Science* **253**, 85–87 (1991).
231. King, A. J., Hutchings, M. E., Moore, D. R. & Blakemore, C. Developmental plasticity in the visual and auditory representations in the mammalian superior colliculus. *Nature* **332**, 73–76 (1988).
232. Knudsen, E. I. & Knudsen, P. F. Sensitive and critical periods for visual calibration of sound localization by barn owls. *The Journal of Neuroscience* **10**, 222 (1990).
233. Bauer, R. W., Matuzsa, J. L., Blackmer, R. F. & Glucksberg, S. Noise Localization after Unilateral Attenuation. *J Acoust Soc Am* **40**, 441 (2005).
234. Kacelnik, O., Nodal, F. R., Parsons, C. H. & King, A. J. Training-Induced Plasticity of Auditory Localization in Adult Mammals. *PLoS Biol* **4**, 627–638 (2006).
235. Kumpik, D. P., Kacelnik, O. & King, A. J. Adaptive Reweighting of Auditory Localization Cues in Response to Chronic Unilateral Earplugging in Humans. *The Journal of Neuroscience* **30**, 4883 (2010).

236. Keating, P., Rosenior-Patten, O., Dahmen, J. C., Bell, O. & King, A. J. Behavioral training promotes multiple adaptive processes following acute hearing loss. *Elife* **5**, (2016).
237. Trapeau, R. & Schönwiesner, M. Adaptation to shifted interaural time differences changes encoding of sound location in human auditory cortex. *Neuroimage* **118**, 26–38 (2015).
238. Zonooz, B. & Van Opstal, A. J. Differential Adaptation in Azimuth and Elevation to Acute Monaural Spatial Hearing after Training with Visual Feedback. *eNeuro* **6**, (2019).
239. David, S. V., Fritz, J. B. & Shamma, S. A. Task reward structure shapes rapid receptive field plasticity in auditory cortex. *Proc Natl Acad Sci U S A* **109**, 2144–2149 (2012).
240. Niwa, M., Johnson, J. S., O'Connor, K. N. & Sutter, M. L. Active Engagement Improves Primary Auditory Cortical Neurons' Ability to Discriminate Temporal Modulation. *The Journal of Neuroscience* **32**, 9323 (2012).
241. Jaramillo, S., Borges, K. & Zador, A. M. Auditory Thalamus and Auditory Cortex Are Equally Modulated by Context during Flexible Categorization of Sounds. *The Journal of Neuroscience* **34**, 5291 (2014).
242. Shamma, S. & Fritz, J. Adaptive Auditory Computations. *Curr Opin Neurobiol* **25**, 164 (2014).
243. Edeline, J.-M. & Weinberger, N. M. Subcortical adaptive filtering in the auditory system: associative receptive field plasticity in the dorsal medial geniculate body. *Behavioral neuroscience* **105**, 154–175 (1991).
244. Weinberger, N. M. AUDITORY ASSOCIATIVE MEMORY AND REPRESENTATIONAL PLASTICITY IN THE PRIMARY AUDITORY CORTEX. *Hear Res* **229**, 54 (2007).
245. Bieszczad, K. M. & Weinberger, N. M. Representational gain in cortical area underlies increase of memory strength. *Proc Natl Acad Sci U S A* **107**, 3793 (2010).
246. Recanzone, G. H., Schreiner, C. E. & Merzenich, M. M. Plasticity in the frequency representation of primary auditory cortex following discrimination training in adult owl monkeys. *The Journal of Neuroscience* **13**, 87 (1993).
247. Polley, D. B., Steinberg, E. E. & Merzenich, M. M. Perceptual Learning Directs Auditory Cortical Map Reorganization through Top-Down Influences. *The Journal of Neuroscience* **26**, 4970 (2006).
248. Reed, A. *et al.* Cortical map plasticity improves learning but is not necessary for improved performance. *Neuron* **70**, 121–131 (2011).
249. Moore, D. R. & Shannon, R. V. Beyond cochlear implants: awakening the deafened brain. *Nat Neurosci* **12**, 686–691 (2009).
250. Cramer, S. C. *et al.* Harnessing neuroplasticity for clinical applications. *Brain* **134**, 1591 (2011).
251. Keating, P. & King, A. J. Developmental plasticity of spatial hearing following asymmetric hearing loss: context-dependent cue integration and its clinical implications. *Front Syst Neurosci* **7**, (2013).
252. Sandmann, P. *et al.* Rapid bilateral improvement in auditory cortex activity in postlingually deafened adults following cochlear implantation. *Clin Neurophysiol* **126**, 594–607 (2015).
253. Irvine, D. R. F. Plasticity in the auditory system. *Hear Res* **362**, 61–73 (2018).
254. Auerbach, B. D. & Gritton, H. J. Hearing in Complex Environments: Auditory Gain Control, Attention, and Hearing Loss. *Front Neurosci* **16**, 799787 (2022).
255. Adrian, E. D. & Zotterman, Y. The impulses produced by sensory nerve endings: Part 3. Impulses set up by Touch and Pressure. *J Physiol* **61**, 465 (1926).
256. Webster, M. Visual Adaptation. *Annu Rev Vis Sci* **1**, 547 (2015).
257. Westerman, L. A. & Smith, R. L. Rapid and short-term adaptation in auditory nerve responses. *Hear Res* **15**, 249–260 (1984).
258. Yates, G. K., Robertson, D. & Johnstone, B. M. Very rapid adaptation in the guinea pig auditory nerve. *Hear Res* **17**, 1–12 (1985).

259. Javel, E. Long-term adaptation in cat auditory-nerve fiber responses. *J Acoust Soc Am* **99**, 1040–1052 (1996).
260. Ó Maoiléidigh, D. & Ricci, A. J. A bundle of mechanisms: Inner-ear hair-cell mechanotransduction. *Trends Neurosci* **42**, 221 (2019).
261. Peng, A. W., Effertz, T. & Ricci, A. J. Adaptation of mammalian auditory hair cell mechanotransduction is independent of calcium entry. *Neuron* **80**, 960 (2013).
262. Russell, I. J. & Sellick, P. M. Intracellular studies of hair cells in the mammalian cochlea. *J Physiol* **284**, 261 (1978).
263. Smith, R. L., Brachman, M. L. & Goodman, D. A. Adaptation in the auditory periphery. *Ann N Y Acad Sci* **405**, 79–93 (1983).
264. Moser, T. & Beutner, D. Kinetics of exocytosis and endocytosis at the cochlear inner hair cell afferent synapse of the mouse. *Proc Natl Acad Sci U S A* **97**, 883 (2000).
265. Goutman, J. D. & Glowatzki, E. Time course and calcium dependence of transmitter release at a single ribbon synapse. *Proc Natl Acad Sci U S A* **104**, 16341 (2007).
266. Goutman, J. D. Mechanisms of synaptic depression at the hair cell ribbon synapse that support auditory nerve function. *Proc Natl Acad Sci U S A* **114**, 9719–9724 (2017).
267. Ingham, N. J. & McAlpine, D. Spike-frequency adaptation in the inferior colliculus. *J Neurophysiol* **91**, 632–645 (2004).
268. Ter-Mikaelian, M., Sanes, D. H. & Semple, M. N. Transformation of Temporal Properties between Auditory Midbrain and Cortex in the Awake Mongolian Gerbil. *The Journal of Neuroscience* **27**, 6091 (2007).
269. Eggermont, J. J. Animal models of auditory temporal processing. *Int J Psychophysiol* **95**, 202–215 (2015).
270. Fairhall, A. L., Lewen, G. D., Bialek, W. & De Ruyter van Steveninck, R. R. Efficiency and ambiguity in an adaptive neural code. *Nature* **412**, 787–792 (2001).
271. Dean, I., Robinson, B. L., Harper, N. S. & McAlpine, D. Rapid Neural Adaptation to Sound Level Statistics. *The Journal of Neuroscience* **28**, 6430 (2008).
272. Winter, I. M., Robertson, D. & Yates, G. K. Diversity of characteristic frequency rate-intensity functions in guinea pig auditory nerve fibres. *Hear Res* **45**, 191–202 (1990).
273. Heilbron, M. & Chait, M. Great Expectations: Is there Evidence for Predictive Coding in Auditory Cortex? *Neuroscience* **389**, 54–73 (2018).
274. Neisser U. Cognition and reality. *cir.nii.ac.jp* (1987).
275. Friston, K. A theory of cortical responses. *Philosophical Transactions of the Royal Society B: Biological Sciences* **360**, 815 (2005).
276. Rao, R. P. N. & Ballard, D. H. Predictive coding in the visual cortex: a functional interpretation of some extra-classical receptive-field effects. *Nat Neurosci* **2**, 79–87 (1999).
277. Knill, D. C. & Pouget, A. The Bayesian brain: the role of uncertainty in neural coding and computation. *Trends Neurosci* **27**, 712–719 (2004).
278. Denham, S. L. & Winkler, I. Predictive coding in auditory perception: challenges and unresolved questions. *Eur J Neurosci* **51**, 1151–1160 (2020).
279. Schröger, E. *et al.* Predictive regularity representations in violation detection and auditory stream segregation: from conceptual to computational models. *Brain Topogr* **27**, 565–577 (2014).
280. Schröger, E., Marzecová, A. & Sanmiguel, I. Attention and prediction in human audition: a lesson from cognitive psychophysiology. *Eur J Neurosci* **41**, 641 (2015).
281. Winkler, I. & Schröger, E. Auditory perceptual objects as generative models: Setting the stage for communication by sound. *Brain Lang* **148**, 1–22 (2015).

282. Zador, A. M. A critique of pure learning and what artificial neural networks can learn from animal brains. *Nat Commun* **10**, (2019).
283. Oja, E. Unsupervised learning in neural computation. *Theor Comput Sci* **287**, 187–207 (2002).
284. Oord, A. van den, Li, Y. & Vinyals, O. Representation Learning with Contrastive Predictive Coding. (2018).
285. Bakhtiari, S., Mineault, P., Lillicrap, T., Pack, C. C. & Richards, B. A. The functional specialization of visual cortex emerges from training parallel pathways with self-supervised predictive learning. *bioRxiv* 2021.06.18.448989 (2021) doi:10.1101/2021.06.18.448989.
286. Zhuang, C. *et al.* Unsupervised neural network models of the ventral visual stream. *Proc Natl Acad Sci U S A* **118**, (2021).
287. Huang, Y. & Rao, R. P. N. Predictive coding. *Wiley Interdiscip Rev Cogn Sci* **2**, 580–593 (2011).
288. Spratling, M. W. A review of predictive coding algorithms. *Brain Cogn* **112**, 92–97 (2017).
289. Whittington, J. C. R. & Bogacz, R. Theories of Error Back-Propagation in the Brain. *Trends Cogn Sci* **23**, 235 (2019).
290. Grossberg, S. Conscious mind, resonant brain: how each brain makes a mind. (2021).
291. Millidge, B., Seth, A. K. & Buckley, C. L. Predictive Coding: a Theoretical and Experimental Review. (2021).
292. Wiskott, L. & Sejnowski, T. J. Slow feature analysis: unsupervised learning of invariances. *Neural Comput* **14**, 715–770 (2002).
293. Bialek, W., De Ruyter Van Steveninck, R. R. & Tishby, N. Efficient representation as a design principle for neural coding and computation. *IEEE International Symposium on Information Theory - Proceedings* 659–663 (2007) doi:10.1109/ISIT.2006.261867.
294. Palmer, S. E., Marre, O., Berry, M. J. & Bialek, W. Predictive information in a sensory population. *Proc Natl Acad Sci U S A* **112**, 6908–6913 (2015).
295. Keller, G. B. & Mrsic-Flogel, T. D. Predictive Processing: A Canonical Cortical Computation. *Neuron* **100**, 424 (2018).
296. Singer, Y. *et al.* Sensory cortex is optimized for prediction of future input. *Elife* **7**, (2018).
297. Näätänen, R., Gaillard, A. W. K. & Mäntysalo, S. Early selective-attention effect on evoked potential reinterpreted. *Acta Psychol (Amst)* **42**, 313–329 (1978).
298. Strauss, M. *et al.* Disruption of hierarchical predictive coding during sleep. *Proc Natl Acad Sci U S A* **112**, E1353–E1362 (2015).
299. Koelsch, S., Heinke, W., Sammler, D. & Olthoff, D. Auditory processing during deep propofol sedation and recovery from unconsciousness. *Clin Neurophysiol* **117**, 1746–1759 (2006).
300. Quaedflieg, C. W., Münte, S., Kalso, E. & Sambeth, A. Effects of remifentanyl on processing of auditory stimuli: a combined MEG/EEG study. *J Psychopharmacol* **28**, 39–48 (2014).
301. Morlet, D. & Fischer, C. MMN and Novelty P3 in Coma and Other Altered States of Consciousness: A Review. *Brain Topogr* **27**, 467 (2014).
302. Cheour, M. *et al.* Speech sounds learned by sleeping newborns. *Nature* **415**, 599–600 (2002).
303. Winkler, I. *et al.* Newborn infants can organize the auditory world. *Proc Natl Acad Sci U S A* **100**, 11812 (2003).
304. Paavilainen, P. The mismatch-negativity (MMN) component of the auditory event-related potential to violations of abstract regularities: a review. *Int J Psychophysiol* **88**, 109–123 (2013).
305. Paavilainen, P., Kaukinen, C., Koskinen, O., Kylmäälä, J. & Rehn, L. Mismatch negativity (MMN) elicited by abstract regularity violations in two concurrent auditory streams. *Heliyon* **4**, 608 (2018).
306. Saarinen, J., Paavilainen, P., Tervaniemi, M. & Naatanen, R. Representation of abstract attributes of auditory stimuli in the human brain. *Neuroreport* **3**, 1149–1151 (1992).

307. Schröger, E., Bendixen, A., Trujillo-Barreto, N. J. & Roeber, U. Processing of Abstract Rule Violations in Audition. *PLoS One* **2**, 1131 (2007).
308. Tervaniemi, M., Maury, S. & Näätänen, R. Neural representations of abstract stimulus features in the human brain as reflected by the mismatch negativity. *Neuroreport* **5**, 844–846 (1994).
309. Näätänen, R., Astikainen, P., Ruusuvirta, T. & Huotilainen, M. Automatic auditory intelligence: an expression of the sensory-cognitive core of cognitive processes. *Brain Res Rev* **64**, 123–136 (2010).
310. Sussman, E., Winkler, I. & Wang, W. MMN and attention: competition for deviance detection. *Psychophysiology* **40**, 430–435 (2003).
311. Fritz, J. B., Elhilali, M., David, S. V. & Shamma, S. A. Auditory attention--focusing the searchlight on sound. *Curr Opin Neurobiol* **17**, 437–455 (2007).
312. Bartha-Doering, L., Deuster, D., Giordano, V., Am Zehnhoff-Dinnesen, A. & Dobel, C. A systematic review of the mismatch negativity as an index for auditory sensory memory: From basic research to clinical and developmental perspectives. *Psychophysiology* **52**, 1115–1130 (2015).
313. Ranganath, C. & Rainer, G. Neural mechanisms for detecting and remembering novel events. *Nat Rev Neurosci* **4**, 193–202 (2003).
314. Baldeweg, T., Klugman, A., Gruzelier, J. & Hirsch, S. R. Mismatch negativity potentials and cognitive impairment in schizophrenia. *Schizophr Res* **69**, 203–217 (2004).
315. Damaso, K. A. M., Michie, P. T. & Todd, J. Paying attention to MMN in schizophrenia. *Brain Res* **1626**, 267–279 (2015).
316. Ells, E. M. L. *et al.* Alterations of complex mismatch negativity (cMMN) elicited by a two-tone pattern paradigm in early-phase psychosis. *Biol Psychol* **135**, 128–135 (2018).
317. Haigh, S. M. *et al.* Mismatch Negativity to Pitch Pattern Deviants in Schizophrenia. *Eur J Neurosci* **46**, 2229 (2017).
318. Javitt, D. C. & Sweet, R. A. Auditory dysfunction in schizophrenia: integrating clinical and basic features. *Nat Rev Neurosci* **16**, 535 (2015).
319. Joshi, Y. B. *et al.* Mismatch Negativity Impairment is Associated with Deficits in Identifying Real-World Environmental Sounds in Schizophrenia. *Schizophr Res* **191**, 5 (2018).
320. Brønneck, K. S., Nordby, H., Larsen, J. P. & Aarsland, D. Disturbance of automatic auditory change detection in dementia associated with Parkinson's disease: A mismatch negativity study. *Neurobiol Aging* **31**, 104–113 (2010).
321. Minks, E. *et al.* Mismatch negativity-like potential (MMN-like) in the subthalamic nuclei in Parkinson's disease patients. *J Neural Transm (Vienna)* **121**, 1507–1522 (2014).
322. Pekkonen, E. Mismatch negativity in aging and in Alzheimer's and Parkinson's diseases. *Audiol Neurootol* **5**, 216–224 (2000).
323. Idrizbegovic, E., Hederstierna, C. & Rosenhall, U. Mismatch Negativity and Ear Laterality in Alzheimer's Disease and in Mild Cognitive Impairment. *J Alzheimers Dis* **53**, 1405–1410 (2016).
324. Jiang, S. *et al.* Mismatch negativity as a potential neurobiological marker of early-stage Alzheimer disease and vascular dementia. *Neurosci Lett* **647**, 26–31 (2017).
325. Papadaniil, C. D. *et al.* Cognitive MMN and P300 in mild cognitive impairment and Alzheimer's disease: A high density EEG-3D vector field tomography approach. *Brain Res* **1648**, 425–433 (2016).
326. Goris, J. *et al.* Sensory Prediction Errors Are Less Modulated by Global Context in Autism Spectrum Disorder. *Biol Psychiatry Cogn Neurosci Neuroimaging* **3**, 667–674 (2018).

327. Hudac, C. M. *et al.* Early enhanced processing and delayed habituation to deviance sounds in autism spectrum disorder. *Brain Cogn* **123**, 110 (2018).
328. Schwartz, S., Shinn-Cunningham, B. & Tager-Flusberg, H. Meta-analysis and systematic review of the literature characterizing auditory mismatch negativity in individuals with autism. *Neurosci Biobehav Rev* **87**, 106 (2018).
329. Davids, N. *et al.* The nature of auditory discrimination problems in children with specific language impairment: an MMN study. *Neuropsychologia* **49**, 19–28 (2011).
330. Kujala, T. & Leminen, M. Low-level neural auditory discrimination dysfunctions in specific language impairment—A review on mismatch negativity findings. *Dev Cogn Neurosci* **28**, 65 (2017).
331. Kujala, T., Tervaniemi, M. & Schröger, E. The mismatch negativity in cognitive and clinical neuroscience: theoretical and methodological considerations. *Biol Psychol* **74**, 1–19 (2007).
332. Näätänen, R., Paavilainen, P., Rinne, T. & Alho, K. The mismatch negativity (MMN) in basic research of central auditory processing: a review. *Clin Neurophysiol* **118**, 2544–2590 (2007).
333. Näätänen, R., Sussman, E. S., Salisbury, D. & Shafer, V. L. Mismatch Negativity (MMN) as an Index of Cognitive Dysfunction. *Brain Topogr* **27**, 451 (2014).
334. Light, G. A. & Näätänen, R. Mismatch negativity is a breakthrough biomarker for understanding and treating psychotic disorders. *Proc Natl Acad Sci U S A* **110**, 15175 (2013).
335. Näätänen, R. *et al.* The mismatch negativity (MMN)—a unique window to disturbed central auditory processing in ageing and different clinical conditions. *Clin Neurophysiol* **123**, 424–458 (2012).
336. Schall, U. Is it time to move mismatch negativity into the clinic? *Biol Psychol* **116**, 41–46 (2016).
337. Ayala, Y. A. & Malmierca, M. S. Cholinergic Modulation of Stimulus-Specific Adaptation in the Inferior Colliculus. *The Journal of Neuroscience* **35**, 12261 (2015).
338. Duque, D., Ayala, Y. A. & Malmierca, M. S. Deviance detection in auditory subcortical structures: what can we learn from neurochemistry and neural connectivity? *Cell Tissue Res* **361**, 215–232 (2015).
339. Ayala, Y. A. & Malmierca, M. S. The effect of inhibition on stimulus-specific adaptation in the inferior colliculus. *Brain Struct Funct* **223**, 1391–1407 (2018).
340. Duque, D., Pérez-González, D., Ayala, Y. A., Palmer, A. R. & Malmierca, M. S. Topographic Distribution, Frequency, and Intensity Dependence of Stimulus-Specific Adaptation in the Inferior Colliculus of the Rat. *The Journal of Neuroscience* **32**, 17762 (2012).
341. Duque, D., Wang, X., Nieto-Diego, J., Krumbholz, K. & Malmierca, M. S. Neurons in the inferior colliculus of the rat show stimulus-specific adaptation for frequency, but not for intensity. *Sci Rep* **6**, (2016).
342. Malmierca, M. S., Cristaudo, S., Pérez-González, D. & Covey, E. Stimulus-Specific Adaptation in the Inferior Colliculus of the Anesthetized Rat. *The Journal of Neuroscience* **29**, 5483 (2009).
343. Zhao, L., Liu, Y., Shen, L., Feng, L. & Hong, B. Stimulus-specific adaptation and its dynamics in the inferior colliculus of rat. *Neuroscience* **181**, 163–174 (2011).
344. Anderson, L. A., Christianson, G. B. & Linden, J. F. Stimulus-Specific Adaptation Occurs in the Auditory Thalamus. *The Journal of Neuroscience* **29**, 7359 (2009).
345. Anderson, L. A. & Malmierca, M. S. The effect of auditory cortex deactivation on stimulus-specific adaptation in the inferior colliculus of the rat. *Eur J Neurosci* **37**, 52–62 (2013).
346. Antunes, F. M. & Malmierca, M. S. An overview of stimulus-specific adaptation in the auditory thalamus. *Brain Topogr* **27**, 480–499 (2014).

347. Antunes, F. M., Nelken, I., Covey, E. & Malmierca, M. S. Stimulus-Specific Adaptation in the Auditory Thalamus of the Anesthetized Rat. *PLoS One* **5**, (2010).
348. Chen, I. W., Helmchen, F. & Lütcke, H. Specific Early and Late Oddball-Evoked Responses in Excitatory and Inhibitory Neurons of Mouse Auditory Cortex. *The Journal of Neuroscience* **35**, 12560 (2015).
349. Farley, B. J., Quirk, M. C., Doherty, J. J. & Christian, E. P. Stimulus-Specific Adaptation in Auditory Cortex Is an NMDA-Independent Process Distinct from the Sensory Novelty Encoded by the Mismatch Negativity. *The Journal of Neuroscience* **30**, 16475 (2010).
350. Klein, C., Von Der Behrens, W. & Gaese, B. H. Stimulus-specific adaptation in field potentials and neuronal responses to frequency-modulated tones in the primary auditory cortex. *Brain Topogr* **27**, 599–610 (2014).
351. Natan, R. G., Rao, W. & Geffen, M. N. Cortical interneurons differentially shape frequency tuning following adaptation. *Cell Rep* **21**, 878 (2017).
352. Natan, R. G. *et al.* Complementary control of sensory adaptation by two types of cortical interneurons. *Elife* **4**, (2015).
353. Nieto-Diego, J. & Malmierca, M. S. Topographic Distribution of Stimulus-Specific Adaptation across Auditory Cortical Fields in the Anesthetized Rat. *PLoS Biol* **14**, (2016).
354. Valdés-Baizabal, C., Parras, G. G., Ayala, Y. A. & Malmierca, M. S. Endocannabinoid Modulation of Stimulus-Specific Adaptation in Inferior Colliculus Neurons of the Rat. *Sci Rep* **7**, (2017).
355. Ulanovsky, N., Las, L. & Nelken, I. Processing of low-probability sounds by cortical neurons. *Nat Neurosci* **6**, 391–398 (2003).
356. Nelken, I. & Ulanovsky, N. Mismatch negativity and stimulus-specific adaptation in animal models. *J Psychophysiol* **21**, 214–223 (2007).
357. Escera, C. & Malmierca, M. S. The auditory novelty system: an attempt to integrate human and animal research. *Psychophysiology* **51**, 111–123 (2014).
358. Malmierca, M. S., Sanchez-Vives, M. V., Escera, C. & Bendixen, A. Neuronal adaptation, novelty detection and regularity encoding in audition. *Front Syst Neurosci* **8**, (2014).
359. Khouri, L. & Nelken, I. Detecting the unexpected. *Curr Opin Neurobiol* **35**, 142–147 (2015).
360. Auztulewicz, R. & Friston, K. Repetition suppression and its contextual determinants in predictive coding. *Cortex* **80**, 125 (2016).
361. Bastos, A. M. *et al.* Canonical microcircuits for predictive coding. *Neuron* **76**, 695 (2012).
362. Carbajal, G. V. & Malmierca, M. S. The Neuronal Basis of Predictive Coding Along the Auditory Pathway: From the Subcortical Roots to Cortical Deviance Detection. *Trends Hear* **22**, (2018).
363. Garrido, M. I., Kilner, J. M., Stephan, K. E. & Friston, K. J. The mismatch negativity: A review of underlying mechanisms. *Clinical Neurophysiology* **120**, 453 (2009).
364. Garrido, M. I. *et al.* Repetition suppression and plasticity in the human brain. *Neuroimage* **48**, 269 (2009).
365. Grill-Spector, K., Henson, R. & Martin, A. Repetition and the brain: neural models of stimulus-specific effects. *Trends Cogn Sci* **10**, 14–23 (2006).
366. Summerfield, C., Trittschuh, E. H., Monti, J. M., Mesulam, M. M. & Egner, T. Neural repetition suppression reflects fulfilled perceptual expectations. *Nat Neurosci* **11**, 1004 (2008).
367. Todorovic, A., van Ede, F., Maris, E. & de Lange, F. P. Prior Expectation Mediates Neural Adaptation to Repeated Sounds in the Auditory Cortex: An MEG Study. *The Journal of Neuroscience* **31**, 9118 (2011).
368. Grotheer, M. & Kovács, G. Can predictive coding explain repetition suppression? *Cortex* **80**, 113–124 (2016).

369. Pajani, A., Kouider, S., Roux, P. & De Gardelle, V. Unsuppressible Repetition Suppression and exemplar-specific Expectation Suppression in the Fusiform Face Area. *Sci Rep* **7**, (2017).
370. Todorovic, A. & de Lange, F. P. Repetition Suppression and Expectation Suppression Are Dissociable in Time in Early Auditory Evoked Fields. *The Journal of Neuroscience* **32**, 13389 (2012).
371. Barascud, N., Pearce, M. T., Griffiths, T. D., Friston, K. J. & Chait, M. Brain responses in humans reveal ideal observer-like sensitivity to complex acoustic patterns. *Proc Natl Acad Sci U S A* **113**, E616–E625 (2016).
372. Southwell, R. *et al.* Is predictability salient? A study of attentional capture by auditory patterns. *Philosophical Transactions of the Royal Society B: Biological Sciences* **372**, (2017).
373. Wacongne, C., Changeux, J. P. & Dehaene, S. A Neuronal Model of Predictive Coding Accounting for the Mismatch Negativity. *The Journal of Neuroscience* **32**, 3665 (2012).
374. Winkler, I., Denham, S. L. & Nelken, I. Modeling the auditory scene: predictive regularity representations and perceptual objects. *Trends Cogn Sci* **13**, 532–540 (2009).
375. Lazard, D. S. *et al.* Pre-, Per- and Postoperative Factors Affecting Performance of Postlinguistically Deaf Adults Using Cochlear Implants: A New Conceptual Model over Time. *PLoS One* **7**, (2012).
376. Blamey, P. *et al.* Factors affecting auditory performance of postlinguistically deaf adults using cochlear implants. *Audiol Neurootol* **1**, 293–306 (1996).
377. Blamey, P. *et al.* Factors affecting auditory performance of postlinguistically deaf adults using cochlear implants: an update with 2251 patients. *Audiol Neurootol* **18**, 36–47 (2013).
378. Blamey, P. *et al.* Factors affecting auditory performance of postlinguistically deaf adults using cochlear implants: an update with 2251 patients. *Audiol Neurootol* **18**, 36–47 (2013).
379. Zimmermann, C. E., Burgess, B. J. & Nadol, J. B. Patterns of degeneration in the human cochlear nerve. *Hear Res* **90**, 192–201 (1995).
380. Shearer, A. E. *et al.* Genetic Variants in the Peripheral Auditory System Significantly Affect Adult Cochlear Implant Performance. *Hear Res* **348**, 138 (2017).
381. Hardie, N. A. & Shepherd, R. K. Sensorineural hearing loss during development: morphological and physiological response of the cochlea and auditory brainstem. *Hear Res* **128**, 147–165 (1999).
382. Leake, P. A. & Hradek, G. T. Cochlear pathology of long term neomycin induced deafness in cats. *Hear Res* **33**, 11–33 (1988).
383. Tagoe, T., Barker, M., Jones, A., Allcock, N. & Hamann, M. Auditory Nerve Perinodal Demyelination in Noise-Induced Hearing Loss. *The Journal of Neuroscience* **34**, 2684 (2014).
384. Cianfrone, G., Turchetta, R., Mazzei, F., Bartolo, M. & Parisi, L. Temperature-dependent auditory neuropathy: is it an acoustic Uthoff-like phenomenon? A case report. *Ann Otol Rhinol Laryngol* **115**, 518–527 (2006).
385. Orabi, A. A., Mawman, D., Al-Zoubi, F., Saeed, S. R. & Ramsden, R. T. Cochlear implant outcomes and quality of life in the elderly: Manchester experience over 13 years. *Clin Otolaryngol* **31**, 116–122 (2006).
386. Litovsky, R. Y. *et al.* Studies on Bilateral Cochlear Implants at the University of Wisconsin's Binaural Hearing and Speech Lab. *J Am Acad Audiol* **23**, 476 (2012).
387. Kan, A. & Litovsky, R. Y. Binaural hearing with electrical stimulation. *Hear Res* **322**, 127 (2015).
388. Basser, P. J. Scaling laws for myelinated axons derived from an electrotonic core-conductor model. *J Integr Neurosci* **3**, 227–244 (2004).
389. Rushton, W. A. H. A theory of the effects of fibre size in medullated nerve. *J Physiol* **115**, 101 (1951).

390. Koles, Z. J. & Rasminsky, M. A computer simulation of conduction in demyelinated nerve fibres. *J Physiol* **227**, 351 (1972).
391. Chow, C. C. & White, J. A. Spontaneous action potentials due to channel fluctuations. *Biophys J* **71**, 3013 (1996).
392. Imennov, N. S. & Rubinstein, J. T. Stochastic population model for electrical stimulation of the auditory nerve. *IEEE Trans Biomed Eng* **56**, 2493–2501 (2009).
393. White, J. A., Rubinstein, J. T. & Kay, A. R. Channel noise in neurons. *Trends Neurosci* **23**, 131–137 (2000).
394. Goldwyn, J. H., Rubinstein, J. T. & Shea-Brown, E. A point process framework for modeling electrical stimulation of the auditory nerve. *J Neurophysiol* **108**, 1430 (2012).
395. Shepherd, R. K. & Javel, E. Electrical stimulation of the auditory nerve: II. Effect of stimulus waveshape on single fibre response properties. *Hear Res* **130**, 171–188 (1999).
396. Joshi, S. N., Dau, T. & Epp, B. A Model of Electrically Stimulated Auditory Nerve Fiber Responses with Peripheral and Central Sites of Spike Generation. *JARO: Journal of the Association for Research in Otolaryngology* **18**, 323 (2017).
397. Rosen, S. Temporal information in speech: acoustic, auditory and linguistic aspects. *Philos Trans R Soc Lond B Biol Sci* **336**, 367–373 (1992).
398. Saberi, K. & Perrott, D. R. Cognitive restoration of reversed speech. *Nature* **398**, 760 (1999).
399. Zwislocki, J. & Feldman, R. S. Just Noticeable Differences in Dichotic Phase. *J Acoust Soc Am* **28**, 860 (1956).
400. Bernstein, L. R. & Trahiotis, C. Converging measures of binaural detection yield estimates of precision of coding of interaural temporal disparities. *J Acoust Soc Am* **138**, EL474–EL479 (2015).
401. Resnick, J. M., Rubinstein, J. T., Perkel, D. J. & Rieke, F. M. Simulating the Effects of Neural Pathology on Cochlear Implant Responses. (2019).
402. Resnick, J. M., O'Brien, G. E. & Rubinstein, J. T. Simulated Auditory Nerve Axon Demyelination Alters Sensitivity and Response Timing to Extracellular Stimulation. *Hear Res* **361**, 121 (2018).
403. Brown, A. D. & Stecker, G. C. Temporal weighting of interaural time and level differences in high-rate click trains. *J Acoust Soc Am* **128**, 332 (2010).
404. Freyman, R. L., Zurek, P. M., Balakrishnan, U. & Chiang, Y.-C. Onset dominance in lateralization. *J Acoust Soc Am* **101**, 1649–1659 (1997).
405. Klein-Hennig, M., Dietz, M., Hohmann, V. & Ewert, S. D. The influence of different segments of the ongoing envelope on sensitivity to interaural time delays. *J Acoust Soc Am* **129**, 3856–3872 (2011).
406. Kolaric, K. V., Thomson, G., Edgar, J. M. & Brown, A. M. Focal axonal swellings and associated ultrastructural changes attenuate conduction velocity in central nervous system axons: a computer modeling study. *Physiol Rep* **1**, 59 (2013).
407. Wise, A. K., Pujol, R., Landry, T. G., Fallon, J. B. & Shepherd, R. K. Structural and Ultrastructural Changes to Type I Spiral Ganglion Neurons and Schwann Cells in the Deafened Guinea Pig Cochlea. *JARO: Journal of the Association for Research in Otolaryngology* **18**, 751 (2017).
408. Craner, M. J., Lo, A. C., Black, J. A. & Waxman, S. G. Abnormal sodium channel distribution in optic nerve axons in a model of inflammatory demyelination. *Brain* **126**, 1552–1561 (2003).
409. McArthur, G. M. & Bishop, D. V. M. Auditory perceptual processing in people with reading and oral language impairments: current issues and recommendations. *Dyslexia* **7**, 150–170 (2001).

410. Vandermosten, M. *et al.* Adults with dyslexia are impaired in categorizing speech and nonspeech sounds on the basis of temporal cues. *Proc Natl Acad Sci U S A* **107**, 10389–10394 (2010).
411. Boets, B., Wouters, J., van Wieringen, A. & Ghesquière, P. Auditory processing, speech perception and phonological ability in pre-school children at high-risk for dyslexia: a longitudinal study of the auditory temporal processing theory. *Neuropsychologia* **45**, 1608–1620 (2007).
412. Torgesen, J. K. *et al.* Developmental and individual differences in performance on phonological synthesis tasks. *J Exp Child Psychol* **47**, 491–505 (1989).
413. RK, W. *et al.* Changing relations between phonological processing abilities and word-level reading as children develop from beginning to skilled readers: a 5-year longitudinal study. *Dev Psychol* **33**, 468–479 (1997).
414. Snowling, M., Bishop, D. V. M. & Stothard, S. E. Is preschool language impairment a risk factor for dyslexia in adolescence? *J Child Psychol Psychiatry* **41**, 587–600 (2000).
415. Vandermosten, M., Boets, B., Wouters, J. & Ghesquière, P. A qualitative and quantitative review of diffusion tensor imaging studies in reading and dyslexia. *Neurosci Biobehav Rev* **36**, 1532–1552 (2012).
416. Yeatman, J. D., Dougherty, R. F., Myall, N. J., Wandell, B. A. & Feldman, H. M. Tract profiles of white matter properties: automating fiber-tract quantification. *PLoS One* **7**, (2012).
417. Kere, J. The molecular genetics and neurobiology of developmental dyslexia as model of a complex phenotype. *Biochem Biophys Res Commun* **452**, 236–243 (2014).
418. Ramus, F., Altarelli, I., Jednoróg, K., Zhao, J. & Scotto di Covella, L. Neuroanatomy of developmental dyslexia: Pitfalls and promise. *Neurosci Biobehav Rev* **84**, 434–452 (2018).
419. Poelmans, G., Buitelaar, J. K., Pauls, D. L. & Franke, B. A theoretical molecular network for dyslexia: integrating available genetic findings. *Mol Psychiatry* **16**, 365–382 (2011).
420. Nopola-Hemmi, J. *et al.* A dominant gene for developmental dyslexia on chromosome 3. *J Med Genet* **38**, 658–664 (2001).
421. Galaburda, A. M., LoTurco, J., Ramus, F., Fitch, R. H. & Rosen, G. D. From genes to behavior in developmental dyslexia. *Nat Neurosci* **9**, 1213–1217 (2006).
422. Rodan, L. H. *et al.* Phenotypic expansion of CACNA1C-associated disorders to include isolated neurological manifestations. *Genet Med* **23**, 1922–1932 (2021).
423. Gabel, M. *et al.* Phosphorylation cycling of Annexin A2 Tyr23 is critical for calcium-regulated exocytosis in neuroendocrine cells. *Biochim Biophys Acta Mol Cell Res* **1866**, 1207–1217 (2019).
424. Klingberg, T. *et al.* Microstructure of temporo-parietal white matter as a basis for reading ability: evidence from diffusion tensor magnetic resonance imaging. *Neuron* **25**, 493–500 (2000).
425. Beaulieu, C. *et al.* Imaging brain connectivity in children with diverse reading ability. *Neuroimage* **25**, 1266–1271 (2005).
426. Norton, E. S., Beach, S. D. & Gabrieli, J. D. E. Neurobiology of dyslexia. *Curr Opin Neurobiol* **30**, 73–78 (2015).
427. Vandermosten, M., Hoeft, F. & Norton, E. S. Integrating MRI brain imaging studies of pre-reading children with current theories of developmental dyslexia: A review and quantitative meta-analysis. *Curr Opin Behav Sci* **10**, 155–161 (2016).
428. Huber, E., Donnelly, P. M., Rokem, A. & Yeatman, J. D. Rapid and widespread white matter plasticity during an intensive reading intervention. *Nat Commun* **9**, (2018).
429. Vidyasagar, T. R. & Pammer, K. Dyslexia: a deficit in visuo-spatial attention, not in phonological processing. *Trends Cogn Sci* **14**, 57–63 (2010).

430. Franceschini, S., Gori, S., Ruffino, M., Pedrolli, K. & Facchetti, A. A causal link between visual spatial attention and reading acquisition. *Curr Biol* **22**, 814–819 (2012).
431. Facchetti, A., Paganoni, P., Turatto, M., Marzola, V. & Mascetti, G. G. Visual-spatial attention in developmental dyslexia. *Cortex* **36**, 109–123 (2000).
432. Facchetti, A. & Molteni, M. The gradient of visual attention in developmental dyslexia. *Neuropsychologia* **39**, 352–357 (2001).
433. Bosse, M. L., Tainturier, M. J. & Valdois, S. Developmental dyslexia: the visual attention span deficit hypothesis. *Cognition* **104**, 198–230 (2007).
434. Sperling, A. J., Lu, Z. L., Manis, F. R. & Seidenberg, M. S. Deficits in perceptual noise exclusion in developmental dyslexia. *Nat Neurosci* **8**, 862–863 (2005).
435. Ziegler, J. C. & Goswami, U. Reading acquisition, developmental dyslexia, and skilled reading across languages: a psycholinguistic grain size theory. *Psychol Bull* **131**, 3–29 (2005).
436. Valdois, S. The visual-attention span deficit in developmental dyslexia: Review of evidence for a visual-attention-based deficit. *Dyslexia* **28**, 397–415 (2022).
437. Shaywitz, B. A. *et al.* Development of left occipitotemporal systems for skilled reading in children after a phonologically-based intervention. *Biol Psychiatry* **55**, 685–691 (2004).
438. Peterson, R. L., Pennington, B. F., Olson, R. K. & Wadsworth, S. J. Longitudinal Stability of Phonological and Surface Subtypes of Developmental Dyslexia. *Sci Stud Read* **18**, 347–362 (2014).
439. Simos, P. G. *et al.* Dyslexia-specific brain activation profile becomes normal following successful remedial training. *Neurology* **58**, 1203–1213 (2002).
440. Wanzek, J. & Vaughn, S. Research-based implications from extensive early reading interventions. *School Psych Rev* **36**, 541–561 (2007).
441. Kluk, K. *et al.* No evidence for hidden hearing loss due to noise exposure in young adults with a normal audiogram. *J Acoust Soc Am* **140**, 3152–3152 (2016).
442. Fulbright, A. N. C., Le Prell, C. G., Griffiths, S. K. & Lobarinas, E. Effects of Recreational Noise on Threshold and Suprathreshold Measures of Auditory Function. *Semin Hear* **38**, 298–318 (2017).
443. Grinn, S. K., Wiseman, K. B., Baker, J. A. & Le Prell, C. G. Hidden hearing loss? No effect of common recreational noise exposure on cochlear nerve response amplitude in humans. *Front Neurosci* **11**, (2017).
444. Prendergast, G. *et al.* Effects of noise exposure on young adults with normal audiograms I: Electrophysiology. *Hear Res* **344**, 68–81 (2017).
445. Prendergast, G. *et al.* Effects of noise exposure on young adults with normal audiograms II: Behavioral measures. *Hear Res* **356**, 74–86 (2017).
446. Guest, H., Munro, K. J., Prendergast, G., Millman, R. E. & Plack, C. J. Impaired speech perception in noise with a normal audiogram: No evidence for cochlear synaptopathy and no relation to lifetime noise exposure. *Hear Res* **364**, 142–151 (2018).
447. Grose, J. H., Buss, E. & Hall, J. W. Loud Music Exposure and Cochlear Synaptopathy in Young Adults: Isolated Auditory Brainstem Response Effects but No Perceptual Consequences. *Trends Hear* **21**, (2017).
448. Valderrama, J. T. *et al.* Effects of lifetime noise exposure on the middle-age human auditory brainstem response, tinnitus and speech-in-noise intelligibility. *Hear Res* **365**, 36–48 (2018).
449. Andrade-Talavera, Y., Fisahn, A. & Rodríguez-Moreno, A. Timing to be precise? An overview of spike timing-dependent plasticity, brain rhythmicity, and glial cells interplay within neuronal circuits. *Molecular Psychiatry* **2023** 1–12 (2023) doi:10.1038/s41380-023-02027-w.
450. Meshberger, F. L. An Interpretation of Michelangelo's Creation of Adam Based on Neuroanatomy. *JAMA* **264**, 1837–1841 (1990).

Author Contributions

Publication 1: Kv3.3 subunits control presynaptic action potential waveform and neurotransmitter release at a central excitatory synapse

Amy Richardson 1†, Victoria Ciampani 1, **Mihai Stancu** 2, Kseniia Bondarenko 1‡, Sherylanne Newton 1§, Joern R Steinert 1#, Nadia Pilati 3, Bruce P Graham 4, Conny Kopp-Scheinpflug 2, Ian D Forsythe 1*

Amy Richardson, Formal analysis, Investigation, Methodology, Writing – original draft, Writing – Review and editing; Victoria Ciampani, **Mihai Stancu**, Sherylanne Newton, Bruce P Graham, **Formal analysis, Investigation, Writing – review and editing**; Kseniia Bondarenko, Formal analysis, Investigation, Methodology, Writing – review and editing; Joern R Steinert, Formal analysis, Investigation, Supervision, Writing – review and editing; Nadia Pilati, Funding acquisition, Investigation, Supervision, Writing – review and editing; Conny Kopp-Scheinpflug, Formal analysis, Funding acquisition, Investigation, Project administration, Supervision, Writing – review and editing; Ian D Forsythe, Conceptualization, Formal analysis, Funding acquisition, Investigation, Methodology, Project administration, Supervision, Writing – original draft, Writing – review and editing

My contribution for this publication in detail:

For this publication, I performed the in-vivo experiments and collected the data for Figure 8; I contributed to writing the corresponding part of the paper manuscript and manuscript review and comments. **Publication 2 (Manuscript pending submission):** Ambient sound stimulation tunes axonal conduction speed by regulating radial growth of myelin in an individual, axon-specific manner.

Mihai Stancu, Hilde Wohlfrom, Martin Heß, Benedikt Grothe, Christian Leibold & Conny Kopp-Scheinpflug*

Division of Neurobiology, Faculty of Biology, Ludwig-Maximilians-University Munich, Großhaderner Straße 2, 82152, Planegg-Martinsried. Germany

Author Contributions: **M.S.** and C.K.-S. designed research; **M.S.**, H.W., M.H. performed research; C.K.-S. supervised work; **M.S.** and C.K.-S. analyzed data; C.L. performed computational modeling, **M.S.**, B.G. and C.K.-S. wrote the paper.

My contribution for this publication in detail:

For this publication, I performed all experiments, gathered and analyzed data (except for the second half of Figure 2 and the modeling from Figure 4 panels G-I). I developed tracing techniques for the lower auditory pathway; I streamlined experimental procedures for in vivo data acquisition and data analysis; I contributed to writing the paper.

For both manuscripts, each author is responsible for the integrity and accuracy of the data and are accountable for the content of the work.

Munich, April 2023

.....

Mihai Stancu

.....

PD. Dr. Conny Kopp-Scheinpflug
(supervisor)